Boundary Element Method for Solving Inverse Heat Source Problems

Areena Hazanee

Submitted in accordance with the requirements for the degree of

Doctor of Philosophy

The University of Leeds

Department of Applied Mathematics

July 2015

The candidate confirms that the work submitted is his/her own, except where work which has formed part of jointly authored publications has been included. The contribution of the candidate and the other authors to this work has been explicitly indicated below. The candidate confirms that appropriate credit has been given within the thesis where reference has been made to the work of others.

Joint Publications

Some material of this thesis is based on five published papers and three conference proceedings as well as one paper pending, as follows:

▶ Publications

1. Hazanee, A., Ismailov, M. I., Lesnic, D. and Kerimov, N. B. (2013) An inverse time-dependent source problem for the heat equation, *Applied Numerical Mathematics*, Vol.69, pp.13–33.

2. Hazanee, A. and Lesnic, D. (2013) Determination of a time-dependent heat source from nonlocal boundary conditions, *Engineering Analysis with Boundary Elements*, Vol.37, No.6, pp.936–956.

3. Hazanee, A. and Lesnic, D. (2013) Reconstruction of an additive space- and time-dependent heat source, *European Journal of Computational Mechanics*, Vol.22, Nos.5–6, pp.304–329.

4. Hazanee, A. and Lesnic, D. (2014) Determination of a time-dependent coefficient in the bioheat equation, *International Journal of Mechanical Sciences*, Vol.88, pp.259–266.

5. Hazanee, A., Ismailov, M. I., Lesnic, D. and Kerimov, N. B. (2015) An inverse time-dependent source problem for the heat equation with a non-classical boundary condition, *Applied Mathematical Modelling*, in press (available online).

▶ Conference Proceedings

1. Hazanee, A. and Lesnic, D. (2013) The boundary element method for solving an inverse time-dependent source problem, *Proceedings of the 9th UK Conference on Boundary Integral Methods*, (ed. O. Menshykov), UniPrint, University of Aberdeen, pp.55–62.

2. Hazanee, A. and Lesnic, D. (2014) A time-dependent coefficient identification problem for the bioheat equation, *ICIPE2014 8th International Conference on Inverse Problems in Engineering*, (eds. I. Szczygiel, A. J. Nowak and M. Rojczyk), Silesian University of Technology, May 12-15, 2014, Poland, pp.127–136.

3. Hazanee, A. and Lesnic, D. (2015) The boundary element method for an inverse time-dependent source problem for the heat equation with a non-classical boundary condition, *Proceedings of the 10th UK Conference on Boundary Integral Methods*, (ed. P. J. Harris), University of Brighton, pp.28–35.

► Possible Publications

1. Hazanee, A. and Lesnic, D. (2015) Reconstruction of multiplicative space- and time-dependent sources, submitted to Inverse Problems in Science and Engineering.

Acknowledgements

In the name of Allah, the most gracious and merciful, Alhamdulillah I thank Allah (subhanahu wa ta'ala) for endowing me with health, patience, and knowledge to complete this work. This thesis appears in its current form due to the assistance and guidance of several people. I would like to extend my sincere appreciation to all of them.

First and foremost, I would like to express my deepest gratitude to my supervisor, Professor Daniel Lesnic, for providing me with this great opportunity to do my PhD under his great supervision. My gratitude extends to Dr. Evy Kersalé, my adviser, for his valuable advice during my whole PhD study. I also would like to extend my thanks to all PhD students in the inverse problem group, Bandar Bin-Mohsin, Mohammed Hussein, Shilan Hussein, Taysir Dyhoum and Dimitra Flouri.

I would like to give my special thanks to all staff in the School of Mathematics for their help. Many thanks to all my friends in this school, Abeer Al-Nahdi, Wafa Al-Mohri, Mufida Mohamed Hmaida, and especially to my best friend and sister, Aolo Bashar Abusaksaka, who was always besides and supported me in any situation I have faced. I am grateful to Thai students, Joy Riyapan, Jeab Pattamawadee, Jiab Dussadee for their very good suggestions and providing me the Thai food which made me felt like I am still in Thailand. And also I am thankful to all Thai Muslim students in the UK for their friendship and fraternity during my time in the UK.

Of course, the indispensable thanks go to my Hazanee family, dad, mom, brothers, and my beloved aunt for unconditional love, support, cheering me up and standing by me. Far distance and time difference could not make me feel I am away from them.

I also gratefully acknowledge the funding support provided by the Ministry of Science and Technology of Thailand, Prince of Songkla University Thailand, for pursuing my PhD at the University of Leeds. I would also like to give special mention to all staff in the Office of Educational Affairs (OEA) in London for their advice and help dealing with my enquiries.

Abstract

In this thesis, the boundary element method (BEM) is applied for solving inverse source problems for the heat equation. Through the employment of the Green's formula and fundamental solution, the BEM naturally reduces the dimensionality of the problem by one although domain integrals are still present due to the initial condition and the heat source. We mainly consider the identification of time-dependent source for heat equation with several types of conditions such as non-local, non-classical, periodic, fixed point, time-average and integral which are considered as boundary or overdetermination conditions. Moreover, the more challenging cases of finding the space- and time-dependent heat source functions for additive and multiplicative cases are also considered.

Under the above additional conditions a unique solution is known to exist, however, the inverse problems are still ill-posed since small errors in the input measurements result in large errors in the output heat source solution. Then some type of regularisation method is required to stabilise the solution. We utilise regularisation methods such as the Tikhonov regularisation with order zero, one, two, or the truncated singular value decomposition (TSVD) together with various choices of the regularisation parameter.

The numerical results obtained from several benchmark test examples are presented in order to verify the efficiency of adopted computational methodology. The retrieved numerical solutions are compared with their analytical solutions, if available, or with the corresponding direct numerical solution, otherwise. Accurate and stable numerical solutions have been obtained throughout for all the inverse heat source problems considered.

Nomenclature

Roman Symbols

A, A_0, A_L, $A_k^{(1)}$, $A_{0,k}^{(1)}$, $A_{L,k}^{(1)}$, A^I, A_i^{II}	BEM coefficient matrices
$A_{0j}(x,t)$, $A_{Lj}(x,t)$	BEM coefficient functions
B, B^*, B_0, B_L, $B_k^{(1)}$, $B_k^{(1)^*}$, $B_{L,k}^{(1)}$, B^I, B_i^{II}, B^{III}	BEM coefficient matrices
$B_{0j}(x,t)$, $B_{Lj}(x,t)$	BEM coefficient integral functions
C, $C_k^{(1)}$, C^I, C_i^{II}, C^{III}	BEM coefficient matrices
$C^k([0,T])$	the space of k-order continuously differentiable functions on $[0,T]$
$C^{k,l}(D_T)$	the space of k-order and l-order continuously differentiable functions in time and space, respectively
$d(x,t)$, $d_0(x,t)$, $d_1(x,t)$, $d_2(x,t)$	BEM integral functions for the source term
d, d^I, d^{II}	BEM coefficient vectors
D, D_0, D_1, D_2, $D_k^{(1)}$, D_1^I, D_2^I, D_1^{II}, D_2^{II}, D^r, D_k^r, D^{rI}, D^{rIII}	BEM coefficient matrices
$D_T := (0,L) \times (0,T)$	solution domain
$\overline{D}_T := [0,L] \times [0,T]$	closure of the solution domain D_T
e_i	discrete components of function $E(t)$
$E(t)$	mass or energy
E	vector of $E(t)$
E^ϵ	noisy vector of $E(t)$
$\mathrm{E} = \mathrm{diag}(e_i)$	diagonal matrix with components e_i
$f(x,t)$, $F(x,t)$, $f(\mathbf{x},t)$	source functions
$\mathbb{F}$, $\mathbb{F}_0$, $\mathbb{F}_\lambda$	objective functions
$G(x,t,\xi,\tau)$	fundamental solution for one-dimensional heat equation

$h(x,t)$	given source function
h_{0j}, h_{Lj}	boundary temperatures
$\mathbb{h}$, $\mathbb{h}_0$, $\mathbb{h}_L$	boundary temperature vectors
$H(t)$	Heaviside step function
$H^{\gamma/2}[0,T]$, $H^{\gamma}[0,L]$, $H^{2+\gamma,1+\gamma/2}(\overline{D}_T)$	Hölder spaces in Chapter 6
i, j, k	indices
$k(t)$, $k_i(t)$	given boundary and overdetermination functions
k^*	the largest index of space x satisfying $x_{k^*} < X_0$
$\mathbb{k}$	vector of function $k(t)$
L	length of one-dimensional space domain
$\mathbf{n}$	outward unit normal to the space boundary
N	number of time steps
N_0	number of space cells
N_t	truncation number (for TSVD)
p, p_0	percentages of perturbation
$P(t)$	perfusion coefficient function
$\mathbb{q}$, $\mathbb{q}_0$, $\mathbb{q}_L$	boundary heat flux vectors
q_{0j}, q_{Lj}	boundary heat fluxes
$r(t)$, $r_1(t)$	time-dependent source functions
R, R_0, R_1, R_2, $R^{(1)}$, $R^{(2)}$, $\mathcal{R}$	regularisation matrices
$s(x)$, $s_1(x)$	space-dependent source functions
S	coefficient matrix
S_0, $\check{S}_0$	values of the sources at the fixed point
T, T_1, T_2	final and fixed times
$u(x,t)$, $u(\mathbf{x},t)$	temperatures
$u_0(x)$, $u_0(\mathbf{x})$	initial temperature
$u_{0,k}$	initial temperature at $\tilde{x}_k$

$\underline{u}_0$, $\underline{\tilde{u}}_0$	initial temperature vectors
$\underline{U}$, $\underline{V}$	orthogonal vectors for SVD
$v(x,t)$	transformation function
$v_1(t)$, $v_2(t)$	given functions
V_1, V_2	diagonal matrices of $v_1(t)$, $v_2(t)$
$\mathbb{W}_2^1(0,T)$, $\mathbb{W}_2^2(0,T)$, $\mathbb{W}_2^2(0,L)$, $\mathbb{W}_2^4(0,L)$, $\mathbb{W}_2^{4,2}(D_T)$	Sobolev space in Chapter 7
$\underline{w}$	unknown vector of $r(t)$ and $s(x)$
x, y, $\mathbf{x}$	spaces (variable)
X, X_i	left-hand side coefficient matrices of BEM linear system
X_0	fixed location
X^ϵ	contaminated left-hand side coefficient matrix
y_n	eigenfunction of the spectral problem
$\underline{y}$, $\underline{y}_i$	right-hand side vector of BEM linear system
$\underline{y}^\epsilon$	noisy right-hand side vector

Greek Symbols

α, a, b	heat transfer coefficients
$\beta(x)$, $\beta_1(x)$, $\beta_2(x)$, $\beta(\mathbf{x},t)$	given functions
δ_{ij}	the Kronecker delta symbol
$\psi(x)$	given function
$\chi(t)$, $\chi_1(t)$	given functions
ϵ, ϵ_0	noise levels
γ_1, γ_2	fixed point source values
$\gamma_{ij}(t)$	given functions
λ, λ_L, λ_{dis}, λ_{GCV}, λ_{opt}	regularisation parameters
$\mu_1(t)$, $\mu_2(t)$, $\mu_0(t)$, $\mu_L(t)$	given boundary temperatures

Ω	domain
$\partial\Omega$	boundary of the domain Ω
$\overline{\Omega} = \Omega \cup \partial\Omega$	closure of the domain Ω
$\Phi^4_{n_0}$	space of functions
τ, t	times (variable)
σ, σ_ψ, σ_χ, σ_μ, σ_r, σ_s	standard deviations
σ_i	singular values
Σ	diagonal matrix with components of σ_i
$\vartheta(\mathbf{x}, t)$	given function

Abbreviations

BEM	boundary element method
CBEM	constant boundary element method
erf, erfc	error and complementary error functions
FDM	finite difference method
FEM	finite element method
FOTR	first-order Tikhonov regularisation
GCV	generalised cross-validation
PDE	partial differential equation
RMSE	root mean square error
SOTR	second-order Tikhonov regularisation
SVD	singular value decomposition
TSVD	truncated singular value decomposition
ZOTR	zeroth-order Tikhonov regularisation

Contents

List of Figures

List of Tables

Chapter 1

General Introduction

1.1 Introduction

Inverse problems are becoming an essential part in the development of several applications in science and engineering such as in medical diagnosis and therapy, groundwater/air pollution phenomena, or the designing of thermal equipment, systems and instruments. Such problems, particularly for the heat equation, have important applications in the field of applied sciences such as in melting and freezing processes, the designing and manufacturing areas in which the strength of heat sources is not exactly recognised, especially in the discovery of the quantity of energy generation in a computer chip, in a microwave heating process, or in a chemical reaction process.

In this thesis, the interest is specialised to solve several inverse source problems for the heat equation using the boundary element method (BEM).

1.2 Inverse and ill-posed problems

A direct problem consists of solving a system where an input cause is given and an output effect is desired. However, if the situation is reversed then we have an inverse problem which is in general ill-posed (improperly-posed, incorrectly-posed). For more definitions and examples of inverse and ill-posed problems see the excellent review by

Kabanikhin [31].

The study of ill-posed problems began in the early 20th century through the definition of well-posedness given by J. Hadamard in 1902. In the sense of Hadamard, a mathematical problem is well-posed if it satisfies the following properties:

- *Existence*: For all (suitable) data, there exists a solution of the problem (in an appropriate sense).
- *Uniqueness*: For all (suitable) data, the solution is unique.
- *Stability*: The solution depends continuously on its data (i.e. small perturbations in the input data do not result in large perturbations in the solution).

According to above definition, any mathematical problem is ill-posed if any one of these three conditions is violated. In the cases investigated in this thesis, the problems violate the third condition, i.e. stability.

The main purpose of this thesis focuses on applying BEM to inverse heat source problems, which are in generally ill-posed in the sense that small measurement errors greatly magnify the sought solutions.

1.3 The boundary element method (BEM)

One of the main advantage of the BEM over domain discretisation methods such as the finite-difference method (FDM) or the finite element mehtod (FEM) is that the discretisation is necessary only on the boundary, i.e. the BEM uses less number of nodes and elements when compared to the FDM and the FEM. The main idea of the BEM, which is based on using the Green's identity and the fundamental solution, is to find the solution inside the domain by using the solution to the partial differential equation (PDE) on the boundary only.

The mathematical background of the BEM is represented by the knowledge of the fundamental solution and the application of the Green's identities. We first introduce

the Heaviside step function and the Dirac delta distribution as follows:

The Heaviside step function:

$$H(t) = \begin{cases} 1, & \text{if} \quad t > 0, \\ 0, & \text{if} \quad t \leq 0. \end{cases}$$

The Dirac delta distribution function:

$$\delta(x, \xi) = \delta(x - \xi) = \begin{cases} 0, & \text{if} \quad x \neq \xi, \\ \infty, & \text{if} \quad x = \xi. \end{cases}$$

The fundamental properties of the Dirac delta distribution are

$$\delta(x) = H'(x), \quad \int_{\Omega} f(\xi)\delta(x, \xi)\, d\xi = f(x), \quad x \in \Omega.$$

Basically, the one-dimensional transient heat equation is governed by the partial differential heat operator $\mathcal{L} := \frac{\partial^2}{\partial x^2} - \frac{\partial}{\partial t}$. Let $L > 0$ and $T > 0$ be the length of the space domain and the time duration, respectively, and define the solution domain

$$D_T := (0, L) \times (0, T]. \tag{1.1}$$

Consider the classical heat equation

$$\mathcal{L}u(x, t) = \frac{\partial^2 u}{\partial x^2}(x, t) - \frac{\partial u}{\partial t}(x, t) = 0, \quad (x, t) \in D_T. \tag{1.2}$$

A function $G(x, t, y, \tau)$ is called a fundamental solution for the heat equation (1.2) if

$$\mathcal{L}^* G(x, t, y, \tau) = -\delta(x, t; y, \tau) = -\delta(|x - y|, |t - \tau|), \tag{1.3}$$

where $\mathcal{L}^* = \frac{\partial^2}{\partial x^2} + \frac{\partial}{\partial t}$ is the adjoint of $\mathcal{L}$, (x, t) is a field point, and (y, τ) is a source point. Solving (1.3) using the method of Fourier transform gives the fundamental

solution, see [60],

$$G(x,t,y,\tau)=\frac{H(t-\tau)}{\sqrt{4\pi(t-\tau)}}\exp\left(-\frac{(x-y)^2}{4(t-\tau)}\right). \tag{1.4}$$

In order to develop the BEM, let us introduce the Green's identities, as follows:

$$\begin{cases} \displaystyle\int_\Omega \left(U\nabla^2 V - V\nabla^2 U\right)\, d\Omega = \int_{\partial\Omega}\left(U\frac{\partial V}{\partial n} - V\frac{\partial U}{\partial n}\right)\, dS, \\ \displaystyle\int_\Omega \left(U\nabla^2 V + \nabla U\cdot\nabla V\right)\, d\Omega = \int_{\partial\Omega} U\frac{\partial V}{\partial n}\, dS, \end{cases} \tag{1.5}$$

for any functions $U, V \in C^2(\Omega)$, where **n** is the outward normal to the boundary $\partial\Omega$ of the bounded domain Ω.

1.4 The BEM for solving one-dimensional direct heat problem

In order to understand how the BEM performs, let us consider the direct classical (one-dimensional) heat conduction problem which requires finding the temperature $u(x,t)$ satisfying the heat equation

$$u_t = u_{xx} + F(x,t), \quad (x,t)\in D_T, \tag{1.6}$$

where F is a heat source, subject to the initial condition

$$u(x,0) = u_0(x), \quad x\in[0,L], \tag{1.7}$$

and the Neumann boundary conditions

$$u_x(0,t)=\mu_1(t), \quad u_x(L,t)=\mu_2(t), \quad t\in(0,T], \tag{1.8}$$

(or the Dirichlet boundary conditions)

$$u(0,t) = \mu_1(t), \quad u(L,t) = \mu_2(t), \quad t \in (0,T]. \tag{1.9}$$

Mixed or Robin boundary conditions can also be considered. For using the BEM, we first multiply (1.6) by G and integrate over D_T to result in

$$\int_{D_T} G(x,t,y,\tau)\frac{\partial u}{\partial \tau}(y,\tau)\,dyd\tau = \int_{D_T} G(x,t,y,\tau)\frac{\partial^2 u}{\partial y^2}(y,\tau)\,dyd\tau + \int_{D_T} G(x,t,y,\tau)F(y,\tau)\,dyd\tau.$$

Using the Green's identities (1.5) gives

$$\begin{aligned}&\int_{D_T} G(x,t,y,\tau)\frac{\partial u}{\partial \tau}(y,\tau)\,dyd\tau \\ &= \int_0^T \left[G(x,t,\xi,\tau)\frac{\partial u}{\partial n(\xi)}(\xi,\tau) - u(\xi,\tau)\frac{\partial G}{\partial n(\xi)}(x,t,\xi,\tau)\right]_{\xi\in\{0,L\}} d\tau \\ &\quad + \int_{D_T} u(y,\tau)\frac{\partial^2 G}{\partial y^2}(x,t,y,\tau)\,dyd\tau + \int_{D_T} G(x,t,y,\tau)F(y,\tau)\,dyd\tau,\end{aligned} \tag{1.10}$$

where **n** is the outward unit normal to the space boundary $\{0,L\}$, i.e. $\frac{\partial}{\partial n(\xi)} = -\frac{\partial}{\partial \xi}$ for $\xi = 0$, and $\frac{\partial}{\partial n(\xi)} = \frac{\partial}{\partial \xi}$ for $\xi = L$. Then, using that the fundamental solution satisfies (1.3) and the property of the Dirac delta function result in the integral equation

$$\begin{aligned}\eta(x)u(x,t) = &\int_0^t \left[G(x,t,\xi,\tau)\frac{\partial u}{\partial n(\xi)}(\xi,\tau) - u(\xi,\tau)\frac{\partial G}{\partial n(\xi)}(x,t,\xi,\tau)\right]_{\xi\in\{0,L\}} d\tau \\ &+ \int_0^L G(x,t,y,0)u(y,0)\,dy + \int_0^L\int_0^T G(x,t,y,\tau)F(y,\tau)\,d\tau dy, \\ &(x,t) \in [0,L]\times(0,T],\end{aligned} \tag{1.11}$$

where $\eta(0) = \eta(L) = \frac{1}{2}$ and $\eta(x) = 1$ for $x \in (0,L)$.

The discretisation of the integral equation (1.11) is performed by dividing the boundaries $\{0\}\times(0,T]$ and $\{L\}\times(0,T]$ into a series of N small boundary elements

$[t_{j-1}, t_j]$ for $j = \overline{1, N}$, $t_j = \frac{jT}{N},\ j = \overline{0, N}$, whilst the space domain $[0, L] \times \{0\}$ is discretised into a series of N_0 small cells $[x_{k-1}, x_k]$ for $k = \overline{1, N_0}$, $x_k = \frac{k}{N_0},\ k = \overline{0, N_0}$. Over each boundary element $(t_{j-1}, t_j]$, the temperature u and the flux $\frac{\partial u}{\partial n}$ are assumed to be constant and take their values at the midpoint $\tilde{t}_j = \dfrac{t_{j-1} + t_j}{2}$, i.e.

$$u(0,t) = u(0,\tilde{t}_j) =: h_{0j},\ \ u(L,t) = u(L,\tilde{t}_j) =: h_{Lj}, \quad t \in (t_{j-1}, t_j] \tag{1.12}$$

$$\frac{\partial u}{\partial n}(0,t) = \frac{\partial u}{\partial n}(0,\tilde{t}_j) =: q_{0j},\ \ \frac{\partial u}{\partial n}(L,t) = \frac{\partial u}{\partial n}(L,\tilde{t}_j) =: q_{Lj},\ \ t \in (t_{j-1}, t_j]. \tag{1.13}$$

Note that since **n** is the outward unit normal to the (one-dimensional) space boundary, then

$$q_{0j} = -\frac{\partial u}{\partial x}(0,\tilde{t}_j), \quad q_{Lj} = \frac{\partial u}{\partial x}(L,\tilde{t}_j). \tag{1.14}$$

In each cell $[x_{k-1}, x_k]$, the temperature u is assumed to be constant and takes its value at the midpoint $\tilde{x}_k = \dfrac{x_{k-1} + x_k}{2}$, i.e.

$$u(x,0) = u(\tilde{x}_k,0) =: u_{0,k}, \quad x \in (x_{k-1}, x_k]. \tag{1.15}$$

Also, for the source function $F(x,t)$, we assume the piecewise constant approximation in time as

$$F(x,t) = F(x,\tilde{t}_j), \quad t \in (t_{j-1}, t_j]. \tag{1.16}$$

With these approximations, the integral equation (1.11) is discretised as

$$\begin{aligned}\eta(x)u(x,t) = &\sum_{j=1}^{N} [A_{0j}(x,t)q_{0j} + A_{Lj}(x,t)q_{Lj} - B_{0j}(x,t)h_{0j} - B_{Lj}(x,t)h_{Lj}] \\ &+ \sum_{k=1}^{N_0} C_k(x,t)u_{0,k} + \sum_{j=1}^{N} D_{0,j}(x,t), \quad (x,t) \in [0,L] \times (0,T],\end{aligned} \tag{1.17}$$

where the integral coefficients are given by

$$A_{\xi j}(x,t) = \int_{t_{j-1}}^{t_j} G(x,t,\xi,\tau)d\tau, \quad \xi = \{0, L\}, \tag{1.18}$$

$$B_{\xi j}(x,t) = \int_{t_{j-1}}^{t_j} \frac{\partial G}{\partial n(\xi)}(x,t,\xi,\tau)d\tau, \quad \xi = \{0, L\}, \tag{1.19}$$

$$C_k(x,t) = \int_{x_{k-1}}^{x_k} G(x,t,y,0)dy, \tag{1.20}$$

and the double integral source term is given by

$$D_{0,j}(x,t) = \int_{t_{j-1}}^{t_j}\int_0^L G(x,t,y,\tau)F(y,\tilde{t}_j)\,dyd\tau. \tag{1.21}$$

The integrals in expressions (1.18)–(1.20) can be evaluated analytically as, see [15],

$$A_{\xi j}(x,t) = \begin{cases} 0 & ;\ t \le t_{j-1}, \\ \sqrt{\dfrac{t-t_{j-1}}{\pi}} & ;\ t_{j-1} < t \le t_j,\ x = \xi, \\ \dfrac{|x-\xi|}{2\sqrt{\pi}}\left(\dfrac{e^{-z_0^2}}{z_0} - \sqrt{\pi}\text{erfc}(z_0)\right) & ;\ t_{j-1} < t \le t_j,\ x \ne \xi, \\ \sqrt{\dfrac{t-t_{j-1}}{\pi}} - \sqrt{\dfrac{t-t_j}{\pi}} & ;\ t > t_j,\ x = \xi, \\ \dfrac{|x-\xi|}{2\sqrt{\pi}}\left(\dfrac{e^{-z_0^2}}{z_0} - \dfrac{e^{-z_1^2}}{z_1} + \sqrt{\pi}\left(\text{erf}(z_0) - \text{erf}(z_1)\right)\right) & \\ & ;\ t > t_j,\ x \ne \xi, \end{cases} \tag{1.22}$$

$$B_{\xi j}(x,t) = \begin{cases} 0 & ;\ t \le t_{j-1}, \\ 0 & ;\ t_{j-1} < t \le t_j,\ x = \xi, \\ -\dfrac{\text{erfc}(z_0)}{2} & ;\ t_{j-1} < t \le t_j,\ x \ne \xi, \\ \dfrac{\text{erf}(z_0) - \text{erf}(z_1)}{2} & ;\ t > t_j, \end{cases} \tag{1.23}$$

$$C_k(x,t) = \frac{1}{2}\left[\text{erf}\left(\frac{x-x_{k-1}}{2\sqrt{t}}\right) - \text{erf}\left(\frac{x-x_k}{2\sqrt{t}}\right)\right], \tag{1.24}$$

where $\xi \in \{0, L\}$, $z_0 = \dfrac{|x-\xi|}{2\sqrt{t-t_{j-1}}}$, $z_1 = \dfrac{|x-\xi|}{2\sqrt{t-t_j}}$ and erf, erfc are the error functions defined by $\text{erf}(x) = \dfrac{2}{\sqrt{\pi}}\displaystyle\int_0^x e^{-\sigma^2}\,d\sigma$, $\text{erfc}(x) = 1 - \text{erf}(x)$, respectively. Mean-

while the double integral (1.21) becomes

$$D_{0,j}(x,t) = \int_{t_{j-1}}^{t_j} \int_0^L G(x,t,y,\tau) F(y,\tilde{t}_j)\, dy d\tau = \int_0^L F(y,\tilde{t}_j) A_{yj}(x,t)\, dy,$$

and can be evaluated using the midpoint rule for numerical integration.

Hence on considering the BEM, we apply the initial condition (1.7) at the nodes $\tilde{x}_k$ for $k = \overline{1, N_0}$, as in (1.15), and the integral equation (1.17) at the boundary nodes $(0,\tilde{t}_i)$ and $(L,\tilde{t}_i)$ for $i = \overline{L, N}$. This gives the system of $2N$ linear equations

$$A\mathfrak{q} - B\mathfrak{h} + C\mathfrak{u}_0 + \mathfrak{d} = \mathfrak{0}, \tag{1.25}$$

where

$$A = \begin{bmatrix} A_{0j}(0,\tilde{t}_i) & A_{Lj}(0,\tilde{t}_i) \\ A_{0j}(L,\tilde{t}_i) & A_{Lj}(L,\tilde{t}_i) \end{bmatrix}_{2N\times 2N},$$

$$B = \begin{bmatrix} B_{0j}(0,\tilde{t}_i) + \frac{1}{2}\delta_{ij} & B_{Lj}(0,\tilde{t}_i) \\ B_{0j}(L,\tilde{t}_i) & B_{Lj}(L,\tilde{t}_i) + \frac{1}{2}\delta_{ij} \end{bmatrix}_{2N\times 2N}, C = \begin{bmatrix} C_k(0,\tilde{t}_i) \\ C_k(L,\tilde{t}_i) \end{bmatrix}_{2N\times N_0},$$

$$\mathfrak{q} = \begin{bmatrix} q_{0j} \\ q_{Lj} \end{bmatrix}_{2N}, \quad \mathfrak{h} = \begin{bmatrix} h_{0j} \\ h_{Lj} \end{bmatrix}_{2N}, \quad \mathfrak{u}_0 = \begin{bmatrix} u_{0,k} \end{bmatrix}_{N_0}, \quad \mathfrak{d} = \begin{bmatrix} \sum_{j=1}^N D_{0,j}(0,\tilde{t}_i) \\ \sum_{j=1}^N D_{0,j}(L,\tilde{t}_i) \end{bmatrix}_{2N},$$

where δ_{ij} is the Kronecker delta symbol, defined by $\delta_{ij} = 1$ for $i = j$, and $\delta_{ij} = 0$ for $i \neq j$. Note that matrix term B also includes the contribution from the left-hand side of equation (1.17). At this stage, we can find the boundary temperature $\mathfrak{h}$, if the Neumann boundary conditions (1.8) are prescribed as

$$\mathfrak{h} = B^{-1}\left(A\mathfrak{q} + C\mathfrak{u}_0 + \mathfrak{d}\right).$$

Whereas if the Dirichlet boundary conditions (1.9) are prescribed, we can then obtain the heat flux $\mathfrak{q}$ as

$$\mathfrak{q} = A^{-1}\left(B\mathfrak{h} - C\mathfrak{u}_0 - \mathfrak{d}\right).$$

1.5 Condition number

The insight into the degree of conditioning of the system of equations (1.25) is merely given by the condition number of a matrix herein defined as the ratio between the largest to the smallest singular values. Obviously, the larger the condition number is the more ill-conditioned is our system of equations.

1.6 Regularisations

Inverse problems are well-known to be in general ill-posed by violating the stability condition at least. Upon discretisation, this results in an ill-conditioned systems of equations to be solved. To deal with these difficulties the inverse problem is usually solved as an optimisation problem with regularisation in order to achieve the stability of the solution. Below we briefly describe two such classical methods of regularisation.

1.6.1 The truncated singular value decomposition (TSVD)

Suppose we wish to solve the system of M linear equations with N unknowns

$$X\underline{\mathrm{r}} = \underline{\mathrm{y}}^{\epsilon}, \tag{1.26}$$

where y^{ϵ} is a noisy perturbation of the exact right-hand side vector $\underline{\mathrm{y}}$, i.e. $\|y - y^{\epsilon}\| \approx \epsilon$. We first decompose the matrix X in the form,

$$X = U\Sigma V^{\mathrm{T}}, \tag{1.27}$$

where $U = [\underline{\mathrm{U}}_1, \underline{\mathrm{U}}_2, \ldots, \underline{\mathrm{U}}_N]$ and $V = [\underline{\mathrm{V}}_1, \underline{\mathrm{V}}_2, \ldots, \underline{\mathrm{V}}_N]$ are $M \times N$ matrices with columns $\underline{\mathrm{U}}_j$ and $\underline{\mathrm{V}}_j$ for $j = \overline{1, N}$, such that $U^{\mathrm{T}}U = I = V^{\mathrm{T}}V$, and
$\Sigma = \mathrm{diag}(\sigma_1, \sigma_2, \ldots, \sigma_N)$ is an N diagonal matrix containing the singular values of

the matrix X, σ_j for $j = \overline{1, N}$, in decreasing order

$$\sigma_1 \geq \sigma_2 \geq \cdots \geq \sigma_N \geq 0.$$

Then the matrix system (1.26) can be reformed to obtain the singular value decomposition (SVD) solution as follows:

$$\underline{\mathrm{r}} = \left(\sum_{j=1}^{N} \frac{1}{\sigma_j} \underline{\mathrm{V}}_j \cdot \underline{\mathrm{U}}_j^{\mathrm{T}} \right) \underline{\mathrm{y}}^{\epsilon}. \tag{1.28}$$

In MATLAB, this decomposition is operated using the command $[U, \Sigma, V] = \text{svd}(X)$ or $[U, \Sigma, V] = \text{svds}(X, N)$. For ill-posed problems, the truncation of (1.28) is needed to be considered as a regularisation method, by omitting its last $N - N_t$ small singular values, where N_t denotes the truncation level. This way, the regularised solution is given by

$$\underline{\mathrm{r}}_{N_t} = \left(\sum_{j=1}^{N_t} \frac{1}{\sigma_j} \underline{\mathrm{V}}_j \cdot \underline{\mathrm{U}}_j^{\mathrm{T}} \right) \underline{\mathrm{y}}^{\epsilon}, \tag{1.29}$$

which is simply a truncated SVD (TSVD) stable solution of the full SVD unstable solution (1.28). And the MATLAB command for the TSVD becomes $[U_{N_t}, \Sigma_{N_t}, V_{N_t}] = \text{svds}(X, N_t)$ where $\Sigma_{N_t} = \text{diag}(\sigma_1, \sigma_2, \ldots, \sigma_{N_t})$ and $U_{N_t} = \left[\underline{\mathrm{U}}_1, \underline{\mathrm{U}}_2, \ldots, \underline{\mathrm{U}}_{N_T}\right]$, $V_{N_t} = \left[\underline{\mathrm{V}}_1, \underline{\mathrm{V}}_2, \ldots, \underline{\mathrm{V}}_{N_t}\right]$.

1.6.2 The Tikhonov regularisation

Alternatively, the Tikhonov regularisation is another way of obtaining a stable solution of the ill-conditioned system of equations (1.26). This method is based on minimising the regularised linear least-squares objective function, [42, 57],

$$\|X\underline{\mathrm{r}} - \underline{\mathrm{y}}^{\epsilon}\|^2 + \lambda \|R\underline{\mathrm{r}}\|^2 \tag{1.30}$$

where R is a (differential) regularisation matrix of order $k \in \{0, 1, 2, \dots\}$ imposing a C^k-smoothing constraint on the solution, and $\lambda > 0$ is a regularisation parameter to be prescribed. Note that the norm $\|\cdot\|$ is defined as the Euclidean norm of vector. In this study, we are considering the order of regularisation matrix R to be order zero, one, two as defined by [15, 57],

$$R_0 = \begin{bmatrix} 1 & 0 & 0 & . \\ 0 & 1 & 0 & . \\ 0 & 0 & 1 & . \\ . & . & . & . \end{bmatrix}, \quad \text{the zeroth-order regularisation,} \tag{1.31}$$

$$R_1 = \begin{bmatrix} 1 & -1 & 0 & 0 & . \\ 0 & 1 & -1 & 0 & . \\ 0 & 0 & 1 & -1 & . \\ . & . & . & . & . \end{bmatrix}, \quad \text{the first-order regularisation,} \tag{1.32}$$

$$R_2 = \begin{bmatrix} 1 & -2 & 1 & 0 & 0 & . \\ 0 & 1 & -2 & 1 & 0 & . \\ 0 & 0 & 1 & -2 & 1 & . \\ . & . & . & . & . & . \end{bmatrix}, \quad \text{the second-order regularisation.} \tag{1.33}$$

On solving the minimisation of (1.30) one obtains the regularised solution

$$\underline{\mathrm{r}}_\lambda = \left(X^{\mathrm{T}}X + \lambda R^{\mathrm{T}}R\right)^{-1} X^{\mathrm{T}}\underline{\mathrm{y}}^\epsilon. \tag{1.34}$$

1.6.3 Choice of the regularisation parameter

The regularisation parameter λ is very important in (1.34) (also the truncation level N_t in (1.29)) and it can be chosen according to many criteria, e.g. the L-curve method [16], the generalised cross-validation (GCV) [63], or the discrepancy principle [40]. The L-curve method suggests choosing λ at the corner of the L-curve which is a plot of the norm of the residual $\|X\underline{\mathrm{r}}_\lambda - \underline{\mathrm{y}}^\epsilon\|$ versus the solution norm $\|\underline{\mathrm{r}}_\lambda\|$. Alternatively, the

discrepancy principle chooses $\lambda > 0$ such that the residual $\|X\underline{\mathrm{r}}_\lambda - \underline{\mathrm{y}}^\epsilon\| \approx \epsilon$. Whereas the GCV criterion suggests choosing the parameter λ as the minimum of the GCV function,

$$GCV(\lambda) = \frac{\|X\underline{\mathrm{r}}_\lambda - \underline{\mathrm{y}}^\epsilon\|^2}{[\text{trace}(I - X(X^{\mathrm{T}}X + \lambda R^{\mathrm{T}}R)^{-1}X^{\mathrm{T}})]^2}, \quad \lambda > 0. \tag{1.35}$$

Note that both the L-curve and the GCV criteria are heuristic methods, which are not always convert [58], because they do not require the knowledge of the level of noise ϵ. Then these two methods do not guarantee to give the regularisation parameter.

1.7 Purpose of the thesis

In this thesis, we mainly consider inverse heat source problems for the heat equation (1.6), where u is the unknown temperature and F is a heat source term to be identified. We focus on the identification of the source term $F(x,t)$ in (1.6) in various special cases. This approach is necessary because otherwise there will be no unique solution to the inverse problem unless $u(x,t)$ is specified or measured throughout the whole solution domain D_T, [56].

Moreover, even though uniqueness of solution can be ensured by restricting the source term to be of certain special forms, e.g. space-dependent, time-dependent, additive or multiplicative, the inverse problem is still ill-posed in the sense that the continuous dependence upon the input data is violated (small errors in the input data give rise to large errors in the estimated results). This has to be dealt with by using some sort of regularisation, e.g. the TSVD as described in Subsection 1.6.1, the Tikhoknov regularisation as described in Subsection 1.6.2 [1, 15, 63], the iterative algorithm [30], the variational method [29], the augmented Tikhonov regularisation derived from a Bayesian perspective [65], the mollification methods [68, 69], the smoothing spline approximation [59], etc.

The structure of the thesis is as follows. In Chapter 1, the background knowledge

of inverse and ill-posed problems is provided. The BEM is detailed together with the application to the classical heat equation.

In Chapter 2, three general boundary conditions of inverse heat source problems are considered to determine the time-dependent heat source $r(t)$ in $F(x,t) = r(t)f_0(x,t) + f_1(x,t)$ and the temperature $u(x,t)$ in the heat equation (1.6), subject to the initial condition (1.7), and the following three general nonlocal boundary and overdetermination conditions:

$$\left.\begin{aligned}
&\gamma_{11}(t)u(0,t) + \gamma_{12}(t)u(L,t) + \gamma_{13}(t)u_x(0,t) + \gamma_{14}(t)u_x(L,t) = k_1(t)\\
&\gamma_{21}(t)u(0,t) + \gamma_{22}(t)u(L,t) + \gamma_{23}(t)u_x(0,t) + \gamma_{24}(t)u_x(L,t) = k_2(t)\\
&\gamma_{31}(t)u(0,t) + \gamma_{32}(t)u(L,t) + \gamma_{33}(t)u_x(0,t) + \gamma_{34}(t)u_x(L,t) = k_3(t)
\end{aligned}\right\}, \tag{1.36}$$

where $(k_i)_{i=\overline{1,3}}$ are given functions and $(\gamma_{ij})_{i=\overline{1,3},j=\overline{1,4}}$ is a given matrix of coefficients having rank 3. The BEM is combined with the Tikhonov regularisation in order to obtain an accurate and stable numerical solution.

In Chapter 3, we investigate an identification of the time-dependent heat source, i.e. we seek $r(t)$ in $F(x,t) = r(t)f(x,t)$, together with the temperature $u(x,t)$ in the heat equation (1.6), subject to the initial condition (1.7), the periodic and Robin boundary conditions

$$u(0,t) = u(1,t), \quad t \in [0,T], \tag{1.37}$$

$$u_x(0,t) + \alpha u(0,t) = 0, \quad t \in [0,T], \tag{1.38}$$

where $\alpha \neq 0$ is a given constant, and the integral additional measurement

$$\int_0^1 u(x,t)dx = E(t), \quad t \in [0,T]. \tag{1.39}$$

In this inverse problem, the BEM is developed as a numerical method and combined with two case studies of the regularisation method. Firstly, we apply the BEM together with the TSVD method in order to obtain a stable solution, and then the BEM is con-

sidered again and combined with various orders of Tikhonov's regularisation method.

In Chapter 4, we determine the time-dependent blood perfusion coefficient function $P(t) \geq 0$ and the temperature $u(x,t)$ in the following bioheat equation

$$u_t(x,t) = u_{xx}(x,t) - P(t)u(x,t) + f(x,t), \quad (x,t) \in (0,1) \times (0,T], \tag{1.40}$$

where f is a given heat source term. We subject this bioheat equation to the initial condition (1.7), the boundary conditions (1.37) and (1.38), and the integral overdetermination condition (1.39). A simple transformation is used to reduce the bioheat equation (1.40) to the classical heat equation (1.6). The BEM for the heat equation is employed, together with either the second-order Tikhonov regularisation combined with finite differences, or with a smoothing spline regularisation technique for computing the first-order derivative of a noisy function.

Chapter 5 presents an investigation for the identification of the time-dependent heat source $r(t)$ in $F(x,t) = r(t)f(x,t)$ and the temperature $u(x,t)$ in the heat equation in (1.6), subject to the initial condition (1.7), the non-classical boundary condition

$$au_{xx}(1,t) + \alpha u_x(1,t) + bu(1,t) = 0, \quad t \in [0,T], \tag{1.41}$$

where a, b, α are given numbers not simultaneously equal to zero, and the overdetermination condition (1.39). We are using the same techniques as before.

More challenging, the purpose in Chapter 6 is the simultaneous determination of an additive space- and time-dependent heat sources, i.e. identifying the unknown components $r(t)$ and $s(x)$ in the source term $F(x,t) = r(t)f(x,t) + s(x)g(x,t) + h(x,t)$, together with the temperature $u(x,t)$ in the heat equation (1.6), subject to the initial condition (1.7), the Dirichlet boundary conditions,

$$u(0,t) = \mu_0(t), \quad u(L,t) = \mu_L(t), \quad t \in [0,T], \tag{1.42}$$

and additional conditions. These latter ones consist of a specified temperature measure-

ment at an internal point $X_0 \in (0, L)$, a time-average temperature, and an additional fixing conditions, as follows:

$$u\left(X_0, t\right) = \chi(t), \quad t \in [0, T], \tag{1.43}$$

$$\int_0^T u(x, t)\, dt = \psi(x), \quad x \in [0, L], \tag{1.44}$$

$$s(X_0) = S_0. \tag{1.45}$$

The mathematical problem is linear but ill-posed since the continuous dependence on the input data is violated. In discretised form the problem reduces to solving an ill-conditioned system of linear equations. We investigate the performances of several regularisation methods, i.e. the TSVD and the Tikhonov regularisation, and examine their stability with respect to noise in the input data.

A nonlinear heat source problem is finally studied in Chapter 7. This consists of the simultaneous determination of multiplicative space- and time-dependent source components $f(t)$ and $g(x)$ in $F(x, t) = r(t)s(x)$, in the heat equation (1.6), subject to the initial condition (1.7), the homogeneous Neumann boundary conditions

$$u_x(0, t) = u_x(L, t) = 0, \quad t \in [0, T], \tag{1.46}$$

the specified interior measurement (1.43), the final time temperature measurement at the 'upper-base' final time $t = T$, and an additional fixing condition, as follows:

$$u(x, T) = \beta(x), \quad x \in [0, L], \tag{1.47}$$

$$s(X_0) = S_0. \tag{1.48}$$

For the numerical discretisation, the BEM combined with a regularised nonlinear optimisation are utilised.

Finally, in Chapter 8, the conclusions which summarise the main work of this thesis and possible future work are highlighted.

Chapter 2

Determination of a Time-dependent Heat Source from Nonlocal Boundary Conditions

2.1 Introduction

Recently, nonlocal boundary and overdetermination conditions have become a centre of interest in the mathematical formulation and numerical solution of several inverse and improperly posed problems in transient heat conduction, see e.g. [23, 24, 33, 51], to mention only a few. They opened a new area of applied numerical and mathematical modelling research. Practical applications of nonlocal boundary value problems are encountered in chemical diffusion for heat conduction in biological processes, see e.g. [11, 41, 46]. For example, in multiphase flows involving fluids, solids and gases, the heat flux is often taken to be proportional to the difference in boundary temperature between the various phases, and the quantities γ_{ij}, $i = \overline{1,3}$, $j = \overline{1,4}$, present in the nonlocal boundary condition (2.3) below (see also equation (1.36)) represent those proportionality factors.

In this chapter, we consider obtaining the numerical solution of several inverse

time-dependent heat source problems for the heat equation with non-local boundary and overdetermination conditions whose unique solvabilities have previously been investigated/established by Ivanchov [28]. The mathematical inverse formulations are described in Section 2.2. Since the inverse problems under investigations are linear, but ill-posed (in the sense that the continuous dependence upon the input data is violated), the numerical method is based on the boundary element direct solver combined with the Tikhonov regularisation, as described in Section 2.3. The choice of the regularisation parameter in the latter procedure is based on the discrepancy principle, [40]. The above combination yields accurate and stable numerical solutions, as it will be presented and discussed in Section 2.4. Finally, Section 2.5 highlights the conclusions of this chapter.

2.2 Mathematical formulation

Consider the problem of finding the time-dependent heat source $r(t) \in C([0,T])$ and the temperature $u(x,t) \in C^{2,1}(D_T) \cap C^{1,0}(\overline{D}_T)$ which satisfy the heat conduction equation

$$u_t = u_{xx} + r(t)f(x,t) + h(x,t), \quad (x,t) \in D_T, \tag{2.1}$$

subject to the initial condition (1.7), namely

$$u(x,0) = u_0(x), \quad x \in [0,L], \tag{2.2}$$

and the following general boundary and overdetermination conditions:

$$\left.\begin{aligned}
&\gamma_{11}(t)u(0,t) + \gamma_{12}(t)u(L,t) + \gamma_{13}(t)u_x(0,t) + \gamma_{14}(t)u_x(L,t) = k_1(t)\\
&\gamma_{21}(t)u(0,t) + \gamma_{22}(t)u(L,t) + \gamma_{23}(t)u_x(0,t) + \gamma_{24}(t)u_x(L,t) = k_2(t)\\
&\gamma_{31}(t)u(0,t) + \gamma_{32}(t)u(L,t) + \gamma_{33}(t)u_x(0,t) + \gamma_{34}(t)u_x(L,t) = k_3(t)
\end{aligned}\right\} \tag{2.3}$$

where

$$f, h \in C^{1,0}(\overline{D}_T), \quad u_0 \in C^2([0, L]), \quad k_i \in C^1([0, T]), \quad i = \overline{1, 3}, \tag{2.4}$$

and the matrix $\gamma = (\gamma_{ij})_{i=\overline{1,3}, j=\overline{1,4}} \in C^1([0, T])$ has rank 3 for all $t \in [0, T]$.

Actually, this inverse problem was studied theoretically by Ivanchov [28] who established its unique solvability. Moreover, by assuming, without any loss of generality, that the same third-order minor of the matrix γ is non-zero we can express three of the four boundary data $u(0, t)$, $u(L, t)$, $u_x(0, t)$, and $u_x(L, t)$ in terms of the fourth one and distinguish the following six cases:

Case 1 $u_x(0, t) = \mu_1(t), \quad u_x(L, t) = \mu_2(t),$ (2.5)

$v_1(t)u(0, t) + v_2(t)u(L, t) = k(t);$ (2.6)

Case 2 $u(0, t) = \mu_1(t), \quad u_x(L, t) = \mu_2(t),$ (2.7)

$v_1(t)u_x(0, t) + v_2(t)u(L, t) = k(t);$ (2.8)

Case 3 $u(0, t) = \mu_1(t), \quad u(L, t) = \mu_2(t),$ (2.9)

$v_1(t)u_x(0, t) + v_2(t)u_x(L, t) = k(t);$ (2.10)

Case 4 $u(0, t) = \mu_1(t), \quad u_x(L, t) + v_1(t)u(L, t) = \mu_2(t),$ (2.11)

$u_x(0, t) + v_2(t)u_x(L, t) = k(t);$ (2.12)

Case 5 $u_x(0, t) = \mu_1(t), \quad u_x(L, t) + v_1(t)u(L, t) = \mu_2(t),$ (2.13)

$u(0, t) + v_2(t)u(L, t) = k(t);$ (2.14)

Case 6 $u_x(0, t) - v_1(t)u(0, t) = \mu_1(t), \;\; u_x(L, t) + v_2(t)u(L, t) = \mu_2(t),$ (2.15)

$v_3(t)u(0, t) + v_4(t)u(L, t) = k(t),$ (2.16)

for $t \in [0, T]$, where $k \in C^1([0, T])$ is a given function resulted from manipulating the system (2.3). The other mixed boundary conditions cases corresponding to Cases 2, 4–6 can be reduced to these ones by the change of variable $y = L - x$.

The following Theorems 2.2.1–2.2.5 from [28] give the unique solvability, i.e. ex-

istence and uniqueness of the solutions of the inverse problem (2.1)–(2.3) in all the above six cases.

Theorem 2.2.1 *Assume that the regularity conditions* (2.4) *are satisfied and that:*

(i) $v_1, v_2 \in C^1([0,T]),\ v_1^2(t) + v_2^2(t) > 0, \quad t \in [0,T];$

(ii) $v_1(t)f(0,t) + v_2(t)f(L,t) \neq 0, \quad t \in [0,T];$

(iii) $\mu_1(0) = u_0'(0),\ \mu_2(0) = u_0'(L),\ v_1(0)u_0(0) + v_2(0)u_0(L) = k(0).$

Then the inverse problem (2.1), (2.2), (2.5), (2.6) *representing Case 1 is uniquely solvable.*

Theorem 2.2.2 *Assume that, in addition to conditions* (2.4) *and* (i) *of Theorem 2.2.1, the following conditions are satisfied:*

(i) $v_1(t)f(0,t) \neq 0, \quad t \in [0,T];$

(ii) $\mu_1(0) = u_0(0),\ \mu_2(0) = u_0'(L),\ v_1(0)u_0'(0) + v_2(0)u_0(L) = k(0).$

Then the inverse problem (2.1), (2.2), (2.7), (2.8) *representing Case 2 is uniquely solvable.*

Theorem 2.2.3 *Assume that, in addition to conditions* (2.4), (i) *and* (ii) *of Theorem 2.2.1, the following conditions are satisfied:*

$$\mu_1(0) = u_0(0),\ \mu_2(0) = u_0(L),\ v_1(0)u_0'(0) + v_2(0)u_0'(L) = k(0).$$

Then the inverse problem (2.1), (2.2), (2.9), (2.10) *representing Case 3 is uniquely solvable.*

Theorem 2.2.4 *Assume that the regularity conditions* (2.4) *are satisfied and that:*

(i) $v_1 \in C[0,T],\ v_2, \mu_i \in C^1[0,T],\ i = \overline{1,2},\ v_1(t) > 0, \quad t \in [0,T];$

(ii) in Case 4,

$$f(0,t) - v_2(t)f(L,t) \neq 0, \quad t \in [0,T],$$
$$\mu_1(0) = u_0(0),\ \mu_2(0) = u_0'(L) + v_1(0)u_0(L),\ k(0) = u_0'(0) + v_2(0)u_0'(L);$$

(iii) in Case 5,

$$f(0,t) + v_2(t)f(L,t) \neq 0, \quad t \in [0,T],$$
$$\mu_1(0) = u_0'(0),\ \mu_2(0) = u_0'(L) + v_1(0)u_0(L),\ k(0) = u_0(0) + v_2(0)u_0(L).$$

Then the inverse problem (2.1), (2.2), (2.11), (2.12) *representing Case 4, and* (2.1), (2.2), (2.13), (2.14) *representing Case 5 are uniquely solvable.*

Theorem 2.2.5 *Assume that the regularity conditions* (2.4) *are satisfied and that:*

(i) $v_i \in C[0,T],\ v_3, v_4, \mu_i \in C^1[0,T],\ v_i(t) > 0,\ i = 1,2,\ t \in [0,T];$

(ii) $v_1(t)f(0,t) + v_2(t)f(L,t) \neq 0,\ v_3^2(t) + v_4^2(t) > 0,\ t \in [0,T];$

(iii) $\mu_1(0) = u_0'(0) - v_1(0)u_0(0),\ \mu_2(0) = u_0'(L) + v_2(0)u_0(L),$
$k(0) = v_3(0)u_0(0) + v_4(0)u_0(L).$

Then the inverse problem (2.1), (2.2), (2.15), (2.16) *representing Case 6 is uniquely solvable.*

Although the problems of Cases 1–6 are uniquely solvable, they are still ill-posed since small errors in the input data $k(t)$ lead to large errors in the output source solution $r(t)$. In the next subsection we describe how the BEM discretising numerically the heat equation (2.1) can be used in conjunction with the Tikhonov regularisation in order to obtain a stable solution.

2.3 The boundary element method (BEM)

In the numerical process, we employ the BEM as introduced in Section 1.3. For the heat equation (2.1) we then obtain the integral equation

$$\begin{aligned}\eta(x)u(x,t) = &\int_0^t \left[G(x,t,\xi,\tau)\frac{\partial u}{\partial n(\xi)}(\xi,\tau) - u(\xi,\tau)\frac{\partial G}{\partial n(\xi)}(x,t,\xi,\tau)\right]_{\xi\in\{0,L\}} d\tau \\ &+ \int_0^L G(x,t,y,0)u(y,0)\,dy + \int_0^L\int_0^t G(x,t,y,\tau)r(\tau)f(y,\tau)\,d\tau dy \\ &+ \int_0^L\int_0^t G(x,t,y,\tau)h(y,\tau)\,d\tau dy, \quad (x,t)\in[0,L]\times(0,T). \quad (2.17)\end{aligned}$$

We use the constant BEM (CBEM) with the midpoint approximations (1.12), (1.13) and (1.15). Nevertheless, higher-order, e.g. linear boundary element approximations will be more accurate than constant boundary elements. This improvement in accuracy will be significant in higher-dimension, see e.g. [49], but in our one-dimensional time-dependent setting the use of the CBEM approximation was found sufficiently accurate. With this, the integral equation (2.17) can be approximated as

$$\begin{aligned}\eta(x)u(x,t) = &\sum_{j=1}^{N}\left[A_{0j}(x,t)q_{0j} + A_{Lj}(x,t)q_{Lj} - B_{0j}(x,t)h_{0j} - B_{Lj}(x,t)h_{Lj}\right] \\ &+ \sum_{k=1}^{N_0} C_k(x,t)u_{0,k} + d(x,t) + d_0(x,t), \quad (2.18)\end{aligned}$$

where the coefficients $A_{\xi j}$, $B_{\xi j}$, $\xi\in\{0,1\}$, and C_k are given by (1.18)–(1.20) and can be evaluated analytically as in (1.22)–(1.24), respectively. Whereas the double integral source terms d and d_0 are given by

$$d(x,t) = \int_0^L\int_0^t G(x,t,y,\tau)r(\tau)f(y,\tau)\,d\tau dy, \quad (2.19)$$

$$d_0(x,t) = \int_0^L\int_0^t G(x,t,y,\tau)h(y,\tau)\,d\tau dy, \quad (2.20)$$

and can be evaluated by assuming the piecewise constant approximations for the source functions $f(x,t)$, $h(x,t)$, and $r(t)$, i.e.

$$f(x,t) = f(x,\tilde{t}_j), \quad h(x,t) = h(x,\tilde{t}_j), \quad r(t) = r(\tilde{t}_j) =: r_j, \tag{2.21}$$

for $t \in (t_{j-1}, t_j]$ and $j = \overline{1,N}$. By these approximations, the integrals (2.19) and (2.20) become

$$d(x,t) = \int_0^t r(\tau) \int_0^L G(x,t,y,\tau) f(y,\tau)\, dy d\tau = \sum_{j=1}^{N} D_j(x,t) r_j, \tag{2.22}$$

$$d_0(x,t) = \int_0^t \int_0^L G(x,t,y,\tau) h(y,\tau)\, dy d\tau = \sum_{j=1}^{N} D_{0,j}(x,t), \tag{2.23}$$

where

$$\begin{aligned} D_j(x,t) &= \int_{t_{j-1}}^{t_j} \int_0^L G(x,t,y,\tau) f(y,\tilde{t}_j)\, dy d\tau = \int_0^L f(y,\tilde{t}_j) \int_{t_{j-1}}^{t_j} G(x,t,y,\tau)\, d\tau dy \\ &= \int_0^L f(y,\tilde{t}_j) A_{yj}(x,t)\, dy, \\ D_{0,j}(x,t) &= \int_{t_{j-1}}^{t_j} \int_0^L G(x,t,y,\tau) h(y,\tilde{t}_j)\, dy d\tau = \int_0^L h(y,\tilde{t}_j) \int_{t_{j-1}}^{t_j} G(x,t,y,\tau)\, d\tau dy \\ &= \int_0^L h(y,\tilde{t}_j) A_{yj}(x,t)\, dy, \end{aligned}$$

are evaluated numerically using the midpoint integral approximation. Here, the integral equation (2.18) can be rewritten as

$$\begin{aligned} \eta(x) u(x,t) = &\sum_{j=1}^{N} \left[A_{0j}(x,t) q_{0j} + A_{Lj}(x,t) q_{Lj} - B_{0j}(x,t) h_{0j} - B_{Lj}(x,t) h_{Lj} \right] \\ &+ \sum_{k=1}^{N_0} C_k(x,t) u_{0,k} + \sum_{j=1}^{N} D_j(x,t) r_j + \sum_{j=1}^{N} D_{0,j}(x,t). \end{aligned} \tag{2.24}$$

Applying (2.24) at the boundary nodes $(0, \tilde{t}_i)$ and $(L, \tilde{t}_i)$ for $i = \overline{1, N}$, we obtain the following system of $2N$ equations

$$A\mathfrak{q} - B\mathfrak{h} + C\mathfrak{u}_0 + D\mathfrak{r} + \mathfrak{d} = \mathfrak{0}, \tag{2.25}$$

where matrices A, B, C, D and vectors $\mathfrak{q}$, $\mathfrak{h}$, $\mathfrak{u}_0$, $\mathfrak{r}$, $\mathfrak{d}$ are defined as same as in Section 1.4, and $D = \begin{bmatrix} D_j(0, \tilde{t}_i) \\ D_j(L, \tilde{t}_i) \end{bmatrix}_{2N \times N}$.

In this section, we consider the heat equation (2.1) with the general conditions (2.3) which can be separated into the 6 cases presented in (2.5)–(2.16). Applying the boundary and the overdetermination conditions of these 6 cases results as follows.

2.3.1 Case 1

The Neumann heat flux boundary conditions (2.5) give

$$\mathfrak{q} = \begin{bmatrix} -u_x(0, \tilde{t}_j) \\ u_x(L, \tilde{t}_j) \end{bmatrix}_{2N} = \begin{bmatrix} -\mu_1(\tilde{t}_j) \\ \mu_2(\tilde{t}_j) \end{bmatrix}_{2N}. \tag{2.26}$$

Also, from (2.25) we obtain

$$\mathfrak{h} = B^{-1} \left(A\mathfrak{q} + C\mathfrak{u}_0 + D\mathfrak{r} + \mathfrak{d} \right). \tag{2.27}$$

The overdetermination condition (2.6) can be rewritten as a matrix equation as follows:

$$\begin{bmatrix} V_1 & V_2 \end{bmatrix} \mathfrak{h} = \mathfrak{k}, \tag{2.28}$$

where V_1, V_2 are $N \times N$ diagonal matrices of components $v_1(\tilde{t_1}), \ldots, v_1(\tilde{t_N})$ and $v_2(\tilde{t_1}), \ldots, v_2(\tilde{t_N})$, respectively, and $\mathfrak{k}$ is an N-column vector of the piecewise constant approximation of $k(t)$, namely

$$k(t) = k(\tilde{t}_i) =: k_i, \text{ for } t \in (t_{j-1}, t_j],\ j = \overline{1, N}.$$

Substituting (2.27) into (2.28) yields

$$\begin{bmatrix} V_1 & V_2 \end{bmatrix} B^{-1} \left(A\mathfrak{q} + C\mathfrak{u}_0 + D\mathfrak{r} + \mathfrak{d} \right) = \mathfrak{k}.$$

Rearranging this expression the inverse source problem in Case 1 reduces to solving the $N \times N$ linear system of equations

$$X_1 \mathfrak{r} = \underline{\mathfrak{y}}_1, \tag{2.29}$$

where $X_1 = \begin{bmatrix} V_1 & V_2 \end{bmatrix} B^{-1} D$, and $\underline{\mathfrak{y}}_1 = \mathfrak{k} - \begin{bmatrix} V_1 & V_2 \end{bmatrix} B^{-1} \left(A\mathfrak{q} + C\mathfrak{u}_0 + \mathfrak{d} \right)$.

2.3.2 Case 2

We rearrange the matrix equation (2.25) as follows:

$$\begin{bmatrix} A_0 & A_L \end{bmatrix} \begin{bmatrix} -u_x(0, \tilde{t}_j) \\ u_x(L, \tilde{t}_j) \end{bmatrix} - \begin{bmatrix} B_0 & B_L \end{bmatrix} \begin{bmatrix} u(0, \tilde{t}_j) \\ u(L, \tilde{t}_j) \end{bmatrix} + C\mathfrak{u}_0 + D\mathfrak{r} + \mathfrak{d} = \mathfrak{0}, \tag{2.30}$$

where $A_0 = \begin{bmatrix} A_{0j}(0, \tilde{t}_j) \\ A_{0j}(L, \tilde{t}_j) \end{bmatrix}$, $A_L = \begin{bmatrix} A_{Lj}(0, \tilde{t}_j) \\ A_{Lj}(L, \tilde{t}_j) \end{bmatrix}$, $B_0 = \begin{bmatrix} B_{0j}(0, \tilde{t}_j) + \frac{1}{2}\delta_{ij} \\ B_{0j}(L, \tilde{t}_j) \end{bmatrix}$, and $B_L = \begin{bmatrix} B_{Lj}(0, \tilde{t}_j) \\ B_{Lj}(L, \tilde{t}_j) + \frac{1}{2}\delta_{ij} \end{bmatrix}$ are $2N \times N$ matrices. Next, we apply the boundary conditions (2.7) such that this system becomes

$$A_0 \mathfrak{q}_0 + A_L \underline{\mu}_2 - B_0 \underline{\mu}_1 - B_L \mathfrak{h}_L + C\mathfrak{u}_0 + D\mathfrak{r} + \mathfrak{d} = \mathfrak{0},$$

where $\underline{\mu}_1 = \left[\mu_1(\tilde{t}_j) \right]_N$, $\underline{\mu}_2 = \left[\mu_2(\tilde{t}_j) \right]_N$, $\mathfrak{q}_0 = \left[q_{0j} \right]_N$, and $\mathfrak{h}_L = \left[h_{Lj} \right]_N$. From this system we obtain

$$\begin{bmatrix} -\mathfrak{q}_0 \\ \mathfrak{h}_L \end{bmatrix} = \begin{bmatrix} A_0 & B_L \end{bmatrix}^{-1} \left(A_L \underline{\mu}_2 - B_0 \underline{\mu}_1 + C\mathfrak{u}_0 + D\mathfrak{r} + \mathfrak{d} \right). \tag{2.31}$$

The overdetermination condition (2.8) can be written in matrix equation as follows:

$$\begin{bmatrix} V_1 & V_2 \end{bmatrix} \begin{bmatrix} -\mathfrak{q}_0 \\ \mathfrak{h}_L \end{bmatrix} = \mathfrak{k}. \tag{2.32}$$

Substituting the expression (2.31) into (2.32) we obtain

$$\begin{bmatrix} V_1 & V_2 \end{bmatrix} \begin{bmatrix} A_0 & B_L \end{bmatrix}^{-1} \Big(A_L \underline{\mu}_2 - B_0 \underline{\mu}_1 + C\mathfrak{u}_0 + D\underline{\mathfrak{r}} + \mathfrak{d} \Big) = \mathfrak{k}.$$

Rearranging this expression the inverse source problem reduces to solving the $N \times N$ linear system of equations

$$X_2 \underline{\mathfrak{r}} = \underline{\mathfrak{y}}_2, \tag{2.33}$$

where $X_2 = \begin{bmatrix} V_1 & V_2 \end{bmatrix} \begin{bmatrix} A_0 & B_L \end{bmatrix}^{-1} D$

and $\underline{\mathfrak{y}}_2 = \mathfrak{k} - \begin{bmatrix} V_1 & V_2 \end{bmatrix} \begin{bmatrix} A_0 & B_L \end{bmatrix}^{-1} \Big(A_L \underline{\mu}_2 - B_0 \underline{\mu}_1 + C\mathfrak{u}_0 + \mathfrak{d} \Big)$.

2.3.3 Case 3

The Dirichlet boundary temperature conditions (2.9) give

$$\mathfrak{h} = \begin{bmatrix} u(0, \tilde{t}_j) \\ u(L, \tilde{t}_j) \end{bmatrix}_{2N} = \begin{bmatrix} \mu_1(\tilde{t}_j) \\ \mu_2(\tilde{t}_j) \end{bmatrix}_{2N}. \tag{2.34}$$

Also, from (2.25) we obtain

$$\underline{\mathfrak{q}} = A^{-1} \left(B\mathfrak{h} - C\mathfrak{u}_0 - D\underline{\mathfrak{r}} - \mathfrak{d} \right). \tag{2.35}$$

The overdetermination condition (2.10) can be written as

$$\begin{bmatrix} -V_1 & V_2 \end{bmatrix} \underline{\mathfrak{q}} = \mathfrak{k}. \tag{2.36}$$

Substituting (2.35) into (2.36) gives the $N \times N$ linear system of equations

$$X_3 \mathbf{r} = \mathbf{y}_3, \tag{2.37}$$

where $X_3 = \begin{bmatrix} -V_1 & V_2 \end{bmatrix} A^{-1} D$ and $y_3 = -\mathbf{k} + \begin{bmatrix} -V_1 & V_2 \end{bmatrix} A^{-1} (B\mathbf{h} - C\mathbf{u}_0 - \mathbf{d})$.

2.3.4 Case 4

Consider the boundary condition (2.11) which can be rewritten as

$$u_x(L,t) = \mu_2(t) - v_1(t)u(L,t).$$

Apply this to the matrix equation (2.30), derived from (2.25), then the system becomes

$$A_0\mathbf{q} + A_L(\underline{\mu}_2 - V_1\mathbf{h}_L) - B_0\underline{\mu}_1 - B_L\mathbf{h}_L + C\mathbf{u}_0 + D\mathbf{r} + \mathbf{d} = \mathbf{0}.$$

We rearrange the matrix equation above as follows:

$$\begin{bmatrix} A_0 & A_L V_1 + B_L \end{bmatrix} \begin{bmatrix} -\mathbf{q}_0 \\ \mathbf{h}_L \end{bmatrix} = A_L\underline{\mu}_2 - B_0\underline{\mu}_1 + C\mathbf{u}_0 + D\mathbf{r} + \mathbf{d}.$$

From this system we obtain

$$\begin{bmatrix} -\mathbf{q}_0 \\ \mathbf{h}_L \end{bmatrix} = \begin{bmatrix} A_0 & A_L V_1 + B_L \end{bmatrix}^{-1} \left(A_L\underline{\mu}_2 - B_0\underline{\mu}_1 + C\mathbf{u}_0 + D\mathbf{r} + \mathbf{d} \right). \tag{2.38}$$

The overdetermined condition (2.12) becomes $u_x(0,t) + v_2(t)\mu_2(t) - v_2(t)v_1(t)u(L,t) = k(t)$ and can be rewritten in the matrix form as,

$$\begin{bmatrix} I & -V_2 V_1 \end{bmatrix} \begin{bmatrix} -\mathbf{q}_0 \\ \mathbf{h}_L \end{bmatrix} = \mathbf{k} - V_2\underline{\mu}_2, \tag{2.39}$$

where I is the $N \times N$ identity matrix. We then substitute (2.38) into (2.39) to obtain the $N \times N$ linear system of equations

$$X_4 \underline{\mathbf{r}} = \underline{\mathbf{y}}_4, \tag{2.40}$$

where $X_4 = \begin{bmatrix} I & -V_2 V_1 \end{bmatrix} \begin{bmatrix} A_0 & A_L V_1 + B_L \end{bmatrix}^{-1} D$
and $\underline{\mathbf{y}}_4 = \mathbf{k} - V_2 \underline{\mu}_2 - \begin{bmatrix} I & -V_2 V_1 \end{bmatrix} \begin{bmatrix} A_0 & A_L V_1 + B_L \end{bmatrix}^{-1} \Big(A_L \underline{\mu}_2 - B_0 \underline{\mu}_1 + C\mathbf{u}_0 + \mathbf{d} \Big)$.

2.3.5 Case 5

Consider the boundary condition (2.13) which can be rewritten as

$$u_x(L,t) = \mu_2(t) - v_1(t) u(L,t). \tag{2.41}$$

Apply this to the matrix equation (2.30), derived from (2.25), then the system becomes

$$-A_0 \underline{\mu}_1 + A_L(\underline{\mu}_2 - V_1 \mathbf{h}_L) - B_0 \mathbf{h}_0 - B_L \mathbf{h}_L + C\mathbf{u}_0 + D\underline{\mathbf{r}} + \mathbf{d} = \underline{0}.$$

We rearrange the matrix equation above as follows:

$$\begin{bmatrix} B_0 & A_L V_1 + B_L \end{bmatrix} \mathbf{h} = -A_0 \underline{\mu}_1 + A_L \underline{\mu}_2 + C\mathbf{u}_0 + D\underline{\mathbf{r}} + \mathbf{d}.$$

From this system we obtain

$$\mathbf{h} = \begin{bmatrix} B_0 & A_L V_1 + B_L \end{bmatrix}^{-1} \Big(-A_0 \underline{\mu}_1 + A_L \underline{\mu}_2 + C\mathbf{u}_0 + D\underline{\mathbf{r}} + \mathbf{d} \Big). \tag{2.42}$$

The overdetermination condition (2.14) gives

$$\begin{bmatrix} I & V_2 \end{bmatrix} \mathbf{h} = \mathbf{k}. \tag{2.43}$$

Substitute (2.42) into (2.43) to obtain the $N \times N$ linear system of equations

$$X_5 \underline{\mathbf{r}} = \underline{\mathbf{y}}_5, \tag{2.44}$$

where $X_5 = \begin{bmatrix} I & V_2 \end{bmatrix} \begin{bmatrix} B_0 & A_L V_1 + B_L \end{bmatrix}^{-1} D$
and $\underline{\mathbf{y}}_5 = \mathbf{k} - \begin{bmatrix} I & V_2 \end{bmatrix} \begin{bmatrix} B_0 & A_L V_1 + B_L \end{bmatrix}^{-1} \left(-A_0 \underline{\mu}_1 + A_L \underline{\mu}_2 + C\mathbf{u}_0 + \mathbf{d} \right)$.

2.3.6 Case 6

Consider the boundary condition (2.15) which can be rearranged as

$$\mathbf{q} = \begin{bmatrix} -u_x(0, \tilde{t}_j) \\ u_x(L, \tilde{t}_j) \end{bmatrix}_{2N} = \begin{bmatrix} -\underline{\mu}_1 - V_1 u(0, \tilde{t}_j) \\ \underline{\mu}_2 - V_2 u(L, \tilde{t}_j) \end{bmatrix}_{2N}.$$

Substituting this into the matrix equation (2.30) we obtain

$$A_0(-\underline{\mu}_1 - V_1 \mathbf{h}_0) + A_L(\underline{\mu}_2 - V_2 \mathbf{h}_L) - B_0 \mathbf{h}_0 - B_L \mathbf{h}_L + C\mathbf{u}_0 + D\underline{\mathbf{r}} + \mathbf{d} = \mathbf{0},$$

and this can be rearranged as

$$\begin{bmatrix} A_0 V_1 + B_0 & A_L V_2 + B_L \end{bmatrix} \mathbf{h} = -A_0 \underline{\mu}_1 + A_L \underline{\mu}_2 + C\mathbf{u}_0 + D\underline{\mathbf{r}} + \mathbf{d}.$$

Then we have

$$\mathbf{h} = \begin{bmatrix} A_0 V_1 + B_0 & A_L V_2 + B_L \end{bmatrix}^{-1} \left(-A_0 \underline{\mu}_1 + A_L \underline{\mu}_2 + C\mathbf{u}_0 + D\underline{\mathbf{r}} + \mathbf{d} \right). \tag{2.45}$$

The overspecified condition (2.16) gives

$$\begin{bmatrix} V_3 & V_4 \end{bmatrix} \mathbf{h} = \mathbf{k}. \tag{2.46}$$

Substitute (2.45) into (2.46) to obtain the $N \times N$ linear system of equations

$$X_6 \mathfrak{r} = \underline{\mathfrak{y}}_6, \tag{2.47}$$

where $\begin{bmatrix} V_3 & V_4 \end{bmatrix} \begin{bmatrix} A_0 V_1 + B_0 & A_L V_2 + B_L \end{bmatrix}^{-1} D$
and $\mathfrak{k} - \begin{bmatrix} V_3 & V_4 \end{bmatrix} \begin{bmatrix} A_0 V_1 + B_0 & A_L V_2 + B_L \end{bmatrix}^{-1} \Big(-A_0 \underline{\mu}_1 + A_L \underline{\mu}_2 + C \mathfrak{u}_0 + \mathfrak{d} \Big)$.

From the above assembly one can see that the solution of the inverse heat source problem (2.1)–(2.3) separated into the 6 cases, has been reduced to solving the $N \times N$ linear system of equations, generally written as

$$X \mathfrak{r} = \underline{\mathfrak{y}}, \tag{2.48}$$

where X and $\underline{\mathfrak{y}}$ are the coefficient matrix and the right-hand side vector, respectively, corresponding to the case we are dealing with; that is, the linear systems of equations, (2.29), (2.33), (2.37), (2.40), (2.44), and (2.47) for Cases 1–6, respectively. We note that the system of equations (2.48) is ill-conditioned since the inverse problems under investigation are ill-posed. Therefore, a straightforward inversion of (2.48) such as the Gaussian elimination or the singular value decomposition will result into an unstable numerical solution, especially when the right-hand side vector $\underline{\mathfrak{y}}$ is contaminated by random noise as $\underline{\mathfrak{y}}^{\epsilon} = \underline{\mathfrak{y}} + \epsilon$ where ϵ represents the noise to contaminate into the problem. In order to ensure a stable solution we employ the Tikhonov regularisation method for (2.48) which gives solution (1.34) together with the regularisation parameter chosen by the discrepancy principle. Let us denote by λ_{dis} the regularisation parameter which is determined by the discrepancy principle, i.e. the largest λ for which the residual $\|X\mathfrak{r} - y^{\epsilon}\|$ becomes less than the noise level ϵ.

2.4 Numerical examples and discussion

In order to test the accuracy of the approximations, let us introduce the root mean square error (RMSE) defined as

$$\text{RMSE}(r(t)) = \sqrt{\frac{T}{N}\sum_{i=1}^{N}\left(r_{exact}(\tilde{t}_i) - r_{numerical}(\tilde{t}_i)\right)^2}. \tag{2.49}$$

2.4.1 Example 1

We consider a smooth benchmark test with the input data

$$\begin{cases} u(x,0) = u_0(x) = 1 + x - x^2, \\ f(x,t) = (1-x^2)e^{-t}, \;\; h(x,t) = (2+x)e^t. \end{cases} \tag{2.50}$$

Assuming that all quantities involved have been non-dimensionalised we can take $T = L = 1$. In addition, the boundary and overdetermination conditions are as follows:

Case 1 $u_x(0,t) = e^t, \quad u_x(1,t) = -e^t,$ (2.51)

$u(0,t) + u(1,t) = 2e^t.$ (2.52)

Case 2 $u(0,t) = e^t, \quad u_x(1,t) = -e^t,$ (2.53)

$u_x(0,t) + u(1,t) = 2e^t.$ (2.54)

Case 3 $u(0,t) = e^t, \quad u(1,t) = e^t,$ (2.55)

$e^t u_x(0,t) + t u_x(1,t) = (e^t - t)e^t,$ (2.56)

where $v_1(t) = e^t,\ v_2(t) = t.$

Case 4 $u(0,t) = e^t, \quad u_x(1,t) + (1+t)u(1,t) = te^t,$ (2.57)

$u_x(0,t) + e^{-t}u_x(1,t) = e^t - 1,$ (2.58)

where $v_1(t) = 1 + t,\ v_2(t) = e^{-t}.$

Case 5 $u_x(0,t) = e^t, \quad u_x(1,t) + e^{-t}u(1,t) = 1 - e^t,$ (2.59)

$u(0,t) + (1+t)u(1,t) = (2+t)e^t,$ (2.60)

where $v_1(t) = e^{-t},\ v_2(t) = 1 + t.$

Case 6 $u_x(0,t) - e^t u(0,t) = e^t - e^{2t}, \quad u_x(1,t) + (1+t)u(1,t) = te^t,$ (2.61)

$tu(0,t) + (1-t)u(1,t) = e^t,$ (2.62)

where $v_1(t) = e^t,\ v_2(t) = 1 + t,\ v_3(t) = t,\ v_4(t) = 1 - t.$

In this example the analytical solution is given by

$$u(x,t) = (1 + x - x^2)e^t, \quad r(t) = e^{2t}, \tag{2.63}$$

for $0 \leq x \leq 1$ and $0 \leq t \leq 1$. Note that the input data in expressions (2.50)–(2.62) satisfy the conditions of Theorems 2.2.1–2.2.5 for the existence and uniqueness of the solution of the inverse problems of Cases 1–6 under investigation.

Figure 2.1 and Table 2.1 show the condition numbers of matrix X in (2.48) corresponding to $N_0 = N \in \{20, 40, 80\}$ for all Cases 1–6. From these it can be seen that the condition numbers of the matrix X for Cases 1, 5, and, 6 are high and this ill-conditioning will need to be dealt with using the Tikhonov regularisation described in Section 1.6.2. On the other hand, the matrices for Cases 2–4 do not have a very large condition number and, in principle, the system of equations (2.48) can be solved directly using, for example, the Gauss elimination method or the SVD. In what follows, we illustrate the numerical results obtained with $N_0 = N = 40$.

Case 1

Figures 2.2(a)–2.2(c) show the analytical and numerical solutions for $r(t)$, $u(0,t)$ and $u(1,t)$, respectively, for exact input data and no regularisation, i.e. $\lambda = 0$. From this figure it can be seen that although the solution for the boundary values of the temperatures $u(0,t)$ and $u(1,t)$ is stable and accurate, the retrieved source term $r(t)$

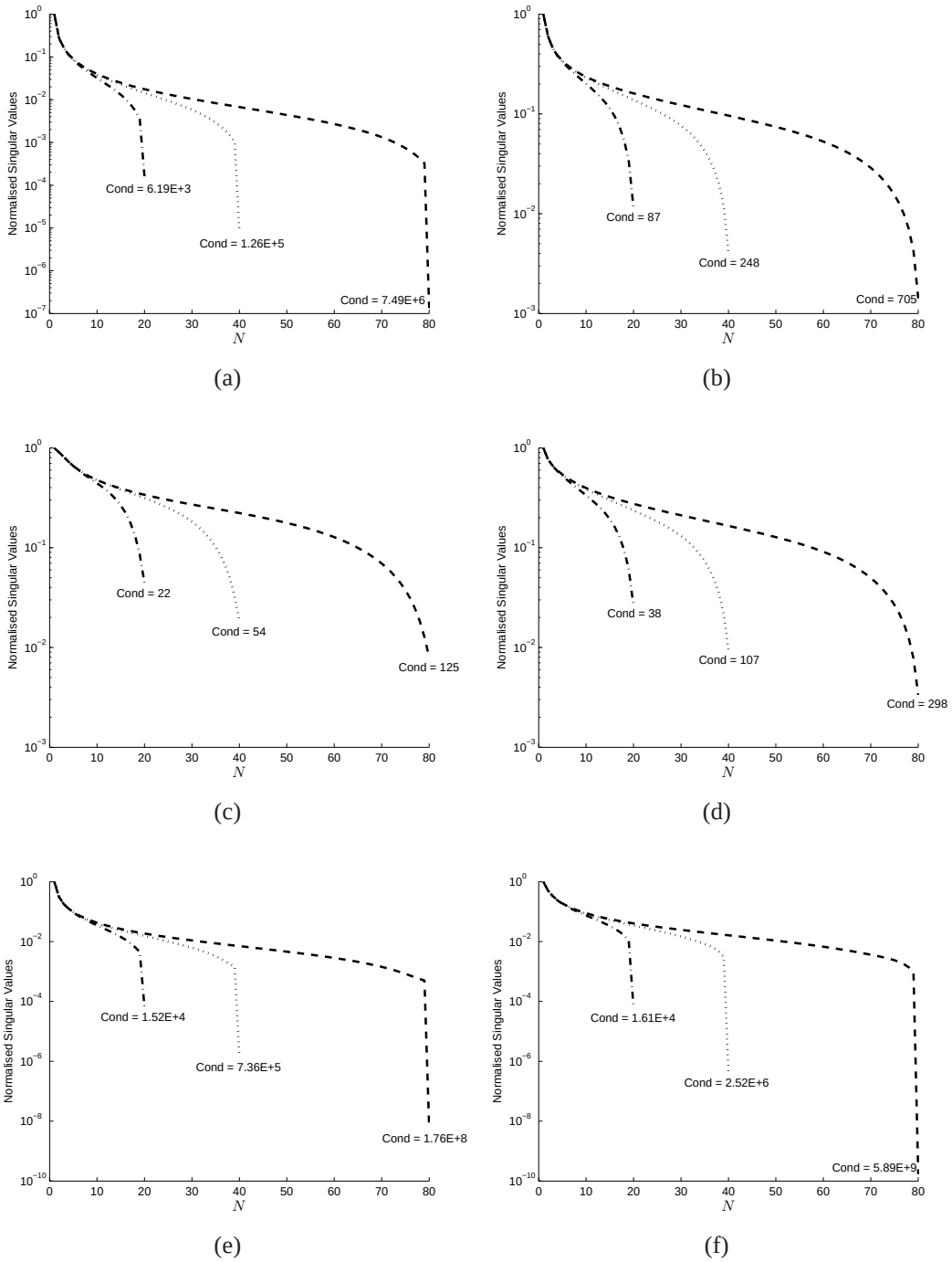

Figure 2.1: The normalised singular values of matrix X for (a) Case 1 – (f) Case 6 for $N_0 = N = \{20\ (- \cdot -), 40\ (\cdots), 80\ (- - -)\}$, for Example 1.

Table 2.1: The condition numbers of the matrix X in equation (2.48) for $N = N_0 \in \{20, 40, 80\}$ for Example 1 Cases 1–6.

Case	Condition Number		
	$N = N_0 = 20$	$N = N_0 = 40$	$N = N_0 = 80$
1	6.19E+3	1.26E+5	7.49E+6
2	87	248	705
3	22	54	125
4	38	107	298
5	1.52E+4	7.36E+5	1.76E+8
6	1.61E+4	2.52E+6	5.89E+9

seems unstable. This is to be expected since the inverse problem in Case 1 is ill-posed, see also the condition number in Table 2.1. Regularisation needs to be employed and more stable results are illustrated in Figure 2.3. In this figure, numerical results obtained with the zeroth-order Tikhonov regularisation. Initially, we have tried the L-curve criterion, but we have found that an L-corner could not be clearly identified. We then have tried with the trial and error and found that the regularisation parameters $\lambda \in \{10^{-7}, 10^{-5}\}$ are most suitable as presented in Figure 2.3. Moreover, although not illustrated, it is reported that the slight inaccuracies near $t = 1$ observed in Figure 2.3(a) can be further eliminated by employing higher-order regularisations such as the first- or second-order.

Table 2.2: The RMSE for the zeroth- and first-order Tikhonov regularisation for $p \in \{0, 1, 3\}\%$ noise, for Example 1 Case 1.

Regularisation	$p(\%)$	parameter λ	RMSE		
			$r(t)$	$u(0,t)$	$u(1,t)$
-	0	0	0.983	3.67E-4	3.67E-4
-	1	0	4.90E+2	1.90E-1	1.81E-1
zeroth-order	0	λ=1.0E-5	0.499	1.27E-3	7.92E-5
	1	λ_{dis}=6.6E-4	1.264	2.01E-2	7.31E-3
	3	λ_{dis}=4.0E-3	1.982	6.25E-2	2.91E-2
first-order	0	λ=1.0E-7	9.49E-3	3.06E-5	3.07E-5
	1	λ_{dis}=4.3E-2	0.364	7.19E-3	3.03E-3
	3	λ_{dis}=9.7E-1	1.007	3.59E-2	1.78E-2

In order to investigate the stability of the numerical solution we add noise to the

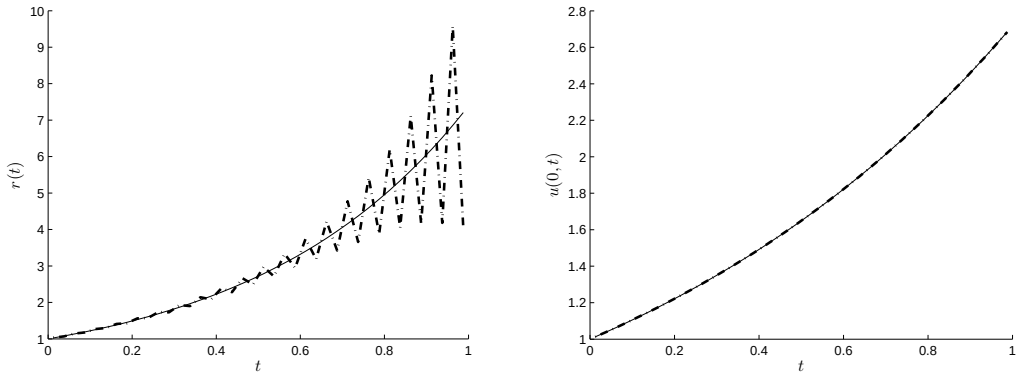

(a) (b)

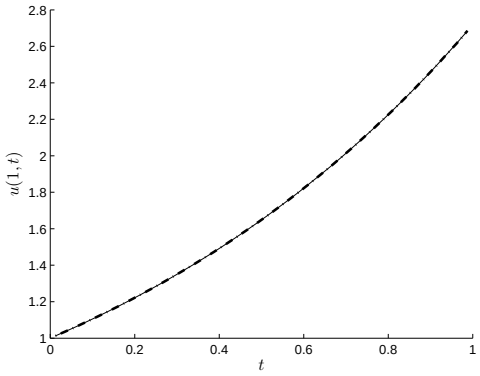

(c)

Figure 2.2: The analytical (——) and numerical ($-\cdot-$) results of (a) $r(t)$, (b) $u(0,t)$, and (c) $u(1,t)$ for exact data and $\lambda = 0$, for Example 1 Case 1.

right-hand side of the overspecified condition (2.6) as

$$\mathrm{k}^{\epsilon} = \mathrm{k} + random('\text{Normal}', 0, \sigma, 1, N), \tag{2.64}$$

where the $random('\text{Normal}', 0, \sigma, 1, N)$ is a command in MATLAB which generates the random variables by normal distribution with zero mean and standard deviation σ, computed as

$$\sigma = p \times \max_{t\in[0,1]} |k(t)|, \tag{2.65}$$

where p represents the percentage of noise. In Case 1, k is given by (2.52) and therefore, $\sigma = 2ep$ in (2.65). The ill-posedness of the inverse problem and the instability of

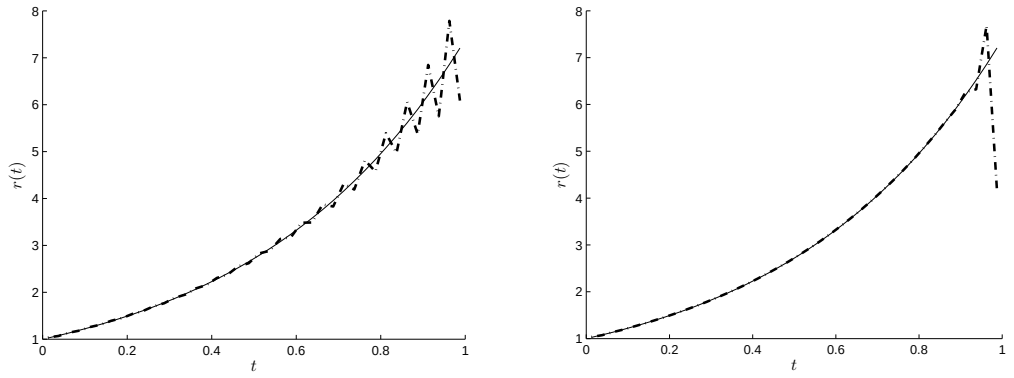

(a) (b)

Figure 2.3: The analytical (——) and numerical ($- \cdot -$) results of $r(t)$ obtained by using the zeroth-order Tikhonov regularisation with the regularisation parameters (a) $\lambda = 10^{-7}$ gives RMSE=0.319, and (b) $\lambda = 10^{-5}$ gives RMSE=0.499, for exact data for Example 1 Case 1.

the numerical solution in Case 1 are further enhanced by the presence of noise in the measured data, as illustrated in Figure 2.4 (compare with Figure 2.2). In order to remove the highly unwanted oscillations recorded in Figure 2.4, we employ the Tikhonov regularisation with the choice of the regularisation parameter λ, as described in (1.34), given by the discrepancy principle as introduced in Section 1.6.3. Figures 2.5(a) and 2.6(a) present the discrepancy principle curves obtained by the Tikhonov regularisation of order zero and one, respectively, for $p = 1\%$ and 3% noisy data. Generated as in (2.64), this results in the amounts of noise $\epsilon = 0.32$ and 1.01 for $p = 1\%$ and 3%, respectively. The intersections between these horizontal lines and the discrepancy (residual) curves yield the regularisation parameter denoted by λ_{dis} and tabulated in Table 2.2. With these values of λ_{dis}, Figures 2.5(b)–2.5(d) and 2.6(b)–2.6(d) present the numerical results for $r(t)$, $u(0,t)$, and $u(1,t)$ obtained using the zeroth- and first-order Tikhonov regularisation, respectively. By comparing Figures 2.5(b) and 2.6(b) it can be seen that the first-order regularisation produces more accurate and stable results than the zeroth-order regularisation since it imposes a higher-order smoothness constraint onto the solution.

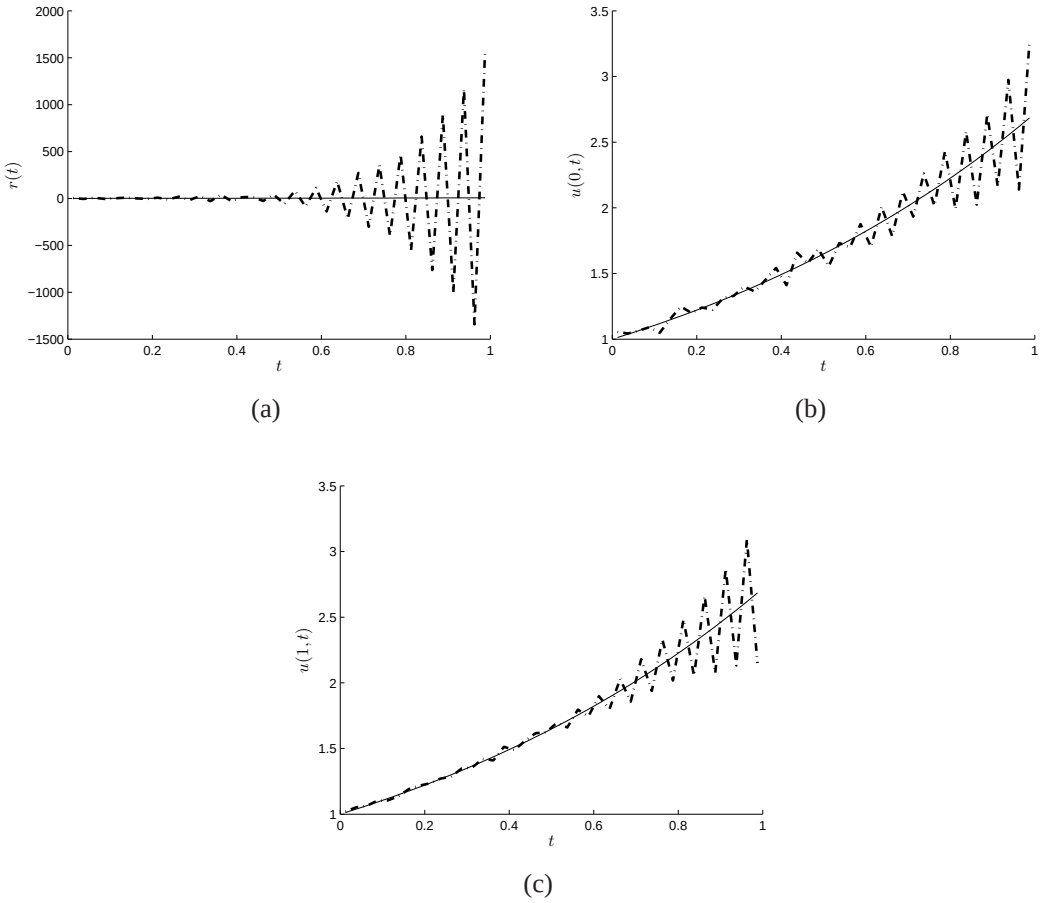

(a) (b)

(c)

Figure 2.4: The analytical (——) and numerical ($- \cdot -$) results of (a) $r(t)$, (b) $u(0,t)$, and (c) $u(1,t)$ for $p = 1\%$ noisy data and $\lambda = 0$, for Example 1 Case 1.

Cases 2–4

In Cases 2–4, Table 2.1 shows that the condition numbers of the matrices X_2, X_3, and X_4 are much smaller than the condition numbers of the matrices for the rest of the cases. Therefore, for exact data, i.e. $p = 0$, we expect accurate and stable results of the inversion even if no regularisation is employed, i.e. $\lambda = 0$. This is clearly illustrated in Figure 2.7 for Case 2 where it can be seen that the agreement between the analytical and numerical solutions for $r(t)$, $u(1,t)$ and $u_x(0,t)$ is excellent. The same overlapping agreement has also been obtained for Cases 3 and 4 and therefore these results are omitted. Next we add $p\%$ noise in the input data, as described in

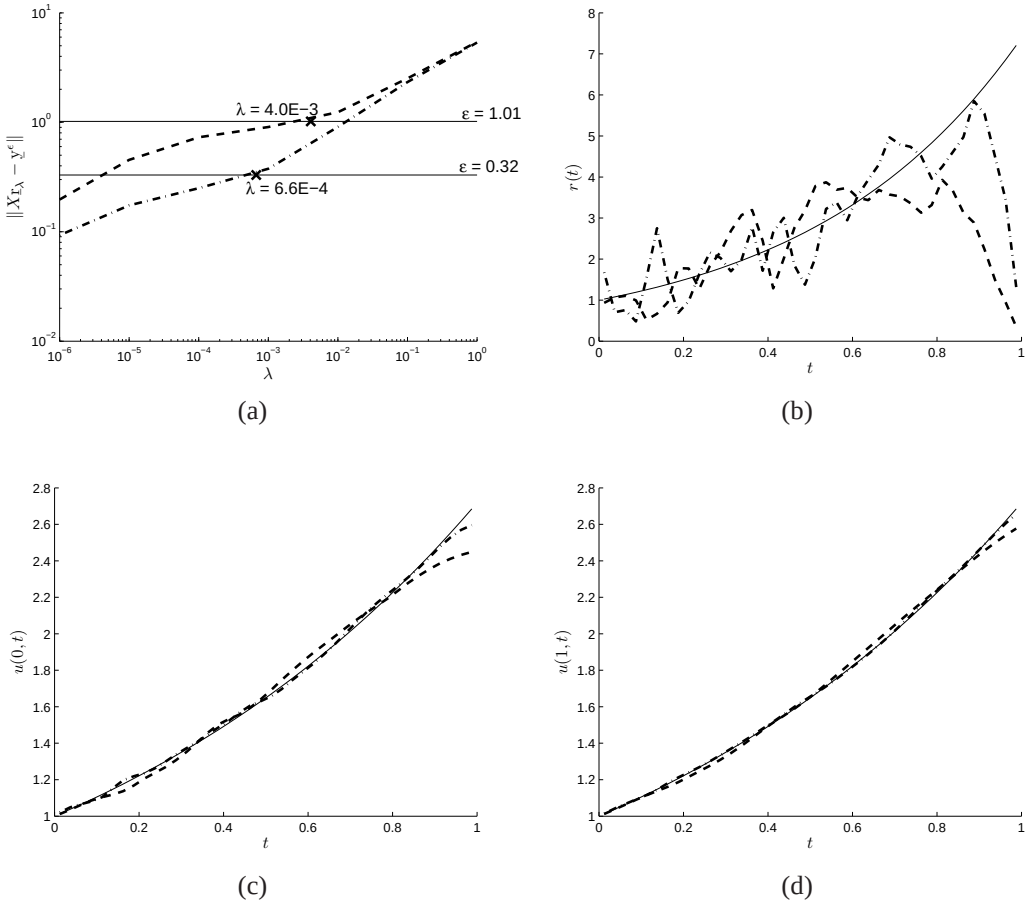

(a) (b)

(c) (d)

Figure 2.5: (a) The discrepancy principle curve, and the analytical (——) and numerical results of (b) $r(t)$, (c) $u(0,t)$, and (d) $u(1,t)$ obtained using the zeroth-order Tikhonov regularisation for $p = 1\%$ $(- \cdot -)$ and $p = 3\%$ $(- - -)$ noise with the regularisation parameters λ_{dis} given in Table 2.2, for Example 1 Case 1.

(2.64). According to expression (2.65), and equations (2.54), (2.56), and (2.58), we have the standard deviations $\sigma = 2ep$, $\sigma = (e^2 - e)p$, and $\sigma = (e - 1)p$ for Cases 2–4, respectively. As expected, and previously reported in Figure 2.4 for Case 1, if no regularisation is imposed, i.e. $\lambda = 0$, when $p = 1\%$ noise contaminates the input data $k(t)$, then an unstable solution for $r(t)$ is obtained, see Figures 2.8, 2.11, and 2.14 for Cases 2–4, respectively. However, the high oscillations in these figures have smaller magnitudes than these reported in Figure 2.4 for Case 1. This is consistent with the fact that the inverse problems of Cases 2–4 are less ill-posed than the inverse

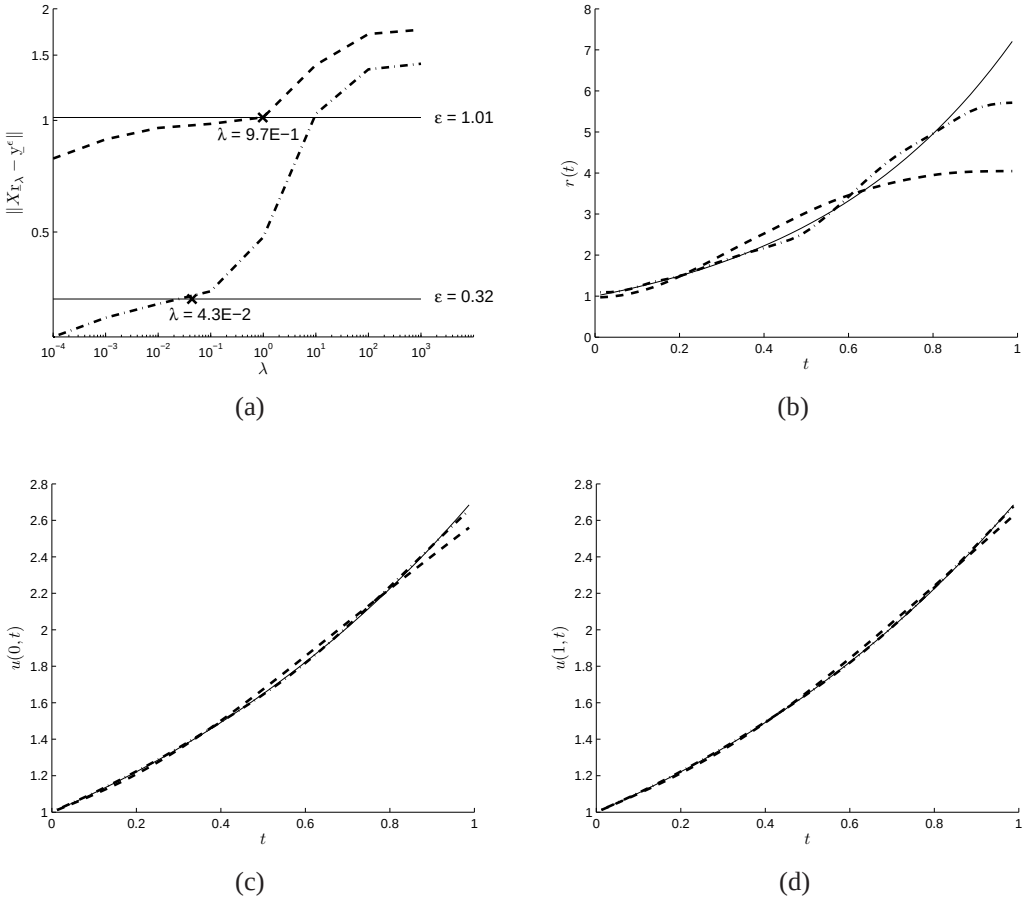

(a) (b) (c) (d)

Figure 2.6: (a) The discrepancy principle curve, and the analytical (——) and numerical results of (b) $r(t)$, (c) $u(0,t)$, and (d) $u(1,t)$ obtained using the first-order Tikhonov regularisation for $p = 1\%$ $(- \cdot -)$ and $p = 3\%$ $(- - -)$ noise with the regularisation parameters λ_{dis} given in Table 2.2, for Example 1 Case 1.

problem of Case 1 (and Cases 5 and 6), see the condition numbers reported in Table 2.1. It is also interesting to remark that the retrieval of the boundary temperature is more accurate and stable than of the heat flux, e.g. compare Figures 2.8(b) and 2.14(b) with Figures 2.8(c) and 2.14(c), see also Figures 2.11(b) and 2.11(c). This is to be expected since retrieving higher-order derivatives is less accurate than retrieving lower-order derivatives, see Lesnic et al. [38]. In order to obtain a stable solution, regularisation needs to be employed. The numerical results obtained for $p \in \{1, 3\}\%$ noise using the zeroth-order Tikhonov regularisation with the regularisation parameter

chosen according to the discrepancy principle are shown in Figures 2.9, 2.12, and 2.15 for Cases 2–4, respectively. The corresponding results obtained using the first-order regularisation illustrated in Figures 2.10, 2.13, and 2.16 show much improvement in terms of both stability and accuracy compared to the results obtained using the zeroth-order regularisation. The regularisation parameters and the RMSE errors of the output solutions are given in Tables 2.3–2.5 for Cases 2–4, respectively. From these tables it can be observed that, as expected, λ_{dis} and RMSE increase with increasing the percentage of noise p.

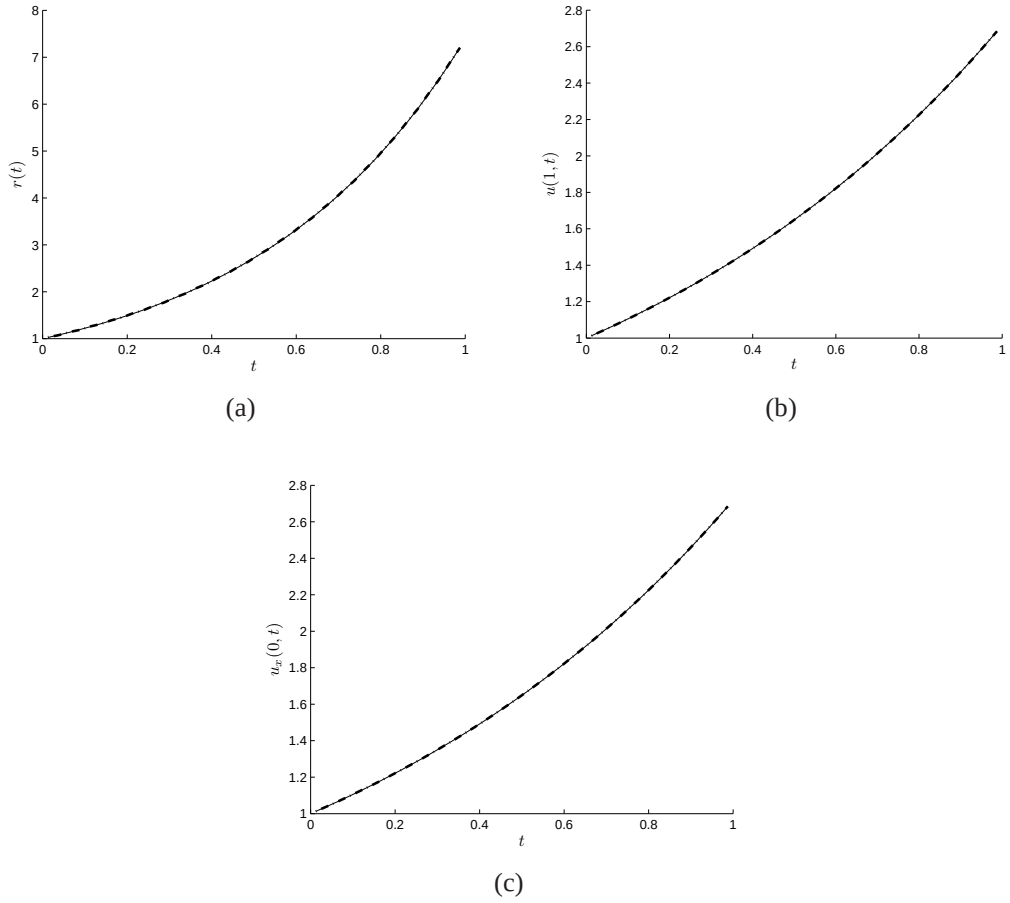

(a) (b)

(c)

Figure 2.7: The analytical (——) and numerical ($- \cdot -$) results of (a) $r(t)$, (b) $u(1,t)$, and (c) $u_x(0,t)$ for exact data and $\lambda = 0$, for Example 1 Case 2.

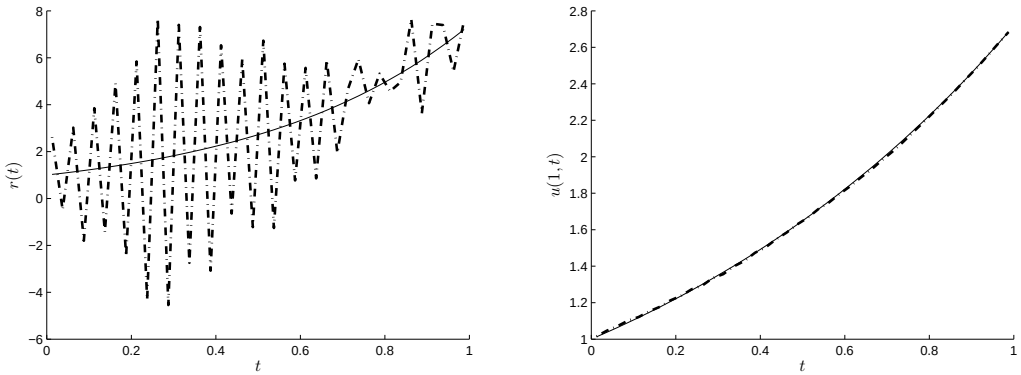

(a) (b)

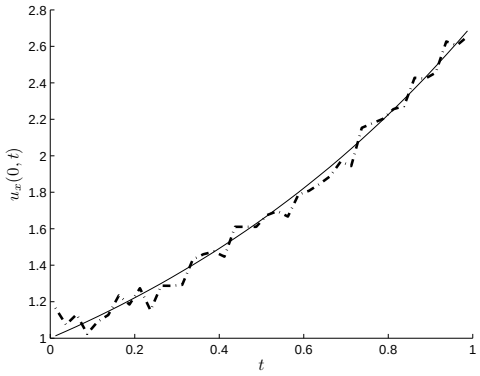

(c)

Figure 2.8: The analytical (——) and numerical ($- \cdot -$) results of (a) $r(t)$, (b) $u(1,t)$, and (c) $u_x(0,t)$ for $p = 1\%$ noisy data and $\lambda = 0$, for Example 1 Case 2.

Cases 5 and 6

In Cases 5 and 6 we expect even higher ill-conditioning to occur in the systems of equations (2.44) and (2.47), compare the condition numbers in Table 2.1. This is reflected indeed in the numerical results presented in Figures 2.17(a) and 2.18 for Case 5, and even more prominently in Figure 2.21 for Case 6 where unstable numerical results can be clearly seen if $\lambda = 0$ even when exact data are inverted. When $p\%$ noise is added to the measured data (2.60) and (2.62), the standard deviations in (2.65) are given by $\sigma = 3ep$ and $\sigma = ep$ for Cases 5 and 6, respectively. Numerical results obtained using the zeroth- and first-order regularisation are presented in Figures 2.19, 2.20 and Table

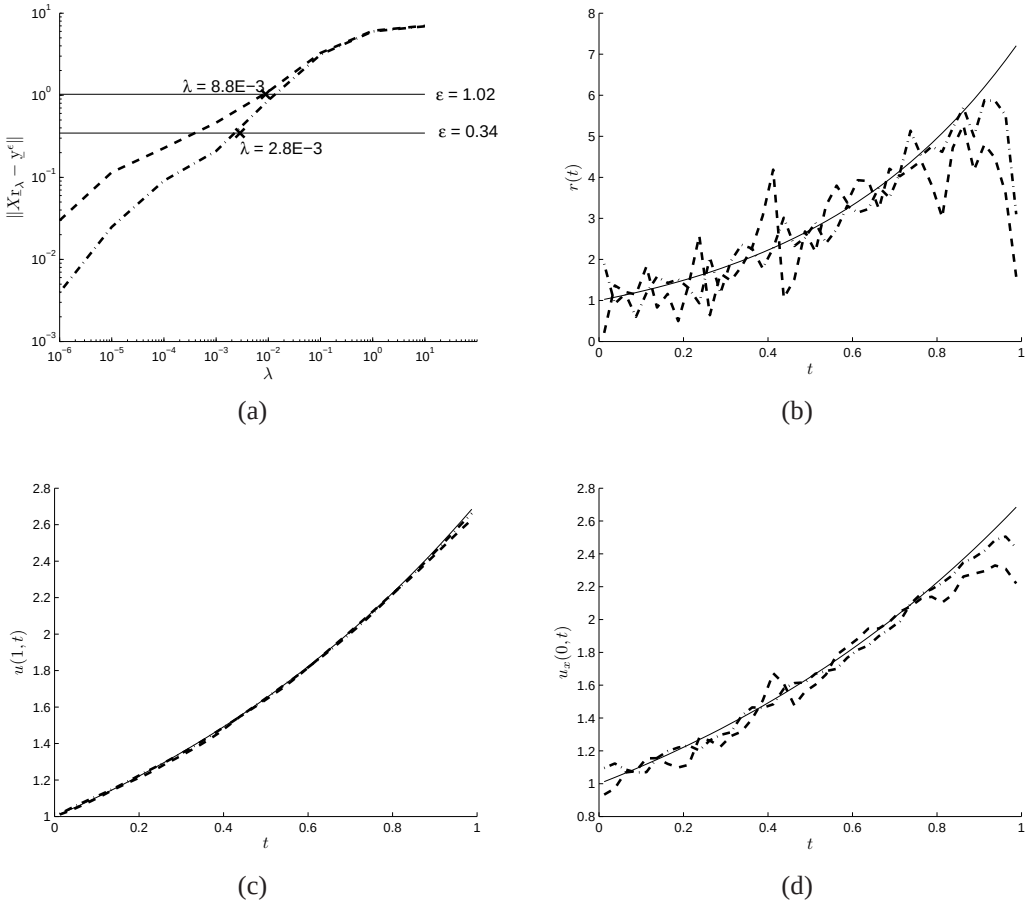

(a) (b)

(c) (d)

Figure 2.9: (a) The discrepancy principle curve, and the analytical (——) and numerical results of (b) $r(t)$, (c) $u(1,t)$, and (d) $u_x(0,t)$ obtained using the zeroth-order Tikhonov regularisation for $p = 1\%$ $(- \cdot -)$ and $p = 3\%$ $(- - -)$ noise with the regularisation parameters λ_{dis} given in Table 2.3, for Example 1 Case 2.

Table 2.3: The RMSE for the zeroth- and first-order Tikhonov regularisation for $p \in \{0, 1, 3\}\%$ noise, for Example 1 Case 2.

Regularisation	$p(\%)$	parameter λ_{dis}	RMSE		
			$r(t)$	$u(1,t)$	$u_x(0,t)$
-	0	0	7.15E-3	4.33E-5	4.33E-5
-	1	0	3.29	5.94E-3	5.31E-2
zeroth-order	1	2.8E-3	0.785	7.63E-3	5.83E-2
	3	8.8E-3	1.331	1.66E-2	1.24E-1
first-order	1	3.0E-1	3.23E-1	3.29E-3	2.95E-2
	3	9.4E-1	5.53E-1	8.58E-3	5.81E-2

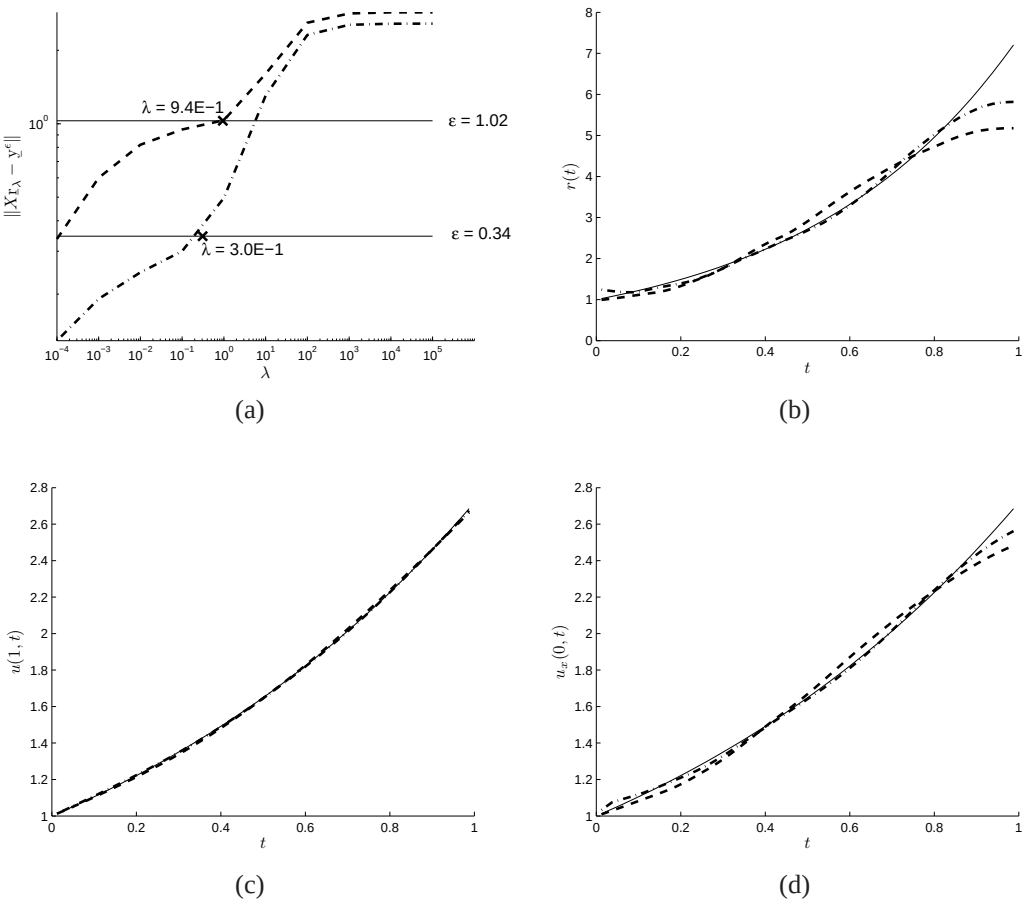

Figure 2.10: (a) The discrepancy principle curve, and the analytical (——) and numerical results of (b) $r(t)$, (c) $u(1,t)$, and (d) $u_x(0,t)$ obtained using the first-order Tikhonov regularisation for $p = 1\%$ $(- \cdot -)$ and $p = 3\%$ $(- - -)$ noise with the regularisation parameters λ_{dis} given in Table 2.3, for Example 1 Case 2.

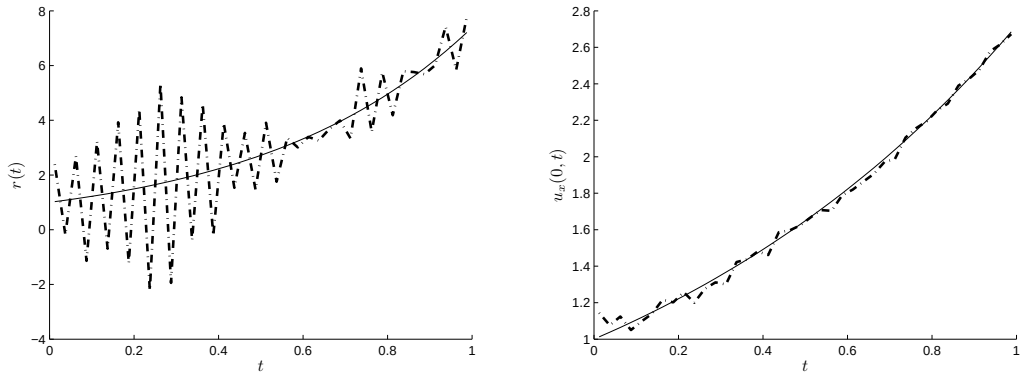

(a) (b)

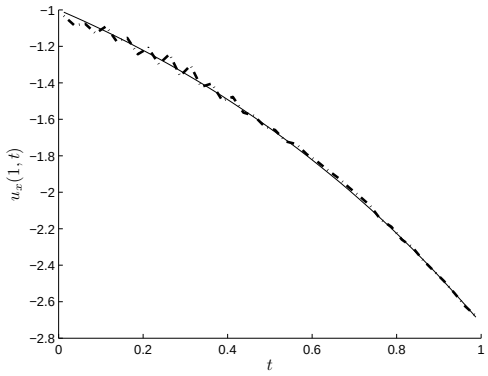

(c)

Figure 2.11: The analytical (——) and numerical ($-\cdot-$) results of (a) $r(t)$, (b) $u_x(0,t)$, and (c) $u_x(1,t)$ for $p = 1\%$ noisy data and $\lambda = 0$, for Example 1 Case 3.

2.6 for Case 5, whilst for Case 6 the corresponding results are presented in Figures 2.22, 2.23 and Table 2.7. Furthermore, for Case 6, which is the most ill-conditioned case, we have increased the percentage of noise to $p = 5\%$ in order to show that the Tikhonov regularisation method combined with the BEM can satisfactorily deal in a stable and accurate manner with higher measurement errors. We finally report that, although not illustrated, we have also implemented the second-order Tikhonov regularisation and similar results, in terms of accuracy and stability, to those given by first-order regularisation have been obtained.

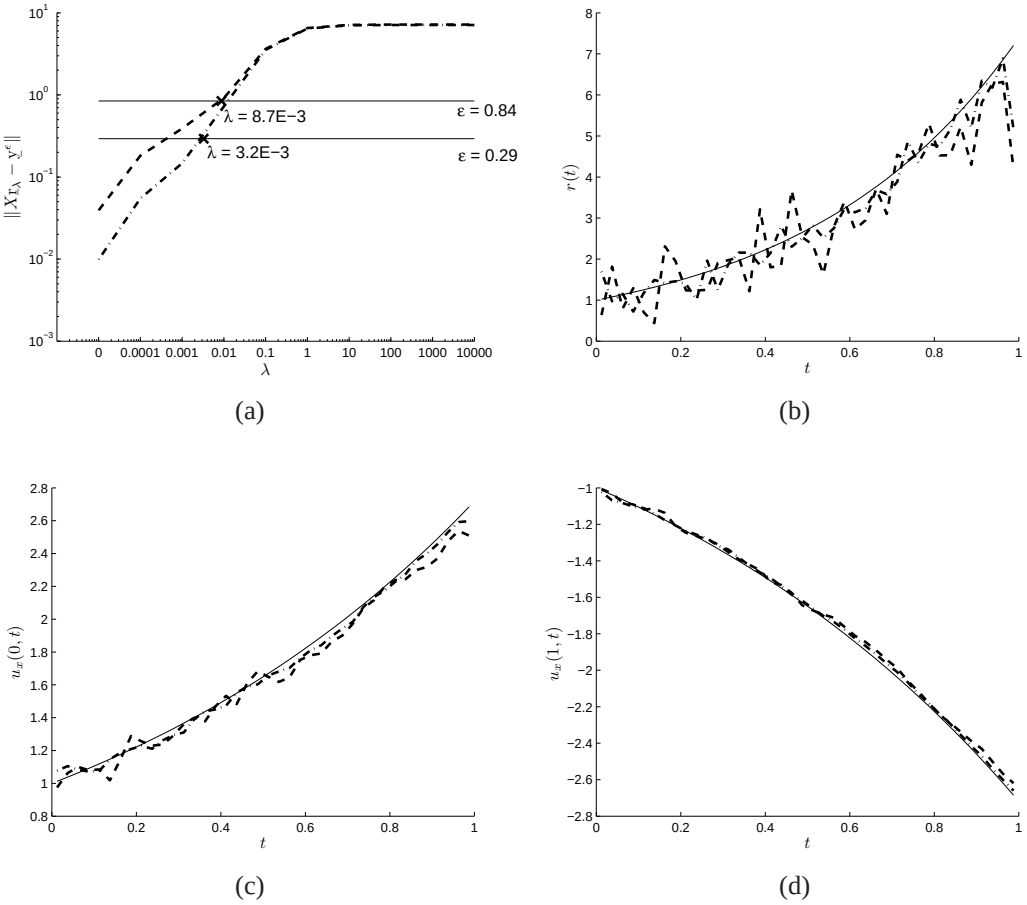

Figure 2.12: (a) The discrepancy principle curve, and the analytical (——) and numerical results of (b) $r(t)$, (c) $u_x(0,t)$, and (d) $u_x(1,t)$ obtained using the zeroth-order Tikhonov regularisation for $p = 1\%$ $(- \cdot -)$ and $p = 3\%$ $(- - -)$ noise with the regularisation parameters λ_{dis} given in Table 2.4, for Example 1 Case 3.

2.4.2 Example 2

We finally investigate specially in the most ill-posed Case 6, the retrieval of a non-smooth heat source given by

$$r(t) = \left| t - \frac{1}{2} \right| + 1, \quad 0 < t < 1 = T, \tag{2.66}$$

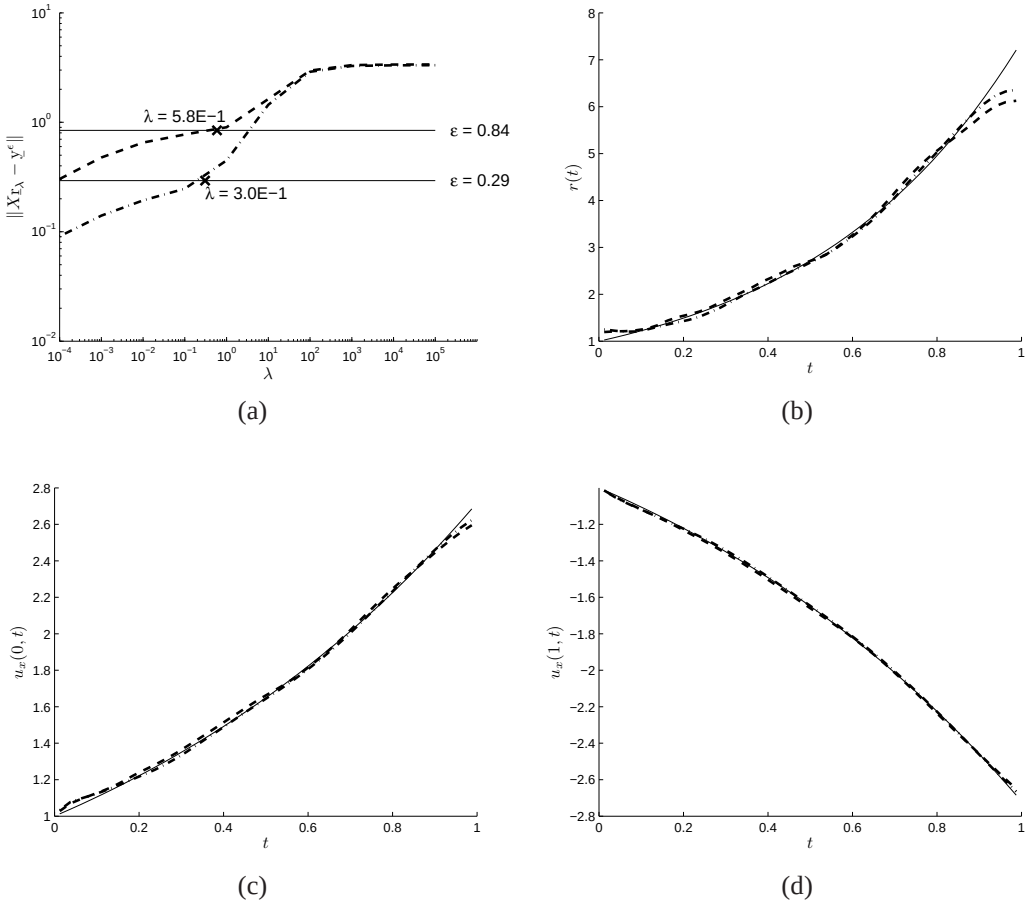

(a) (b)

(c) (d)

Figure 2.13: (a) The discrepancy principle curve, and the analytical (——) and numerical results of (b) $r(t)$, (c) $u_x(0,t)$, and (d) $u_x(1,t)$ obtained using the first-order Tikhonov regularisation for $p = 1\%$ $(- \cdot -)$ and $p = 3\%$ $(- - -)$ noise with the regularisation parameters λ_{dis} given in Table 2.4, for Example 1 Case 3.

and, for brevity, the boundary and overdetermination conditions as given by (2.61), (2.62) and the input data as follows:

$$\begin{cases} u(x,0) = u_0(x) = 1 + x - x^2, \;\; f(x,t) = (1-x^2)e^{-t}, \\ h(x,t) = (3 + x - x^2)e^t - (1-x^2)\left(\left|t - \dfrac{1}{2}\right| + 1\right)e^{-t}, \end{cases} \tag{2.67}$$

which are generated from the analytical temperature solution

$$u(x,t) = (1 + x - x^2)e^t. \tag{2.68}$$

Table 2.4: The RMSE for the zeroth- and first-order Tikhonov regularisation for $p \in \{0, 1, 3\}\%$ noise, for Example 1 Case 3.

Regularisation	$p(\%)$	parameter λ_{dis}	RMSE		
			$r(t)$	$u_x(0,t)$	$u_x(1,t)$
-	0	0	3.29E-3	4.04E-5	1.49E-4
-	1	0	1.776	3.58E-2	2.41E-2
zeroth-order	1	3.2E-3	4.42E-1	3.65E-2	1.74E-2
	3	8.7E-3	7.80E-1	6.81E-2	3.09E-2
first-order	1	3.0E-1	1.78E-1	1.72E-2	7.58E-3
	3	5.8E-1	2.47E-1	2.41E-2	1.07E-2

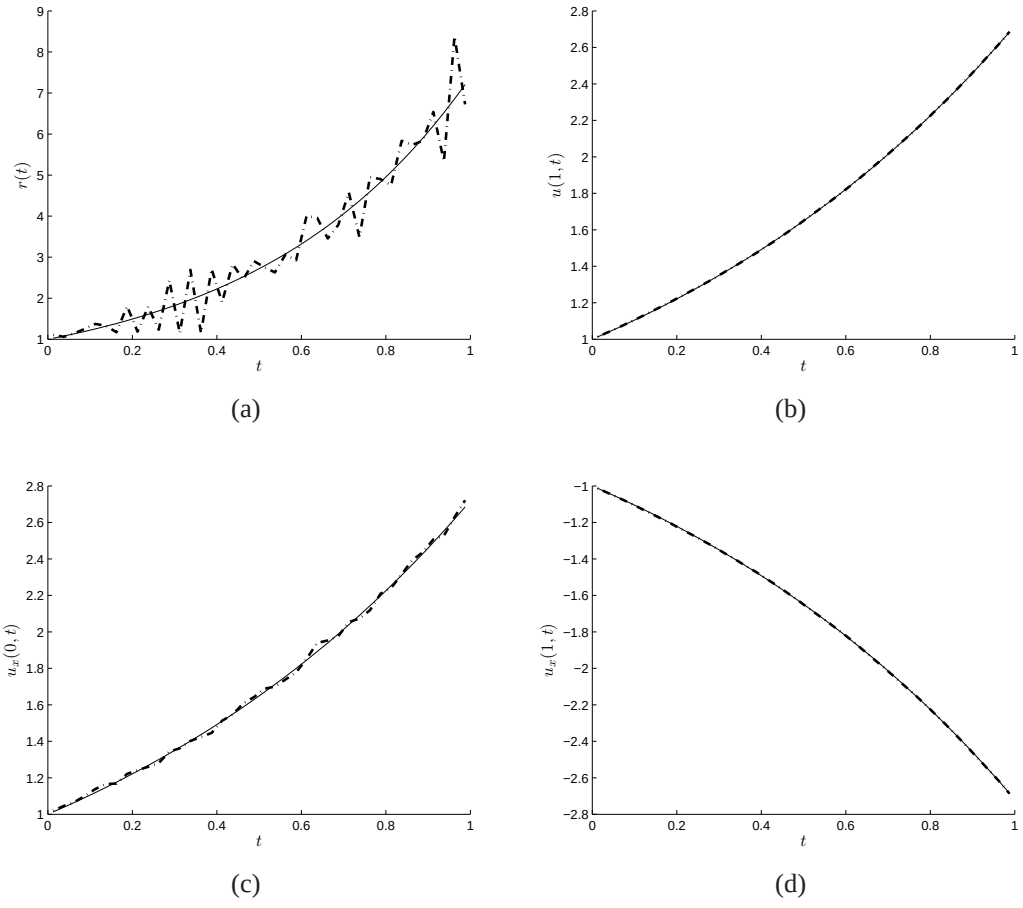

(a) (b)

(c) (d)

Figure 2.14: The analytical (——) and numerical ($- \cdot -$) results of (a) $r(t)$, (b) $u(1,t)$, (c) $u_x(0,t)$, and $u_x(1,t)$ for $p = 1\%$ noisy data and $\lambda = 0$, for Example 1 Case 4.

Numerical results are presented for $N = N_0 = 80$. Also, results are illustrated for the first-order Tikhonov regularisation only, as for the zeroth-order regularisation the re-

Table 2.5: The RMSE for the zeroth- and first-order Tikhonov regularisation for $p \in \{0, 1, 3\}\%$ noise, for Example 1 Case 4.

Regularisation	$p(\%)$	parameter λ_{dis}	RMSE			
			$r(t)$	$u(1,t)$	$u_x(0,t)$	$u_x(1,t)$
-	0	0	4.13E-3	3.63E-5	3.19E-5	5.77E-5
-	1	0	4.98E-1	9.11E-4	1.71E-2	1.33E-3
zeroth-order	1	6.2E-4	4.35E-1	1.52E-3	1.89E-2	2.70E-3
	3	2.0E-3	7.31E-1	4.55E-3	4.95E-2	8.24E-3
first-order	1	4.8E-2	1.23E-1	9.29E-4	9.61E-3	1.38E-3
	3	1.3E-1	1.77E-1	2.16E-3	1.72E-2	3.15E-3

Table 2.6: The RMSE for the zeroth- and first-order Tikhonov regularisation for $p \in \{0, 1, 3\}\%$ noise, for Example 1 Case 5.

Regularisation	$p(\%)$	parameter λ_{dis}	RMSE			
			$r(t)$	$u(0,t)$	$u(1,t)$	$u_x(1,t)$
-	0	0	5.598	3.35E-3	1.72E-3	6.76E-4
-	1	0	2.9E+3	1.776	9.09E-1	3.56E-1
zeroth-order	1	2.2E-3	1.584	3.92E-2	1.60E-2	7.79E-3
	3	9.5E-3	2.033	9.38E-2	4.73E-2	2.53E-2
first-order	1	1.7E-1	0.673	2.29E-2	1.02E-2	4.93E-3
	3	3.4	1.334	7.52E-2	3.92E-2	2.00E-2

Table 2.7: The RMSE for the zeroth- and first-order Tikhonov regularisation for $p \in \{0, 1, 3, 5\}\%$ noise, for Example 1 Case 6.

Regularisation	$p(\%)$	parameter λ_{dis}	RMSE				
			$r(t)$	$u(0,t)$	$u(1,t)$	$u_x(0,t)$	$u_x(1,t)$
-	0	0	1.49E+2	2.58E-2	6.08E-2	4.66E-2	1.09E-1
-	1	0	6.78E+4	1.17E+1	2.77E+1	2.13E+1	4.98E+1
zeroth-order	1	1.8E-4	1.380	1.96E-2	9.67E-3	4.59E-2	1.68E-2
	3	6.3E-4	1.559	4.03E-2	2.61E-2	8.14E-2	4.28E-2
	5	8.8E-4	1.737	4.07E-2	2.23E-2	8.51E-2	3.78E-2
first-order	1	2.4E-2	5.90E-1	1.19E-2	6.82E-3	2.59E-2	1.10E-2
	3	8.4E-2	5.36E-1	1.71E-2	1.12E-2	2.81E-2	1.52E-2
	5	9.5E-2	5.04E-1	1.80E-2	1.36E-2	3.49E-2	2.31E-2

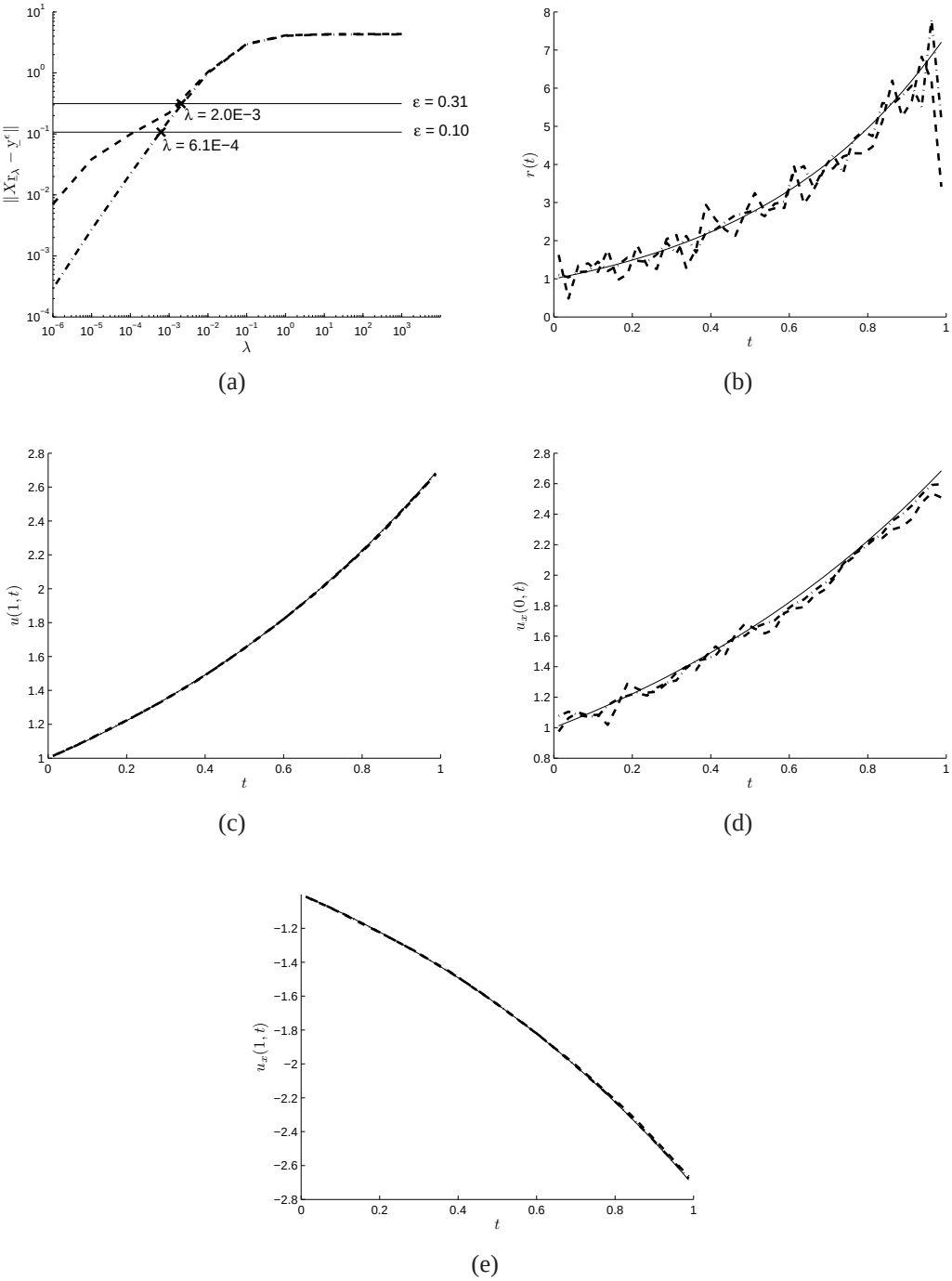

Figure 2.15: (a) The discrepancy principle curve, and the analytical (——) and numerical results of (b) $r(t)$, (c) $u(1,t)$, (d) $u_x(0,t)$, and (e) $u_x(1,t)$ obtained using the zeroth-order Tikhonov regularisation for $p = 1\%$ $(- \cdot -)$ and $p = 3\%$ $(- - -)$ noise with the regularisation parameters λ_{dis} given in Table 2.5, for Example 1 Case 4.

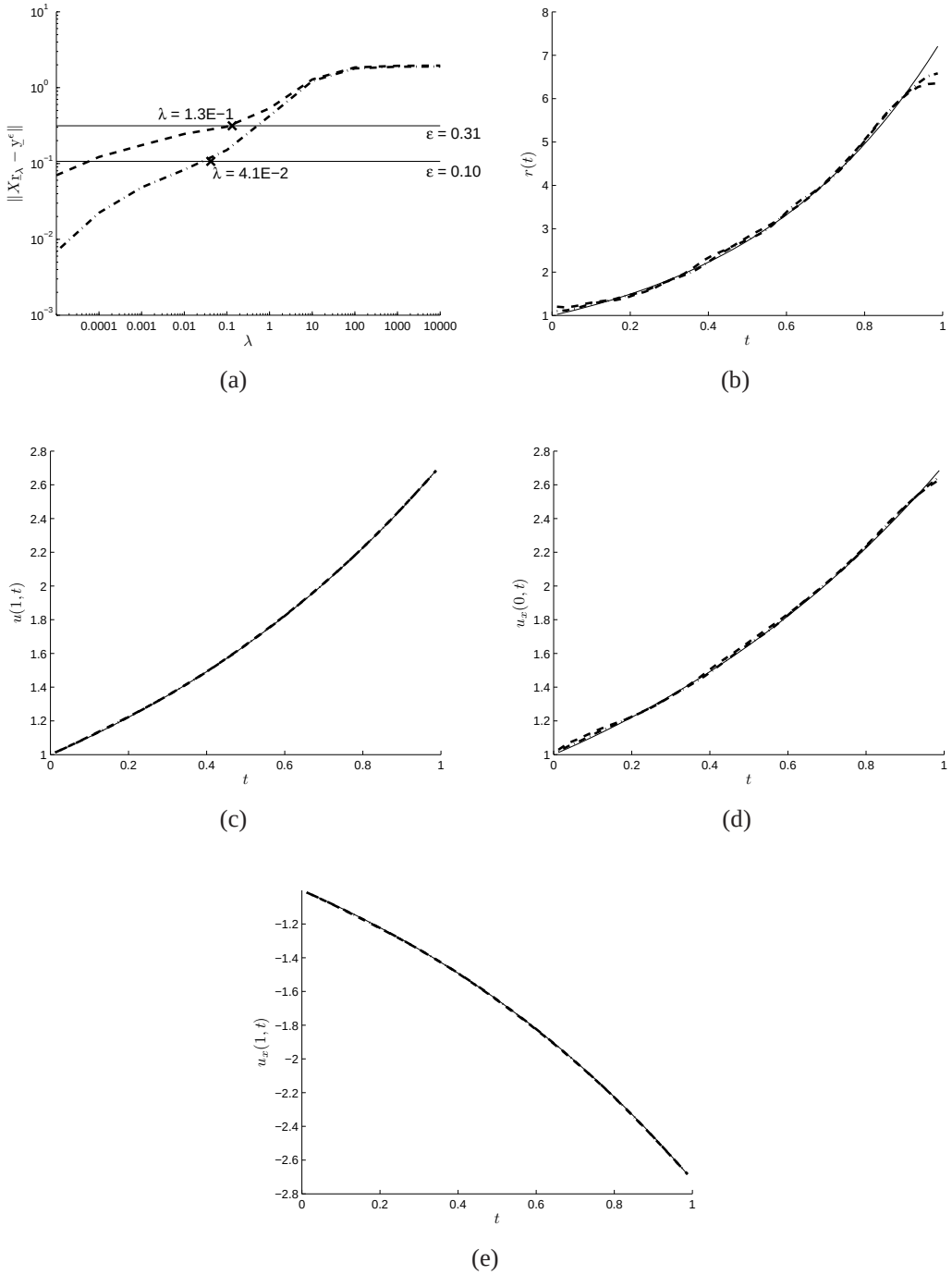

(a) (b) (c) (d) (e)

Figure 2.16: (a) The discrepancy principle curve, and the analytical (——) and numerical results of (b) $r(t)$, (c) $u(1,t)$, (d) $u_x(0,t)$, and (e) $u_x(1,t)$ obtained using the first-order Tikhonov regularisation for $p = 1\%$ $(- \cdot -)$ and $p = 3\%$ $(- - -)$ noise with the regularisation parameters λ_{dis} given in Table 2.5, for Example 1 Case 4.

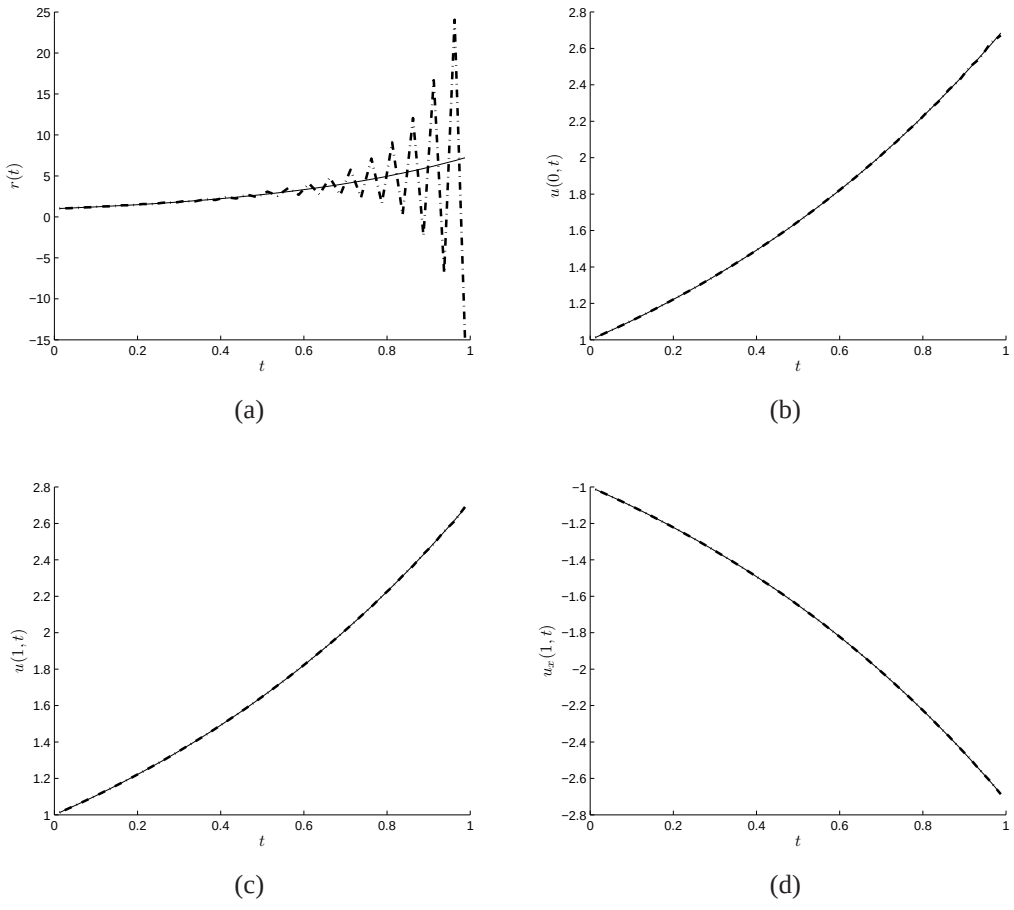

(a) (b)

(c) (d)

Figure 2.17: The analytical (——) and numerical ($- \cdot -$) results of (a) $r(t)$, (b) $u(0,t)$, (c) $u(1,t)$ and (d) $u_x(1,t)$ for exact data and $\lambda = 0$, for Example 1 Case 5.

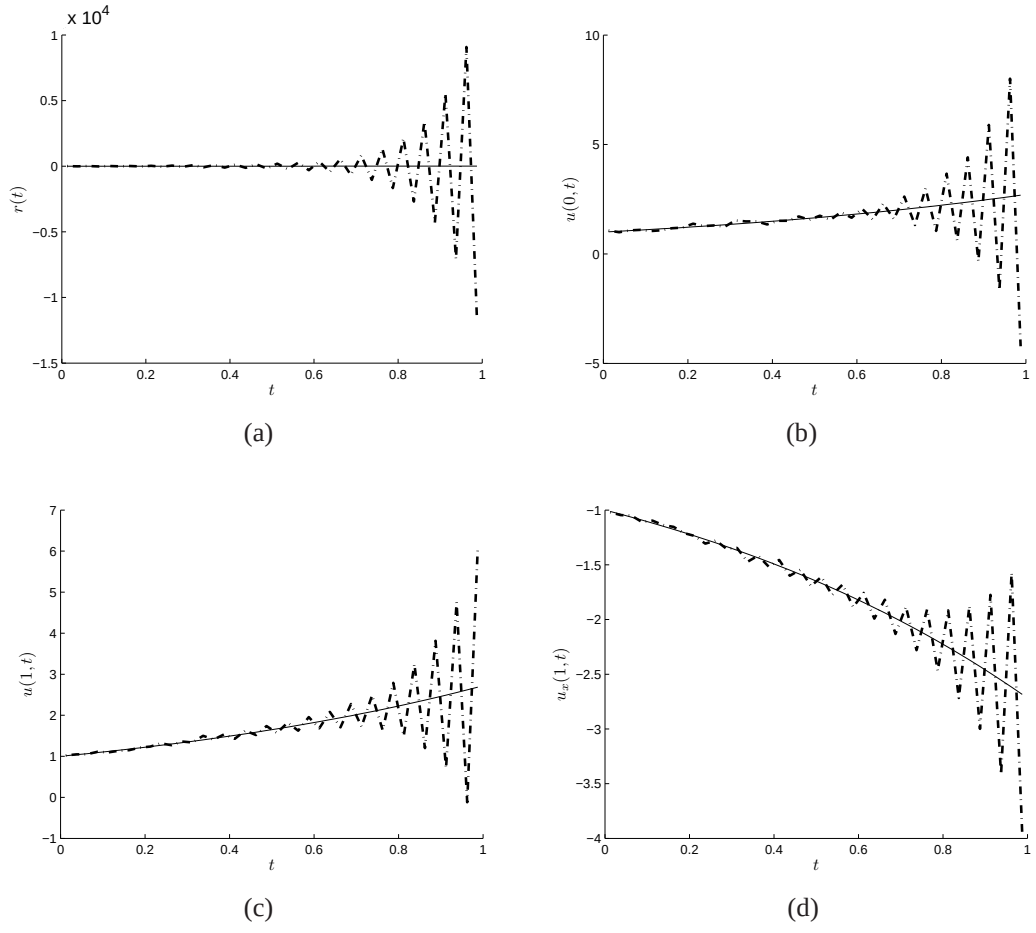

(a) (b)

(c) (d)

Figure 2.18: The analytical (——) and numerical ($- \cdot -$) results of (a) $r(t)$, (b) $u(0,t)$, (c) $u(1,t)$ and (d) $u_x(1,t)$ for $p = 1\%$ noisy data and $\lambda = 0$, for Example 1 Case 5.

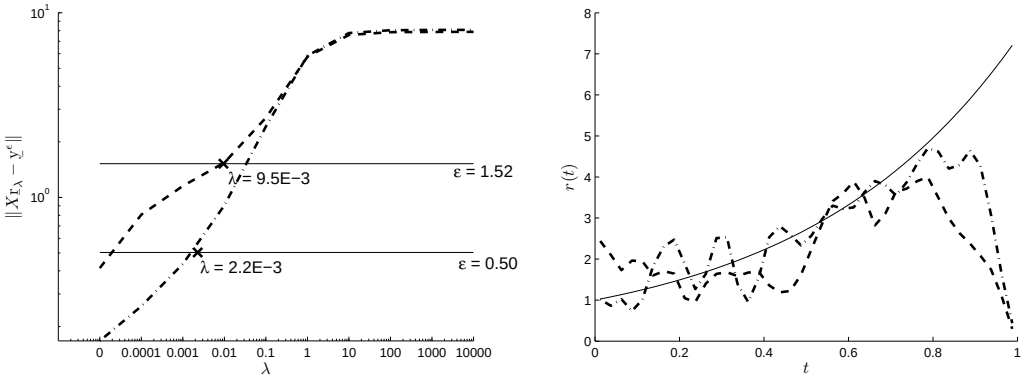

(a) (b)

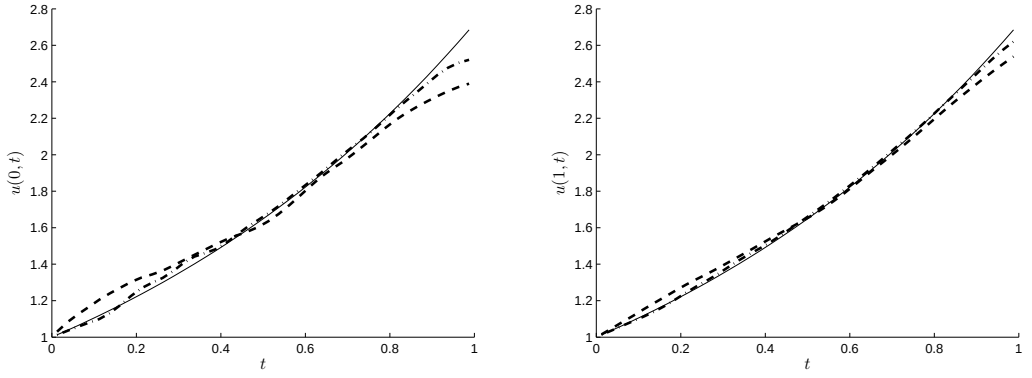

(c) (d)

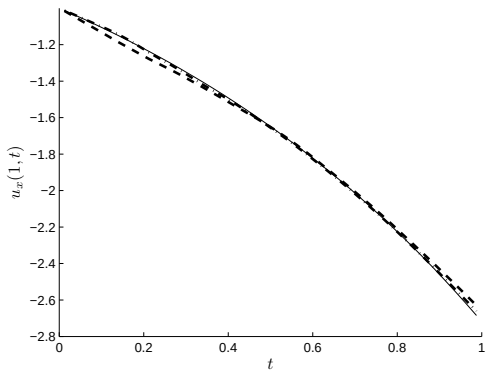

(e)

Figure 2.19: (a) The discrepancy principle curve, and the analytical (——) and numerical results of (b) $r(t)$, (c) $u(0,t)$, (d) $u(1,t)$, and (e) $u_x(1,t)$ obtained using the zeroth-order Tikhonov regularisation for $p = 1\%$ $(- \cdot -)$ and $p = 3\%$ $(- - -)$ noise with the regularisation parameters λ_{dis} given in Table 2.6, for Example 1 Case 5.

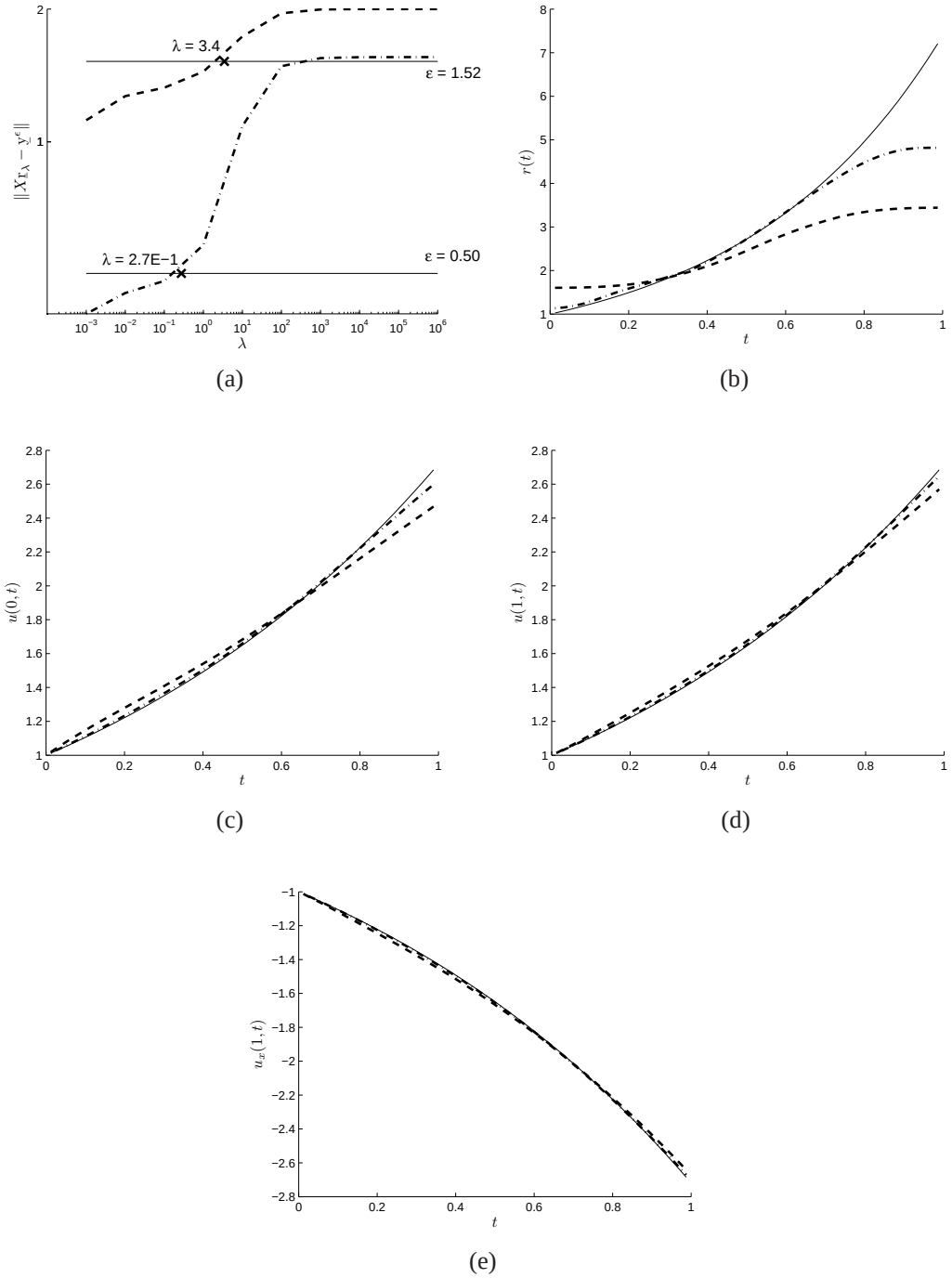

Figure 2.20: (a) The discrepancy principle curve, and the analytical (——) and numerical results of (b) $r(t)$, (c) $u(0,t)$, (d) $u(1,t)$, and (e) $u_x(1,t)$ obtained using the first-order Tikhonov regularisation for $p = 1\%$ $(- \cdot -)$ and $p = 3\%$ $(- - -)$ noise with the regularisation parameters λ_{dis} given in Table 2.6, for Example 1 Case 5.

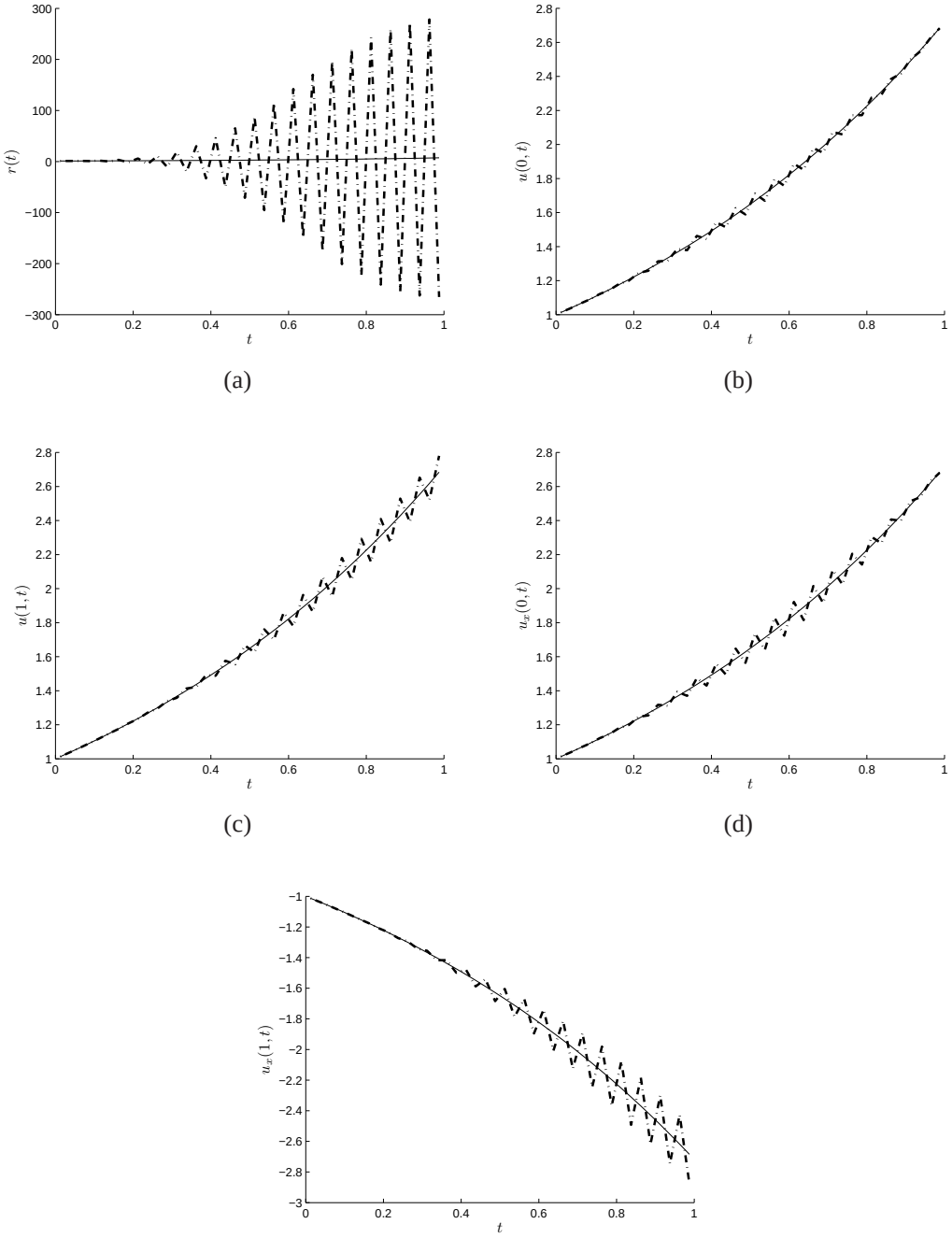

(a) (b) (c) (d) (e)

Figure 2.21: The analytical (——) and numerical ($- \cdot -$) results of (a) $r(t)$, (b) $u(0,t)$, (c) $u(1,t)$, (d) $u_x(0,t)$, and (e) $u_x(1,t)$ for exact data and $\lambda = 0$, for Example 1 Case 6.

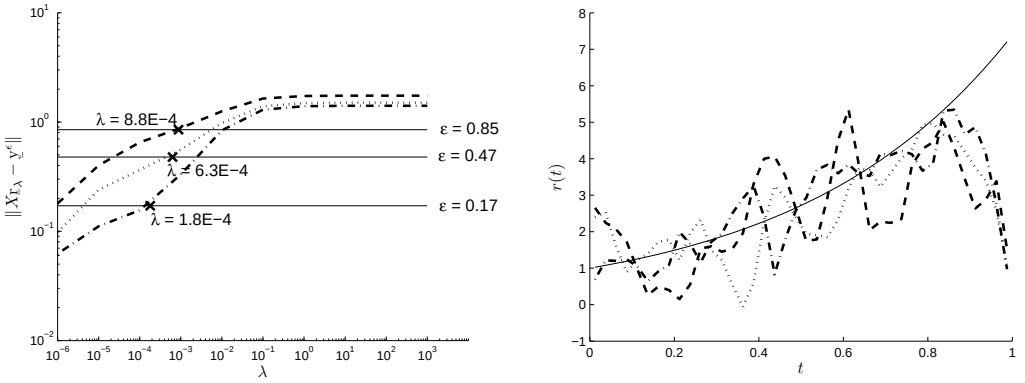

(a)

(b)

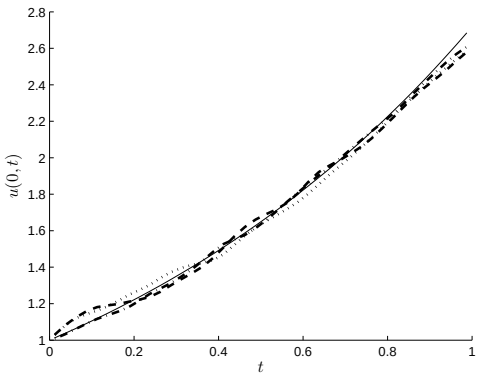

(c)

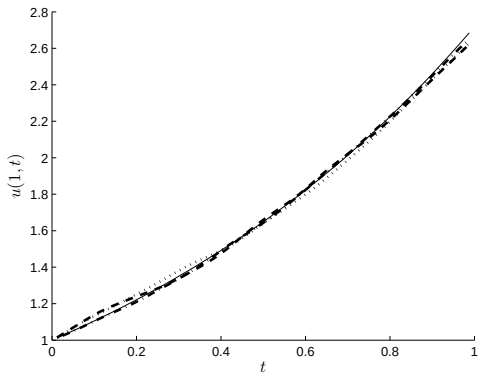

(d)

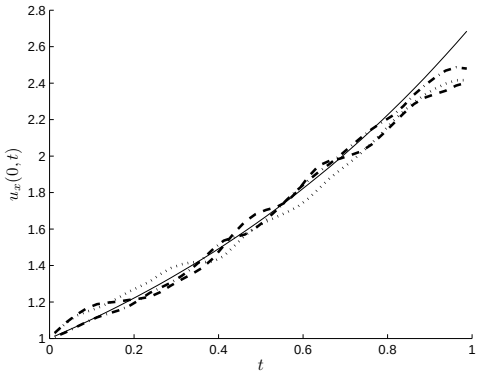

(e)

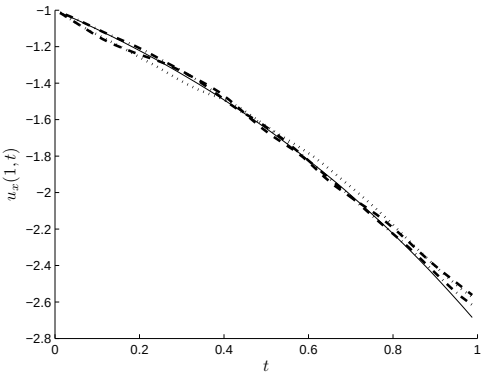

(f)

Figure 2.22: (a) The discrepancy principle curve, and the analytical (——) and numerical results of (b) $r(t)$, (c) $u(0,t)$, (d) $u(1,t)$, (e)$u_x(0,t)$, and (f) $u_x(1,t)$ obtained using the zeroth-order Tikhonov regularisation for $p \in \{1(-\cdot-),\ 3(\cdots),\ 5(---)\}\%$ noise with the regularisation parameters λ_{dis} given in Table 2.7, for Example 1 Case 6.

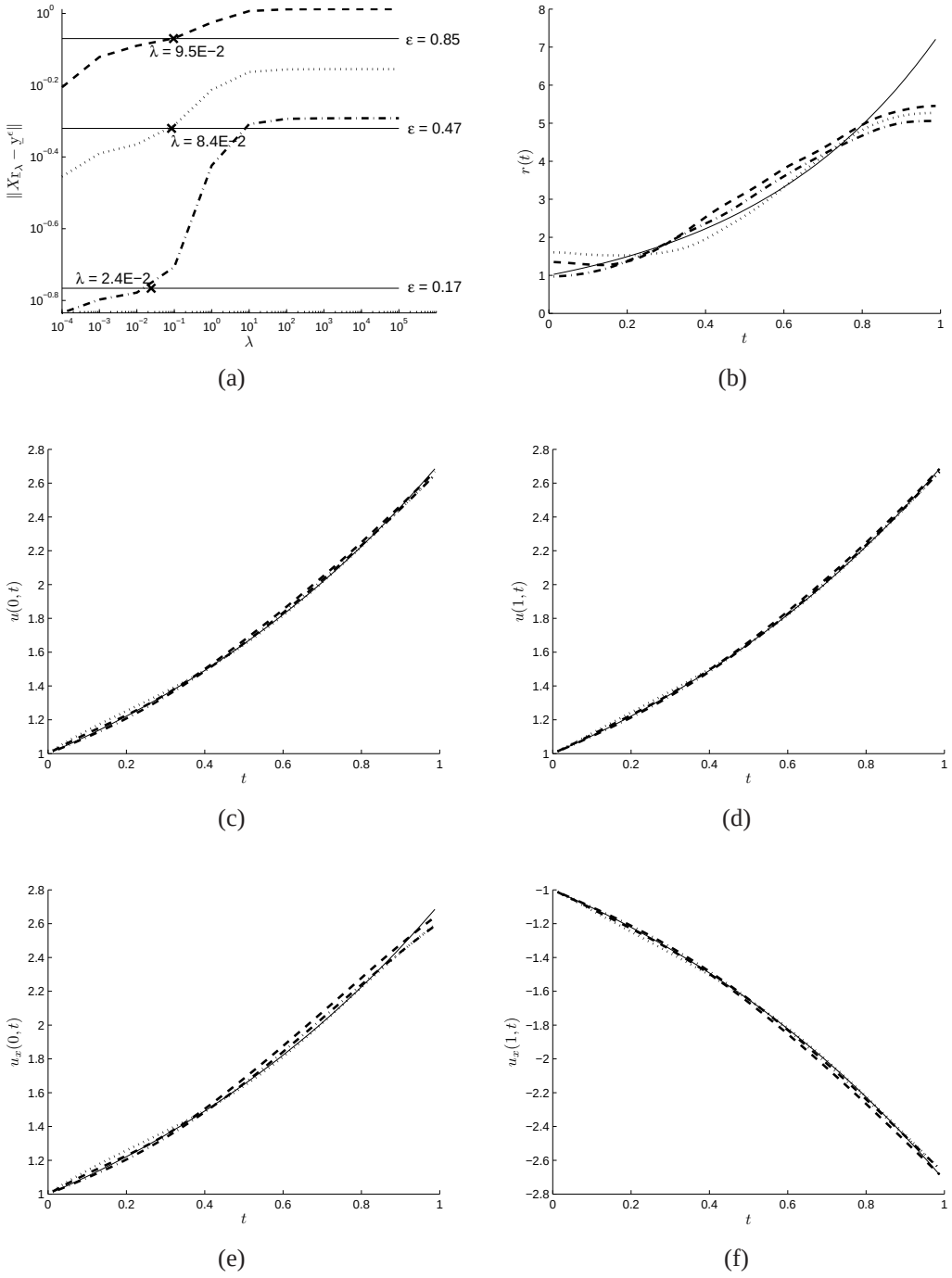

(a) (b)

(c) (d)

(e) (f)

Figure 2.23: (a) The discrepancy principle curve, and the analytical (——) and numerical results of (b) $r(t)$, (c) $u(0,t)$, (d) $u(1,t)$, (e)$u_x(0,t)$, and (f) $u_x(1,t)$ obtained using the first-order Tikhonov regularisation for $p \in \{1(- \cdot -),\ 3(\cdots),\ 5(- - -)\}\%$ noise with the regularisation parameters λ_{dis} given in Table 2.7, for Example 1 Case 6.

sults obtained were oscillatory as in Figure 2.22(b). Figure 2.24 shows the numerical results obtained for various amounts of noise $p \in \{0, 0.1, 0.5, 1\}\%$ for the regularisation parameters λ_{dis} given in Table 2.8. From this figure it can be seen that the regularised BEM can invert accurately up to about 0.1% noisy data. For higher levels of noise the reconstruction of the non-smooth heat source (2.66) starts to deteriorate.

Table 2.8: The RMSE for the first-order Tikhonov regularisation for $p \in \{0, 0.1, 0.5, 1\}\%$ noise, for Example 2.

$p(\%)$	parameter λ	RMSE				
		$r(t)$	$u(0,t)$	$u(1,t)$	$u_x(0,t)$	$u_x(1,t)$
0	λ=1.0E-5	1.63E-3	1.40E-5	9.88E-6	1.77E-5	1.54E-5
0.1	λ_{dis}=2.7E-2	2.60E-2	1.11E-3	7.93E-4	1.48E-3	1.02E-3
0.5	λ_{dis}=3.1E-1	1.02E-1	4.51E-3	3.11E-3	6.84E-3	4.21E-3
1	λ_{dis}=1.1	1.28E-1	8.10E-3	5.84E-3	1.09E-2	7.61E-3

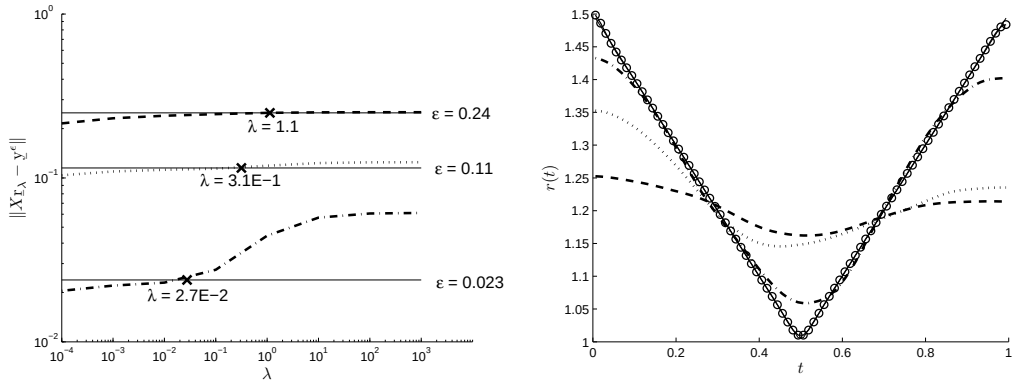

(a) (b)

Figure 2.24: (a) The discrepancy principle curve, and the analytical (——) and numerical results of (b) $r(t)$ obtained using the first-order Tikhonov regularisation for $p \in \{0(\circ\circ\circ),\ 0.1(-\cdot-),\ 0.5(\cdots),\ 1(---)\}\%$ noise with the regularisation parameters λ_{dis} given in Table 2.8, for Example 2.

2.5 Conclusions

In this chapter, inverse problems with nonlocal boundary conditions have been investigated in order to find the time-dependent heat source and the temperature entering

equation (2.1). Three general boundary and overdetermination conditions (2.3) have been expanded into 6 separate Cases 1–6 generating six inverse problems to solve in the context of inverse time-dependent source identification. It was found, see Table 2.1, that most ill-posed problems are given by Cases 6 and 5 followed by Case 1. It turns out that Cases 2–4 are less ill-posed compared to the previous ones. This is consistently reflected in the accuracy and stability of the numerical results obtained with no regularisation for both exact and noisy data. Regularisation was found essential in all cases investigated, with the first-order regularisation performing better than the zeroth-order one.

As we have studied in this chapter, the nonlocal boundary and overdetermination conditions are considered in general boundary condition form. In the next chapter, the nonlocal boundary condition will be considered together with an integral overdetermination to find the time-dependent heat source.

Chapter 3

Determination of a Time-dependent Heat Source from Nonlocal Boundary and Integral Conditions

3.1 Introduction

In many of studies of solving inverse source problems for the heat equation, see e.g. [15, 17, 29, 61, 63, 66–68], the overdetermination conditions were selected among classical boundary conditions and similar conditions given at interior points located inside the body under investigation. More general, nonlocal and integral overdetermination conditions have also been considered, see the monographs [25] and [43].

In the previous chapter, we have investigated the retrieval of the time-dependent heat source $r(t)$ and the temperature $u(x,t)$ in the heat equation (2.1) with the three general boundary and overdetermination conditions (2.3). In this chapter, the investigation of finding the time-dependent heat source and the temperature for the heat equation is still of our interest, but an integral condition is considered as overdetermination condition.

This chapter is organised as follows. In Section 3.2, the mathematical inverse for-

mulation is described and the numerical discretisation of the problem using the BEM is presented in Section 3.3. The TSVD and the Tikhonov regularisation are described in Section 3.4, as procedures for overcoming the instability of the solution. Finally, Sections 3.5 and 3.6 discuss the numerical results and highlight the conclusions of this chapter.

3.2 Mathematical formulation

Consider the problem of finding the time-dependent heat source $r(t) \in C([0,T])$ and the temperature $u(x,t) \in C^{2,1}(D_T) \cap C^{1,0}(\overline{D}_T)$ which satisfy the heat conduction equation

$$u_t = u_{xx} + r(t)f(x,t), \quad (x,t) \in D_T, \tag{3.1}$$

where $L = 1$ in the definition of D_T in (1.1), subject to the initial condition (1.7), namely

$$u(x,0) = u_0(x), \quad x \in [0,1], \tag{3.2}$$

the boundary conditions

$$u(0,t) = u(1,t), \quad u_x(0,t) + \alpha u(0,t) = 0, \quad t \in [0,T], \tag{3.3}$$

and the energy/mass specification

$$\int_0^1 u(x,t)dx = E(t), \quad t \in [0,T], \tag{3.4}$$

where $\alpha \neq 0$ is a given constant and f, u_0, E are given functions. The first periodicity condition in (3.3) is nonlocal, whilst (3.4) specifies an integral specification of the energy of the thermal system. The nature of the boundary conditions (3.3) in mathematical biology is demonstrated in [41], whilst the prescription of the energy, or mass, (3.4), is encountered in heat transfer applications, [10, 22].

The unique solvability of the inverse problem (3.1)–(3.4) has been established in

[18], as given by the following theorem.

Theorem 3.2.1 *Let the following conditions be satisfied:*

(A_1) $u_0(x) \in C^2[0,1];\ u_0(0) = u_0(1),\ u_0'(0) + \alpha u_0(0) = 0$*;*

(A_2) $E(t) \in C^1[0,T];\ E(0) = \int_0^1 u_0(x)dx$*;*

(A_3) $f(x,t) \in C(\overline{D}_T);\ f(\cdot,t) \in C^2[0,1],\ \forall t \in [0,T];\ f(0,t) = f(1,t)$*,*
$f_x(0,t) + \alpha f(0,t) = 0$; *and* $\int_0^1 f(x,t)dx \neq 0,\ \forall t \in [0,T]$*.*

Then the inverse problem (3.1)–(3.4) *has a unique solution* $(r(t), u(x,t)) \in C[0,T] \times (C^{2,1}(D_T) \cap C^{1,0}(\overline{D}_T))$.

Although the inverse problem (3.1)–(3.4) is uniquely solvable, it is still ill-posed. In the next section we will demonstrate how the BEM discretising numerically, the heat equation (3.1) can be used together with the regularisation, to be described in Section 3.4 either the TSVD or the Tikhonov regularisation, in order to obtain stable solutions.

3.3 The boundary element method (BEM)

In this section, we use the BEM to discretise the heat equation (3.1). As introduced in Section 1.3, the use of BEM results in the boundary integral equation

$$\begin{aligned}\eta(x)u(x,t) = &\int_0^t \left[G(x,t,\xi,\tau)\frac{\partial u}{\partial n(\xi)}(\xi,\tau) - u(\xi,\tau)\frac{\partial G}{\partial n(\xi)}(x,t,\xi,\tau)\right]_{\xi\in\{0,1\}} d\tau \\ &+ \int_0^1 G(x,t,y,0)u(y,0)\,dy + \int_0^1\int_0^t G(x,t,y,\tau)r(\tau)f(y,\tau)\,d\tau dy, \\ &(x,t) \in [0,1] \times (0,T]. \end{aligned} \tag{3.5}$$

Using the same discretisation as described in Section 2.3, we obtain

$$\eta(x)u(x,t) = \sum_{j=1}^{N} [A_{0j}(x,t)q_{0j} + A_{Lj}(x,t)q_{Lj} - B_{0j}(x,t)h_{0j} - B_{Lj}(x,t)h_{Lj}] + \sum_{k=1}^{N_0} C_k(x,t)u_{0,k} + d(x,t), \tag{3.6}$$

where source functions $r(t)$ and $f(x,t)$ are assumed to be piecewise constant approximations as defined in (2.21). Then, the double integral term is approximated as

$$d(x,t) = \int_0^t r(\tau) \left(\int_0^1 G(x,t,y,\tau) f(y,\tau)\, dy \right) d\tau = \sum_{j=1}^{N} D_j(x,t) r_j,$$

where

$$D_j(x,t) = \int_{t_{j-1}}^{t_j} \int_0^1 G(x,t,y,\tau) f(y,\tilde{t}_j) dy d\tau = \int_0^1 f(y,\tilde{t}_j) A_{yj}(x,t)\, dy,$$

is calculated using the midpoint integration rule. Here, the integral equation (3.6) can be written as

$$\eta(x)u(x,t) = \sum_{j=1}^{N} [A_{0j}(x,t)q_{0j} + A_{Lj}(x,t)q_{Lj} - B_{0j}(x,t)h_{0j} - B_{Lj}(x,t)h_{Lj}] + \sum_{k=1}^{N_0} C_k(x,t)u_{0,k} + \sum_{j=1}^{N} D_j(x,t) r_j. \tag{3.7}$$

By applying (3.7) at the boundary nodes $(0,\tilde{t}_i)$ and $(1,\tilde{t}_i)$ for $i = \overline{1,N}$, we obtain the system of $2N$ equations

$$A\mathfrak{q} - B\mathfrak{h} + C\mathfrak{u}_0 + D\mathfrak{r} = \mathfrak{0}, \tag{3.8}$$

where all matrices and vectors are defined the same as in (2.25). From the boundary conditions (3.3), we can express the boundary temperature $\mathtt{h}$ as

$$\mathtt{h} = \begin{bmatrix} h_{0j} \\ h_{Lj} \end{bmatrix} = \begin{bmatrix} u(0,\tilde{t}_j) \\ u(1,\tilde{t}_j) \end{bmatrix} = \begin{bmatrix} -\frac{1}{\alpha}u_x(0,\tilde{t}_j) \\ u(0,\tilde{t}_j) \end{bmatrix} = \begin{bmatrix} -\frac{1}{\alpha}u_x(0,\tilde{t}_j) \\ -\frac{1}{\alpha}u_x(0,\tilde{t}_j) \end{bmatrix} = \frac{1}{\alpha}\begin{bmatrix} q_{0j} \\ q_{0j} \end{bmatrix}.$$

Then, the system of equations (3.8) can be rewritten as

$$\left(A - \frac{1}{\alpha}(B + B^*)\right)\mathtt{q} + C\mathtt{u}_0 + D\mathtt{r} = \mathtt{0}, \tag{3.9}$$

where $B^* = \begin{bmatrix} B_{Lj}(0,\tilde{t}_i) & -B_{Lj}(0,\tilde{t}_i) \\ B_{Lj}(1,\tilde{t}_i) + \frac{1}{2}\delta_{ij} & -B_{Lj}(1,\tilde{t}_i) - \frac{1}{2}\delta_{ij} \end{bmatrix}_{2N\times 2N}$. Then, we can express the flux $\mathtt{q}$ as

$$\mathtt{q} = -\left(A - \frac{1}{\alpha}(B + B^*)\right)^{-1}(C\mathtt{u}_0 + D\mathtt{r}). \tag{3.10}$$

We now discretise the integral expression in (3.4), via the midpoint numerical integral approximation, as

$$\int_0^1 u(x,t)\,dx = \frac{1}{N_0}\sum_{k=1}^{N_0} u(\tilde{x}_k, t).$$

Applying this at $t = \tilde{t}_i$ for $i = \overline{1,N}$, we obtain

$$\frac{1}{N_0}\sum_{k=1}^{N_0} u(\tilde{x}_k,\tilde{t}_i) = \int_0^1 u(x,\tilde{t}_i)\,dx = E(\tilde{t}_i) =: e_i \quad \text{for } i = \overline{1,N}. \tag{3.11}$$

Using the integral equation (3.5), as before, equation (3.11) results in the system of N equations

$$\frac{1}{N_0}\sum_{k=1}^{N_0}\left[\left(A_k^{(1)} - \frac{1}{\alpha}(B_k^{(1)} + B_k^{(1)^*})\right)\mathtt{q} + C_k^{(1)}\mathtt{u}_0 + D_k^{(1)}\mathtt{r}\right] = \mathtt{E}, \tag{3.12}$$

where

$$A_k^{(1)} = \left[A_{0j}(\tilde{x}_k, \tilde{t}_i) \quad A_{Lj}(\tilde{x}_k, \tilde{t}_i)\right]_{N\times 2N}, \quad B_k^{(1)} = \left[B_{0j}(\tilde{x}_k, \tilde{t}_i) \quad B_{Lj}(\tilde{x}_k, \tilde{t}_i)\right]_{N\times 2N},$$
$$B_k^{(1)^*} = \left[B_{Lj}(\tilde{x}_k, \tilde{t}_i) \quad -B_{Lj}(\tilde{x}_k, \tilde{t}_i)\right]_{N\times 2N}, \quad C_k^{(1)} = \left[C_l(\tilde{x}_k, \tilde{t}_i)\right]_{N\times N_0},$$
$$\text{and} \quad D_k^{(1)} = \left[D_j(\tilde{x}_k, \tilde{t}_i)\right]_{N\times N}, \quad \mathrm{E} = \left[e_i\right]_N, \quad \text{for} \quad k, l = \overline{1, N_0}, \;\; i, j = \overline{1, N}.$$

Substituting the expression (3.10) into (3.12), we obtain a system of $N \times N$ linear equations as follows:

$$X\mathrm{r} = \underline{\mathrm{y}}, \tag{3.13}$$

$$\text{where} \quad X = \frac{1}{N_0}\sum_{k=1}^{N_0}\left[-\left(A_k^{(1)} - \frac{1}{\alpha}(B_k^{(1)} + B_k^{(1)^*})\right)\left(A - \frac{1}{\alpha}(B + B^*)\right)^{-1} D + D_k^{(1)}\right]$$

$$\text{and} \quad \underline{\mathrm{y}} = \mathrm{E} + \frac{1}{N_0}\sum_{k=1}^{N_0}\left[\left(A_k^{(1)} - \frac{1}{\alpha}(B_k^{(1)} + B_k^{(1)^*})\right)\left(A - \frac{1}{\alpha}(B + B^*)\right)^{-1} C - C_k^{(1)}\right]\mathrm{u}_0.$$

Since the problem is ill-posed, then the system of equations (3.13) is ill-conditioned. In the next section, we will deal with this ill-conditioning using regularisation in order to obtain a stable solution.

3.4 Regularisation

As we have mentioned before, the inverse time-dependent heat source problem (3.1)–(3.4) has a unique solution. However this inverse problem is still ill-posed since small errors into the energy measurement (3.4) result in large errors in the solution r. In order to model this, we investigate the stability of the numerical solution with respect to noise in the energy data (3.4), defined as

$$\mathrm{E}^{\epsilon} = \mathrm{E} + random('\text{Normal}', 0, \sigma, 1, N), \tag{3.14}$$

with the standard deviation computed by

$$\sigma = p \times \max_{t\in[0,T]} |E(t)|. \tag{3.15}$$

When the noise is present the right-hand side of equation (3.13) is contaminated by some noise ϵ,

$$\|\underline{\mathrm{y}}^{\epsilon} - \underline{\mathrm{y}}\| \approx \epsilon, \tag{3.16}$$

therefore we have to solve the following system of linear equations instead of (3.13):

$$X\underline{\mathrm{r}} = \underline{\mathrm{y}}^{\epsilon}, \tag{3.17}$$

then the inverse solution $\underline{\mathrm{r}} = X^{-1}\underline{\mathrm{y}}^{\epsilon}$ of (3.13) will be a poor unstable approximation to the exact solution. This instability can be overcome by employing the regularisation method, and this study, we utilise either the TSVD or the Tikhonov regularisation methods to solve the linear and ill-conditioned system of equations (3.17).

When the noise is present, we employ the TSVD procedure, as described in Section 1.6.1 by using the *[U,Σ,V]=svds(X,N_t)* command in MATLAB where the N_t is the truncated level indicated by the L-curve method or the discrepancy principle. Alternatively, the regularisation namely the Tikhonov regularisation is another way to obtain a stable solution, as described in Subsection 1.6.2, yielding the regularised solution (1.34).

3.5 Numerical examples and discussion

In this section, we present a couple of benchmark test examples to illustrate the accuracy and stability of the BEM combined with the Tikhonov regularisation technique presented in Section 3.4. In order to illustrate the accuracy of the numerical results, the RMSE defined in (2.49) is also used here.

3.5.1 Example 1

In the first example, we consider the inverse problem (3.1)–(3.4) with $T = 1$, the input data

$$\left.\begin{aligned} &u(x,0) = u_0(x) = 1 + x - x^2, \;\; f(x,t) = (3 + x - x^2)e^{-t}, \\ &\int_0^1 u(x,t)\,dx = E(t) = \frac{7e^t}{6}, \end{aligned}\right\} \tag{3.18}$$

and subject to the boundary condition (3.3) with $\alpha = -1$. Then the analytical solution of the inverse problem (3.1)–(3.4) is given by

$$u(x,t) = (1 + x - x^2)e^t, \quad r(t) = e^{2t}. \tag{3.19}$$

The normalised singular values of matrix X in equation (3.13) for $N_0 = N \in \{20, 40, 80\}$ are shown in Figure 3.1. The corresponding condition numbers of matrix X are 248, 780, and 2393 for $N_0 = N \in \{20, 40, 80\}$, respectively. These values indicate that the system of equations (3.13) is mildly ill-conditioned [42].

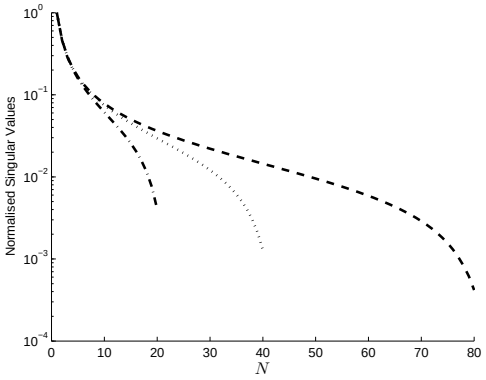

Figure 3.1: The normalised singular values of matrix X for $N_0 = N \in \{20\ (- \cdot -), 40\ (\cdots), 80\ (- - -)\}$, for Example 1.

In what follows, we present numerical results obtained with $N_0 = N = 40$. We consider first the case of exact data, i.e. there is no noise in the input data (3.4). Figure 3.2(a) shows the analytical and numerical results of $r(t)$ from which it can be

seen that the numerical solution is very accurate. Figure 3.2(b) shows the numerical solution of $u(0,t)$ in comparison with the analytical value $u(0,t) = e^t$. The same very good agreement between the numerical and analytical solutions is recorded. We do not present the results for the flux at $x = 1$ since these were found to be equal to the negative of the boundary temperature at $x = 0$. This is to be expected since from (3.18) we have $u_0(x) = u_0(1-x)$, $f(x,t) = f(1-x,t)$ and it can easily be verified that from (3.8), using (3.3) with $\alpha = -1$, it follows that $\mathfrak{q}_L = -\mathfrak{h}_0$. Furthermore, note that $\lambda = 0$, i.e. no regularisation, was found necessary for $N_0 = N = 40$ and exact input data (3.4).

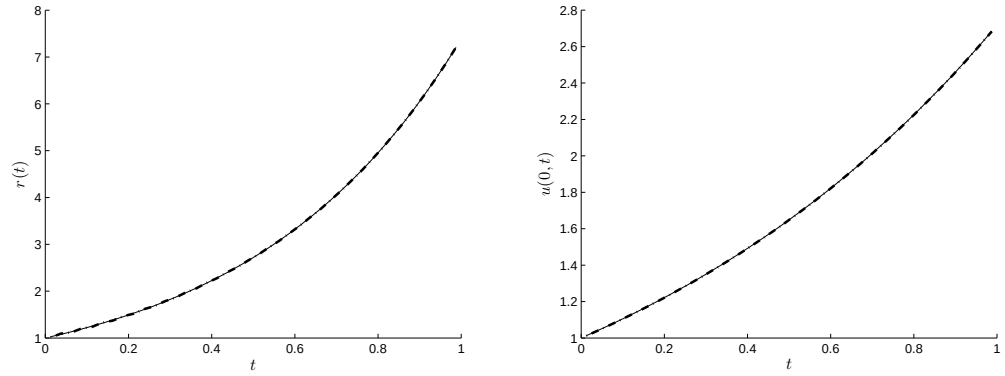

(a) (b)

Figure 3.2: The analytical (——) and numerical ($-\cdot-$) results of (a) $r(t)$ and (b) $u(0,t)$ for exact data and $\lambda = 0$, for Example 1.

Next, we investigate the stability of the numerical solution with respect to noise in the energy data (3.4), we add noise to the right-hand side of the oversdetermination condition (3.4), E^ϵ, as generated in (3.14) with the standard deviation given by $\sigma = \dfrac{7ep}{6}$. The contaminated data input with $p = 1\%$ is firstly inverted by using the Gaussian elimination procedure as shown in Figure 3.3. Although from Figure 3.3(b) the numerical solution for $u(0,t)$ seems to remain stable and accurate, whereas Figure 3.3(a) shows that the numerical solution for $r(t)$, with no regularisation, is unstable, i.e. highly oscillatory and unbounded. This phenomenon is to be expected since the inverse problem under investigation is ill-posed with the smallest normalised singular

value for $N = 40$ being of $O(10^3)$. Moreover, similar unstable results are obtained by using the untruncated SVD or with $\lambda = 0$ in regularised solution (1.34), instead of the Gaussian elimination method.

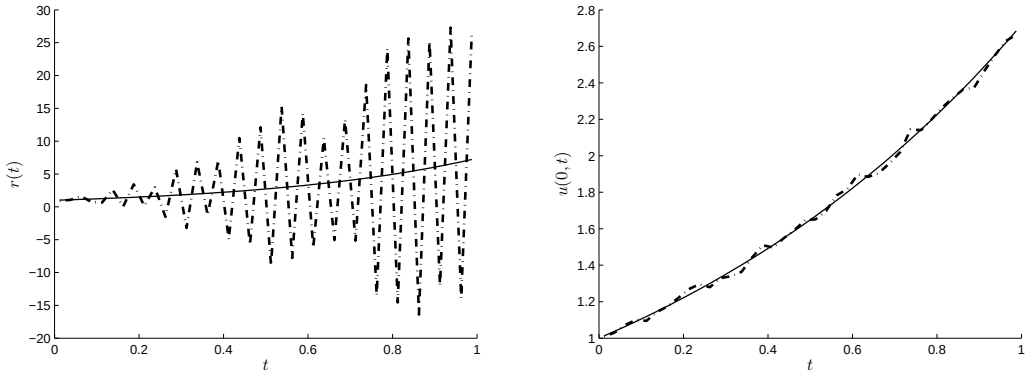

(a) (b)

Figure 3.3: The analytical (——) and numerical ($-\cdot-$) results of (a) $r(t)$ and (b) $u(0,t)$ for $p = 1\%$ noisy data and $\lambda = 0$, for Example 1.

In order to avoid the over amplification of noise and maintain the stability of the results when the noise is presented, we employ the regularisation of either the TSVD or the Tikhonov regularisation of orders zero, one and two. Furthermore, the L-curve method and the discrepancy principle are investigated to indicate the truncation level N_t for using TSVD, and choose the regularisation parameter λ for using the Tikhonov regularisation. Firstly, we consider the BEM together with the TSVD in the case of $p \in \{1, 3, 5\}\%$. Initially, we have tried the L-curve criterion which should select the truncated number N_t at the corner of L-curve graph. Figure 3.4 displays the L-curves for various percentages of noise $p \in \{1, 3, 5\}\%$. From this figure, especially on the normal scale one can see that L-shaped curves appear and their corners indicate the level of truncation N_t in the following intervals $\{9, \ldots, 32\}$, $\{12, \ldots, 24\}$ and $\{10, \ldots, 17\}$ for $p \in \{1, 3, 5\}\%$, respectively. Alternatively, one can choose the truncation level by the more rigorous discrepancy principle which uses the knowledge of the level of noise as in (3.16), i.e. $\epsilon = \|\underline{\mathrm{y}}^{\epsilon} - \underline{\mathrm{y}}\| = \|\mathrm{E}^{\epsilon} - \mathrm{E}\|$. Figure 3.5(a) represents the discrepancy principle to select N_t for $p \in \{1, 3, 5\}\%$. These truncated numbers N_t are obtained

within the intervals which have been recommended by the L-curve criterion of Figure 3.4. Besides, the numerical results for $r(t)$ and $u(0,t)$ are illustrated in Figures 3.5(b) and 3.5(c), respectively, and the RMSE for these results are given in Table 3.1. From Table 3.1 it can be remarked that the accuracy of the numerical results for $u(0,t)$ improves as the percentage of noise decreases; however, the convergence of the numerical solution for $r(t)$ towards the analytical solution is non-monotonic as p decreases (to zero), see also Figure 3.5(b). Further, from Figure 3.5(c), it can be seen that the numerical results for $u(0,t)$ are stable, although by comparing with Figure 3.3(b) it can be seen that for $p = 1\%$ noise the results with untruncation, i.e. no regularisation, are slightly more accurate than the results with $N_t = 15$. This is somewhat to be expected since the pair of solutions $(u(x,t), r(t))$ of the inverse problem is stable in the temperature $u(x,t)$ component, but unstable in the heat source $r(t)$ component. This latter instability in $r(t)$ which has already been illustrated in Figure 3.3(b), is alleviated in Figure 3.5(b) which shows the numerical results with regularisation.

Alternatively for comparison, the zeroth-order Tikhonov regularisation (ZOTR) is also utilised here. Initially, we have tried the L-curve plot of the residual $\|X\underline{\mathrm{r}}_\lambda - \underline{\mathrm{y}}^\epsilon\|$ versus the norm of the solution $\|\underline{\mathrm{r}}_\lambda\|$, but we have found that an L-corner could not be clearly identified. This is to be somewhat expected because the L-curve is a heuristic method which is not always convergent [58]. Another optional method, the more rigorous discrepancy principle which uses the knowledge of the level of noise ϵ is recommended.

Figure 3.6(a) shows the discrepancy principle curves, for various percentages of noise $p \in \{1,3,5\}\%$ where the intersection of the residual curve with the horizontal level noisy line ϵ yields the value of λ_{dis}. The RMSE for the output solutions of $r(t)$ and $u(0,t)$ obtained with these values of λ_{dis} are given in Table 3.1 and the numerical results are illustrated in Figures 3.6(b) and 3.6(c). From this table it can be seen that the ZOTR slightly outperforms the TSVD. As it can be seen from Figures 3.6(b) and 3.6(c) the numerical results obtained by the ZOTR are stable and in good agreement with the analytical solution. Although Figure 3.6(b) represents a significant improvement over

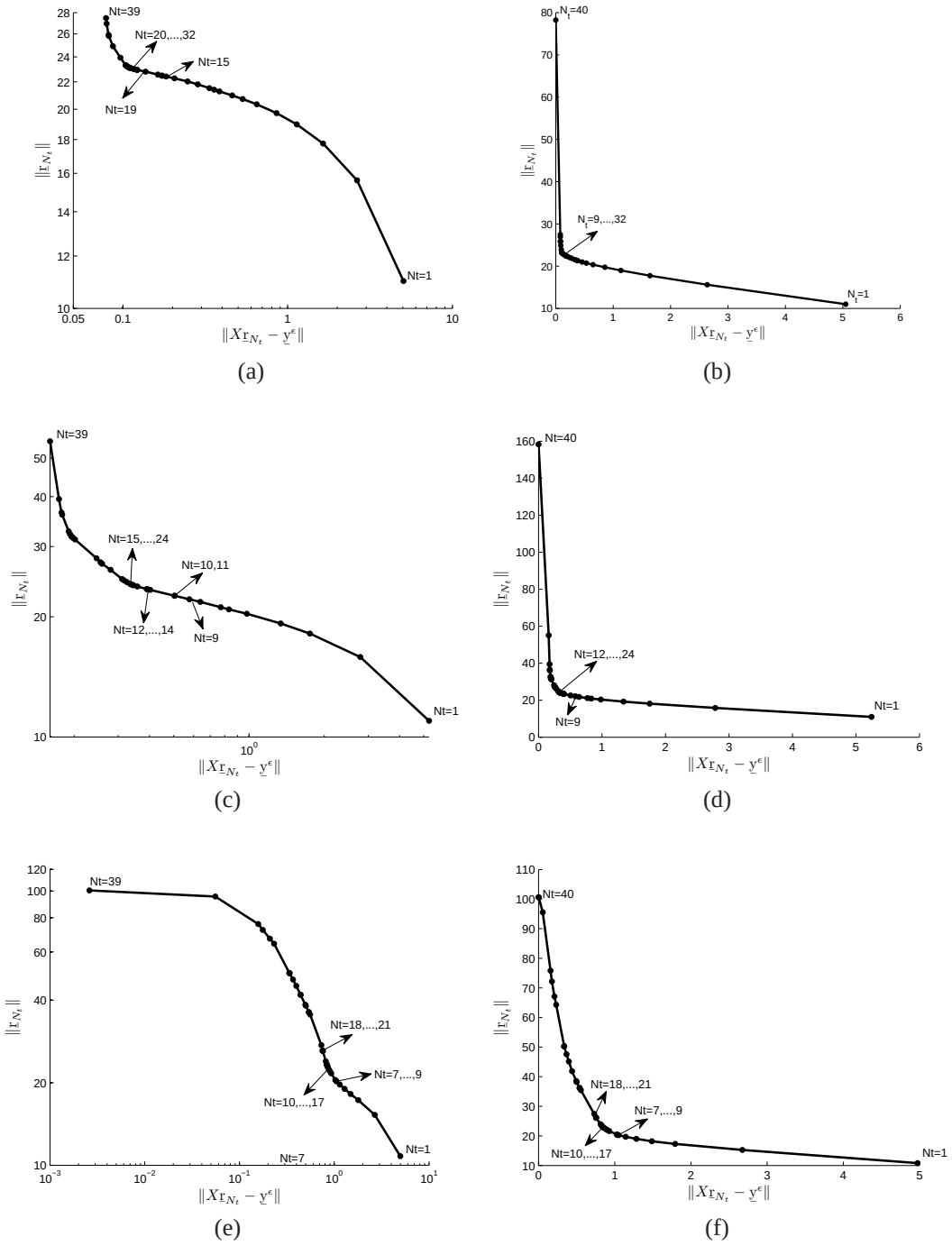

Figure 3.4: The L-curve on (a), (c), (e) log-log scale and (b), (d), (f) normal scale, obtained using TSVD for $p \in \{1(\text{top}),\ 3(\text{middle}),\ 5(\text{bottom})\}\%$ noise, for Example 1.

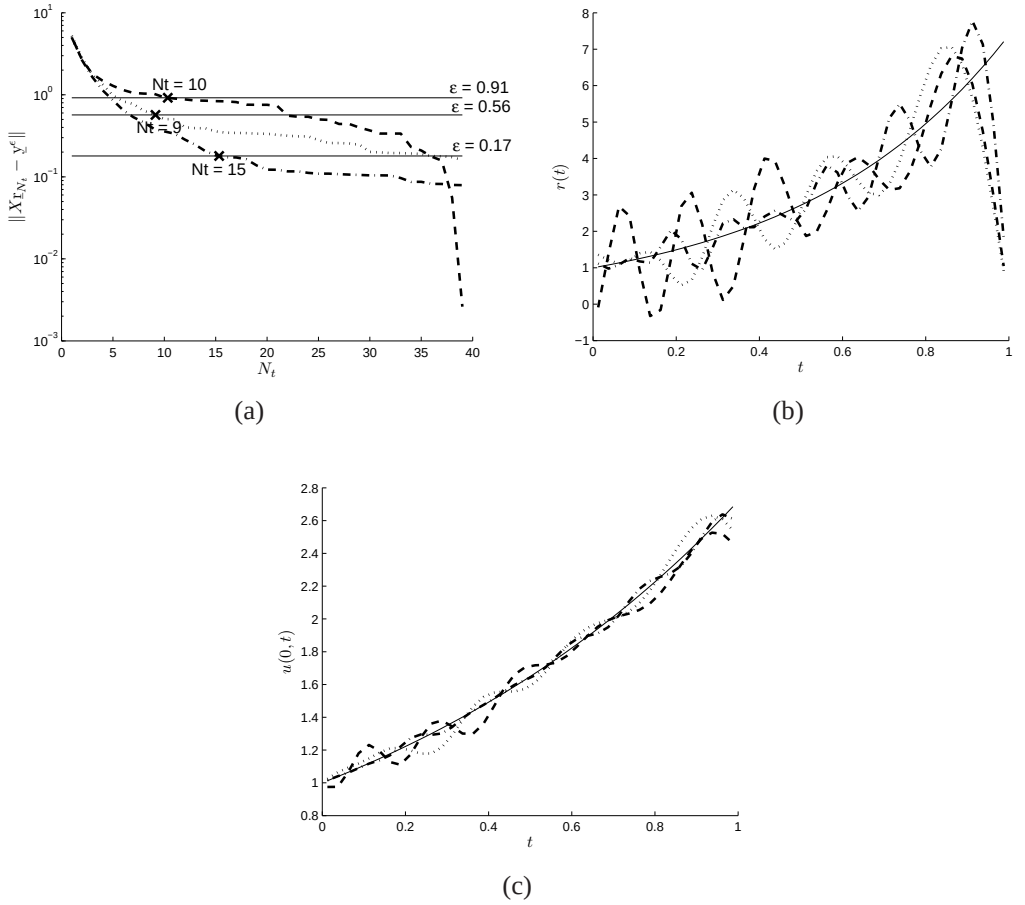

(a) (b)

(c)

Figure 3.5: (a) The discrepancy principle curve, and the analytical (——) and numerical results of (b) $r(t)$, and (c) $u(0,t)$ obtained using the TSVD for $p \in \{1(- \cdot -),\ 3(\cdots),\ 5(- - -)\}\%$ noise at the truncation level N_t given in Table 3.1, for Example 1.

Figure 3.3(a) the numerical results are still oscillatory. In order to further improve on the accuracy and stability of the numerical results of Figure 3.6(b), next we employ the regularisation with the higher-order Tikhonov regularisation of orders one and two.

Figures 3.7 and 3.8 show the analogous numerical results to Figure 3.6, but for the first- and second-order Tikhonov regularisation, denoted FOTR and SOTR, respectively. The corresponding values of the regularisation parameters λ_{dis} chosen according to the discrepancy principle are given in Table 3.1. By comparing Figures 3.6–3.8 and Table 3.1, it can be seen that the use of higher-order regularisation improves the

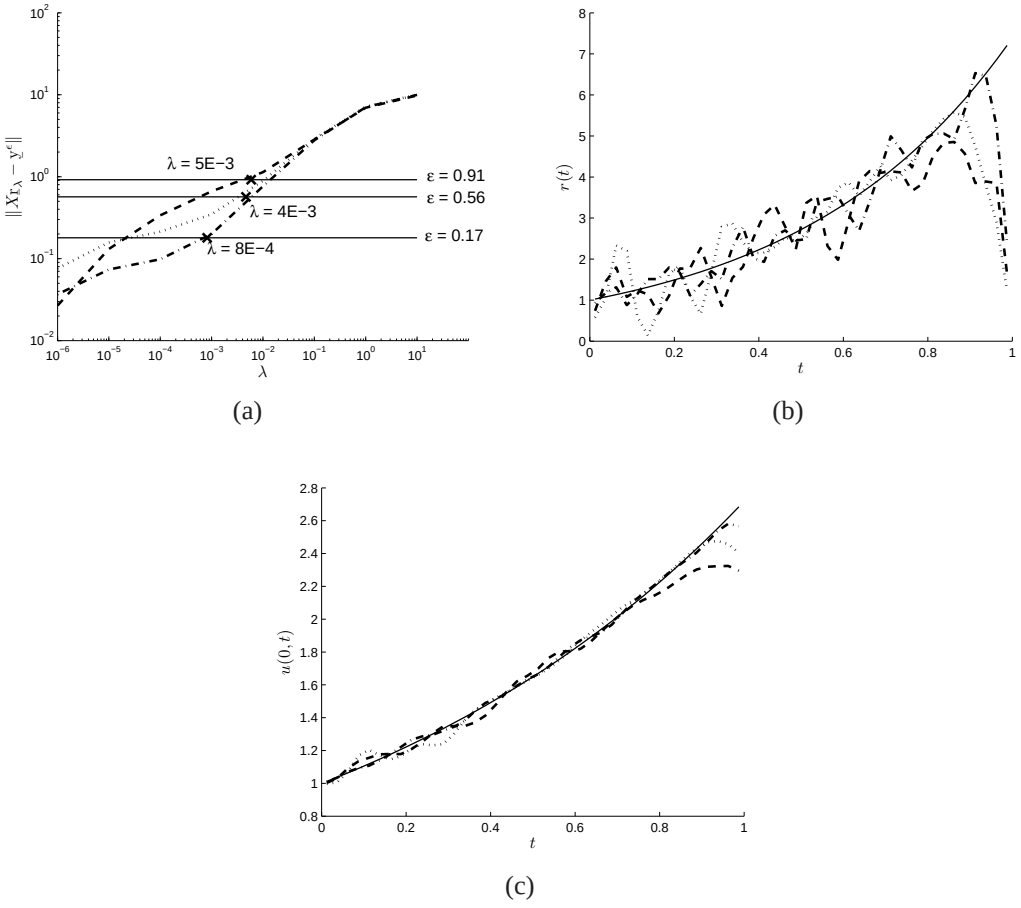

(a) (b)

(c)

Figure 3.6: (a) The discrepancy principle curve, and the analytical (——) and numerical results of (b) $r(t)$, and (c) $u(0,t)$ obtained using the ZOTR for $p \in \{1(- \cdot -),\ 3(\cdots),\ 5(- - -)\}\%$ noise with the regularisation parameters λ_{dis} given in Table 3.1, for Example 1.

accuracy and stability of the numerical results. This is to be expected since the analytical solution (3.19) to be retrieved is infinitely differentiable. However, if less smooth sources are attempted to be retrieved, the use of higher-order regularisation does not necessarily improve the accuracy of the numerical results, as can be seen from the next example.

Table 3.1: The RMSE for the TSVD, ZOTR, FOTR, SOTR for $p \in \{0, 1, 3, 5\}\%$ noise, for Example 1.

Regularisation	$p(\%)$	parameter	RMSE	
			$r(t)$	$u(0,t)$
-	0	0	8.1E-3	6.6E-4
	1%	0	11.66	0.023
TSVD	1%	N_t=15	1.080	2.47E-2
	3%	N_t=9	1.443	6.03E-2
	5%	N_t=10	1.521	7.25E-2
ZOTR	1%	λ_{dis}=8E-4	0.878	2.40E-2
	3%	λ_{dis}=4E-3	1.324	6.22E-2
	5%	λ_{dis}=5E-3	1.280	9.90E-2
FOTR	1%	λ_{dis}=0.05	0.246	1.17E-2
	3%	λ_{dis}=0.45	0.435	3.14E-2
	5%	λ_{dis}=0.64	0.595	5.81E-2
SOTR	1%	λ_{dis}=5.2	0.113	6.86E-3
	3%	λ_{dis}=81	0.198	2.67E-2
	5%	λ_{dis}=324	0.473	5.48E-2

3.5.2 Example 2

The previous Example 1 involved retrieving a smooth source function given by $r(t) = e^{2t}$. In this example, we are considering the BEM combined only with the Tikhonov regularisation as we found in the previous example that the ZOTR slightly outperforms the TSVD. Consider a more severe discontinuous test function given by [63],

$$r(t) = \begin{cases} -1, & t \in [0, 0.25), \\ 1, & t \in [0.25, 0.5), \\ -1, & t \in [0.5, 0.75), \\ 1, & t \in [0.75, 1]. \end{cases} \tag{3.20}$$

We also take $T = 1$, $\alpha = -1$, $u_0 = 0$, and $f = 1$. Since the inverse problem (3.1)–(3.4) does not have an analytical solution available for the temperature $u(x, t)$, the input energy data (3.4) is numerically simulated by solving first the direct problem (3.1)–(3.2)

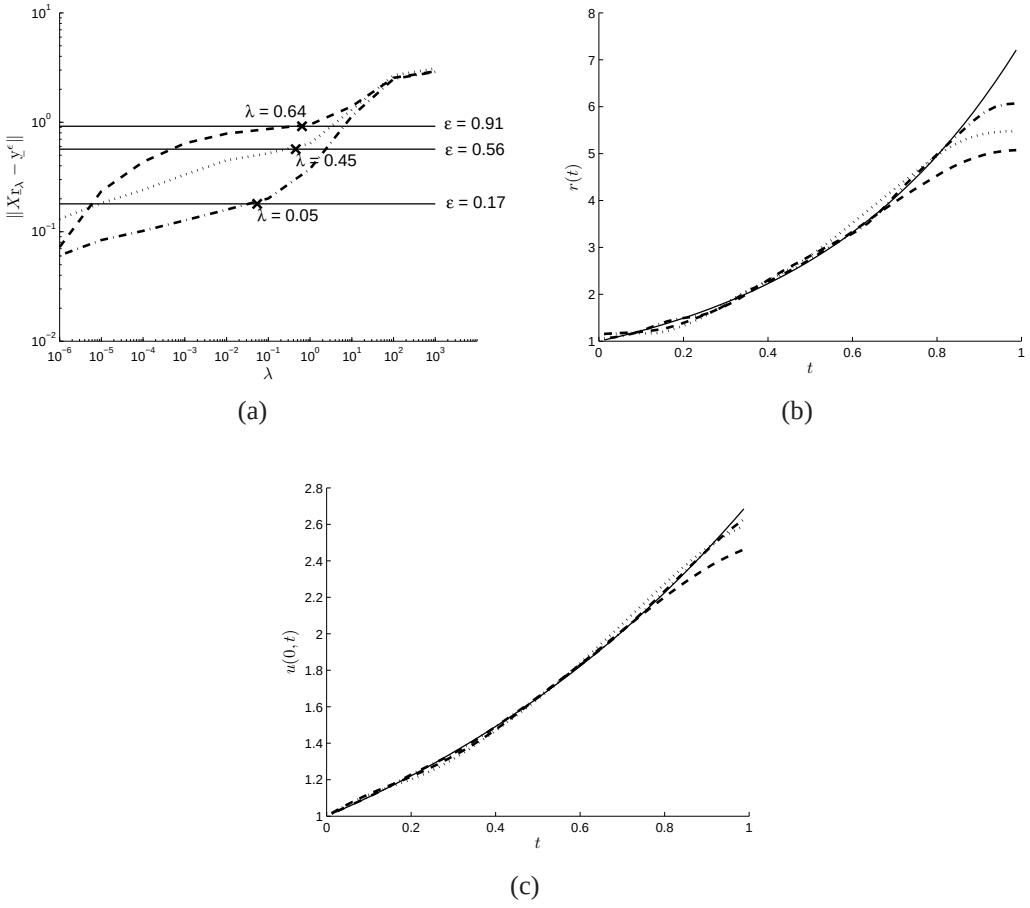

(a) (b)

(c)

Figure 3.7: (a) The discrepancy principle curve, and the analytical (——) and numerical results of (b) $r(t)$, and (c) $u(0,t)$ obtained using the FOTR for $p \in \{1(- \cdot -),\ 3(\cdots),\ 5(- - -)\}\%$ noise with the regularisation parameters λ_{dis} given in Table 3.1, for Example 1.

with r given by (3.20). The numerical results for $E(t)$ and $u(0,t)$ are shown in Figures 3.9(a) and 3.9(b), respectively, for various numbers of boundary elements/cells $N = N_0 \in \{20, 40, 80\}$. From Figure 3.9 it can be seen that the numerical solution is convergent as the number of boundary elements increases. Also, there is little difference between the numerical results obtained with the various mesh sizes showing that the independence of the mesh has been achieved. We can therefore take the numerical results for $E(t)$, simulated from the direct problem with $N = N_0 = 40$ and shown in Figure 3.9(a), as our input (3.4) in the inverse problem (3.1)–(3.4). Furthermore, in

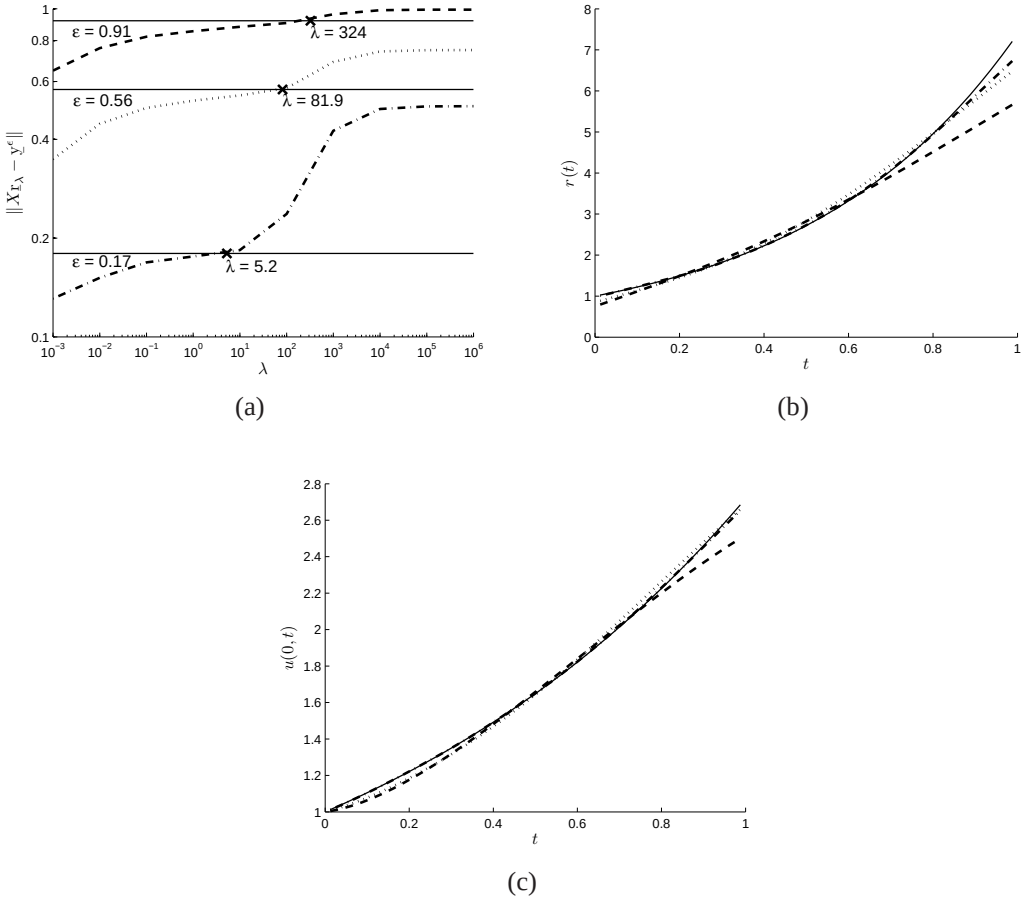

(a) (b)

(c)

Figure 3.8: (a) The discrepancy principle curve, and the analytical (——) and numerical results of (b) $r(t)$, and (c) $u(0,t)$ obtained using the SOTR for $p \in \{1(- \cdot -),\ 3(\cdots),\ 5(- - -)\}\%$ noise with the regularisation parameters λ_{dis} given in Table 3.1, for Example 1.

order to avoid committing an inverse crime [32], in the inverse problem the number of cells is taken $N_0 = 30$ (different than 40) while the number of boundary elements is kept the same $N = 40$.

First, Figures 3.10(a) and 3.10(b) show the numerical results for $r(t)$ and $u(0,t)$, respectively, for no noise in the input data (3.4) obtained with no regularisation, i.e. $\lambda = 0$. The exact solution (3.20) for $r(t)$ is also included, and the numerical solution for $u(0,t)$ from Figure 3.9(b) with $N = N_0 = 40$ is also referred to as 'analytical'. From Figure 3.10 it can be seen that the agreement between the numerical and the

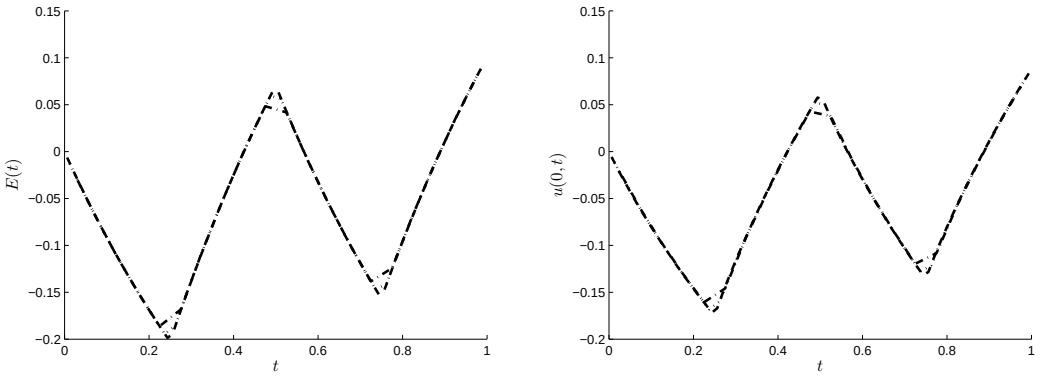

(a) (b)

Figure 3.9: The numerical results of (a) $E(t)$ and (b) $u(0,t)$ obtained by solving the direct problem with $N_0 = N \in \{20\ (- \cdot -), 40\ (\cdots), 80\ (- - -)\}$, for Example 2.

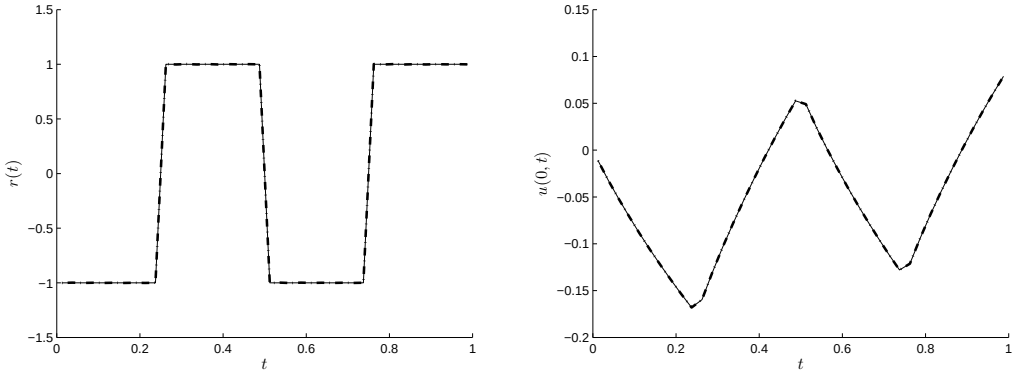

(a) (b)

Figure 3.10: The analytical (——) and numerical $(- \cdot -)$ results of (a) $r(t)$ and (b) $u(0,t)$ for exact data and $\lambda = 0$, for Example 2.

analytical solutions is excellent. Next we add noise to the input data (3.4) numerically simulated in Figure 3.9(a). This is generated as in (3.14) with the standard deviation given by $\sigma = 0.19p$. If $\lambda = 0$, the numerically retrieved results for $r(t)$ were found highly unbounded and oscillatory and therefore, they are not presented. The numerical results for the discrepancy principle, $r(t)$ and $u(0,t)$ for various amounts of noise and regularisation of various orders zero, one, and two are shown in Figures 3.11–3.13, respectively, and Table 3.2. The use of higher-order regularisation imposes higher-order

Table 3.2: The RMSE for the ZOTR, FOTR, SOTR for $p \in \{1, 3, 5\}\%$ noise and $N = 40$, $N_0 = 30$, for Example 2.

Regularisation	$p(\%)$	parameter λ_{dis}	RMSE	
			$r(t)$	$u(0,t)$
ZOTR	1%	8.7E-5	0.195	1.90E-3
	3%	3.3E-4	0.284	4.66E-3
	5%	4.3E-4	0.287	5.80E-3
FOTR	1%	9.9E-5	0.211	1.98E-3
	3%	8.1E-4	0.289	4.38E-3
	5%	7.8E-4	0.280	4.69E-3
SOTR	1%	7.7E-5	0.223	2.06E-3
	3%	9.2E-4	0.292	4.48E-3
	5%	7.3E-4	0.279	4.48E-3

smoothness of the desired output hence, since the solution (3.20) is discontinuous, more accurate results are obtained with the ZOTR, whilst the FOTR and the SOTR, although they achieve stability, they slightly oversmooth the retrieved solution.

3.6 Conclusions

In this chapter, the inverse problem of finding the time-dependent heat source together with the temperature of heat equation under non-local boundary and integral overdetermination conditions has been investigated. The general ill-posed problem, a numerical method based on the BEM combined with either the TSVD or the Tikhonov regularisation has been proposed. The TSVD has been truncated at the optimal truncation level given by the L-curve criterion and the discrepancy principle. Whereas the discrepancy principle for choosing the regularisation parameter with three orders of Tikhonov regularisation have also been employed. The numerical results were found to be accurate and stable. These features of the numerical solution increase with decreasing the amount of noise included in the input data and with increasing the order of regularisation for smooth sources. However, as expected, non-smooth sources are more accurately reconstructed by lower-order regularisation.

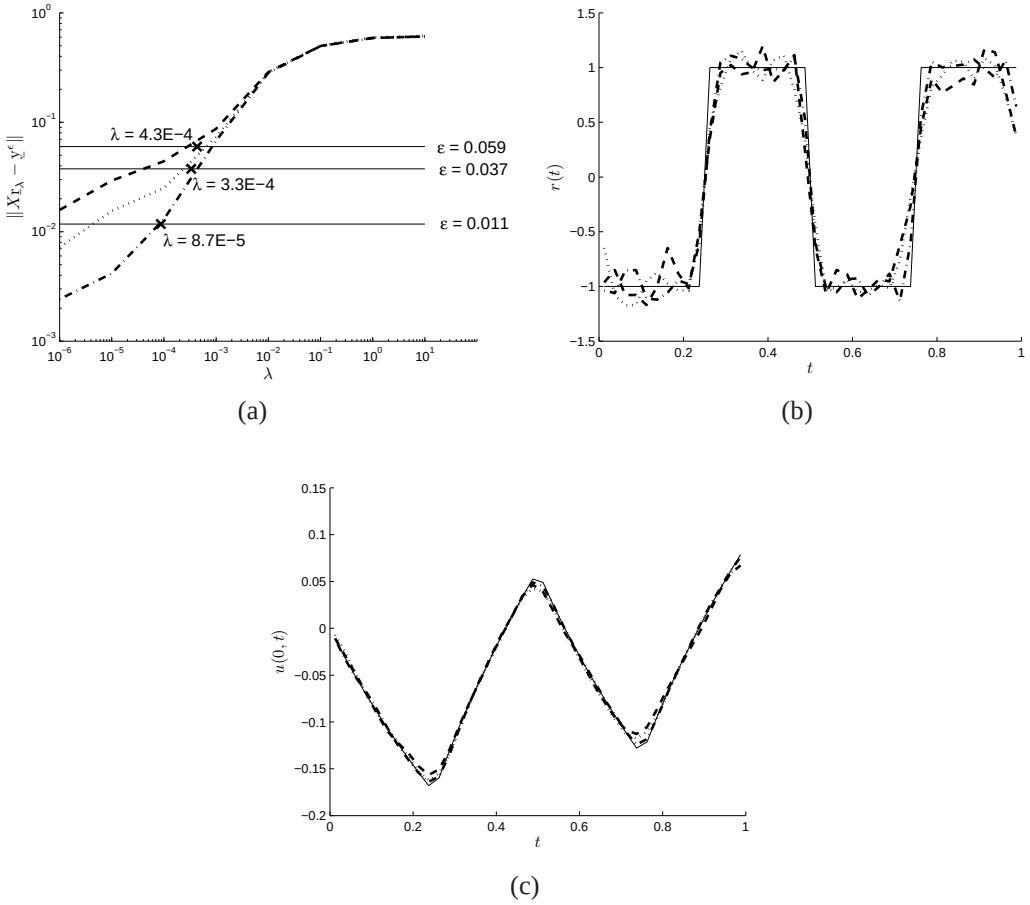

(a) (b)

(c)

Figure 3.11: (a) The discrepancy principle curve, and the analytical (——) and numerical results of (b) $r(t)$, and (c) $u(0,t)$ obtained using the ZOTR for $p \in \{1(- \cdot -),\ 3(\cdots),\ 5(- - -)\}\%$ noise with the regularisation parameters λ_{dis} given in Table 3.2, for Example 2.

We have studied the nonlocal boundary and integral overdetermination condition for the inverse source problem for the heat equation. In the next chapter, we will subject these conditions to a coefficient identification problem for the bioheat equation.

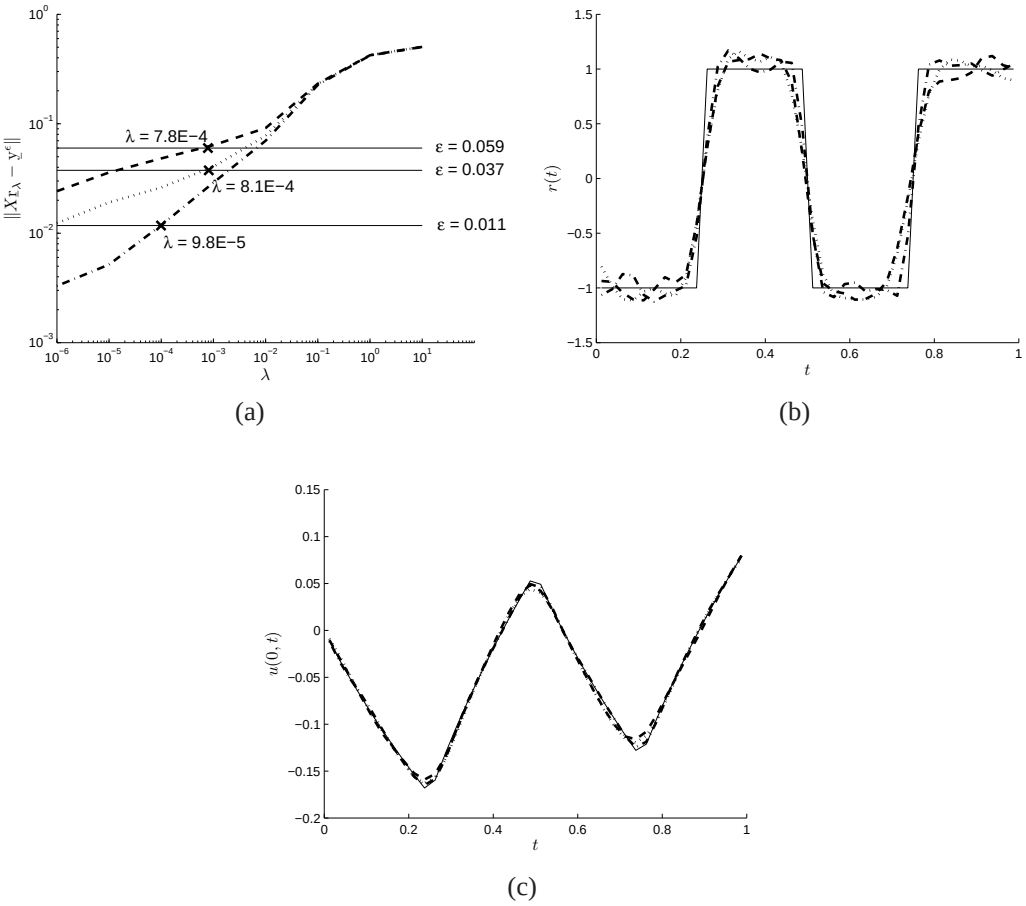

(a) (b)

(c)

Figure 3.12: (a) The discrepancy principle curve, and the analytical (——) and numerical results of (b) $r(t)$, and (c) $u(0,t)$ obtained using the FOTR for $p \in \{1(- \cdot -),\ 3(\cdots),\ 5(- - -)\}\%$ noise with the regularisation parameters λ_{dis} given in Table 3.2, for Example 2.

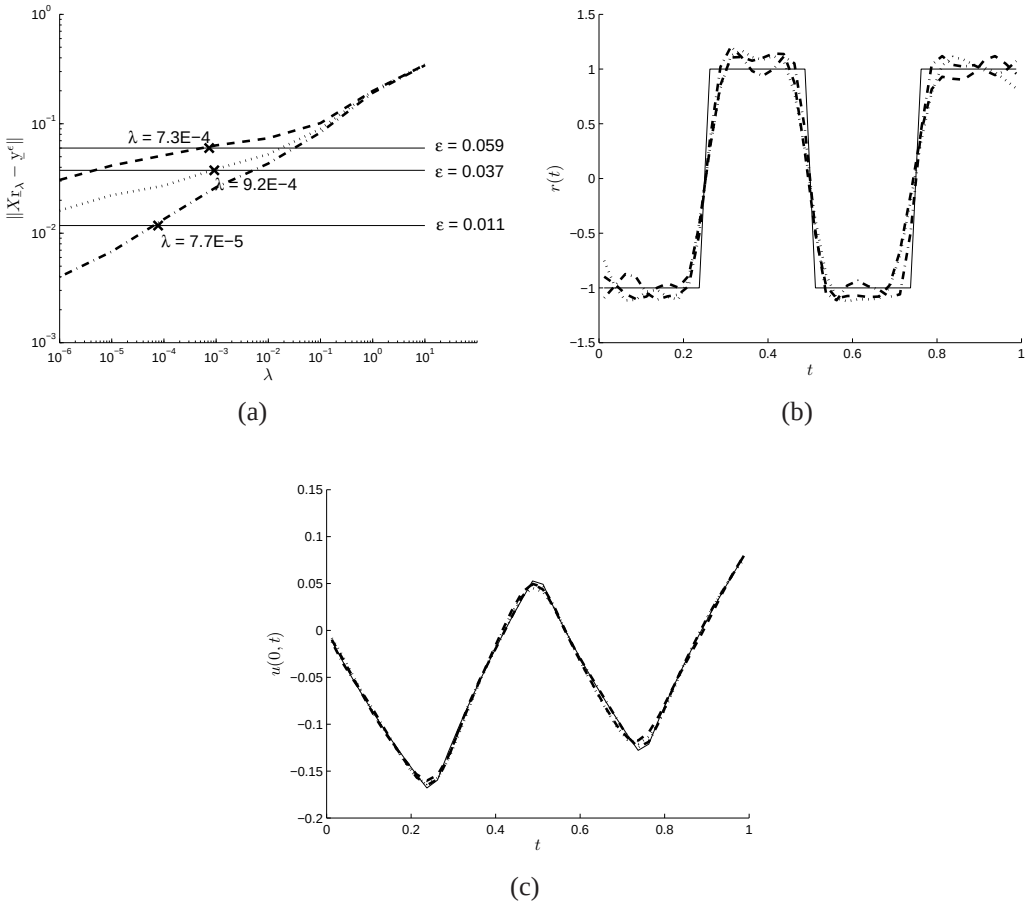

(a) (b)

(c)

Figure 3.13: (a) The discrepancy principle curve, and the analytical (——) and numerical results of (b) $r(t)$, and (c) $u(0,t)$ obtained using the SOTR for $p \in \{1(- \cdot -),\ 3(\cdots),\ 5(- - -)\}\%$ noise with the regularisation parameters λ_{dis} given in Table 3.2, for Example 2.

Chapter 4

Determination of a Time-dependent Coefficient in the Bioheat Equation

4.1 Introduction

The bioheat equation establishes a mathematical connection between the tissue temperature and the arterial blood perfusion which are the dominant components in human physiology, see [55]. It involves a blood perfusion coefficient whose determination is of much interest, [53].

In the previous chapter, we have considered the identification of the time-dependent heat source $r(t)$ and the temperature $u(x,t)$ in the heat equation (3.1) with nonlocal boundary and integral conditions. In this chapter, we aim to find the time-dependent blood perfusion coefficient function $P(t)$ and the temperature of the tissue $u(x,t)$ entering the bioheat equation (4.1) below. The initial (3.2), nonlocal boundary (3.3) and integral (3.4) conditions are the same as in the previous chapter. We mention that time-dependent coefficient identification problems with nonlocal boundary and/or integral overdetermination conditions have recently attracted revitalising interest, e.g. the reconstruction of a time-dependent diffusivity [27], a blood perfusion coefficient [23], or a heat source [18, 24].

The inverse problem investigated in this chapter has already been proved to be uniquely solvable in [33], but no numerical reconstruction has been attempted. Therefore, the purpose of this chapter is to devise a numerical stable method for obtaining the solution of the inverse problem.

4.2 Mathematical formulation

Let us consider the inverse problem consisting of finding the time-dependent blood perfusion coefficient function $P(t) \in C[0,T]$ and the temperature of the tissue $u(x,t) \in C^{2,1}(D_T) \cap C^{1,0}(\overline{D}_T)$ satisfying the one-dimensional time-dependent bioheat equation, [33, 54],

$$u_t(x,t) = u_{xx}(x,t) - P(t)u(x,t) + f(x,t), \quad (x,t) \in D_T, \tag{4.1}$$

where f is a known heat source term and $L = 1$ in the definition of D_T in (1.1), subject to the following initial, boundary and overdetermination conditions:

$$u(x,0) = u_0(x), \quad x \in [0,1], \tag{4.2}$$

$$u(0,t) = u(1,t), \quad u_x(0,t) + \alpha u(0,t) = 0, \quad t \in [0,T], \tag{4.3}$$

$$\int_0^1 u(x,t)dx = E(t), \quad t \in [0,T], \tag{4.4}$$

where the function u_0 is given and it denotes the initial temperature, α is a given constant heat transfer coefficient, and E represents the mass or energy of the system. Note that the nonlocal periodic boundary condition (4.3) is encountered in biological applications, [41], whilst the mass/energy specification (4.4) models processes related to particle diffusion in turbulent plasma, [22], or heat conduction, [10]. The physical constraint that the blood perfusion $P(t)$ is positive can also be imposed, [37].

Note that the case $\alpha = 0$ has been dealt with in [24]. Herein, we consider the case $\alpha \neq 0$ whose unique solvability and local continuous dependence of the solution upon

the data of the inverse problem (4.1)–(4.4) have been established in [33]. Moreover, the continuous dependence of the solution upon the data also was established, [21].

Consider now the following transformation, [11],

$$v(x,t) = r(t)u(x,t), \quad r(t) = \exp\left(\int_0^t P(\tau)\,d\tau\right). \tag{4.5}$$

Then the inverse problem (4.1)–(4.3) becomes

$$v_t = v_{xx} + r(t)f(x,t), \quad (x,t) \in D_T, \tag{4.6}$$

$$v(x,0) = u_0(x), \quad x \in [0,t], \tag{4.7}$$

$$v(0,t) = v(1,t), \quad v_x(0,t) + \alpha v(0,t) = 0, \quad t \in [0,T], \tag{4.8}$$

with the transformed integral condition

$$\int_0^1 v(x,t)dx = E(t)r(t), \quad t \in [0,T]. \tag{4.9}$$

We also have that $r \in C^1[0,T]$, $r(0) = 1$, $r(t) > 0$, for $t \in [0,T]$. Solving the inverse problem (4.6)–(4.9) for the solution pair $(r(t), v(x,t))$ yields afterwards the solution pair $(P(t), u(x,t))$ for the inverse problem (4.1)–(4.4) as given by

$$P(t) = \frac{r'(t)}{r(t)} \quad \text{and} \quad u(x,t) = \frac{v(x,t)}{r(t)}, \quad (x,t) \in D_T. \tag{4.10}$$

From equation (4.10) one can observe that the ill-posedness of the inverse problem consists of the numerical differentiation of the noisy function $r(t)$ which would need regularisation.

4.3 The boundary element method (BEM)

In this section, we apply the BEM to the one-dimensional inverse problem (4.6)–(4.9), in order to approximate the solution $(r(t), v(x,t))$ which in turn, via (4.10), leads to

the original solution $(P(t), u(x,t))$ of the inverse problem (4.1)–(4.4). Utilising the BEM is classical with the use of the fundamental solution for the heat equation and Green's identities. As introduced in Section 1.3, we then obtain the boundary integral equation

$$\begin{aligned}\eta(x)v(x,t) = &\int_0^t \left[G(x,t,\xi,\tau)\frac{\partial v}{\partial n(\xi)}(\xi,\tau) - v(\xi,\tau)\frac{\partial G}{\partial n(\xi)}(x,t,\xi,\tau)\right]_{\xi\in\{0,1\}} d\tau \\ &+ \int_0^1 G(x,t,y,0)v(y,0)\,dy + \int_0^1\int_0^T G(x,t,y,\tau)r(\tau)f(y,\tau)\,d\tau dy, \\ &(x,t)\in[0,1]\times(0,T]. \end{aligned} \tag{4.11}$$

Using the same discretisation as in Chapters 1–3, then the integral equation above can be approximate as

$$\begin{aligned}\eta(x)v(x,t) = &\sum_{j=1}^{N}\left[A_{0j}(x,t)q_{0j} + A_{Lj}(x,t)q_{Lj} - B_{0j}(x,t)h_{0j} - B_{Lj}(x,t)h_{Lj}\right] \\ &+ \sum_{k=1}^{N_0} C_k(x,t)u_{0,k} + \sum_{j=1}^{N} D_j(x,t)r_j. \end{aligned} \tag{4.12}$$

By applying the boundary condition (4.3), we obtain the system of $2N$ linear equations, the same as in (3.9),

$$\left(A - \frac{1}{\alpha}(B+B^*)\right)\mathbf{q} + C\mathbf{u}_0 + D\mathbf{r} = \mathbf{0}. \tag{4.13}$$

The transformed integral condition (4.9) can also be expressed, via the midpoint numerical integral approximation, as

$$\frac{1}{N_0}\sum_{k=1}^{N_0} v(\tilde{x}_k,\tilde{t}_i), = \int_0^1 v(x,\tilde{t}_i)\,dx = E(\tilde{t}_i)r(\tilde{t}_i) = e_i r_i, \quad i = \overline{1,N}. \tag{4.14}$$

By using the integral equation (4.12), via (4.13), and (4.14) as the same in Chapter 3 yields

$$\frac{1}{N_0}\sum_{k=1}^{N_0}\left[\left(A_k^{(1)}-\frac{1}{\alpha}(B_k^{(1)}+B_k^{(1)^*})\right)\mathfrak{q}+C_k^{(1)}\mathfrak{u}_0+D_k^{(1)}\mathfrak{r}\right]=\mathrm{E}\mathfrak{r}, \tag{4.15}$$

where $\mathrm{E}=\mathrm{diag}(\overline{e_1,e_N})$. Eliminating $\mathfrak{q}$ from (4.13) and (4.15) yields a linear system of N equations

$$X\mathfrak{r}=\mathfrak{y}, \tag{4.16}$$

with N unknowns, where

$$X=\frac{1}{N_0}\sum_{k=1}^{N_0}\left[-\left(A_k^{(1)}-\frac{1}{\alpha}(B_k^{(1)}+B_k^{(1)^*})\right)\left(A-\frac{1}{\alpha}(B+B^*)\right)^{-1}D+D_k^{(1)}\right]-\mathrm{E},$$
$$\mathfrak{y}=\frac{1}{N_0}\sum_{k=1}^{N_0}\left[\left(A_k^{(1)}-\frac{1}{\alpha}(B_k^{(1)}+B_k^{(1)^*})\right)\left(A-\frac{1}{\alpha}(B+B^*)\right)^{-1}C-C_k^{(1)}\right]\mathfrak{u}_0.$$

As we have mention before, this inverse problem is ill-posed, then we need to employ the regularisation in order to retrieve the stability of the solution which will be present in the next section.

4.4 Regularisation

In practical measurements, the data (4.4) is usually contaminated with noise. In order to model this, we perturb (4.4) with random noise as defined in (3.14), i.e. $\mathrm{E}^\epsilon=\mathrm{E}+\epsilon$. Then, from the contamination, it means that the left-hand side matrix X is contaminated with noise, denoted by X^ϵ, where

$$\epsilon\approx\|X^\epsilon-X\|. \tag{4.17}$$

The norm of the matrix above is defined as the square root of the sum of squares of all its elements. Hence, instead of (4.16) we have to solve the following linear system of

equations:

$$X^{\epsilon}\underline{\mathrm{r}} = \underline{\mathrm{y}}. \tag{4.18}$$

When the noise is presented, we employ the Tikhonov regularisation, as described in Subsection 1.6.2, yielding the regularised solution

$$\underline{\mathrm{r}}_{\lambda} = \left((X^{\epsilon})^{\mathrm{T}} X^{\epsilon} + \lambda R^{\mathrm{T}} R\right)^{-1} (X^{\epsilon})^{\mathrm{T}} \underline{\mathrm{y}}. \tag{4.19}$$

where $\lambda \geq 0$ is a regularisation parameter to be prescribed and R is a second-order derivative regularisation matrix given by, [57],

$$R = \frac{1}{(T/N)^2} \begin{bmatrix} 1 & -2 & 1 & 0 & 0 & . \\ 0 & 1 & -2 & 1 & 0 & . \\ 0 & 0 & 1 & -2 & 1 & . \\ . & . & . & . & . & . \end{bmatrix}. \tag{4.20}$$

Note that we have kept the multiple of $\dfrac{1}{(T/N)^2}$ to the regularisation matrix which is different from the regularisation matrix introduced in Subsection 1.6.2, this is in order to keep the scaling technique of the computation. In (4.19), the regularisation parameter can be selected according to the GCV criterion which chooses $\lambda > 0$ as the minimum of the GCV function, see e.g. [63] and (1.35),

$$GCV(\lambda) = \frac{\|X^{\epsilon}\underline{\mathrm{r}}_{\lambda} - \underline{\mathrm{y}}\|^2}{[\mathrm{trace}(I - X^{\epsilon}((X^{\epsilon})^{\mathrm{T}} X^{\epsilon} + \lambda R^{\mathrm{T}} R)^{-1} (X^{\epsilon})^{\mathrm{T}})]^2}. \tag{4.21}$$

The solution of the original inverse problem (4.1)–(4.4) can be obtained by substituting all approximate solutions v, r, and r' into (4.10). In order to obtain the solution $P(t)$, we also need to find the derivative function $r'(t)$ which can be approximated using finite differences as

$$r'(\tilde{t}_1) = \frac{r_{\lambda}(\tilde{t}_1) - 1}{T/(2N)}, \quad r'(\tilde{t}_i) = \frac{r_{\lambda}(\tilde{t}_i) - r_{\lambda}(\tilde{t}_{i-1})}{T/N}, \quad i = \overline{2, N}. \tag{4.22}$$

In the next section, we will test numerical examples in order to illustrate the accuracy and stability of the BEM combined with the regularisation technique.

4.5 Numerical examples and discussion

This section presents two benchmark test examples in order to test the accuracy and stability of the BEM numerical procedure introduced earlier. The RMSE defined in (2.49) is also used here to evaluate the accuracy of the numerical results.

4.5.1 Example 1

We consider a benchmark test example with the input $T = 1$, $\alpha = -1$ and

$$\begin{cases} u(x,0) = u_0(x) = 1 + x - x^2, \quad f(x,t) = (3 + x - x^2)e^{-t}, \\ \displaystyle\int_0^1 u(x,t)\,dx = E(t) = 7e^{-t}/6, \end{cases} \tag{4.23}$$

Then the analytical solution of the problem (4.1)–(4.4) is given by

$$u(x,t) = (1 + x - x^2)e^{-t}, \quad P(t) = 2, \tag{4.24}$$

whilst the analytical solution for the transformed problem (4.6)–(4.9) is

$$v(x,t) = (1 + x - x^2)e^{t}, \quad r(t) = e^{2t}, \tag{4.25}$$

In this example, we present the numerical results obtained with a BEM mesh of $N = N_0 = 40$.

We start first with the case of exact data, i.e. $p = 0$. The numerical results for the unknowns $r(t)$, $u(0,t)$, $r'(t)$, and $P(t)$ obtained using the straightforward inversion $\underline{\mathrm{r}} = X^{-1}\underline{\mathrm{y}}$, i.e. without regularisation $\lambda = 0$ in (4.19), are compared with their corresponding analytic values e^{2t}, e^{-t}, $2e^{2t}$, and 2, in Figures 4.1(a)–4.1(d), respectively.

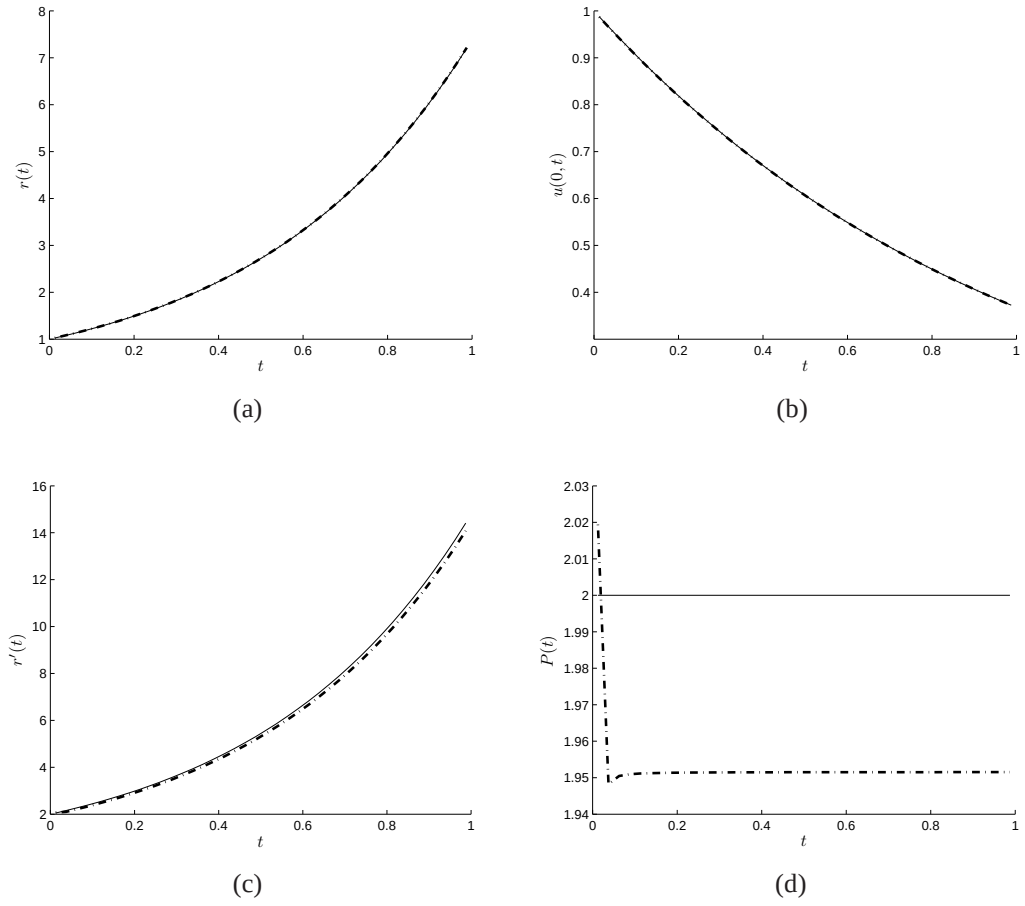

(a) (b)

(c) (d)

Figure 4.1: The analytical (——) and numerical $(- \cdot -)$ results of (a) $r(t)$, (b) $u(0,t)$, (c) $r'(t)$, and (d) $P(t)$ obtained using no regularisation, i.e. $\lambda = 0$, for exact data, for Example 1.

From Figure 4.1 it can be seen that all the quantities of interest are accurate.

Next we investigate the stability of the numerical solution with respect to some $p = 1\%$ noise included in the input energy data E, as mentioned in Section 4.4. The corresponding numerical results to Figure 4.1 (for exact data) are presented in Figure 4.2 (for noisy data). In Figures 4.2(a) and 4.2(b) the numerical results obtained for $r(t)$ and $u(0,t)$, respectively, are relatively accurate. However, the numerical results obtained for $r'(t)$ and $P(t) = r'(t)/r(t)$ shown in Figures 4.2(c) and 4.2(d), respectively, are highly unstable. This is because the differentiation of the noisy function $r(t)$, shown in Figure 4.2(a) with dashed line, using the finite differences (4.22)

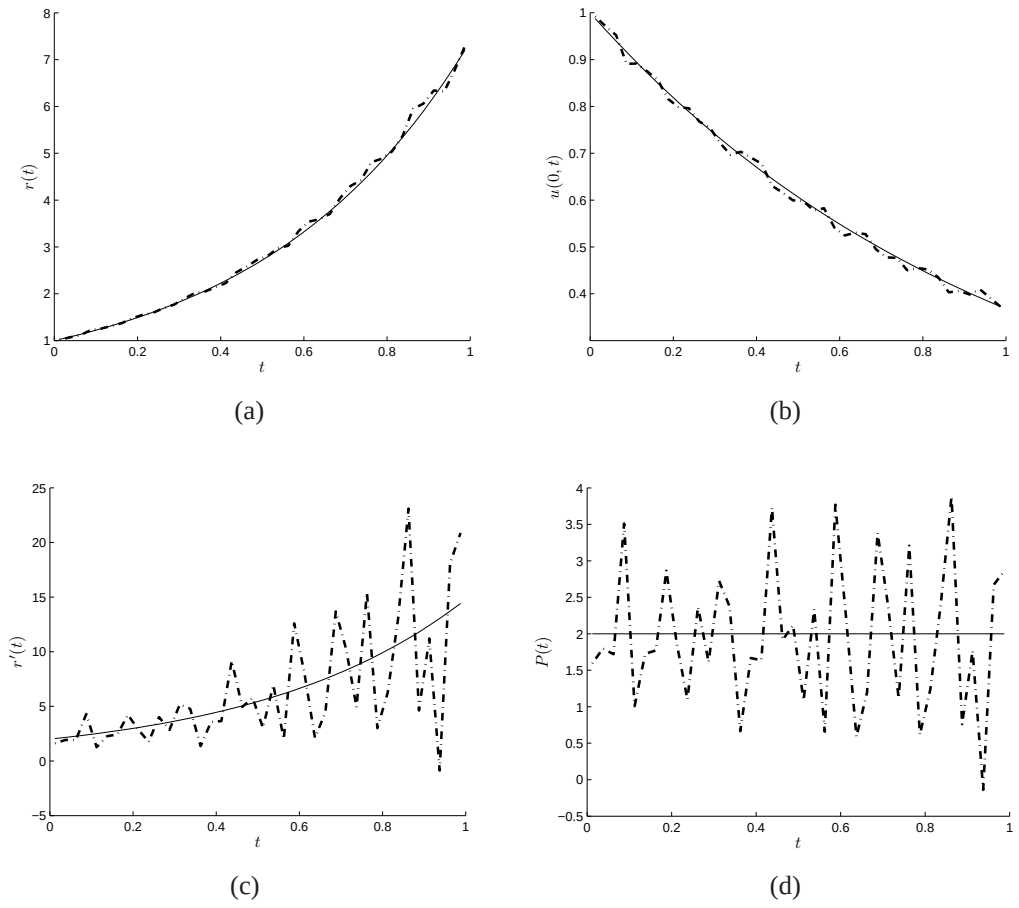

Figure 4.2: The analytical (——) and numerical $(- \cdot -)$ results of (a) $r(t)$, (b) $u(0,t)$, (c) $r'(t)$, and (d) $P(t)$ obtained using no regularisation, i.e. $\lambda = 0$, for $p = 1\%$ noise, for Example 1.

is an unstable procedure. In order to deal with this instability one can employ the smoothing spline regularisation of [59], but this requires the knowledge of the discrepancy between the analytical and numerical values of $r(t)$ in Figure 4.2(a), which is not available if the analytical solution is not available. We shall elaborate in applying this technique later on for Example 2. Alternatively, we employ the second-order Tikhonov regularised solution (4.19) with the choice of the regularisation parameter given by the minimum point of the GCV function (4.21). This is plotted in Figure 4.3 for $p = 1\%$ noise and the minimum yields the value $\lambda_{GCV} = 1.25 \times 10^{-5}$. With the value of $\lambda_{GCV} = 1.25 \times 10^{-5}$, the solution (4.19) for $r(t)$ is plotted in Figure 4.4(a).

By comparing with the previous unregularised solution shown in Figure 4.2(a), one can now see that the obtained solution for $r(t)$ is indeed smooth. Then the process of numerical differentiation (4.22) is permitted and a stable approximation can be obtained, as shown in Figures 4.4(c) and 4.4(d). There are some inaccuracies manifested at the end points $t = 0$ and 1, but this is commonly observed elsewhere when using other stabilising techniques such as the mollification method or, the Tikhonov regularisation for the Fredholm integral equation of the first kind presented in detail in [56]. In Figure 4.4 we have also included for comparative purposes the numerical results obtained with the optimal value, in circle line $(\circ\ \circ\ \circ)$ of the regularisation parameter $\lambda_{opt} = 1.05 \times 10^{-6}$ selected by the trail and error. The RMSE for $\lambda_{GCV} = 1.25 \times 10^{-5}$ and $\lambda_{opt} = 1.05 \times 10^{-6}$ for the numerical results presented in Figure 4.4(d) in comparison with the analytical solution, are 0.324 and 0.219, respectively. Overall from Figure 4.4 it can be seen that there are not much differences between the numerical results obtained with the two values of the regularisation parameter. This confirms that the GCV criterion performs well in choosing a suitable regularisation parameter for obtaining a stable and accurate numerical solution.

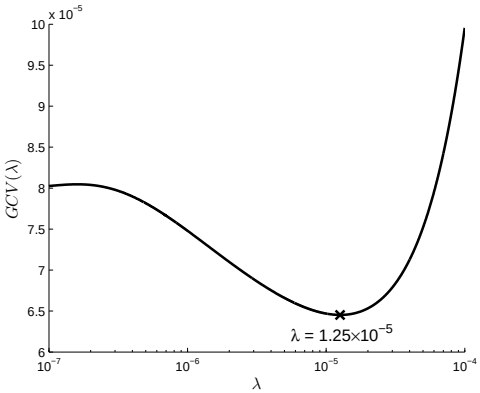

Figure 4.3: The GCV function (4.21), obtained using the second-order Tikhonov regularisation for $p = 1\%$ noise, for Example 1.

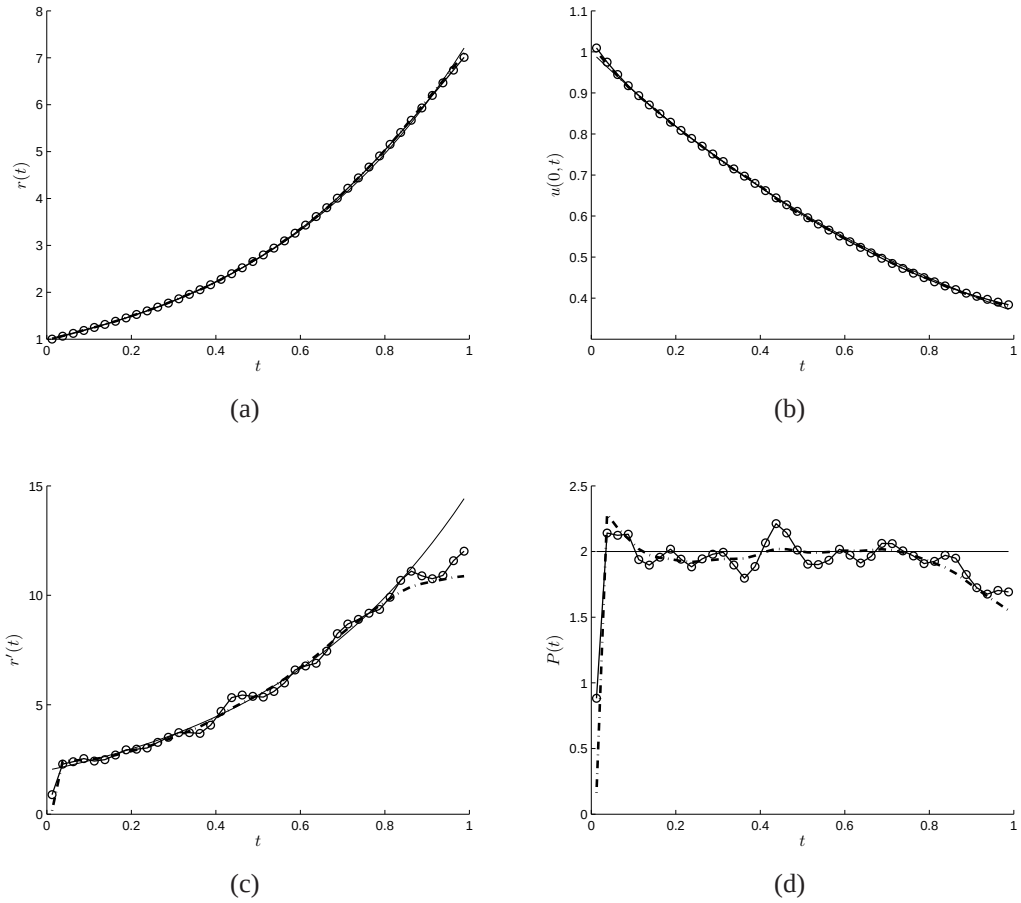

(a) (b)

(c) (d)

Figure 4.4: The analytical (——) and numerical results of (a) $r(t)$, (b) $u(0,t)$, (c) $r'(t)$, and (d) $P(t)$ obtained using the second-order Tikhonov regularisation with $\lambda_{GCV} = 1.25 \times 10^{-5}$ $(- \cdot -)$ and $\lambda_{opt} = 1.05 \times 10^{-6}$ $(\circ \circ \circ)$, for $p = 1\%$ noise, for Example 1.

4.5.2 Example 2

In the previous example, the BEM together with the second-order regularisation and finite differences has been used to solve the inverse problem for the bioheat equation (4.1)–(4.4). In this example we present the BEM together with a smoothing spline regularisation, to be utilised as another regularisation technique, for computing the first-order derivative of a noisy function, see [59]. We consider the inverse problem

(4.1)–(4.4) with the input $L = T = 1$, $\alpha = -1$ and

$$\begin{cases} u_0(x) = x^4(1-x)^3, \quad E(t) = \frac{1}{280}e^{-(t+t^2/2)}, \\ f(x,t) = 6x^2(x-1)(7x^2-8x+2)e^{-(t+t^2/2)}. \end{cases} \tag{4.26}$$

Then the solution of the transformed inverse problem (4.6)–(4.9) is given by

$$v(x,t) = x^4(1-x)^3, \quad r(t) = e^{t+t^2/2}, \tag{4.27}$$

whereas the solution of the original inverse bioheat conduction problem (4.1)–(4.4) is

$$u(x,t) = x^4(1-x)^3e^{-(t+t^2/2)}, \quad P(t) = 1+t.$$

From Figure 4.2(a) of the previous example, we have noticed that the numerical results for the perfusion coefficient $P(t)$ are highly oscillatory and unbounded because the numerical differentiation of a noisy function is an unstable procedure. For Example 1, we have used the second-order Tikhonov regularisation for solving the system of equations (4.19) and this resulted in a smooth approximation for the function $r(t)$, as shown in Figure 4.4(a). Alternatively, for Example 2 we investigate smoothing *a posteriori* the discrete noisy data $\underline{r}$ obtained (without regularisation) like in Figure 4.2(a). This is applied as the smoothing spline technique of [59]. We are seeking therefore a smooth function $\mathfrak{r} \in C^1(\mathbb{R})$ with $\mathfrak{r}'' \in L^2(\mathbb{R})$ which minimises the second-order Tikhonov regularisation functional

$$\mathcal{I}_\Lambda(\mathfrak{r}) := \frac{T}{N}\sum_{j=1}^{N}(\mathfrak{r}(\tilde{t}_j) - \hat{r}_j)^2 + \Lambda\|\mathfrak{r}''\|^2_{L^2(\mathbb{R})}, \tag{4.28}$$

where $\Lambda \geq 0$ is a regularisation parameter to be prescribed and

$$\hat{\underline{r}} = (\hat{r}_j)_{j=\overline{1,N}} = (X^\epsilon)^{-1}\underline{y}, \tag{4.29}$$

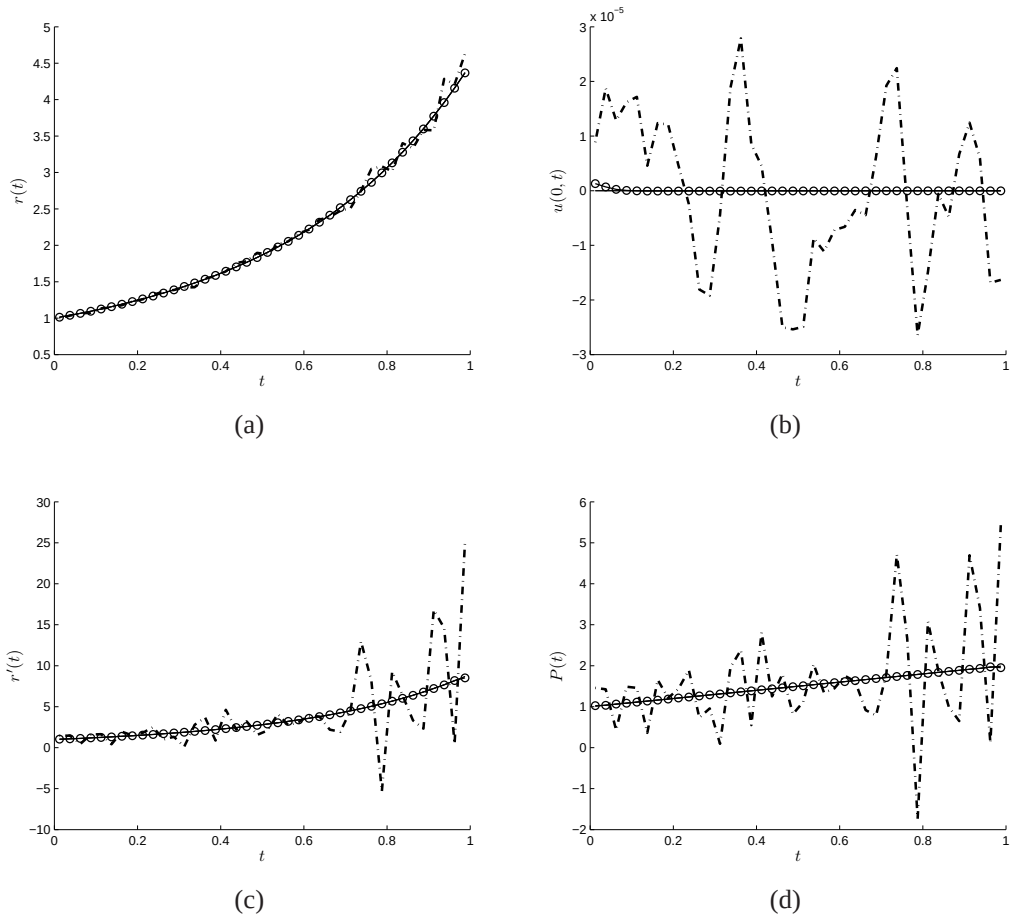

(a) (b)

(c) (d)

Figure 4.5: The analytical (——) and numerical results of (a) $r(t)$, (b) $u(0,t)(t)$, (c) $r'(t)$, and (d) $P(t)$ obtained using no regularisation in (4.31), i.e. $\Lambda = 0$, for exact data $(\circ\circ\circ)$ and for $p = 1\%$ noisy data $(-\cdot-)$, for Example 2.

obtained from Figure 4.2(a). We further approximate the function $\mathfrak{r}$ using cubic splines as

$$\mathfrak{r}(t) = d_1 + d_2 t + \sum_{j=1}^{N} c_j |t - \tilde{t}_j|^3, \tag{4.30}$$

where the coefficients $(c_j)_{j=\overline{1,N}}$ and $(d_j)_{j=\overline{1,2}}$ satisfy the conditions (4.31) and (4.32) below. Inserting (4.30) into (4.28) and minimising the resulting expression with respect to the coefficients $(c_j)_{j=\overline{1,N}}$ and $(d_j)_{j=\overline{1,2}}$ yields the following system of $(N+2)$

equations with $(N+2)$ unknowns, [59],

$$\mathfrak{r}_\Lambda(\tilde{t}_j) + 12\Lambda N c_j = \hat{r}_j, \quad j = \overline{1,N}, \tag{4.31}$$

$$\sum_{j=1}^{N} c_j = \sum_{j=1}^{N} c_j t_j = 0. \tag{4.32}$$

By solving the system of equations (4.31) and (4.32) we obtain the coefficients $(c_j)_{j=\overline{1,N}}$ and $(d_j)_{j=\overline{1,2}}$, and therefore the expression for the smooth function $\mathfrak{r}$, given by (4.30). By differentiating this expression with respect to t we obtain the first-order derivative $\mathfrak{r}'(t)$ given by

$$\mathfrak{r}'(t) = d_2 + 3\sum_{j=1}^{N} c_j (t-\tilde{t}_j)^2 \text{sign}(t-\tilde{t}_j), \tag{4.33}$$

where sign$(\cdot)$ is the signum function. This derivative $\mathfrak{r}'(t)$ is presented as $r'(t)$ in (4.27). From (4.31), one can observe that if $\Lambda = 0$ then $\mathfrak{r}_0(\tilde{t}_i) = \hat{r}(\tilde{t}_i)$ for $i = \overline{1,N}$. In the case of exact data actually one can take $\Lambda = 0$, but for noisy data taking $\Lambda = 0$ produces a highly unbounded and oscillatory solution for $r'(t)$ and $P(t)$, as shown in Figures 4.5(c) and 4.5(d). For noisy data, reference [59] suggests the *a priori* choice

$$\Lambda = \frac{T}{N}\sum_{j=1}^{N}(r_{exact,j} - \hat{r}_j)^2, \tag{4.34}$$

where $r_{exact,j} = r_{exact}(\tilde{t}_j)$ represents an analytical solution r, given by (4.27), at time $\tilde{t}_j$ for $j = \overline{1,N}$. For $p = 1\%$ noise, we have $\Lambda \approx 8 \times 10^{-3}$. The numerical results for $r'(t)$ and $P(t)$ obtained using the smoothing spline regularisation technique with this choice of Λ oversmoothes the exact solution, as shown in Figure 4.6 in dash-dot line $(- \cdot -)$. However, the Morozov's discrepancy principle [40] based on the *a posteriori* choice of Λ such that

$$\frac{T}{N}\sum_{j=1}^{N}(\mathfrak{r}_\Lambda(\tilde{t}_j) - \hat{r}_j)^2 \approx \frac{T}{N}\sum_{j=1}^{N}(r_{exact,j} - \hat{r}_j)^2, \tag{4.35}$$

produces $\Lambda_{dis} = 7 \times 10^{-5}$ which yields more accurate approximations, as also shown

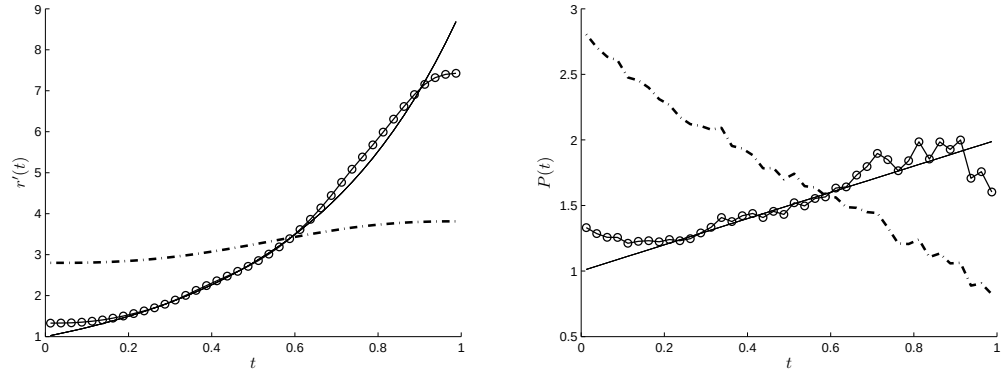

(a) (b)

Figure 4.6: The analytical (——) and numerical results of (a) $r'(t)$ and (b) $P(t)$ obtained using the smoothing spline regularisation with $\Lambda_{dis} = 7\times10^{-5}$ $(\circ\circ\circ)$ and $\Lambda = 8\times10^{-3}$ $(- \cdot -)$, as defined in (4.34), for $p = 1\%$ noise, for Example 2.

in Figure 4.6 in circle line $(\circ\circ\circ)$.

Finally, although not illustrated, it is reported that for higher amounts of noise the numerical reconstructions are less stable.

4.6 Conclusions

The inverse problem of finding a time-dependent blood perfusion coefficient for the bioheat equation with nonlocal boundary conditions and mass/energy specification has been investigated. The inverse problem has been transformed to an inverse heat source problem with an unknown term present in the integral over-determination condition. The numerical discretisation was based on the BEM together with the Tikhonov regularisation and the GCV for the choice of the regularisation parameter. We have also applied the smoothing spline technique for differentiating a noisy function with *a priori* and *a posteriori* choices of the regularisation parameters. For a couple of typical benchmark test examples, accurate and stable numerical solutions have been obtained.

Chapter 5

Determination of a Time-dependent Heat Source with a Dynamic Boundary Condition

5.1 Introduction

In the Chapters 3 and 4, we have considered inverse time-dependent source problems for the heat equation with various types of conditions such as integral, local or nonlocal. In the present chapter, we consider yet another reconstruction of a time-dependent heat source with the integral over-determination measurement of the thermal energy of the system and a new dynamic-type boundary condition. This model can be used in heat transfer and diffusion processes with a time-dependent source parameter to be determined. Also, in acoustic scattering or damage corrosion the new dynamic-type boundary condition (5.4) below is also known as a generalised impedance boundary condition, [4–7].

The well-posedness of the inverse problem studied in this chapter was established in [19], and we aim to obtain the numerical solution by using the BEM together with a regularisation method.

This chapter is organised as follows. In Section 5.2, the mathematical formulation of the inverse problem is described. The numerical discretisation of the problem based on the BEM is described in Section 5.3. Section 5.4 discusses numerical results obtained for three of benchmark test examples and emphasises the importance of employing the Tikhonov regularisation with the choice of regularisation parameter based on either the GCV criterion or the discrepancy principle, in order to achieve a stable numerical solution. Finally, Section 5.5 presents the conclusions of the chapter.

5.2 Mathematical formulation

Consider the following initial-boundary value problem of finding the time-depending heat source $r(t) \in C([0,T])$ and the temperature $u(x,t) \in C^{2,1}(D_T) \cap C^{1,0}(\overline{D}_T)$ which satisfy the heat equation:

$$u_t = u_{xx} + r(t)f(x,t), \quad (x,t) \in \overline{D}_T, \tag{5.1}$$

where $L = 1$ in the definition of D_T in (1.1), subject to the initial condition (1.7), namely

$$u(x,0) = u_0(x), \quad x \in [0,1], \tag{5.2}$$

and the boundary conditions

$$u(0,t) = 0, \quad t \in (0,T], \tag{5.3}$$

$$au_{xx}(1,t) + \alpha u_x(1,t) + bu(1,t) = 0, \quad t \in (0,T], \tag{5.4}$$

where f and u_0 are given functions and a, b, α are given numbers not simultaneously equal to zero. The well-posedness of this direct problem was established in [34].

Taking into account the equation (5.1) at $x = 1$, the boundary condition (5.4)

becomes

$$au_t(1,t) + \alpha u_x(1,t) + bu(1,t) = ar(t)f(1,t), \quad t \in (0,T]. \tag{5.5}$$

In order to add further physics to the problem, we mention that the boundary condition (5.5) is observed in the process of cooling of a thin solid bar one end of which is placed in contact with a fluid [36]. Another possible application of such type of boundary condition is announced in [9, p.79], as this boundary condition represents a boundary reaction in diffusion of a chemical. We finally mention that we have also previously encountered the dynamic boundary condition (5.5) when modelling a transient flow pump experiment in a porous medium [39].

When the function $r(t)$ for $t \in [0,T]$ is unknown, the inverse problem formulates as a problem of finding a pair of functions $(r(t), u(x,t))$ which satisfy the equation (5.1), initial condition (5.2), the boundary conditions (5.3) and (5.4) (or (5.5)), and the energy/mass overdetermination measurement

$$\int_0^1 u(x,t)\,dx = E(t), \quad t \in [0,T]. \tag{5.6}$$

This overdetermination condition is encountered in modelling applications related to particle diffusion in turbulent plasma, as well as in heat conduction problems in which the law of variation $E(t)$ of the total energy of heat in a rod is given, [22].

If we let $u(x,t)$ represent the temperature distribution, then the above-mentioned inverse problem can be regarded as a source control problem. The source control parameter $r(t)$ needs to be determined from the measurement of the thermal energy $E(t)$.

Denote $\Phi^4_{n_0}[0,1] := \{\phi(x) \in C^4[0,1]; \phi(0) = \phi''(0) = 0,\ \phi(1) = \phi'(1) = \phi''(1) = \phi'''(1) = 0,\ \int_0^1 \phi(x) y_{n_0}(x) dx = 0\}$, where $(y_n)_{n\geq 0}$ denote the eigenfunctions

of the spectral problem

$$\begin{cases} y''(x) + \mu y(x) = 0, \quad x \in [0,1], \\ y(0) = 0, \\ (a\mu - b)y(1) = \alpha y'(1), \end{cases} \tag{5.7}$$

where its eigenvalue μ_n and eigenfunctions $y_n(x)$, for $n = 0, 1, 2, \ldots$, have the following asymptotic behavior:

$$\sqrt{\mu_n} = \pi n + O\left(\frac{1}{n}\right), \quad y_n(x) = \sin(\pi n x) + O\left(\frac{1}{n}\right),$$

for sufficiently large n. The following theorem proved in [19] established the existence of a unique solution of the inverse problem (5.1)–(5.3), (5.5) and (5.6).

Theorem 5.2.1 *Let $a\alpha > 0$ and assume that the following conditions are satisfied:*

(A_1) $u_0(x) \in \Phi^4_{n_0}[0,1]$;

(A_2) $E(t) \in C^1[0,T]$; $E(0) = \int_0^1 u_0(x)dx$;

(A_3) $f(x,t) \in C(\overline{D}_T)$; $f(\cdot,t) \in \Phi^4_{n_0}[0,1]$, $\forall t \in [0,T]$; *and* $\int_0^1 f(x,t)dx \neq 0$, $\forall t \in [0,T]$;

Then the inverse problem (5.1)–(5.3), (5.5) *and* (5.6) *has a unique solution* $(r(t), u(x,t)) \in C[0,T] \times (C^{2,1}(D_T) \cap C^{2,0}(\overline{D}_T))$. *Moreover,* $u(x,t) \in C^{2,1}(\overline{D}_T)$.

Although the inverse problem is uniquely solvable, it is still ill-posed since small errors in the input data (5.6) cause large errors in the input source $r(t)$.

In the next section we will describes the discretisation of the inverse problem using the BEM, whilst Section 5.4 will discuss the regularisation of the numerical solution.

5.3 Boundary element method (BEM)

In this section, we explain the numerical procedure for discretising the inverse problem (5.1)–(5.3), (5.5) and (5.6) by using the BEM. As introduced in Section 1.3, the use of BEM recasts the heat equation (5.1) in the boundary integral form (3.5). Using the same discretisation as described in Chapters 2–4, and applying the boundary condition (5.3), the boundary integral equation (3.5) becomes

$$\eta(x)u(x,t) = \sum_{j=1}^{N} [A_{0j}(x,t)q_{0j} + A_{Lj}(x,t)q_{lj} - B_{Lj}(x,t)h_{Lj}] + \sum_{k=1}^{N_0} C_k(x,t)u_{0,k} + \sum_{j=1}^{N} D_j(x,t)r_j, \quad (x,t) \in [0,1] \times (0,T]. \tag{5.8}$$

On applying the BEM and the boundary condition (5.3), we obtain the system of $2N$ linear equations,

$$A_0\mathbf{q}_0 + A_L\mathbf{q}_L - B_L\mathbf{h}_L + C\mathbf{u}_0 + D\mathbf{r} = \mathbf{0}. \tag{5.9}$$

In order to apply the boundary condition (5.5) we need to approximate the time-derivative $u_t(1,t)$ by using finite differences. For this, we use the $O(h^2)$ finite difference formulae

$$\begin{cases} u_t(1,\tilde{t}_1) = \dfrac{u(1,\tilde{t}_2)/3 + u(1,\tilde{t}_1) - 4u_0(1)/3}{h}, \\ u_t(1,\tilde{t}_2) = \dfrac{5u(1,\tilde{t}_2)/3 - 3u(1,\tilde{t}_1) + 4u_0(1)/3}{h}, \\ u_t(1,\tilde{t}_i) = \dfrac{3u(1,\tilde{t}_i)/2 - 2u(1,\tilde{t}_{i-1}) + u(1,\tilde{t}_{i-2})/2}{h}, \quad i = \overline{3,N}, \end{cases}$$

where the step size $h = T/N$ and $\tilde{t}_i = \frac{t_{i-1}+t_i}{2}$ as defined in Chapter 1. Applying the expressions above into the boundary condition (5.5) yields the linear system of N

equations as follows:

$$\begin{cases} \frac{a}{h}u(1,\tilde{t}_1) + \frac{a}{3h}u(1,\tilde{t}_2) + bu(1,\tilde{t}_1) = ar(\tilde{t}_1)f(1,\tilde{t}_1) + \frac{4a}{3h}u_0(1) - \alpha u_x(1,\tilde{t}_1), \\ -\frac{3a}{h}u(1,\tilde{t}_1) + \frac{5a}{3h}u(1,\tilde{t}_2) + bu(1,\tilde{t}_2) = ar(\tilde{t}_2)f(1,\tilde{t}_2) - \frac{4a}{3h}u_0(1) - \alpha u_x(1,\tilde{t}_2), \\ \frac{a}{2h}u(1,\tilde{t}_{i-2}) - \frac{2a}{h}u(1,\tilde{t}_{i-1}) + \frac{3a}{2h}u(1,\tilde{t}_i) + bu(1,\tilde{t}_i) = ar(\tilde{t}_i)f(1,\tilde{t}_i) - \alpha u_x(1,\tilde{t}_i), \end{cases}$$

for $i = \overline{3,N}$. This system can be rewritten as

$$\mathrm{Sh}_L = \mathrm{Fr} + \tilde{\mathrm{u}}_0 - \alpha \mathrm{q}_L, \tag{5.10}$$

where $\mathrm{F} = \mathrm{diag}(af(1,\tilde{t}_1), \ldots, af(1,\tilde{t}_N))$, and

$$\mathrm{S} = \begin{bmatrix} a/h+b & a/3h & 0 & . \\ -3a/h & 5a/3h+b & 0 & . \\ a/2h & -2a/h & 3a/2h+b & . \\ . & . & . & . \\ 0 & a/2h & -2a/h & 3a/2h+b \end{bmatrix}_{N\times N}, \quad \tilde{\mathrm{u}}_0 = \begin{bmatrix} 4au_0(1)/3h \\ -4au_0(1)/3h \\ 0 \\ . \\ 0 \end{bmatrix}_N.$$

Assuming $\alpha \neq 0$, eliminating q_L can be done by applying the derived matrix form of (5.10), i.e.

$$\mathrm{q}_L = \frac{1}{\alpha}\left(\mathrm{Fr} + \tilde{\mathrm{u}}_0 - \mathrm{Sh}_L\right), \tag{5.11}$$

into (5.9), this gives (5.9) and (5.10) results as

$$\begin{bmatrix} \mathrm{h}_L \\ \mathrm{q}_0 \end{bmatrix} = \left[\left(\frac{1}{\alpha}A_L\mathrm{S} + B_L\right) \;\middle|\; -A_0\right]^{-1}\left(\frac{1}{\alpha}A_L\mathrm{Fr} + \frac{1}{\alpha}A_L\tilde{\mathrm{u}}_0 + C\mathrm{u}_0 + D\mathrm{r}\right), \tag{5.12}$$

where the invertible matrix $\left[\left(\frac{1}{\alpha}A_L\mathrm{S} + B_L\right) \;\middle|\; -A_0\right]$ is a $2N \times 2N$ matrix formed with the $2N \times N$ block matrices $\left(\frac{1}{\alpha}A_L\mathrm{S} + B_L\right)$ and $-A_0$ separated by the vertical line.

Next, we collocate the over-determination condition (5.6) by using the midpoint

numerical integration approximation as same as in (3.11). Then the expression (5.8) at $(\tilde{x}_k, \tilde{t}_i)$, can be rewritten as

$$\frac{1}{N_0}\sum_{k=1}^{N_0}\left[A_{0,k}^{(1)}\mathfrak{q}_0 + A_{L,k}^{(1)}\mathfrak{q}_L - B_{L,k}^{(1)}\mathfrak{h}_L + C_k^{(1)}\mathfrak{u}_0 + D_k^{(1)}\mathfrak{r}\right] = \mathfrak{E}, \tag{5.13}$$

where

$$A_{0,k}^{(1)} = \left[A_{0j}(\tilde{x}_k, \tilde{t}_i)\right]_{N\times N}, \quad A_{L,k}^{(1)} = \left[A_{Lj}(\tilde{x}_k, \tilde{t}_i)\right]_{N\times N}, \quad B_{L,k}^{(1)} = \left[B_{Lj}(\tilde{x}_k, \tilde{t}_i)\right]_{N\times N},$$
$$C_k^{(1)} = \left[C_l(\tilde{x}_k, \tilde{t}_i)\right]_{N\times N_0}, \quad D_k^{(1)} = \left[D_j(\tilde{x}_k, \tilde{t}_i)\right]_{N\times N}, \quad k, l = \overline{1, N_0}, i, j = \overline{1, N}.$$

When the boundary condition (5.3) is applied, the expression (5.13) can be, via (5.11), rewritten as

$$\frac{1}{N_0}\sum_{k=1}^{N_0}\left[A_{0,k}^{(1)}\mathfrak{q}_0 + \frac{1}{\alpha}A_{L,k}^{(1)}\left(\mathrm{F}\mathfrak{r} + \tilde{\mathfrak{u}}_0 - \mathrm{S}\mathfrak{h}_L\right) - B_{L,k}^{(1)}\mathfrak{h}_L + C_k^{(1)}\mathfrak{u}_0 + D_k^{(1)}\mathfrak{r}\right] = \mathfrak{E}. \tag{5.14}$$

Finally, eliminating $\mathfrak{q}_0$ and $\mathfrak{h}_L$ between (5.12) and (5.14), the unknown discretised source $\mathfrak{r}$ can be found by solving the $N \times N$ linear system of equations

$$X\mathfrak{r} = \underline{\mathfrak{y}}, \tag{5.15}$$

where

$$X = \frac{1}{N_0}\sum_{k=1}^{N_0}\left\{\left[\left(\frac{1}{\alpha}A_{L,k}^{(1)}\mathrm{S} + B_{L,k}^{(1)}\right) \;\middle|\; -A_{0,k}^{(1)}\right]\left[\left(\frac{1}{\alpha}A_L\mathrm{S} + B_L\right) \;\middle|\; -A_0\right]^{-1}\right.$$
$$\left.\times\left(\frac{1}{\alpha}A_L\mathrm{F} + D\right) - \left(\frac{1}{\alpha}A_{L,k}^{(1)}\mathrm{F} + D_k^{(1)}\right)\right\},$$
$$\underline{\mathfrak{y}} = \frac{1}{N_0}\sum_{k=1}^{N_0}\left\{C_k^{(1)}\mathfrak{u}_0 + \frac{1}{\alpha}A_{L,k}^{(1)}\tilde{\mathfrak{u}}_0 - \left[\left(\frac{1}{\alpha}A_{L,k}^{(1)}\mathrm{S} + B_{L,k}^{(1)}\right) \;\middle|\; -A_{0,k}^{(1)}\right]\right.$$
$$\left.\times\left[\left(\frac{1}{\alpha}A_L\mathrm{S} + B_L\right) \;\middle|\; -A_0\right]^{-1}\left(C\mathfrak{u}_0 + \frac{1}{\alpha}A_L\tilde{\mathfrak{u}}_0\right)\right\} - \mathfrak{E}.$$

As we have mentioned previously the inverse problem under investigation is ill-posed, and consequently, the system of equation (5.15) is ill-conditioned. In the next section, we will discuss the regularisation of the numerical solution together with choices of regularisation parameter based on either the GCV criterion or the discrepancy principle.

5.4 Numerical examples and discussion

This section presents three benchmark test examples with smooth and non-smooth continuous source functions in order to test the accuracy of the BEM numerical procedure introduced earlier in Section 5.3. In order to illustrate the accuracy of the numerical results, the RMSE defined in (2.49) is also used here.

5.4.1 Example 1

In the first example, we consider the case of smooth continuous unknown source function, given by the analytical solution

$$u(x,t) = x^2 e^t, \quad r(t) = e^t, \tag{5.16}$$

for the inverse problem (5.1)–(5.3), (5.5) and (5.6) with the input data $T = 1$, $a = \alpha = 1$, $b = -4$,

$$u(x,0) = u_0(x) = x^2, \quad f(x,t) = x^2 - 2, \tag{5.17}$$

The direct problem (5.1)–(5.3) and (5.5), when $r(t) = e^t$ is known, is considered first with $N = N_0 \in \{20, 40, 80\}$ obtained by (5.11), (5.12) and (5.13), and the RMSE results are shown in Table 5.1. From this table it can be concluded that the BEM numerical solution is convergent to the corresponding exact values

$$u(1,t) = e^t, \quad u_x(0,t) = 0, \quad u_x(1,t) = 2e^t, \quad E(t) = e^t/3, \tag{5.18}$$

for $t \in [0, 1]$, as the number of boundary elements increases.

Table 5.1: The RMSE for $u(1,t)$, $u_x(0,t)$, $u_x(1,t)$ and $E(t)$ obtained using the BEM for the direct problem with $N = N_0 \in \{20, 40, 80\}$, for Example 1.

$N = N_0$	RMSE			
	$u(1,t)$	$u_x(0,t)$	$u_x(1,t)$	$E(t)$
20	6.43E-3	2.79E-3	8.85E-3	2.65E-3
40	2.20E-3	9.68E-4	2.98E-3	9.07E-4
80	7.46E-4	3.32E-4	1.00E-3	3.08E-4

Next, we consider the inverse problem (5.1)–(5.3), (5.5) and (5.6) and we use the BEM with $N = N_0 = 40$ for solving the resulting system of equations (5.15). Figure 5.1 displays the analytical and numerical results of $r(t)$, $u(1,t)$, $u_x(0,t)$, and $u_x(1,t)$ and very good agreement can be observed.

In practice, the contamination of measured data by unplanned error is unavoidable. Thus we add noise to the input energy data $E(t)$ in (5.6) in order to test the stability of the solution. Here, the perturbed input data E^{ϵ} is defined as same as described in (3.14), with the standard deviation $\sigma = \dfrac{ep}{3}$ and $p \in \{1, 3, 5\}\%$. This perturbation means that the known right-hand side vector $\underline{\mathrm{y}}$ of the linear system (5.15) is contaminated with noise, denoted as $\underline{\mathrm{y}}^{\epsilon}$. Then, when noise is present, we have to solve the following system of linear equations instead of (5.15):

$$X\mathrm{r} = \underline{\mathrm{y}}^{\epsilon}. \tag{5.19}$$

Initially, we have tried to solve the above disturbed system (5.19) with $p = 1\%$ noise in the input data (5.6) by using the straightforward inversion of (5.19), i.e. $\mathrm{r} = X^{-1}\underline{\mathrm{y}}^{\epsilon}$, illustrated in Figure 5.2. From this figure it can be seen that the numerical solutions for $r(t)$, $u_x(0,t)$ and $u_x(1,t)$ shown by the dash-dot line ($-\cdot-$) are unstable. However, the result for $u(1,t)$ seems to remain stable.

To overcome this instability, we employ the Tikhonov regularisation method as described in (1.34) with a second-order differential regularisation matrix in (4.20). As happened previously with some of our investigations in Chapters 2 and 3, we report that

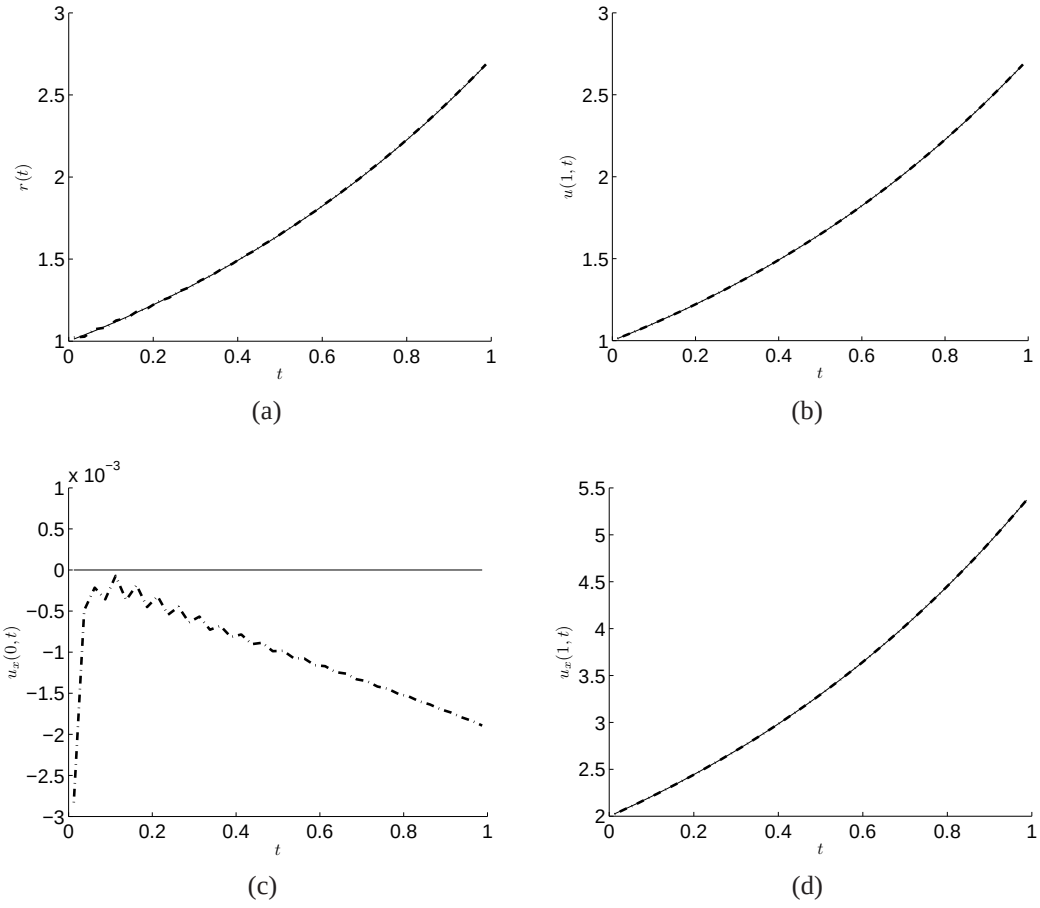

Figure 5.1: The analytical (——) and numerical results $(- \cdot -)$ of (a) $r(t)$, (b) $u(1,t)$, (c) $u_x(0,t)$, and (d) $u_x(1,t)$ for exact data, for Example 1.

the second-order Tikhonov regularisation has produced more accurate results than the zeroth- or first-order regularisation and therefore, only the numerical results obtained using the former regularisation are illustrated in this section.

A popular method for choosing the regularisation parameter is the GCV criterion which is based on the minimisation technique, as we have detailed in Section 1.6. For $p = 1\%$ noise, this minimisation yields the minimum point of the GCV function (1.35) occurring at λ_{GCV}=4.3E-6. Then the numerical results obtained using the Tikhonov regularisation with this value of λ_{GCV}, illustrated by circles $(\circ\circ\circ)$ in Figure 5.2, show that accurate and stable numerical solutions are achieved.

Next, we increase to $p = 3\%$ and 5% the percentage of noise. Figure 5.3 presents

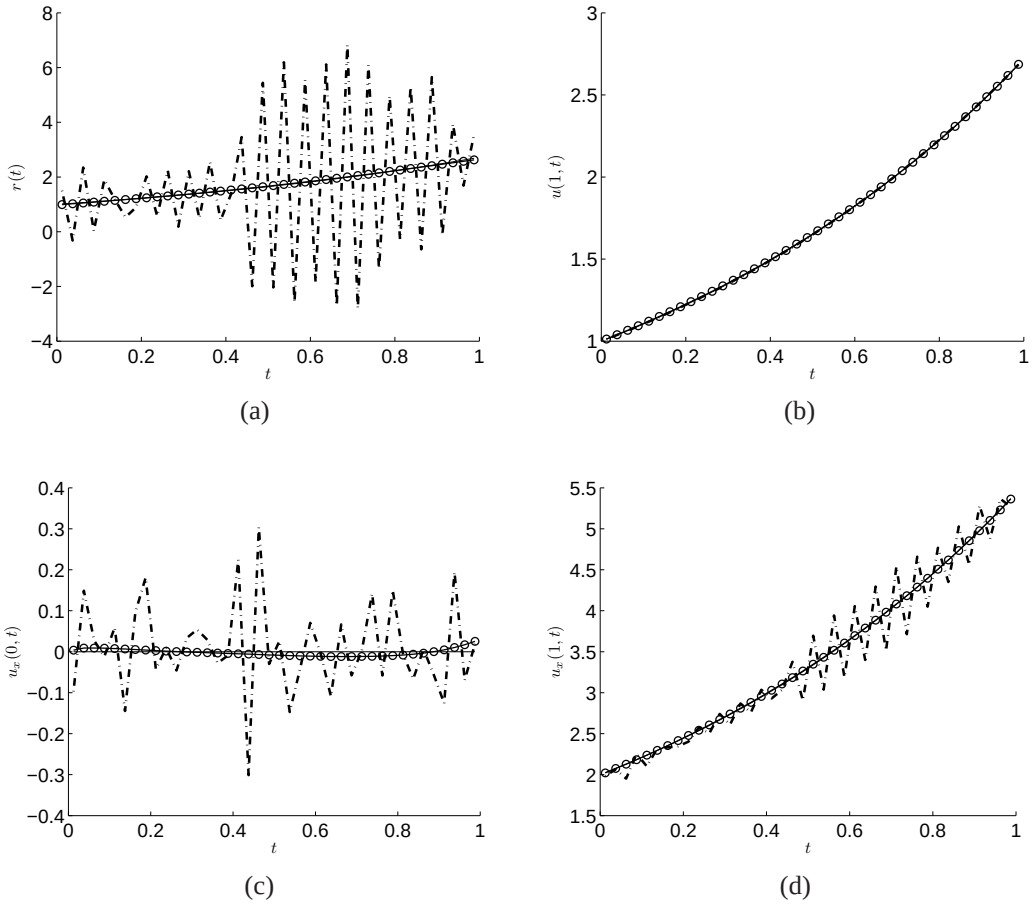

Figure 5.2: The analytical (——) and numerical results of (a) $r(t)$, (b) $u(1,t)$, (c) $u_x(0,t)$, and (d) $u_x(1,t)$ obtained using the straightforward inversion $(- \cdot -)$ with no regularisation, and the second-order Tikhonov regularisation $(\circ \circ \circ)$ with the regularisation parameter λ=4.3E-6 suggested by the GCV method, for $p = 1\%$ noise, for Example 1.

the analytical and numerical results obtained using the second-order Tikhonov regularisation with the regularisation parameter suggested by the GCV method, namely λ_{GCV}=7.4E-6 for $p = 3\%$, and λ_{GCV}=2.7E-5 for $p = 5\%$. From this figure one can observe that stable and accurate results for $r(t)$, $u(1,t)$, $u_x(0,t)$ and $u_x(1,t)$ with $p = 3\%$ noise are attained, whereas the numerical results for $p = 5\%$ noisy input are rather inaccurate, but they remain stable. For completeness, the RMSE errors are displayed in Table 5.2.

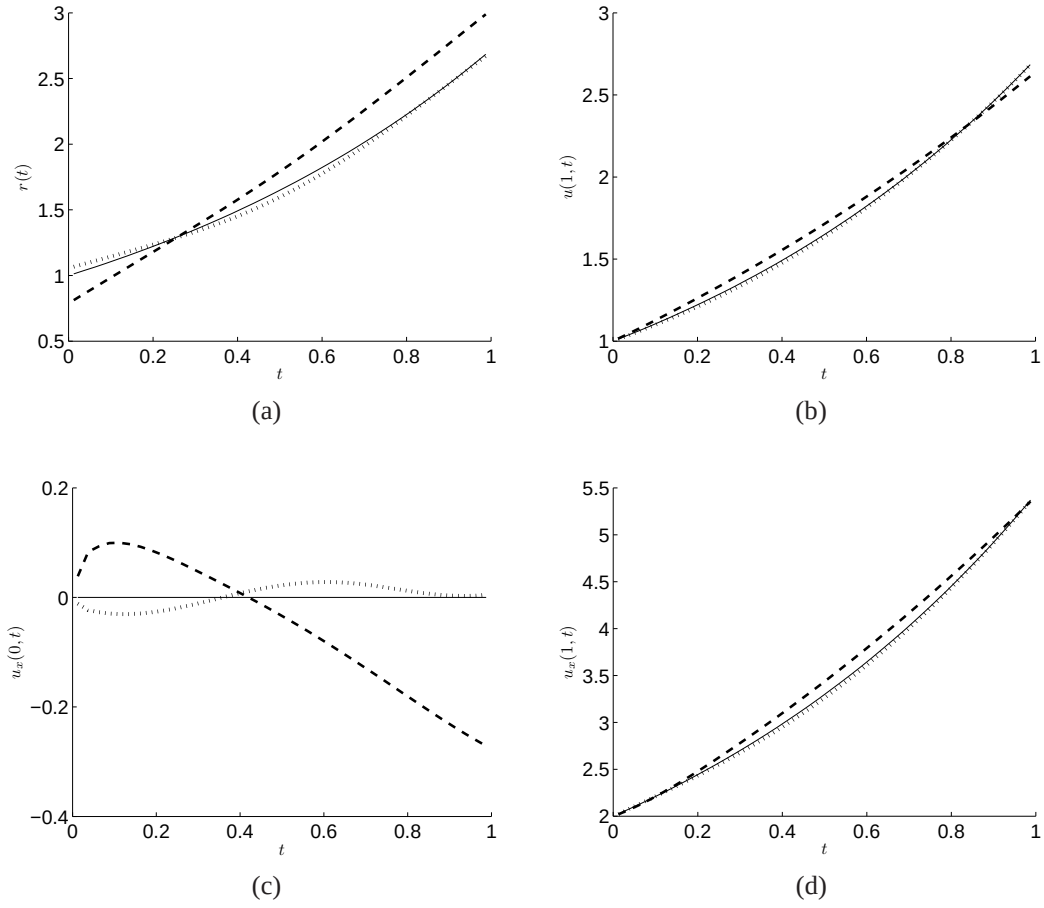

Figure 5.3: The analytical (——) and numerical results of (a) $r(t)$, (b) $u(1,t)$, (c) $u_x(0,t)$, and (d) $u_x(1,t)$ obtained using the second-order Tikhonov regularisation with the regularisation parameter suggested by the GCV method, for $p = 3\%$ $(\cdots)$ and $p = 5\%$ $(---)$, for Example 1.

5.4.2 Example 2

The previous example possessed an analytical solution being explicitly available; however the source function $f(x,t)$ chosen did not satisfy the condition in (A_3) of Theorem 5.2.1 that $f \in \Phi^4_{n_0}[0,1]$. Therefore, in this subsection we aim to construct an example for which the conditions of existence and uniqueness of solution of Theorem 5.2.1 are satisfied. We choose $T = 1$, $a = \alpha = 1$, $b = 0$ and $u_0(x) = 0$.

In the case $a = \alpha = 1$, $b = 0$ the problem (5.7) has the eigenvalues $\mu_n = \nu_n^2$, where ν_n are the positive roots of the transcendental equation $\nu \sin(\nu) = \cos(\nu)$. The

Table 5.2: The regularisation parameters λ and the RMSE for $r(t)$, $u(1,t)$, $u_x(0,t)$ and $u_x(1,t)$, obtained using the BEM with $N = N_0 = 40$ combined with the second-order Tikhonov regularisation for $p \in \{0, 1, 3, 5\}\%$ noise, for Example 1.

p	parameter λ	RMSE			
		$r(t)$	$u(1,t)$	$u_x(0,t)$	$u_x(1,t)$
0	0	4.16E-3	2.47E-4	1.20E-3	8.85E-4
1%	0	2.70	1.72E-2	1.12E-1	2.64E-1
1%	λ_{GCV}=4.3E-6	1.73E-2	2.57E-3	8.92E-3	5.47E-3
3%	0	5.21	4.13E-2	3.51E-1	5.02E-1
3%	λ_{GCV}=7.4E-6	3.32E-2	9.73E-3	1.97E-2	2.25E-2
5%	0	4.74	5.51E-2	4.64E-1	4.54E-1
5%	λ_{GCV}=2.7E-5	1.95E-1	4.63E-2	1.29E-1	9.79E-2

corresponding eigenfunctions are $y_n(x) = \sin(\nu_n x)$. The first eigenvalue is given by $\nu_0 = \sqrt{\mu_0} = 0.860333$. Then choosing

$$f(x,t) = x^3(1-x)^4(\beta_1 x + \beta_2), \tag{5.20}$$

we can determine the constants β_1 and β_2 such that $f \in \Phi_0^4[0,1]$ (choosing $n_0 = 0$ for simplicity), as required by the condition (A_3) of Theorem 5.2.1, i.e. $f(x,t) \in \Phi_{n_0}^4[0,1]$, $\forall t \in [0,t]$. This imposes

$$0 = \int_0^1 f(x,t)\sin(\nu_0 x)\,dx = \int_0^1 x^3(1-x)^4(\beta_1 x + \beta_2)\sin(\nu_0 x)\,dx.$$

After some calculus, choosing $\beta_2 = -1$ it follows that $\beta_1 \approx 2.011$. With these values of β_1 and β_2 we also satisfy that $\int_0^1 f(x,t)\,dx = -0.00037$ is non-zero, as required by condition (A_3). We aim to retrieve a non-smooth source function given by

$$r(t) = \left| t - \frac{1}{2} \right|, \quad t \in [0,t]. \tag{5.21}$$

In this case, the analytical solution of the direct problem for the temperature $u(x,t)$ is not available. Thus the energy $E(t)$ is not available either. In such a situation, we simulate the data (5.6) numerically by solving first the direct problem (5.1)–(5.3) and

(5.5) with r known and given by (5.21). The numerical solutions for $u(1,t)$, $u_x(0,t)$, $u_x(1,t)$ and $E(t)$ obtained using the BEM with $N = N_0 \in \{20, 40, 80\}$ are shown in Figure 5.4. From this figure it can be seen that convergent numerical solutions are obtained.

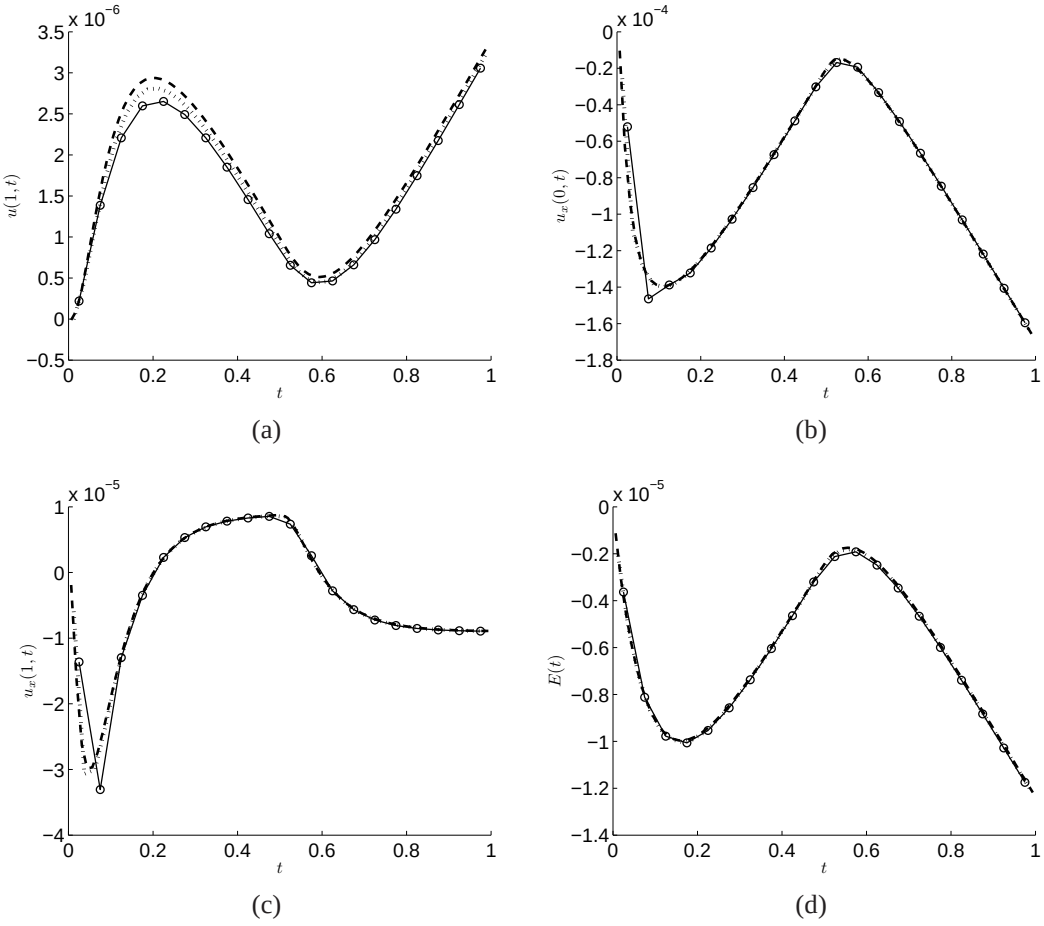

Figure 5.4: The numerical results of (a) $u(1,t)$, (b) $u_x(0,t)$, (c) $u_x(1,t)$, and (d) $E(t)$ obtained by solving the direct problem with $N = N_0 \in \{20(\circ\circ\circ),\ 40(\cdots),\ 80(---)\}$, for Example 2.

To investigate the inverse problem (5.1)–(5.3), (5.5) and (5.6), we use the numerical results for $E(t)$ in Figure 5.4(d) obtained using the BEM with $N = N_0 = 40$, as the input data (5.6). In order to avoid committing an inverse crime we keep $N = 40$, but we use a different N_0, say $N_0 = 30$, than 40 which was used in the direct problem simulation. Figure 5.5 shows the numerical results obtained without regularisation,

i.e. $\lambda = 0$, for $p = 0$ (exact) and $p = 1\%$ (noisy) data. Remark that from Figure 5.4(d), the standard deviation for generating noise is given by $\sigma = 1.2 \times 10^{-5}p$. From Figure 5.5 it can be seen that, for exact data, the straightforward inversion of (5.15) produces very accurate results. However, when noise is introduced into the measured data E^{ϵ}, here we are solving the linear system of equations $X\mathrm{r} = \underline{\mathrm{y}}^{\epsilon}$ instead of $X\mathrm{r} = \underline{\mathrm{y}}$, the numerical retrievals of especially $r(t)$ and $u_x(1,t)$ become highly oscillatory unstable.

In order to retrieve the stability, as in Example 1, the second-order Tikhonov regularisation with the GCV criterion are employed and the numerically obtained results are shown in Figure 5.6. The numerical results from the direct problem presented in Figures 5.7(a)–5.7(c) are used to compare in Figures 5.6(b)–5.6(d) the numerical results for $u(1,t)$, $u_x(0,t)$, and $u_x(1,t)$, respectively, of the inverse problem. Whereas the numerical solution for $r(t)$ of the inverse problem is compared with the analytical solution (5.21) in Figure 5.6(a). From Figure 5.6 it can be seen that stable and accurate numerical solutions are obtained. For completeness, the RMSE errors and the GCV values for λ are displayed in Table 5.3.

Table 5.3: The regularisation parameters λ and the RMSE for $r(t)$, $u(1,t)$, $u_x(0,t)$ and $u_x(1,t)$, obtained using the BEM with $N = 40$ and $N_0 = 30$ combined with the second-order Tikhonov regularisation for $p \in \{0, 1, 3, 5\}\%$ noise, for Example 2.

$p(\%)$	parameter λ	RMSE			
		$r(t)$	$u(1,t)$	$u_x(0,t)$	$u_x(1,t)$
0	0	2.90E-4	2.12E-10	2.94E-8	1.07E-8
1%	0	9.98E-2	2.71E-8	9.55E-6	3.55E-6
1%	λ_{GCV}=3.2E-16	5.47E-3	1.62E-8	1.28E-6	4.12E-7
3%	0	3.63E-1	1.05E-7	3.39E-5	1.27E-5
3%	λ_{GCV}=1.1E-15	1.37E-2	5.96E-8	3.56E-6	9.37E-7
5%	0	5.03E-1	1.70E-7	4.85E-5	1.80E-5
5%	λ_{GCV}=9.0E-16	2.17E-2	9.88E-8	5.68E-6	1.21E-6

If one would like to make a fair comparison between the accuracy of the numerical results obtained for Examples 1 and 2, the RMSE values presented in Tables 5.2 and 5.3 should be divided by the maximum absolute values of the corresponding quantities involved. For example, if we divide the columns of RMSE values for $r(t)$ in Tables

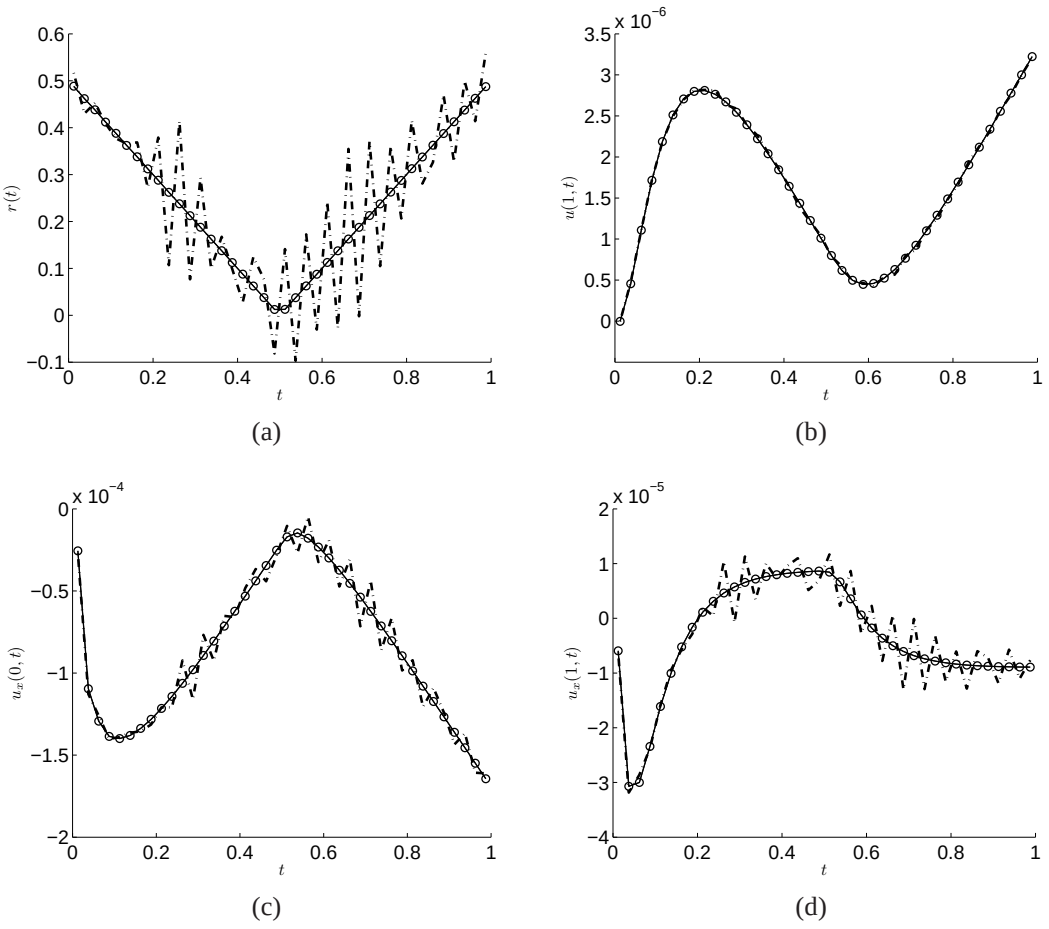

Figure 5.5: The analytical solution (5.21) and the direct problem numerical solution from Figures 5.7(a)–5.7(c) (——) and numerical results of (a) $r(t)$, (b) $u(1,t)$, (c) $u_x(0,t)$, and (d) $u_x(1,t)$, with no regularisation, for exact data $(\circ\,\circ\,\circ)$ and noisy data $p = 1\%$ $(-\,\cdot\,-)$, for Example 2.

5.2 and 5.3 by e (maximum value of $r(t)$ in (5.16)) and 0.5 (maximum value of $r(t)$ in (5.21)), respectively, then the relative errors for $r(t)$ in Example 1 are actually lower than those in Example 2, as expected from the regularity of these solution.

Finally, although not illustrated, it is reported that for both Examples 1 and 2 we have experienced with other values of λ close to the optimal ones but there was not much difference obtained in comparison with the numerical results of Figures 5.2, 5.3 and 5.6. This confirms that the GCV criterion performs well in choosing a suitable regularisation parameter for obtaining a stable and accurate numerical solution.

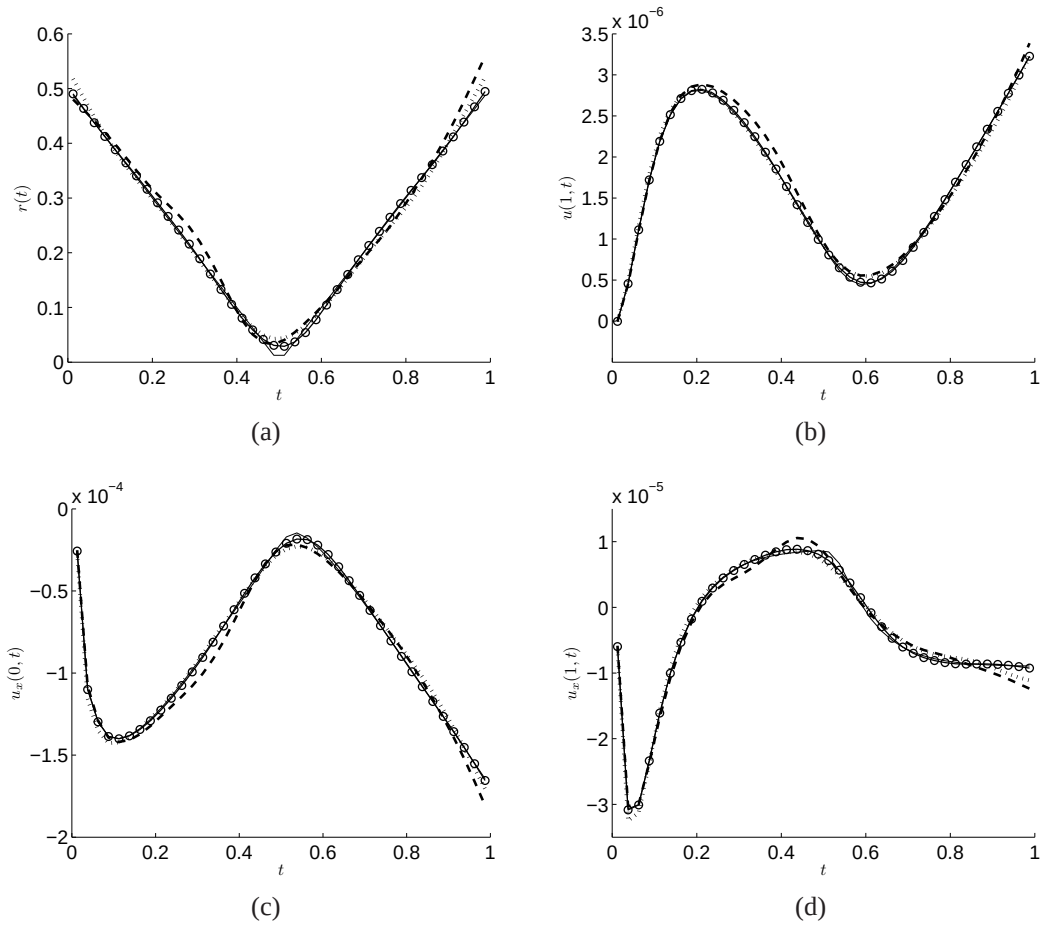

Figure 5.6: The analytical solution (5.21) and the direct problem numerical solutions from Figures 5.7(a)–5.7(c) (——), and the numerical results of (a) $r(t)$, (b) $u(1,t)$, (c) $u_x(0,t)$, and (d) $u_x(1,t)$ obtained using the second-order Tikhonov regularisation with the regularisation parameters suggested by GCV method, for $p \in \{1(\circ\circ\circ),\ 3(\cdots),\ 5(---)\}\%$ noise, for Example 2.

5.4.3 Example 3

In previous examples, we have use the BEM together with the second-order Tikhonov regularisation with the value of the regularisation parameter suggested by the GCV method, on both cases for identification of the smooth and non-smooth source functions in Example 1 and 2, respectively. In this example, we consider yet another case

example of non-smooth source function given by

$$r(t) = \left| t - \frac{1}{2} \right|,$$

with the input data $T = 1$, $a = \alpha = 1$, $b = 0$,

$$u_0(x) = 0, \quad f(x,t) = 1. \tag{5.22}$$

We remark that the condition in (A_3) of Theorem 5.2.1 does not hold.

In this case, as with Example 2 that the analytical solution of the direct problem for the temperature $u(x,t)$ is not available, thus the energy $E(t)$ is not available either. Therefore as we have done in previous example, the direct problem has been solved first with the BEM and $N = N_0 \in \{20, 40, 80\}$, as illustrated in Figure 5.7. From this figure it can be seen that rapidly convergent numerical solutions are obtained. The numerical results obtained using the BEM with $N = N_0 = 40$ are kept as an input data for $E(t)$ and the reference (analytical) solution for $u(1,t)$, $u_x(0,t)$ and $u_x(1,t)$.

In what follows, we present numerical results obtained with $N = 40$ and $N_0 = 30$ instead of 40, in order to avoid committing an inverse crime. The energy data $E(t)$ obtained from the numerical result in Figure 5.7(d) is perturbed, as described in (3.14) with the standard deviation $\sigma = 0.15p$. Figure 5.8 shows that the numerical results obtained by the straightforward inversion of (5.15), i.e. $\underline{\mathrm{r}} = X^{-1}\underline{\mathrm{y}}$, without regularisation, for $p = 0$ (exact) and $p = 1\%$ (noisy) data. For exact data, the same very good agreement between the analytical and numerical solutions is recorded. Whereas for the noisy data, the numerical solutions for $r(t)$ and $u_x(1,t)$ becomes highly oscillatory and unbounded. This is somewhat to be expected since the inverse problem under investigation is ill-posed.

We retrieve the stability, as previous, by the second-order Tikhonov regularisation with the proper choice of the regularisation parameter λ. Firstly, we have used the rigorous discrepancy principle, as introduced in Section 1.6.3, for $p \in \{1, 3, 5\}\%$ which yields $\lambda_{dis} \in \{$5.7E-8, 2.0E-6, 7.0E-6$\}$, respectively. The results are obtained as shown

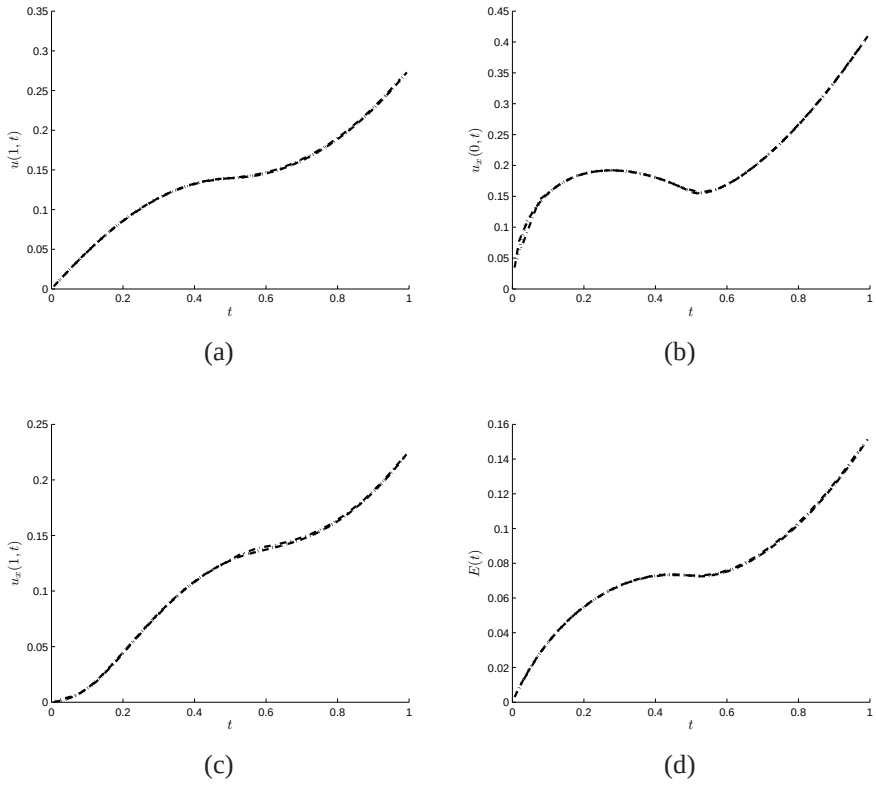

Figure 5.7: The numerical results of (a) $u(1,t)$, (b) $u_x(0,t)$, (c) $u_x(1,t)$, and (d) $E(t)$ obtained by solving the direct problem with $N = N_0 \in \{20\,(-\cdot-),\, 40\,(\cdots),\, 80\,(--)\}$, for Example 3.

in Figure 5.9 and Table 5.4. From Figure 5.9 it can be seen that stable and accurate numerical solutions are obtained. Table 5.4 also shows that the values of the regularisation parameter λ_{dis} and λ_{GCV} given by the discrepancy principle and the GCV are similar and not very different from the optimal value λ_{opt} given by the minimum of the RMSE for $r(t)$. It can also be seen that the GCV produces slightly better predictions than the discrepancy principle.

5.5 Conclusions

The inverse problem of finding the time-dependent heat source together with the temperature in the heat equation, under a non-classical dynamic boundary condition and

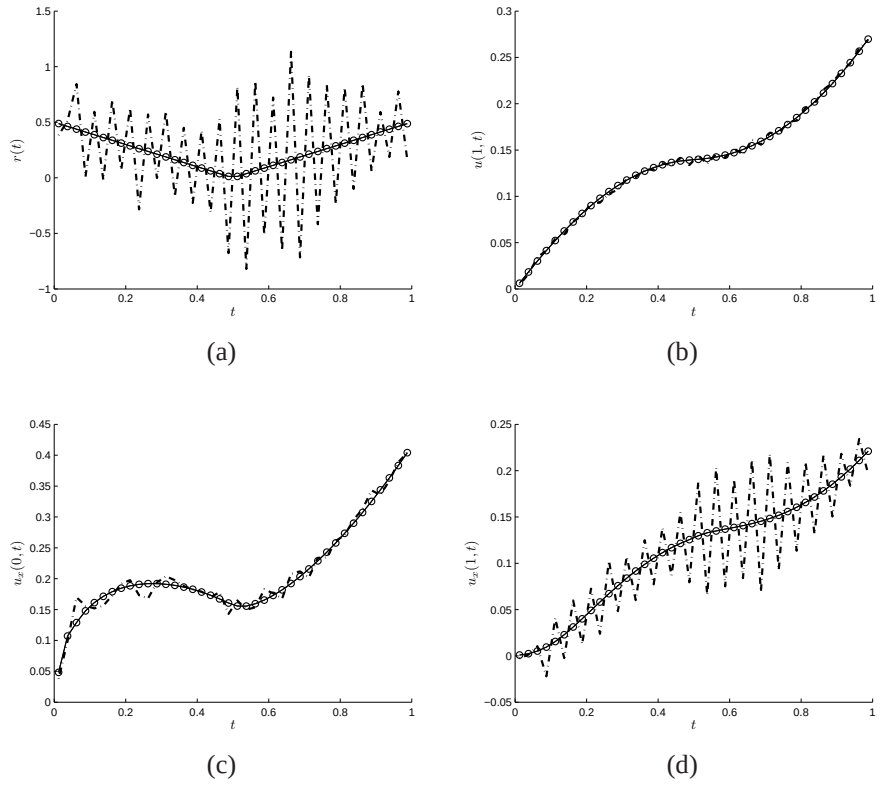

(a) (b)

(c) (d)

Figure 5.8: The analytical solution (5.4.3) and the direct problem numerical solution from Figures 5.7(a)–5.7(c) (——), and numerical results of (a) $r(t)$, (b) $u(1,t)$, (c) $u_x(0,t)$, and (d) $u_x(1,t)$, with no regularisation, for exact data $(\circ\,\circ\,\circ)$ and noisy data $p = 1\%$ $(-\cdot-)$, for Example 3.

an integral over-determination condition has been investigated. A numerical method based on the BEM combined with the second-order Tikhonov regularisation has been proposed together with the use of either the GCV criterion or the discrepancy principle for the selection of the regularisation parameter. The retrieved numerical results were found to be accurate and stable on both smooth and non-smooth continuous examples.

As for the experimental validation of the proposed inverse mathematical model in terms of bias and inverting real noisy data we defer this challenging task to possible future work. We only remark that unlike certain applications, e.g. some significant mismatch has been reported in [2, 35, 52] between experimental data of electromagnetic waves propagating in a non-attenuating medium and data produced by idealised computational simulations, in inverse heat conduction the mathematical models have

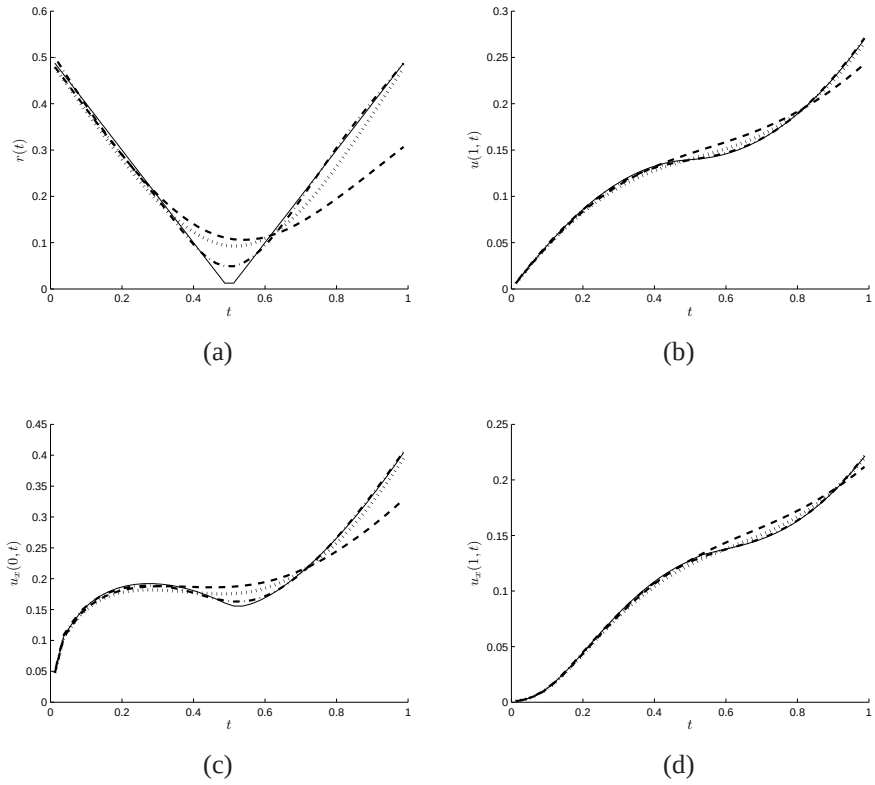

(a) (b)

(c) (d)

Figure 5.9: The analytical solution (5.4.3) and the direct problem numerical solutions from Figures 5.7(a)–5.7(c) (——), and the numerical results of (a) $r(t)$, (b) $u(1,t)$, (c) $u_x(0,t)$, and (d) $u_x(1,t)$ obtained using the second-order Tikhonov regularisation with the regularisation parameters suggested by the discrepancy method, for $p \in \{1(- \cdot -),\ 3(\cdots),\ 5(- - -)\}\%$ noise, for Example 3.

been shown to perform much better in industrial applications with actual real measured data, [13].

So far in previous chapters, the identification of a single time-dependent heat source function has been the main aim. In the next two chapters, we will consider the more challenging cases of simultaneous determination of the components of an additive or multiplicative space- and time-dependent heat source function.

Table 5.4: The regularisation parameters λ given by the discrepancy principle and by the GCV, and the RMSE for $r(t)$, $u(1,t)$, $u_x(0,t)$ and $u_x(1,t)$, obtained using the BEM with $N = 40$ and $N_0 = 30$ combined with the second-order Tikhonov regularisation for $p \in \{0,1,3,5\}\%$ noise. The optimal regularisation parameter given by the minimum of RMSE of $r(t)$ is also included, for Example 3.

p	parameter λ	RMSE			
		$r(t)$	$u(1,t)$	$u_x(0,t)$	$u_x(1,t)$
0	0	2.46E-4	8.06E-6	1.41E-5	2.27E-5
1%	0	5.13E-1	3.26E-3	1.20E-2	4.19E-2
1%	λ_{dis}=5.7E-8	1.11E-2	9.25E-4	2.89E-3	5.82E-4
1%	λ_{GCV}=5.7E-9	1.19E-2	8.26E-4	2.76E-3	5.96E-4
1%	λ_{opt}=2.2E-8	9.85E-3	8.06E-4	2.46E-3	5.65E-4
3%	0	1.53	9.86E-3	3.71E-2	1.23E-1
3%	λ_{dis}=2.0E-6	3.13E-2	3.67E-3	9.99E-3	2.85E-3
3%	λ_{GCV}=3.3E-7	3.01E-2	2.53E-3	8.08E-3	1.81E-3
3%	λ_{opt}=9.0E-7	2.75E-2	2.77E-3	8.05E-3	2.07E-3
5%	0	1.30	1.31E-2	6.26E-2	1.03E-1
5%	λ_{dis}=7.0E-6	7.86E-2	8.95E-3	2.68E-2	5.25E-3
5%	λ_{GCV}=7.9E-7	4.57E-2	6.80E-3	1.72E-2	4.43E-3
5%	λ_{opt}=9.1E-8	4.15E-2	6.68E-3	1.59E-2	4.61E-3

Chapter 6

Determination of an Additive Space- and Time-dependent Heat Source

6.1 Introduction

Inverse source problems for the heat equation have recently attracted considerable interest, see [1, 18, 24, 61, 64, 67] to name just a few. These studies have sought a coefficient source function depending on either space- or time-dependent variables using various techniques. In Chapters 2–5 we have focused on the inverse problem of finding the time-dependent coefficient source function and the temperature for the heat equation. In this chapter we extend our study to determine inverse heat source functions depending on both space and time, but which are additively separated into two unknown coefficient source functions, namely, one component dependent on space and another component dependent on time. The measurement/overspecified conditions are one temperature measurement, as a function of time, at one specified interior location and a time-average temperature throughout the space solution domain.

Since the governing partial differential equation is the linear heat equation with constant coefficients, the preferred method of discretisation is the BEM. Even though the inverse heat source problem is uniquely solvable, it is still ill-posed since small

errors which inherently occur in any practical measurement cause largely oscillating solutions. To overcome this instability, in this chapter regularisation such as the TSVD or the Tikhonov regularisation method are employed. Moreover, the L-curve method, the GCV criterion, or the discrepancy principle are employed for the selection of the regularisation parameter. Additionally in the case of two different regularisation parameters are considered, the L-surface criterion, [3], is utilised.

This chapter is organised as follows. In Section 6.2 the mathematical inverse formulation is described and the numerical discretisation of the problem using the BEM is presented in Section 6.3. The TSVD and the Tikhonov regularisation are described in Section 6.4, as procedures for overcoming the instability of the solution. Finally, Sections 6.5 and 6.6 discuss the numerical results and highlight the conclusions of this research.

6.2 Mathematical formulation

Consider the inverse problem of finding the time-dependent heat source $r(t)$, the space-dependent heat source $s(x)$ and the temperature $u(x,t)$ satisfying the heat conduction equation

$$u_t = u_{xx} + r(t)f(x,t) + s(x)g(x,t) + h(x,t), \quad (x,t) \in D_T, \tag{6.1}$$

subject to the initial condition (1.7), namely

$$u(x,0) = u_0(x), \quad x \in [0,L], \tag{6.2}$$

the Dirichlet boundary conditions

$$u(0,t) = \mu_0(t), \quad u(L,t) = \mu_L(t), \quad t \in [0,T], \tag{6.3}$$

and the over-determination conditions

$$u\left(X_0, t\right) = \chi(t), \quad t \in [0, T], \tag{6.4}$$

$$\int_0^T u(x,t)\, dt = \psi(x), \quad x \in [0, L], \tag{6.5}$$

$$s(X_0) = S_0, \tag{6.6}$$

when f, g, h, u_0, μ_0, μ_L, χ, ψ are given functions, X_0 is a given sensor location within the interval $(0, L)$, and S_0 is a given value of the source function s at the given point X_0.

One can remark that the time-average temperature measurement (6.5) represents a non-local condition/measurement. It is convenient to use in practical situations where a local measurement of the temperature at a fixed time $T_1 \in (0, T]$, namely,

$$u(x, T_1) =: \psi_{T_1}(x), \quad x \in [0, L]$$

contains a large amount of noise. This may be due to harsh external conditions, or to the fact that many space measurements can, in fact, never be recorded at a fixed instant instantaneously. If this is the case, one can have a selection of such large noise local temperature measurements, but which on average produce a less noisy nonlocal measurement (6.5).

The individual separate cases concerning the identification of a single time-dependent heat source $r(t)$, when $s(x)$ is known, or the identification of a single space-dependent heat source $s(x)$, when $r(t)$ is known, have been theoretically investigated in Prilepko and Solov'ev [44] and Prilepko and Tkachenko [45], respectively.

The unique solvability of this inverse source problem was already established by Ivanchov [26] and it is the objective of this study to obtain a stable numerical solution of this still ill-posed problem. Note that condition (6.6) was omitted in [26], but it should be included in order to avoid non-uniqueness and instability cases which have been given as counterexamples in [20]. For the inverse problem (6.1)–(6.6) we have

the following local unique solvability theorem.

Theorem 6.2.1 *Assume that the following conditions are satisfied:*

(i) $u_0(x), \psi(x) \in H^{2+\gamma}[0,L], \mu_0(t), \mu_L(t), \chi(t) \in H^{1+\gamma/2}[0,T], h(x,t) \in H^{\gamma,\gamma/2}(\overline{D_T})$ *with* $\gamma \in (0,1)$,
f *independent of* t *and* $f(x) \in H^{\gamma}[0,L]$,
g *independent of* x *and* $g(t) \in H^{\gamma/2}[0,T]$;

(ii) $f(X_0) \neq 0$, $\displaystyle\int_0^T g(t)\,dt \neq 0$, $\dfrac{g(t)}{\int_0^T g(\tau)\,d\tau} \geq 0$, $\forall t \in [0,T]$;

(iii) $u_0(0) = \mu_0(0)$, $u_0(L) = \mu_L(0)$, $u_0(X_0) = \chi(0)$,
$\displaystyle\int_0^T \chi(t)\,dt = \psi(X_0)$, $\psi(0) = \int_0^T \mu_0(t)\,dt$, $\psi(L) = \int_0^T \mu_L(t)\,dt$.

Then for sufficiently small $T > 0$ *there exists a unique solution* $(r(t), s(x), u(x,t)) \in H^{\gamma/2}[0,T] \times H^{\gamma}[0,L] \times H^{2+\gamma,1+\gamma/2}(\overline{D}_T)$ *of the inverse problem* (6.1)–(6.6).

In this theorem the functions are required to lie in Hölder spaces, defined as follows:

- $H^{i+\gamma_1,j+\gamma_2}(\overline{D}_T)$, with $i,j = 0,1,2$ and $0 < \gamma_1, \gamma_2 \leq 1$, denotes the space of continuous functions with ith partial derivative with respect to x and jth partial derivative with respect to t such that there exist $m_1 > 0$ and $m_2 > 0$ satisfying

$$|\partial_x^i u(x_1,t) - \partial_x^i u(x_2,t)| \leq m_1 |x_1 - x_2|^{\gamma_1}, \quad |\partial_t^j u(x,t_1) - \partial_t^j u(x,t_2)| \leq m_2 |t_1 - t_2|^{\gamma_2}$$

  for all $x_1, x_2 \in [0,L]$ and $t_1, t_2 \in [0,T]$.

- $H^{\gamma}(\Omega)$, with $\Omega = (0,L)$ or $(0,T)$, denotes the space of continuous functions $s : \Omega \to \mathbb{R}$ with exponent $0 < \gamma \leq 1$ such that there exists $m > 0$ satisfying

$$|s(x_1) - s(x_2)| \leq m|x_1 - x_2|^{\gamma} \quad \text{for all} \quad x_1, x_2 \in \Omega.$$

In the next Sections 6.3 and 6.4, we will demonstrate how to solve the inverse heat source problem (6.1)–(6.6) by using a regularised BEM.

6.3 The boundary element method (BEM)

In the numerical process, we utilise the BEM as introduced in Section 1.3 to the heat conduction equation (6.1). We then obtain the following boundary integral equation

$$\begin{aligned}
&\eta(x)u(x,t)\\
&= \int_0^t \left[G(x,t,\xi,\tau)\frac{\partial u}{\partial n(\xi)}(\xi,\tau) - u(\xi,\tau)\frac{\partial G}{\partial n(\xi)}(x,t,\xi,\tau) \right]_{\xi\in\{0,L\}} d\tau\\
&\quad + \int_0^L G(x,t,y,0)u(y,0)\,dy + \int_0^L \int_0^T G(x,t,y,\tau)r(\tau)f(y,\tau)\,d\tau dy\\
&\quad + \int_0^L \int_0^T G(x,t,y,\tau)s(y)g(y,\tau)\,d\tau dy + \int_0^L \int_0^T G(x,t,y,\tau)h(y,\tau)\,d\tau dy,\\
&\quad (x,t)\in[0,L]\times(0,T].
\end{aligned} \tag{6.7}$$

Using the same discretisation as described in the previous chapters, we obtain

$$\begin{aligned}
\eta(x)u(x,t) = &\sum_{j=1}^{N} [A_{0j}(x,t)q_{0j} + A_{Lj}(x,t)q_{Lj} - B_{0j}(x,t)h_{0j} - B_{Lj}(x,t)h_{Lj}]\\
&+ \sum_{k=1}^{N_0} C_k(x,t)u_{0,k} + d_1(x,t) + d_2(x,t) + d_0(x,t).
\end{aligned} \tag{6.8}$$

where

$$d_1(x,t) = \int_0^L \int_0^T G(x,t,y,\tau)r(\tau)f(y,\tau)\,d\tau dy, \tag{6.9}$$

$$d_2(x,t) = \int_0^L \int_0^T G(x,t,y,\tau)s(y)g(y,\tau)\,d\tau dy, \tag{6.10}$$

and can be calculated by applying the piecewise constant approximations to the functions $f(x,t)$ and $r(t)$ as the same in (2.21), and the functions $g(x,t)$ and $s(x)$ as as

$$g(x,t) = g(\tilde{x}_k,t), \quad s(x) = s(\tilde{x}_k) =: s_k, \tag{6.11}$$

for $x \in (x_{k-1}, x_k]$, $k = \overline{1, N_0}$. Then the double integrals (6.9) and (6.10) can be approximated as

$$d_1(x,t) = \int_0^T r(\tau) \int_0^L G(x,t,y,\tau) f(y,\tau)\, dy d\tau = \sum_{j=1}^{N} D_{1,j}(x,t) r_j,$$
$$d_2(x,t) = \int_0^L s(y) \int_0^T G(x,t,y,\tau) g(y,\tau)\, d\tau dy = \sum_{k=1}^{N_0} D_{2,k}(x,t) s_k,$$

where

$$D_{1,j}(x,t) = \int_0^L f(y,\tilde{t}_j) A_{yj}(x,t)\, dy,$$
$$D_{2,k}(x,t) = \frac{1}{2} \int_0^T g(\tilde{x}_k,t) H(t-\tau) \left[\text{erf}\left(\frac{x - x_{k-1}}{2\sqrt{t-\tau}} \right) - \text{erf}\left(\frac{x - x_k}{2\sqrt{t-\tau}} \right) \right] d\tau,$$

These integrals are evaluated using Simpson's rule for numerical integration. With these approximations, the integral equation (6.8) becomes

$$\begin{aligned} \eta(x) u(x,t) = & \sum_{j=1}^{N} [A_{0j}(x,t) q_{0j} + A_{Lj}(x,t) q_{Lj} - B_{0j}(x,t) h_{0j} - B_{Lj}(x,t) h_{Lj}] \\ & + \sum_{k=1}^{N_0} C_k(x,t) u_{0,k} + \sum_{j=1}^{N} D_{1,j}(x,t) r_j + \sum_{k=1}^{N_0} D_{2,k}(x,t) s_k \\ & + \sum_{j=1}^{N} D_{0,j}(x,t). \end{aligned} \tag{6.12}$$

Applying the equation (6.12) at the boundary nodes $(0, \tilde{t}_i)$ and $(L, \tilde{t}_i)$ for $i = \overline{1, N}$ yields the system of $2N$ linear equations

$$A\mathbf{q} - B\mathbf{h} + C\mathbf{u}_0 + D_1\mathbf{r} + D_2\mathbf{s} + \mathbf{d} = \mathbf{0}, \tag{6.13}$$

where matrices A, B, C and vectors $\underline{\mathtt{q}}$, $\underline{\mathtt{h}}$, $\underline{\mathtt{u}}_0$, $\underline{\mathtt{d}}$ are defined the same as in (2.25), and

$$D_1 = \begin{bmatrix} D_{1,j}(0,\tilde{t}_i) \\ D_{1,j}(L,\tilde{t}_i) \end{bmatrix}_{2N\times N}, \quad D_2 = \begin{bmatrix} D_{2,k}(0,\tilde{t}_i) \\ D_{2,k}(L,\tilde{t}_i) \end{bmatrix}_{2N\times N_0}, \quad \underline{\mathtt{s}} = \begin{bmatrix} s_k \end{bmatrix}_{N_0}.$$

Here, the boundary temperature $\underline{\mathtt{h}}$ is known by the boundary condition (6.3), i.e.

$$\underline{\mathtt{h}} = \begin{bmatrix} u(0,\tilde{t}_j) \\ u(L,\tilde{t}_j) \end{bmatrix}_{2N} = \begin{bmatrix} \underline{\mu}_0 \\ \underline{\mu}_L \end{bmatrix}_{2N} =: \underline{\mu}. \tag{6.14}$$

Therefore from (6.13), we obtain

$$\underline{\mathtt{q}} = A^{-1}\left(B\underline{\mu} - C\underline{\mathtt{u}}_0 - D_1\underline{\mathtt{r}} - D_2\underline{\mathtt{s}} - \underline{\mathtt{d}}\right). \tag{6.15}$$

To determine $\underline{\mathtt{r}}$ and $\underline{\mathtt{s}}$, the conditions (6.4)–(6.6) are imposed. Firstly, we consider the interior points $(X_0,\tilde{t}_i)$ for $i = \overline{1,N}$ which can be written as

$$\chi_i := \chi(\tilde{t}_i) = u(X_0,\tilde{t}_i), \quad i = \overline{1,N}. \tag{6.16}$$

Applying the interior points above to the equation (6.12) can give rise to the following linear system of N equations:

$$A^I\underline{\mathtt{q}} - B^I\underline{\mu} + C^I\underline{\mathtt{u}}_0 + D_1^I\underline{\mathtt{r}} + D_2^I\underline{\mathtt{s}} + \underline{\mathtt{d}}^I = \underline{\chi}, \tag{6.17}$$

where

$$A^I = \begin{bmatrix} A_{0j}(X_0,\tilde{t}_i) & A_{Lj}(X_0,\tilde{t}_i) \end{bmatrix}_{N\times 2N}, \quad B^I = \begin{bmatrix} B_{0j}(X_0,\tilde{t}_i) & B_{Lj}(X_0,\tilde{t}_i) \end{bmatrix}_{N\times 2N},$$
$$C^I = \begin{bmatrix} C_k(X_0,\tilde{t}_i) \end{bmatrix}_{N\times N_0}, \quad D_1^I = \begin{bmatrix} D_{1,j}(X_0,\tilde{t}_i) \end{bmatrix}_{N\times N}, \quad D_2^I = \begin{bmatrix} D_{2,k}(X_0,\tilde{t}_i) \end{bmatrix}_{N\times N_0},$$
$$\underline{\mathtt{d}}^I = \begin{bmatrix} \sum_{j=1}^{N} D_{0,j}(X_0,\tilde{t}_i) \end{bmatrix}_N, \quad \underline{\chi} = \begin{bmatrix} \chi_i \end{bmatrix}_N.$$

Whereas the time-integral condition (6.5) is approximated by the midpoint numerical

integration, as in the parallel way as (3.11), at $x = \tilde{x}_k$ for $k = \overline{1, N_0}$, then we obtain

$$\frac{T}{N}\sum_{i=1}^{N} u(\tilde{x}_k, \tilde{t}_i) = \int_0^T u(\tilde{x}_k, t)\, dt = \psi(\tilde{x}_k) =: \psi_k \quad \text{for} \quad k = \overline{1, N_0}. \tag{6.18}$$

Using (6.12), equation (6.18) yields

$$\frac{T}{N}\sum_{i=1}^{N} \left[A_i^{II}\mathfrak{q} - B_i^{II}\underline{\mu} + C_i^{II}\mathfrak{u}_0 + D_{1,i}^{II}\mathfrak{r} + D_{2,i}^{II}\mathfrak{s} + \mathfrak{d}_i^{II} \right] = \underline{\psi}, \tag{6.19}$$

where

$$A_i^{II} = \Big[A_{0j}(\tilde{x}_k, \tilde{t}_i) \quad A_{Lj}(\tilde{x}_k, \tilde{t}_i) \Big]_{N_0 \times 2N}, \quad B_i^{II} = \Big[B_{0j}(\tilde{x}_k, \tilde{t}_i) \quad B_{Lj}(\tilde{x}_k, \tilde{t}_i) \Big]_{N_0 \times 2N},$$
$$C_i^{II} = \Big[C_k(\tilde{x}_k, \tilde{t}_i) \Big]_{N_0 \times N_0}, \quad D_{1,i}^{II} = \Big[D_{1,j}(\tilde{x}_k, \tilde{t}_i) \Big]_{N_0 \times N}, \quad D_{2,i}^{II} = \Big[D_{2,k}(\tilde{x}_k, \tilde{t}_i) \Big]_{N_0 \times N_0},$$
$$\mathfrak{d}_i^{II} = \Big[\textstyle\sum_{j=1}^{N} D_{0,j}(\tilde{x}_k, \tilde{t}_i) \Big]_{N_0}, \quad \underline{\psi} = \Big[\psi_k \Big]_{N_0}.$$

Finally, we consider the condition (6.6). Since we have used the space midpoint discretisation, we then approximate S_0 at the given point $X_0 \in (0, L)$ as

$$S_0 = s(X_0) \approx \frac{s(\tilde{x}_{k^*}) + s(\tilde{x}_{k^*+1})}{2}, \tag{6.20}$$

where index $k^* \in \{1, \ldots, N_0 - 1\}$ satisfies $\tilde{x}_{k^*} \le X_0 < \tilde{x}_{k^*+1}$.

Now the approximate solutions $\mathfrak{r}$ and $\mathfrak{s}$ can be found by eliminating $\mathfrak{q}$ from (6.13) and combining expressions (6.17), (6.19), and (6.20), to obtain, after some manipulations, a linear system of $(N + N_0 + 1)$ equations with $(N + N_0)$ unknowns as follows:

$$X\mathfrak{w} = \underline{\mathfrak{y}}, \tag{6.21}$$

where

$$X = \begin{bmatrix} A^I A^{-1} D_1 - D_1^I & A^I A^{-1} D_2 - D_2^I \\ \dfrac{T}{N}\displaystyle\sum_{i=1}^{N}(A_i^{II} A^{-1} D_1 - D_{1,i}^{II}) & \dfrac{T}{N}\displaystyle\sum_{i=1}^{N}(A_i^{II} A^{-1} D_2 - D_{2,i}^{II}) \\ 0 \ldots 0 & 0 \ldots 0 \ \frac{1}{2} \ \frac{1}{2} \ 0 \ldots 0 \end{bmatrix}_{(N+N_0+1)\times(N+N_0)},$$

$$\underline{\mathrm{y}} = \begin{bmatrix} -\underline{\chi} + A^I A^{-1}(B\underline{\mu} - C\mathfrak{u}_0 - \mathfrak{d}) - B^I \underline{\mu} + C^I \mathfrak{u}_0 + \mathfrak{d}^I \\ -\underline{\psi} + \dfrac{T}{N}\displaystyle\sum_{i=1}^{N}\left(A_i^{II} A^{-1}(B\underline{\mu} - C\mathfrak{u}_0 - \mathfrak{d}) - B_i^{II}\underline{\mu} + C_i^{II}\mathfrak{u}_0 + \mathfrak{d}_i^{II}\right) \\ S_0 \end{bmatrix}_{N+N_0+1},$$

and $\underline{\mathrm{w}} = \begin{bmatrix} \underline{\mathrm{r}} \\ \underline{\mathrm{s}} \end{bmatrix}_{N+N_0}$.

Since the problem is ill-posed, then the system of equations (6.21) is ill-conditioned. In the next section, we will deal with this ill-conditioning using regularisation in order to obtain a stable solution.

6.4 Regularisation

In practice, the measured data is unavoidably contaminated by unplanned error. In order to model this, we add noise into the input functions $\chi(t)$ and $\psi(x)$ representing the over-determination conditions (6.4) and (6.5) as follows:

$$\underline{\chi}^{\epsilon} = \underline{\chi} + random('\text{Normal}', 0, \sigma_\chi, 1, N), \tag{6.22}$$

and

$$\underline{\psi}^{\epsilon} = \underline{\psi} + random('\text{Normal}', 0, \sigma_\psi, 1, N_0), \tag{6.23}$$

with the standard deviations σ_χ and σ_ψ to be taken as

$$\sigma_\chi = p \times \max_{t\in[0,T]} |\chi(t)|, \quad \text{and} \quad \sigma_\psi = p \times \max_{x\in[0,L]} |\psi(x)|, \tag{6.24}$$

respectively. Note that the measurement (6.6) is already contaminated by error due to the approximation made in (6.20).

If we consider the contamination of the right-hand side of equation (6.21) as $\|\underline{\mathbf{y}}^{\epsilon} - \underline{\mathbf{y}}\| \approx \epsilon$, then the direct least-squares solution $\underline{\mathbf{w}} = (X^{\mathrm{T}}X)^{-1}X^{\mathrm{T}}\underline{\mathbf{y}}^{\epsilon}$ will be unstable. To overcome this instability, regularisation method needs to be utilised. In this study, we employ either the TSVD or the Tikhonov regularisation methods.

We first consider the use of the TSVD method as a regularisation procedure. To use this method we use the *[U,Σ,V]=svds(X,N_t)* command in MATLAB, as we have used previously in Chapter 3. In order to indicate the appropriate truncation level N_t, the L-curve criterion, the GCV method, and the discrepancy principle are utilised.

Alternatively, the Tikhonov regularisation is another way of obtaining a stable solution of the ill-conditioned system of equations (6.21) which based on minimising the regularised linear least-squares objective function

$$\|X\underline{\mathbf{w}} - \underline{\mathbf{y}}^{\epsilon}\|^2 + \lambda_r\|R^{(1)}\underline{\mathbf{r}}\|^2 + \lambda_s\|R^{(2)}\underline{\mathbf{s}}\|^2 \tag{6.25}$$

where $R^{(1)}$, $R^{(2)}$ are (differential) regularisation matrices corresponding to a regularisation parameter $\lambda_r, \lambda_s > 0$, respectively. Solving (6.25) one obtains the regularised solution

$$\underline{\mathbf{w}}_{\lambda_r,\lambda_s} = \left(X^{\mathrm{T}}X + \mathcal{R}^{\mathrm{T}}\mathcal{R}\right)^{-1} X^{\mathrm{T}}\underline{\mathbf{y}}^{\epsilon}. \tag{6.26}$$

where the matrix $\mathcal{R}$ represents a block matrix of upper-left subblock $\lambda_r R^{(1)}$ and lower-right subblock $\lambda_s R^{(2)}$. Initially, we take $\lambda := \lambda_r = \lambda_s$ and consider the L-curve criterion, the GCV method, and the discrepancy principle as choices for indicating the single regularisation parameter λ. Note that both the L-curve and the GCV are heuristic methods because they do not require the knowledge of the level of noise ϵ. More rigorously, one can use the discrepancy principle, [40], which selects λ such that

$$\|X\underline{\mathbf{w}}_{\lambda} - \underline{\mathbf{y}}^{\epsilon}\| \approx \epsilon. \tag{6.27}$$

If we allow for general multiple regularisation parameters λ_r and λ_s in (6.25) then, for their selection one could employ the L-surface criterion, [3], which plots the residual $\|X\mathfrak{w}_{\lambda_r,\lambda_s} - \underline{\mathfrak{y}}^{\epsilon}\|$ versus $\|R^{(1)}\mathfrak{r}\|$ and $\|R^{(2)}\mathfrak{s}\|$ for various values of λ_r and λ_s.

6.5 Numerical examples and discussion

In this section, we present two benchmark test examples in order to test the accuracy of the approximate solutions. We are using the RMSE for $r(t)$ as defined in (2.49) whereas the RMSE for $s(x)$ can be defined as

$$\text{RMSE}(s(x)) = \sqrt{\frac{L}{N_0}\sum_{k=1}^{N_0}\left(s_{exact}(\tilde{x}_k) - s_{numerical}(\tilde{x}_k)\right)^2}. \tag{6.28}$$

6.5.1 Example 1

In the first example, we consider a smooth benchmark test with $T = L = 1$, $X_0 = \frac{1}{2}$ and the input data

$$\begin{cases} u_0(x) = u(x,0) = x^2, \quad \mu_0(t) = u(0,t) = 0, \quad \mu_L(t) = u(1,t) = e^t, \\ \chi(t) = u(\frac{1}{2},t) = \dfrac{e^t}{4}, \quad \psi(x) = \displaystyle\int_0^1 u(x,t)\,dt = x^2(e-1), \\ S_0 = s(\frac{1}{2}) = 1, \quad f(x,t) = e^x, \quad g(x,t) = t+1, \\ h(x,t) = (x^2-2)e^t - t^2e^x - (t+1)\sin(\pi x). \end{cases} \tag{6.29}$$

One can check that the conditions of Theorem 6.2.1 are satisfied hence the inverse source problem (6.1)–(6.6) with the data (6.29) has a unique solution. It can easily be verified through direct substitution that this solution is given by

$$u(x,t) = x^2e^t, \quad r(t) = t^2, \quad s(x) = \sin(\pi x). \tag{6.30}$$

As mentioned in Section 6.2, the inverse heat source problem (6.1)–(6.6) is ill-

posed since small errors in the measured data (6.4)–(6.6) cause large errors in the solution. In order to quantify the degree of ill-conditioning we calculate the condition number of the matrix X. The condition numbers for $N = N_0 \in \{20, 40, 80\}$ and $X_0 \in \{\frac{1}{4}, \frac{1}{2}, \frac{3}{4}\}$ are shown in Table 6.1. In addition, the normalised singular values of the matrix X are displayed in Figure 6.1, and the rapidly decreasing values indicate that the system of equations (6.21) is ill-conditioned. Looking at the columns of Table 6.1 it can be seen that the condition number only slightly decreases as X_0 increase, hence we do not expect the numerical results to be significantly influenced by the choice of X_0 within some interval $[\frac{1}{4}, \frac{3}{4}]$ away from the end points $x = 0$ and $x = L = 1$. Of course, as X_0 gets closer to the boundary point $x = 0$ or $x = L$ then the specification of the interval temperature measurement (6.4) resembles a heat flux prescription, namely

$$u_x(0,t) = \lim_{X_0 \searrow 0} \frac{u(X_0,t) - u(0,t)}{X_0}, \quad \text{or} \quad u_x(L,t) = \lim_{X_0 \nearrow L} \frac{u(X_0,t) - u(L,t)}{X_0 - L}.$$

However, this newly generated inverse problem in which Cauchy data are specified at $x = 0$ or $x = L$ is not addressed herein and it is deferred to a future work.

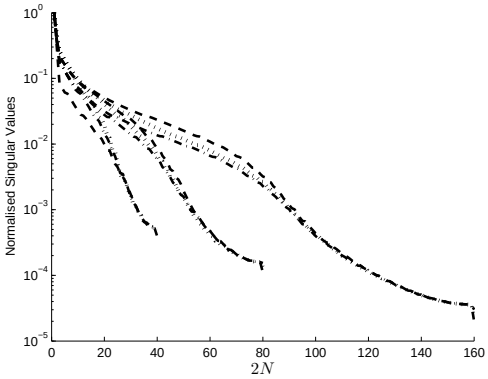

Figure 6.1: The normalised singular values of matrix X for $N = N_0 \in \{20, 40, 80\}$ and $X_0 \in \{\frac{1}{4}\,(-\cdot-), \frac{1}{2}\,(\cdots), \frac{3}{4}\,(---)\}$, for Example 1.

In what follows, the numerical results are illustrated for a fixed discretisation $N = N_0 = 40$ and $X_0 = \frac{1}{2}$.

Table 6.1: The condition numbers of the matrix X in equation (6.21) for various $N = N_0 \in \{20, 40, 80\}$ and $X_0 \in \{\frac{1}{4}, \frac{1}{2}, \frac{3}{4}\}$, for Example 1.

$N = N_0$	20	40	80
$X_0 = 1/4$	1.94E+3	9.07E+3	5.04E+4
$X_0 = 1/2$	1.97E+3	7.51E+3	4.06E+4
$X_0 = 3/4$	1.93E+3	6.50E+3	3.33E+4

Exact Data

We consider first the case of exact data, i.e. $p = 0$ in (6.24). We directly solve the linear system of equations (6.21) with the untruncated SVD method, and display the numerical solutions for $r(t)$, $s(x)$, $u_x(0,t)$, and $u_x(1,t)$ in Figures 6.2(a)–6.2(d), respectively. From these figures, it can be seen that the solutions for $r(t)$ and $s(x)$ are inaccurate, but the fluxes $u_x(0,t)$ and $u_x(1,t)$ are stable and accurate with small RMSEs of 9.32E-3 and 4.58E-2, respectively, see Table 6.2. This is somewhat to be expected since the inverse problem is ill-posed. Hence, regularisation is required to overcome this instability.

For this, we utilise the TSVD and the Tikhonov regularisation of orders zero, one, and two. The selection method of the regularisation parameters is first considered. The L-curves of the TSVD and the Tikhonov regularisations are presented in Figures 6.3(a) and 6.4(a), respectively. It can be seen that there is no L-shape obtained for either the TSVD, ZOTR, or FOTR, whereas the SOTR shows more clearly an L-corner at λ_L=1E-1. Alternatively, the GCV method is utilised as another choice for the regularisation parameter, as shown in Figure 6.3(b). The minimum of the GCV function suggests $N_t = 56$ to be the truncation number for the TSVD, whilst for the Tikhonov regularisation which is displayed in Figure 6.4(b), the minima indicate the parameters λ_{GCV}=1.0E-7, 1.2E-7, and 4.5E-8 for ZOTR, FOTR and SOTR, respectively. Note that for the exact data, $\epsilon \approx 0$ and the discrepancy principle cannot be employed. With the GCV selection for the regularisation parameters determined from Figures 6.3(b) and 6.4(b), the TSVD and the Tikhonov regularisation results are shown in Figure 6.5. Compared to Figure 6.2, one can see that the instability of the numerical solutions is

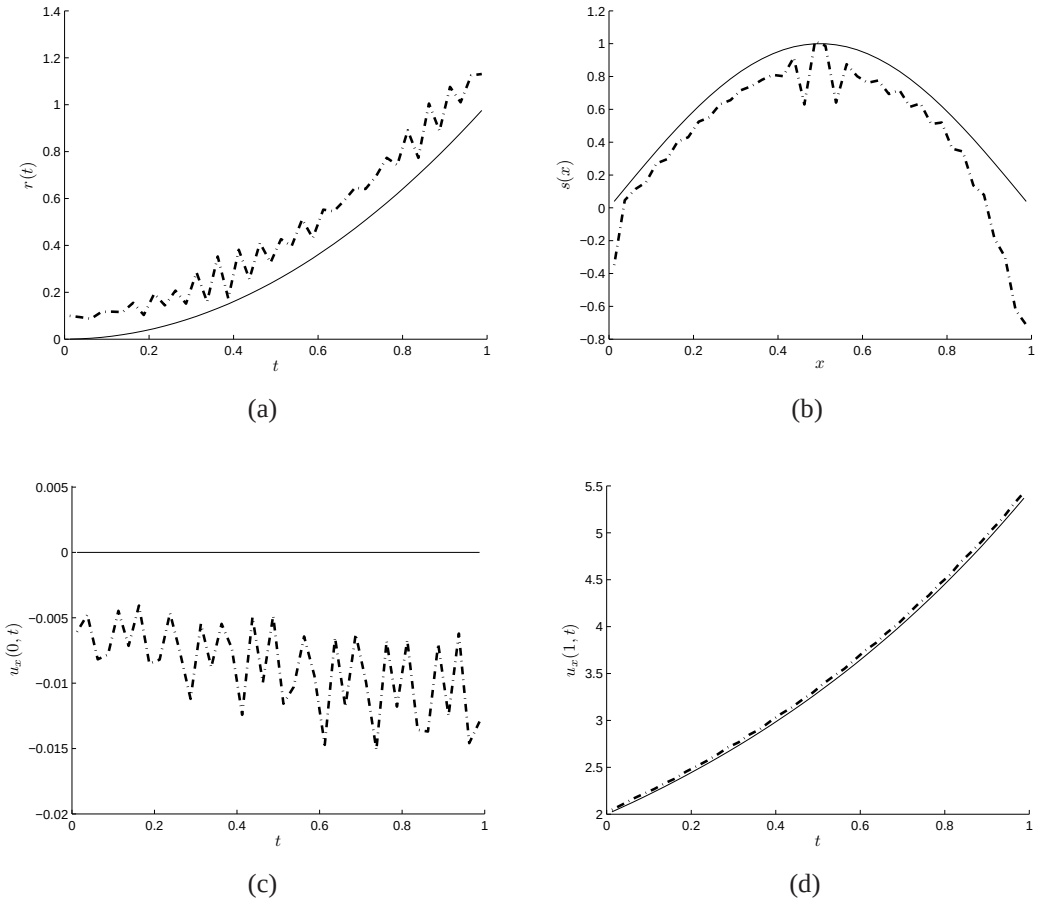

(a) (b)

(c) (d)

Figure 6.2: The analytical (——) and numerical results $(- \cdot -)$ of (a) $r(t)$, (b) $s(x)$, (c) $u_x(0,t)$, and (d) $u_x(1,t)$ obtained using the SVD for exact data, for Example 1.

not alleviated. We then employ another choice of the regularisation parameter based on the L-curve method. This suggests λ_L=1E-1 for the SOTR displayed in Figure 6.4(b). Then with this choice for λ we obtain the stable and accurate numerical results shown in Figure 6.6 and Table 6.2.

Noisy Data

Next, the case of noise contamination with percentage $p = 1\%$ is considered by adding random noise into the input functions $\chi(t)$ and $\psi(x)$ in (6.29), as in (6.22) and (6.23), respectively. It is of crucial importance to utilise the regularisation in this case, and selecting the regularisation parameter is the first step of the regularisation process. Here,

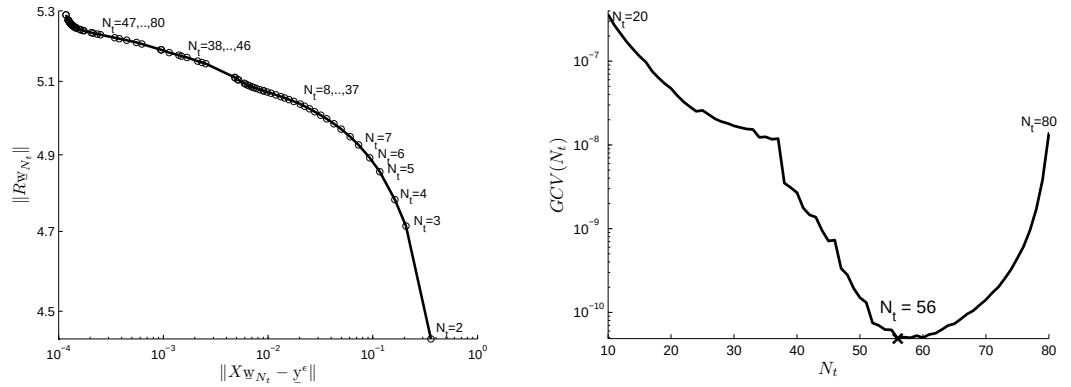

(a) (b)

Figure 6.3: (a) The L-curve and (b) the GCV function obtained by the TSVD for exact data, for Example 1.

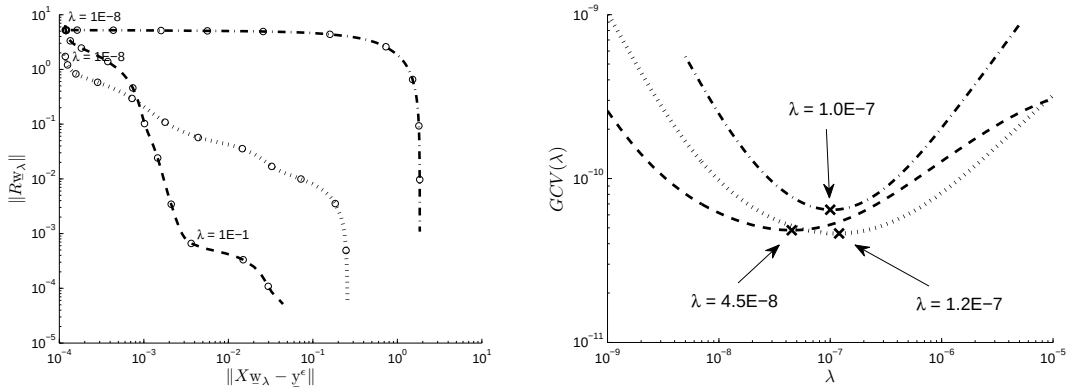

(a) (b)

Figure 6.4: (a) The L-curve, and (b) the GCV function, obtained by the ZOTR $(-\cdot-)$, FOTR $(\cdots)$, and SOTR $(---)$ for exact data, with $\lambda = \lambda_r = \lambda_s$, for Example 1.

the L-curve method and the discrepancy principle are employed as criteria for choosing the regularisation parameters. These are displayed in Figures 6.7 and 6.8 using the TSVD and the Tikhonov regularisation, respectively. The suggested parameters are given in Table 6.2. Figure 6.9 presents all results obtained using the TSVD and the Tikhonov regularisation of orders zero, one, and two with the regularisation parameters suggested by the discrepancy principle, see Table 6.2. Looking more closely at Figure 6.9(a), it can be seen that the approximate solutions for $r(t)$ obtained by the

first- and the second-order Tikhonov regularisation are reasonably stable, whereas the numerical solution for $s(x)$, as shown in Figure 6.9(b) is rather in accurate.

We consider the second-order Tikhonov regularisation with the regularisation parameter suggested by the L-curve method λ_L=10 and obtain the results shown in Figure 6.11. After analyzing this numerical solution, it can be clearly observed that we cannot obtain accurate solutions for both r and s using $\lambda_r = \lambda_s$. Therefore, the case $\lambda_r \neq \lambda_s$ is considered and the L-surfaces are shown in Figure 6.10. On the plane of logarithm of residual norm, $\log \|X\underline{\mathbf{w}}_\lambda - \underline{\mathbf{y}}^\epsilon\|$, versus logarithm of the second deriva-

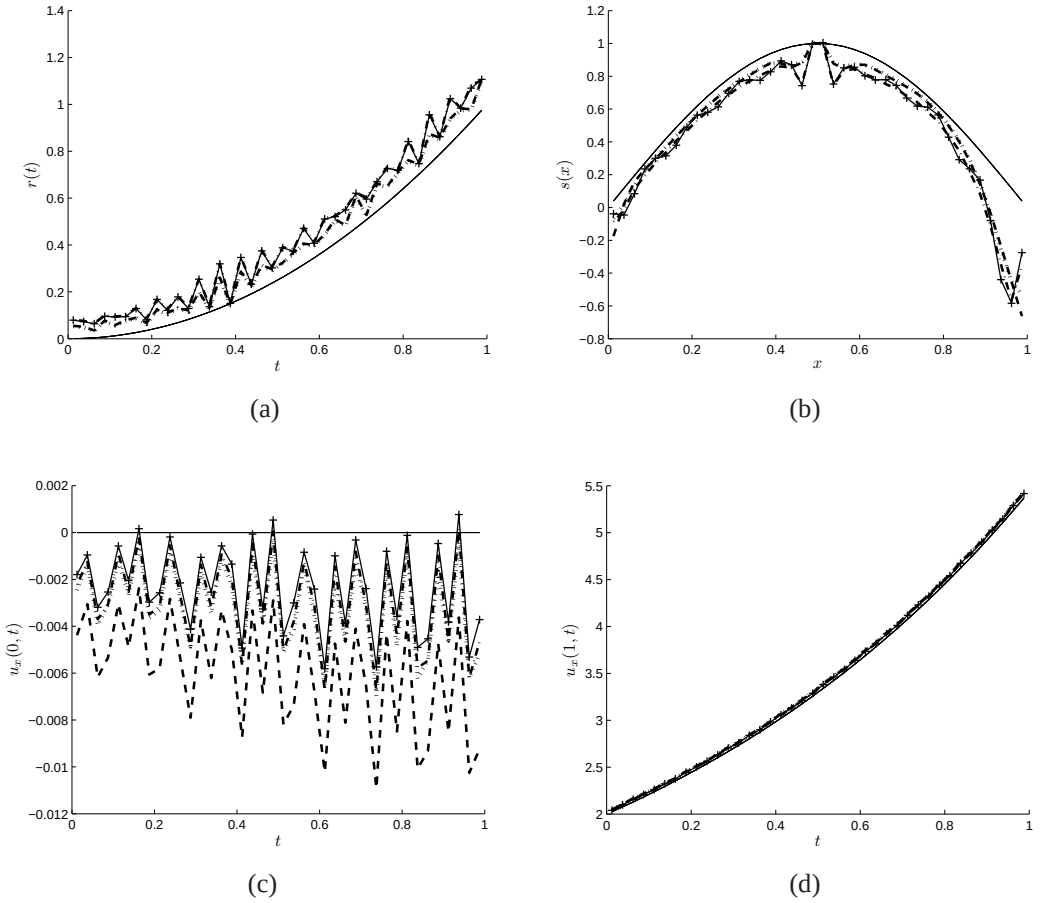

(a) (b)

(c) (d)

Figure 6.5: The analytical (——) and numerical results of (a) $r(t)$, (b) $s(x)$, (c) $u_x(0,t)$, and (d) $u_x(1,t)$ obtained using the TSVD $(-+-)$, ZOTR $(-\cdot-)$, FOTR $(\cdots)$, and SOTR $(---)$ with regularisation parameters suggested by the GCV function of Figure 6.3(b) and 6.4(b) for exact data, for Example 1.

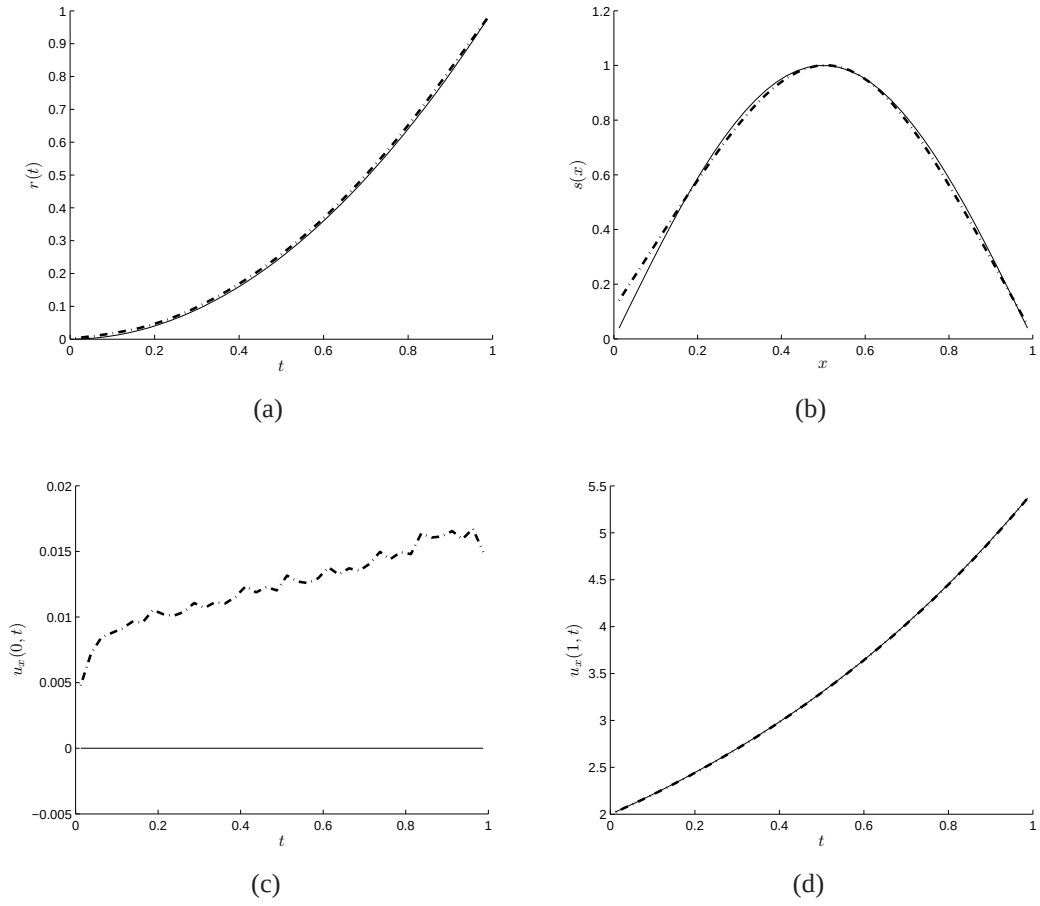

Figure 6.6: The analytical (——) and numerical results $(- \cdot -)$ of (a) $r(t)$, (b) $s(x)$, (c) $u_x(0,t)$, and (d) $u_x(1,t)$ obtained using the SOTR with the regularisation parameter λ_L=1E-1 suggested by the L-curve of Figure 6.4(a) for exact data, for Example 1.

tive of r, $\log \|R^{(1)} r_{\lambda_r}\|$, forms an L-shaped corner at λ_r=1E+1, while λ_s=1 is based around the area of the L-corner on the plane of $\log \|X \underline{\mathbf{w}}_\lambda - \underline{\mathbf{y}}^\epsilon\|$ versus $\log \|R^{(2)} r_{\lambda_s}\|$. However, the numerical solution for $s(x)$ obtained using the parameters $\lambda_{r,L} = 10$, $\lambda_{s,L} = 1$ suggested by the L-surface method, is still inaccurate. We finally use the trial and error process to seek out the appropriated regularisation parameters, and found that regularisation parameters $\lambda_{r,opt}$=8 and $\lambda_{s,opt}$=5.2E-2 can yield an accurate and stable numerical solution, see Figure 6.11. Nevertheless, more research has to be undertaken in the future for the selection of appropriate multiple regularisation parameters, [12]. for completeness, the RMSE of all results which we have mentioned so far are detailed

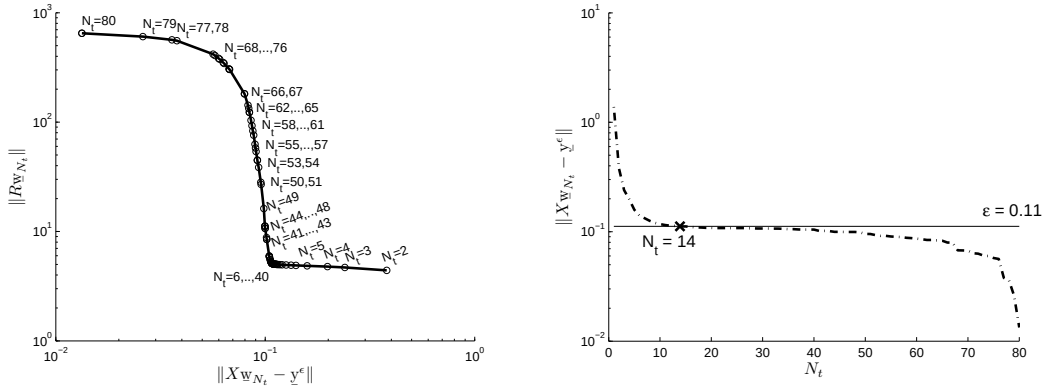

(a) (b)

Figure 6.7: (a) The L-curve and (b) the discrepancy principle obtained using the TSVD for noisy input $p = 1\%$, for Example 1.

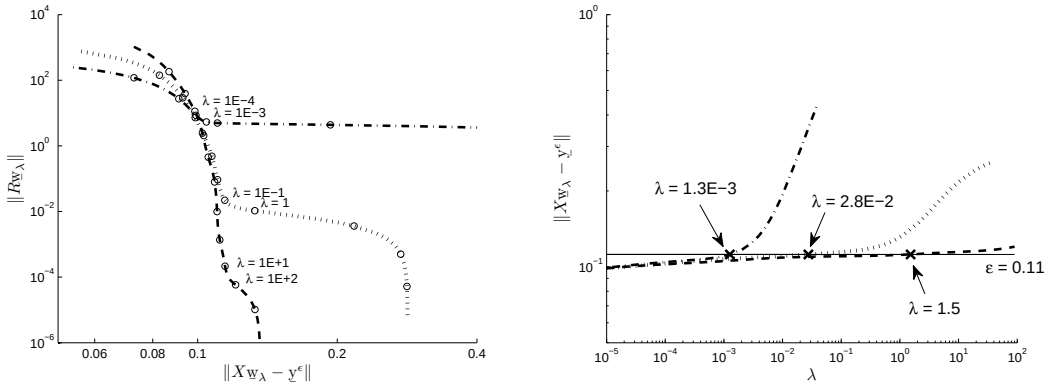

(a) (b)

Figure 6.8: (a) The L-curve and (b) the discrepancy principle obtained using the ZOTR $(- \cdot -)$, FOTR $(\cdots)$, and SOTR $(- - -)$ for noisy input $p = 1\%$, with $\lambda = \lambda_r = \lambda_s$, for Example 1.

in Table 6.2.

6.5.2 Example 2

In example 1, the case of smooth source functions has been investigated and it can retrieved the instability with the use of BEM together with the regularisation based on either the TSVD and the Tikhonov regularisation. In this example, we are considering

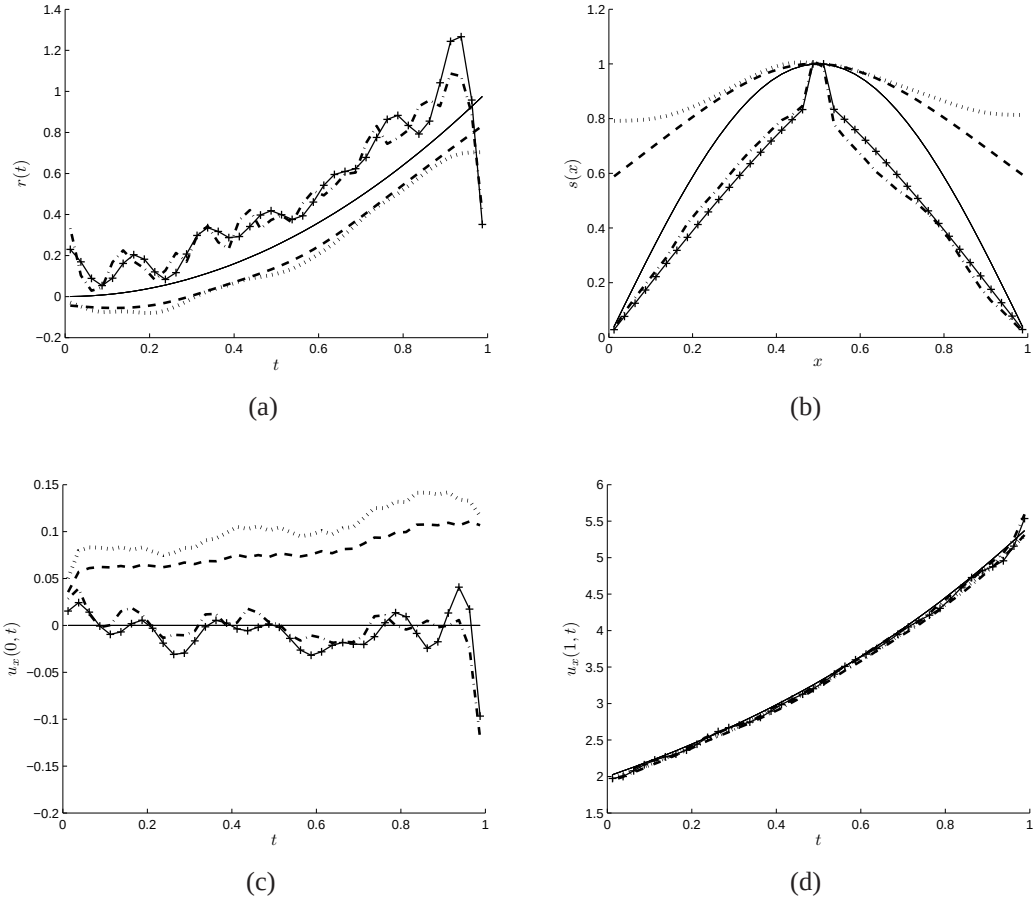

Figure 6.9: The analytical (——) and numerical results of (a) $r(t)$, (b) $s(x)$, (c) $u_x(0,t)$, and (d) $u_x(1,t)$ obtained using the TSVD $(- + -)$ with $N_t = 14$, and the ZOTR $(- \cdot -)$, FOTR $(\cdots)$, SOTR $(- - -)$ with regularisation parameters suggested by the discrepancy principle of Figure 6.8(b) for noisy input $p = 1\%$, for Example 1.

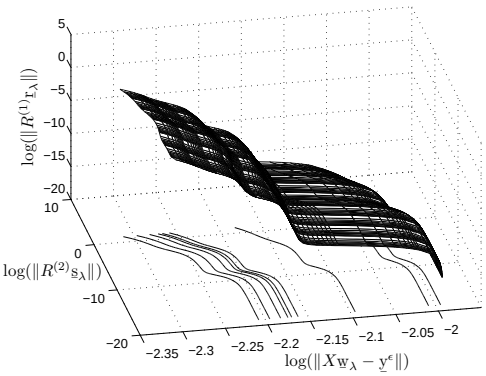

(a)

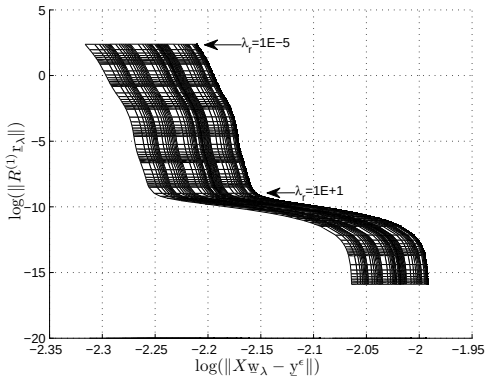

(b)

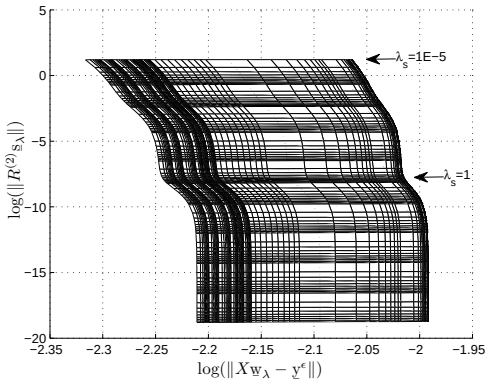

(c)

Figure 6.10: The L-surface on (a) a three-dimensional plot, (b) plane of $\log \|X\mathbf{w}_\lambda - \underline{\mathbf{y}}^\epsilon\|$ versus $\log \|R^{(1)}\mathbf{r}_\lambda\|$, and (c) plane of $\log \|X\mathbf{w}_\lambda - \underline{\mathbf{y}}^\epsilon\|$ versus $\log \|R^{(2)}\mathbf{s}_\lambda\|$, obtained using the SOTR for noisy input $p = 1\%$, for Example 1.

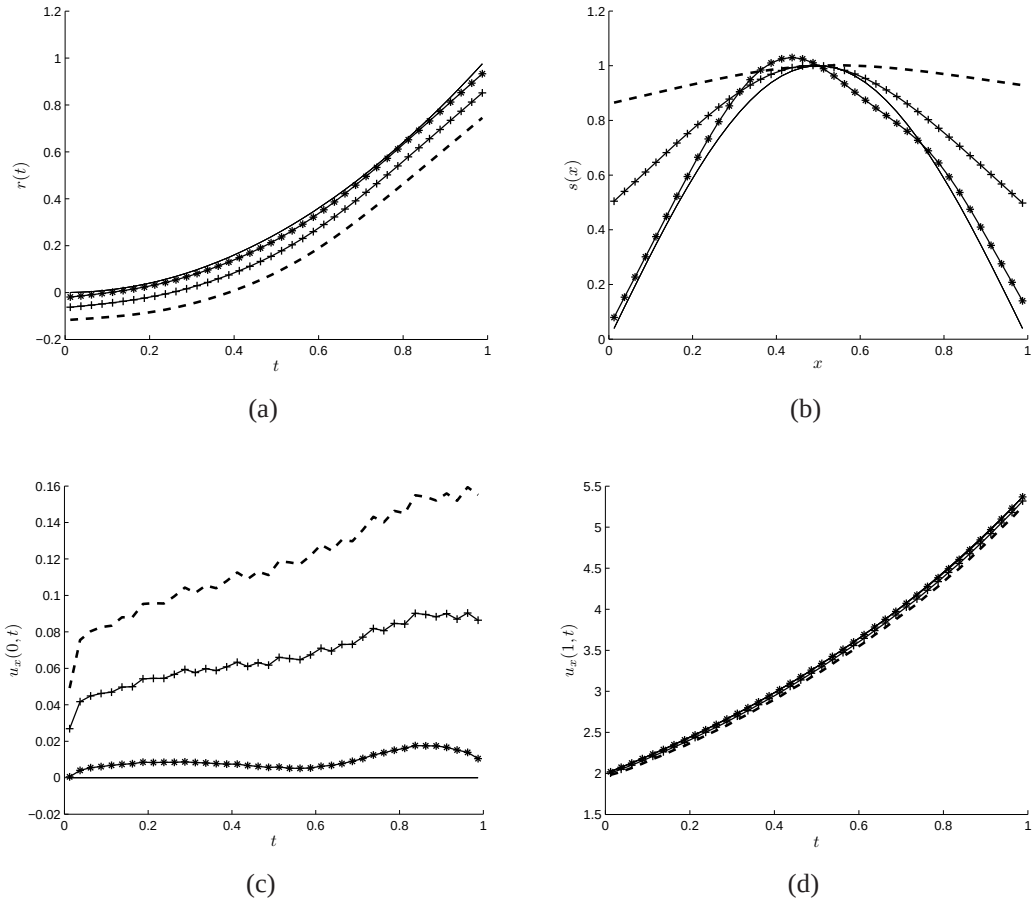

Figure 6.11: The analytical (——) and numerical results of (a) $r(t)$, (b) $s(x)$, (c) $u_x(0,t)$, and (d) $u_x(1,t)$ obtained using the SOTR with regularisation parameters suggested by the L-curve criterion $\lambda_L = \lambda_r = \lambda_s = 10$ $(- - -)$, the L-surface method $(\lambda_{r,L}, \lambda_{s,L})$=(10,1) $(- + -)$, and the trial and error $(\lambda_{r,opt}, \lambda_{s,opt})$=(8,5.2E-2) $(- * -)$, for noisy input $p = 1\%$, for Example 1.

Table 6.2: The RMSE for $r(t)$, $s(x)$, $u_x(0,t)$, and $u_x(1,t)$ obtained using the SVD, TSVD, ZOTR, FOTR, and SOTR, for $p \in \{0,1\}\%$, for Example 1.

Method	p	Parameter	RMSE			
			$r(t)$	$s(x)$	$u_x(0,t)$	$u_x(1,t)$
SVD	0	-	1.47E-1	2.55E-1	9.32E-3	4.58E-2
TSVD	0	N_t=56	1.17E-1	2.03E-1	2.94E-3	3.57E-2
ZOTR	0	λ_{GCV}=1.0E-7	1.20E-1	2.02E-1	3.53E-3	3.65E-2
FOTR	0	λ_{GCV}=1.2E-7	7.62E-2	1.70E-1	3.68E-3	4.35E-2
SOTR	0	λ_{GCV}=4.5E-8	7.96E-2	1.85E-1	6.48E-3	4.70E-2
SOTR	0	λ_L=1.0E-1	8.70E-3	2.81E-2	1.27E-2	3.09E-3
SVD	1%	-	1.62E+1	1.01E+2	2.84	2.48E-1
TSVD	1%	N_t=14	2.04E-1	1.77E-1	2.29E-2	5.83E-2
ZOTR	1%	λ_{dis}=1.3E-3	1.87E-1	1.83E-1	2.32E-2	4.87E-2
FOTR	1%	λ_{dis}=2.8E-2	1.28E-1	3.50E-1	1.05E-1	7.91E-2
SOTR	1%	λ_{dis}=1.5	9.72E-2	2.65E-1	8.05E-2	5.58E-2
SOTR	1%	λ_L=10	1.61E-1	4.23E-1	1.20E-1	9.36E-2
SOTR	1%	λ_r=10,λ_s=1	7.93E-2	2.18E-1	6.81E-2	4.40E-2
SOTR	1%	λ_r=8,λ_s=5.2E-2	1.92E-3	5.34E-2	1.00E-2	6.39E-3

in more severe case with the non-smooth source functions. Let $T = L = 1$, $X_0 = \frac{1}{2}$ and the input data

$$\begin{cases} u_0(x) = \mu_0(t) = \mu_L(t) = 0, \quad S_0 = s(\frac{1}{2}) = \dfrac{1}{4}, \\ \chi(t) = u(\frac{1}{2}, t) = t^2 \sin(\frac{1}{4}), \quad \psi(x) = \displaystyle\int_0^1 u(x,t)\, dt = \frac{\sin(x - x^2)}{3}, \\ f(x,t) = x, \quad g(x,t) = e^t, \\ h(x,t) = (2t + t^2(1-2x)^2)\sin(x - x^2) + 2t^2\cos(x - x^2) \\ \qquad\qquad -x|t - \frac{1}{2}| - e^t|x - \frac{3}{4}|. \end{cases} \tag{6.31}$$

Note that the input data (6.31) satisfy the conditions of Theorem 6.2.1 to ensure the existence and uniqueness of solution of the inverse problem (6.1)–(6.5). In fact, the exact solution is given by

$$u(x,t) = t^2 \sin(x - x^2), \quad r(t) = |t - \tfrac{1}{2}|, \quad s(x) = |x - \tfrac{3}{4}|.$$

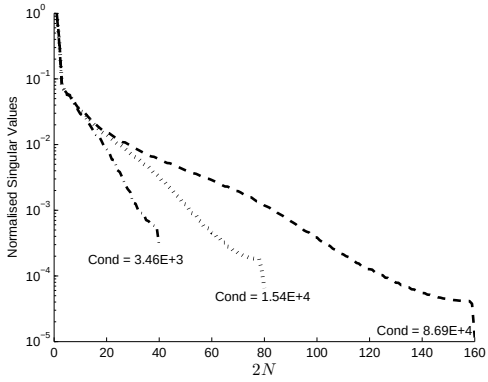

Figure 6.12: The normalised singular values of matrix X for $N = N_0 = 20$ $(- \cdot -)$, $N = N_0 = 40$ $(\cdots)$, and $N = N_0 = 80$ $(- - -)$, for Example 2.

This is a more severe test example than Example 1 since the source components $r(t)$ and $s(x)$ are not smooth functions.

We have calculated the condition numbers of the matrix X and obtained the condition numbers 3.46E+3, 1.54E+4, and 8.69E+4 for $N = N_0 = 20$, 40, and 80, respectively. Moreover, the corresponding normalised singular values are shown in Figure 6.12. In Example 2, the condition numbers of the matrix X are not much different from the condition numbers for Example 1. Then we expect to solve this inverse problem by using wither the TSVD or the Tikhonov regularisation as means to reduce the instability of the solution. Here, we fix $N = N_0 = 40$ and $X_0 = \frac{1}{2}$.

Exact Data

First we have tried the TSVD, ZOTR, FOTR and SOTR with the regularisation parameter given by the GCV function. This yields $N_t = 65$, λ_{GCV}=2.9E-8, 3.2E-8, and 8.3E-9, respectively. But we have found that the solutions for $r(t)$ and $s(x)$ are not so accurate. We then considered the L-curve method for choosing the regularisation parameter. Figures 6.13(a) and 6.13(b) display the L-curves for the TSVD and the Tikhonov regularisation, respectively. The same as the L-curve in Example 1, an L-shape is obtained only when using the SOTR with suggests an L-corner around λ=1E-4 to 1E-3. In particular, for λ_L=1E-4 we obtain the stable solutions presented in Figure

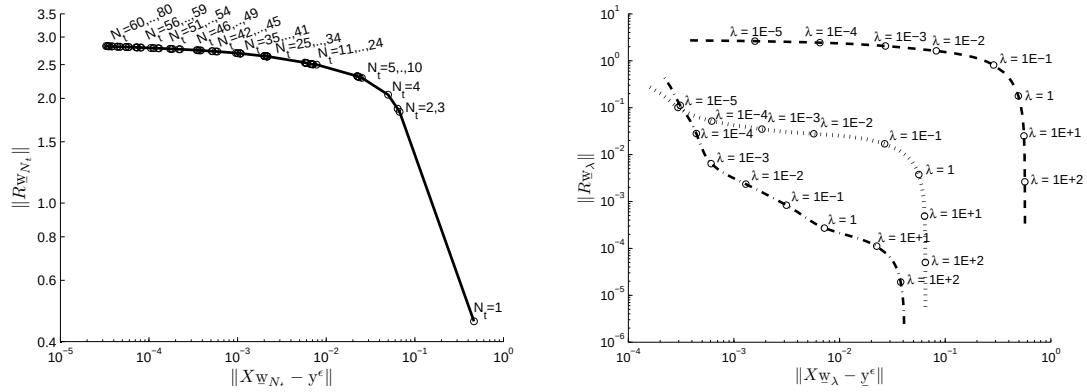

(a) (b)

Figure 6.13: The L-curve obtained using (a) the TSVD and (b) the ZOTR $(- \cdot -)$, FOTR $(\cdots)$, and SOTR $(- - -)$ with $\lambda = \lambda_r = \lambda_s$, for exact data, for Example 2.

6.14 and Table 6.3. The untruncated SVD, i.e. $N_t = 80$, whose numerical results are also included is not so accurate and stable in retrieving the functions $r(t)$ and $s(x)$.

Table 6.3: The RMSE for $r(t)$, $s(x)$, $u_x(0,t)$, and $u_x(1,t)$ obtained using the SVD, TSVD, ZOTR, FOTR, and SOTR, for $p \in \{0,1\}\%$, for Example 2.

Method	p	Parameter	RMSE			
			$r(t)$	$s(x)$	$u_x(0,t)$	$u_x(1,t)$
SVD	0	-	1.15E-1	4.12E-2	2.05E-3	6.95E-4
TSVD	0	N_t=65	1.17E-1	7.92E-2	1.15E-1	4.12E-2
ZOTR	0	λ_{GCV}=2.9E-8	1.67E-1	6.63E-2	5.21E-3	2.19E-3
FOTR	0	λ_{GCV}=3.2E-8	8.94E-2	2.99E-2	2.12E-3	6.01E-4
SOTR	0	λ_{GCV}=8.3E-9	9.20E-2	3.13E-2	2.10E-3	7.61E-4
SOTR	0	λ_L=1.0E-4	5.88E-3	8.94E-3	2.39E-3	1.04E-3
SVD	1%	-	5.31E+1	8.91E+1	2.88	2.42E-1
TSVD	1%	N_t=10	2.16E-1	2.37E-1	1.15E-1	9.05E-2
ZOTR	1%	λ_{dis}=7.3E-4	1.20E-1	2.12E-1	1.15E-1	4.72E-2
FOTR	1%	λ_{dis}=3.2E-2	1.66E-1	6.77E-2	2.21E-2	2.51E-2
SOTR	1%	λ_{dis}=2.3	5.78E-2	7.90E-2	9.98E-3	4.95E-2
SOTR	1%	λ_L=1	9.24E-2	6.63E-2	1.55E-2	4.04E-2
SOTR	1%	$\lambda_{r,L}$=1,$\lambda_{s,L}$=10	3.96E-2	1.13E-1	4.67E-3	6.40E-2
SOTR	1%	$\lambda_{r,opt}$=2.2,$\lambda_{s,opt}$=5.9	2.37E-2	1.01E-1	3.42E-3	5.98E-2

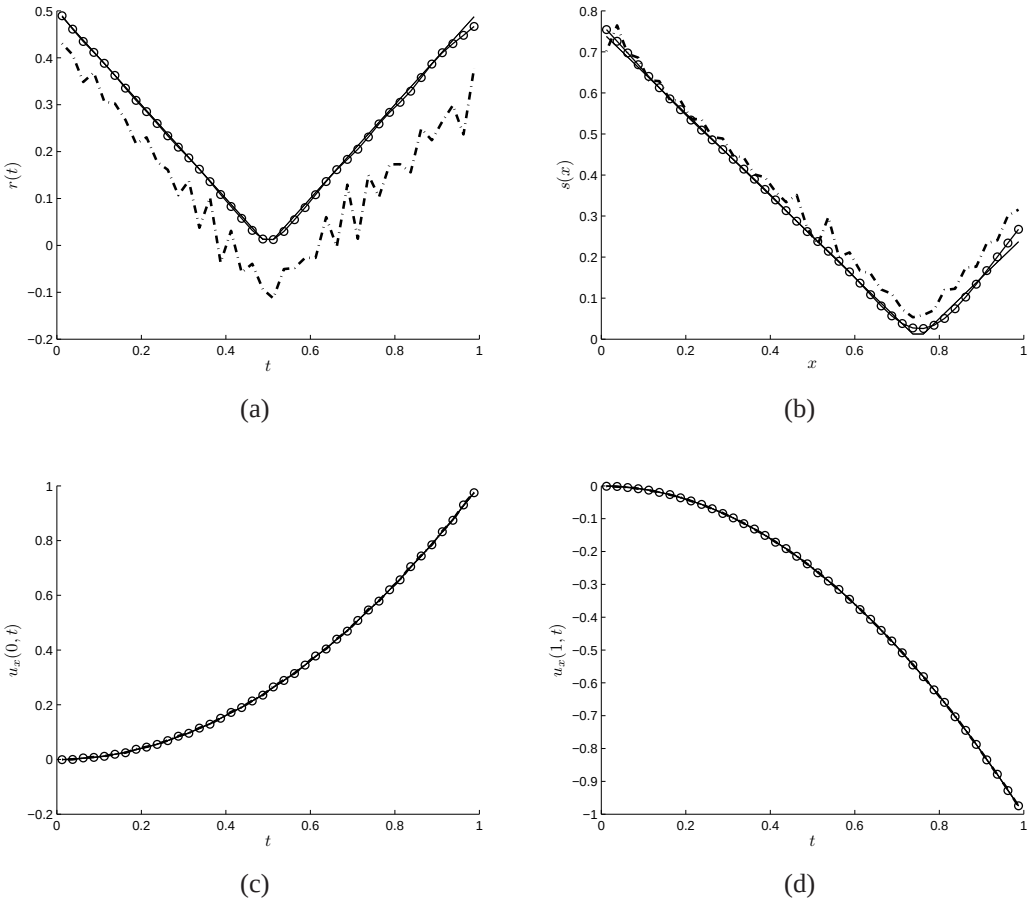

Figure 6.14: The analytical (——) and numerical results of (a) $r(t)$, (b) $s(x)$, (c) $u_x(0,t)$, and (d) $u_x(1,t)$ obtained using the SVD $(- \cdot -)$ and the SOTR $(-\mathrm{o}-)$ with the regularisation parameter λ_L=1E-4 suggested by the L-curve of Figure 6.13(b) for exact data, for Example 2.

Noisy Data

When noise is present in the measured data $\chi(t)$ and $\psi(x)$, the regularisation with an appropriate parameter has to be carefully considered. Here we have tried solving the perturbed problem with $p = 1\%$ noisy input by using the TSVD, ZOTR, FOTR, and SOTR, with the regularisation parameter given by the discrepancy principle. This yields $N_t = 10$, λ_{dis}=7.3E-4, 3.2E-2, and 2.3, respectively. Although the discrepancy principle is a rigorous method which uses the knowledge of noise, the RMSE errors displayed in Table 6.3 are quite large. Alternatively, we consider the L-curve method

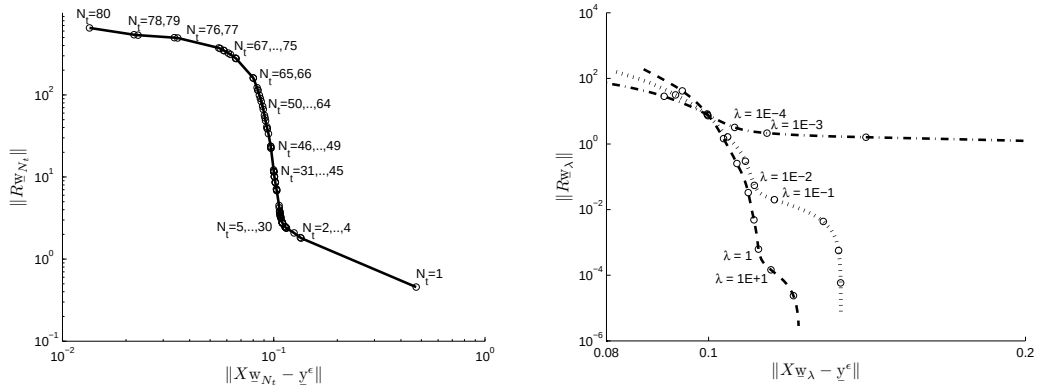

(a) (b)

Figure 6.15: The L-curve obtained using (a) the TSVD and (b) the ZOTR $(- \cdot -)$, FOTR $(\cdots)$, and SOTR $(- - -)$ with $\lambda = \lambda_r = \lambda_s$, for noisy input $p = 1\%$, for Example 2.

for the choice of regularisation parameter displayed in Figure 6.15. This suggests the appropriate parameters as N_t between 5 and 30, λ_L=1E-4, 1E-2, and 1 for the TSVD, ZOTR, FOTR, and SOTR,, respectively. We then solved the inverse problem with these parameters and found that the numerical results obtained using the TSVD, ZOTR and FOTR, are not so accurate. Whereas the SOTR yields a more accurate solution, as shown in Figure 6.17 with dashed line. Hence, as in Example 1, the case of $\lambda_r \neq \lambda_s$ needs to be considered by using the L-surface method for choosing the appropriate regularisation parameters. Figures 6.16 displays the L-surface which selects $\lambda_{r,L}$=10 and $\lambda_{s,L}$=1, and the results obtained using the SOTR with these parameters are shown in Figure 6.17. Furthermore, the regularisation parameters selected by the trial and error have also been considered and these results have also been included in Figure 6.17. The accurate retrieval of $r(t)$ is possible, but for $s(x)$ this is less accurate.

6.6 Conclusions

This chapter has presented a numerical approach to the simultaneous numerical determination of the space- and the time-dependent coefficient source functions of an

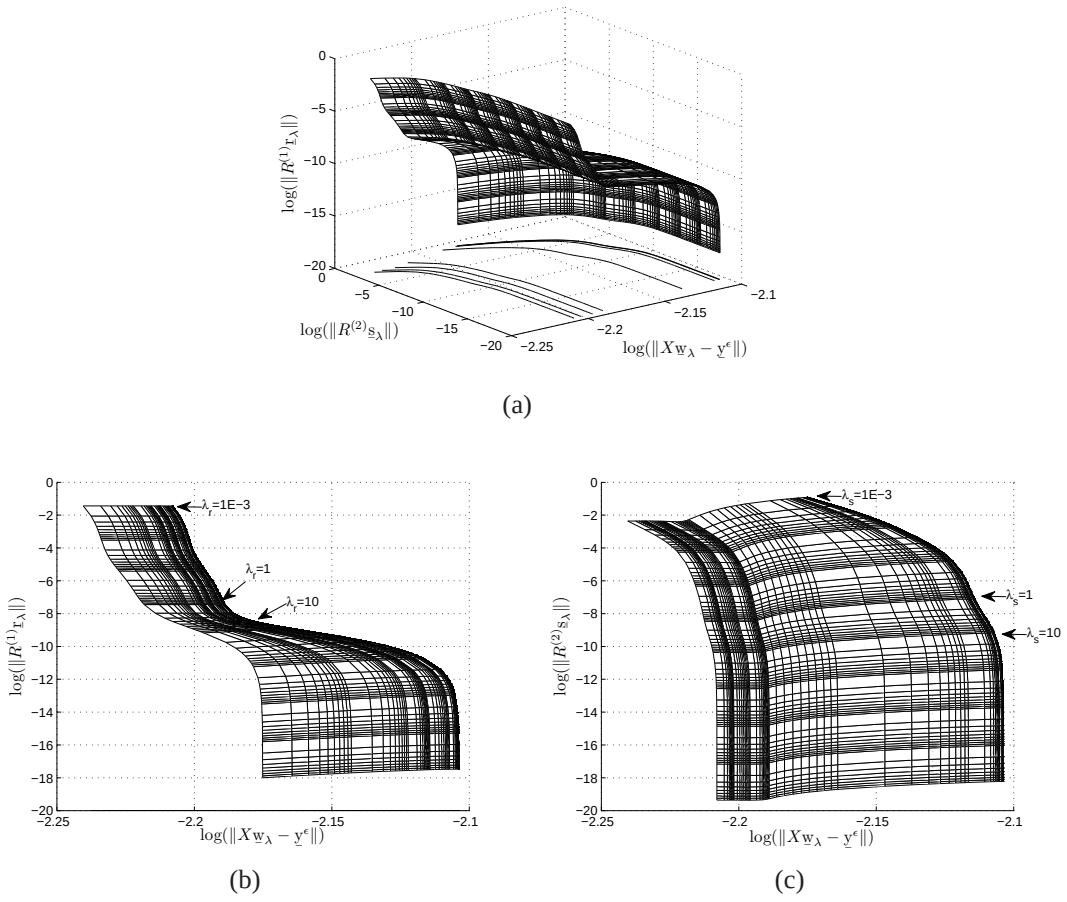

(a)

(b) (c)

Figure 6.16: The L-surface on (a) a three-dimensional plot, (b) plane of $\log \|X\mathrm{w}_\lambda - \underline{\mathrm{y}}^\epsilon\|$ versus $\log \|R^{(1)}\mathrm{r}_\lambda\|$, and (c) plane of $\log \|X\mathrm{w}_\lambda - \underline{\mathrm{y}}^\epsilon\|$ versus $\log \|R^{(2)}\mathrm{s}_\lambda\|$, obtained using the SOTR for noisy input $p = 1\%$, for Example 2.

inverse heat conduction problem with Dirichlet boundary conditions together with specified interior temperature measurement and time-integral condition, as the over-determination conditions.

The numerical discretisation was based on the BEM together with either the TSVD, or the Tikhonov regularisation. Additionally, various methods for choosing the regularisation parameters have been utilised. The numerical results presented show that accurate and stable numerical solutions can be achieved provided that the regularisation parameters are appropriately selected. The two-parameter selection has proved to be difficult, as some of our numerical results obtained using several criteria, e.g.

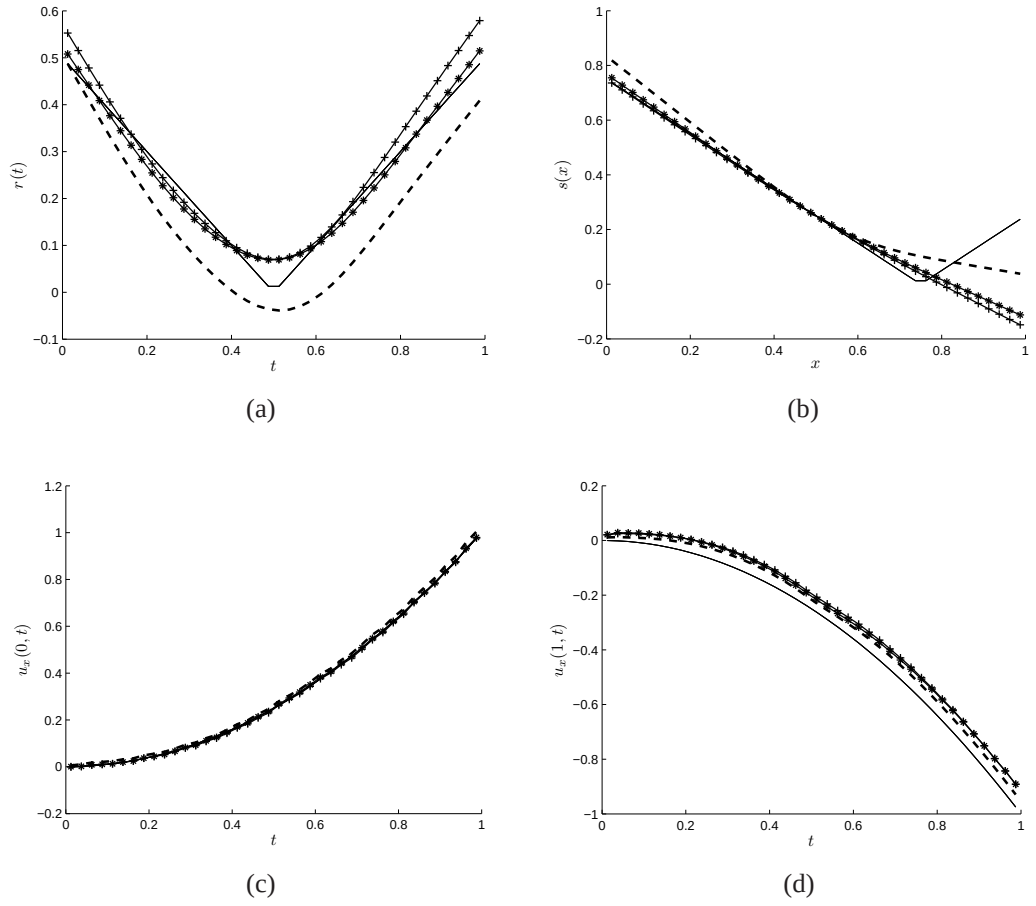

(a) (b)

(c) (d)

Figure 6.17: The analytical (——) and numerical results of (a) $r(t)$, (b) $s(x)$, (c) $u_x(0,t)$, and (d) $u_x(1,t)$ obtained using the SOTR with regularisation parameters suggested by the L-curve criterion $\lambda_L = \lambda_r = \lambda_s = 1$ $(---)$, the L-surface method $(\lambda_{r,L}, \lambda_{s,L})$=(1,10) $(-+-)$, and the trial and error $(\lambda_{r,opt}, \lambda_{s,opt})$=(2.2,5.9) $(-*-)$, for noisy input $p = 1\%$, for Example 2.

discrepancy principle, GCV, L-curve, L-surface, have shown. Nevertheless, more research has to be undertaken in the future for the selection of multiple regularisation parameters, [12].

In the next chapter we will consider reconstructing multiplicative space- and time-dependent heat sources.

Chapter 7

Determination of Multiplicative Space- and Time-dependent Heat Sources

7.1 Introduction

In the previous chapter, we have investigated the reconstruction of an additive source of the form $r(t)f(x,t) + s(x)g(x,t)$. In this chapter, we consider the reconstruction of a multiplicative source of the form $r(t)s(x)$, in which both $r(t)$ and $s(x)$ are unknown functions. In contrast to the previously investigated linear reconstruction of the additive source, Chapter 6, this new inverse source problem formulation is more difficult to solve because it now becomes nonlinear. Moreover, its ill-posedness with respect to small errors in the input data being blown up in the output source solution adds even further difficulty.

The existence and uniqueness of the sources $r(t)$, $s(x)$ and the temperature $u(x,t)$ of the inverse problem were already established in [47]. In this chapter, we consider obtaining a stable solution by using the BEM together with a nonlinear minimisation.

The plan of the chapter is as follows. In Section 7.2, we give the mathematical formulation of the inverse multiplicative source problem and state its unique solvability. In Section 7.3, we describe the numerical discretisation of the problem based on the

BEM, whilst in Section 7.4 we introduce the inverse method for obtaining the solution based on a nonlinear least-squares minimisation. Section 7.5 presents and discusses numerical results and illustrates the need for employing regularisation in order to stabilise the solution. Finally, Section 7.6 presents the conclusions of the study.

7.2 Mathematical formulation

Consider the following inverse initial-boundary value problem of finding the temperature $u(x,t)$ and the multiplicatively separable source function $F(x,t) := r(t)s(x)$ satisfying the heat equation

$$u_t = u_{xx} + r(t)s(x), \quad (x,t) \in D_T, \tag{7.1}$$

subject to the initial condition (1.7), namely

$$u(x,0) = u_0(x), \quad x \in [0,L], \tag{7.2}$$

the homogeneous Neumann boundary conditions

$$u_x(0,t) = u_x(L,t) = 0, \quad t \in [0,T], \tag{7.3}$$

the additional temperature measurement

$$u(X_0,t) = \chi(t), \quad t \in [0,T], \tag{7.4}$$

at a fixed sensor location $X_0 \in (0,L)$, and

$$u(x,T) = \beta(x), \quad x \in [0,L], \tag{7.5}$$

at the 'upper-base' final time $t = T$. Conditions (7.3) express that the ends $\{0,L\}$ of the finite slab $(0,L)$ are insulated. In order to avoid trivial non-uniqueness represented

by the identity $r(t)s(x) = \frac{r(t)}{c} \cdot cs(x)$, with c arbitrary non-zero constant, we impose a fixing condition, say

$$s(X_0) = S_0. \tag{7.6}$$

In the above setting, the functions u_0, χ, β and the constant S_0 are given. We further assume that the conditions (7.2)–(7.5) are consistent, i.e. the following compatibility conditions are satisfied:

$$u_0'(0) = u_0'(L) = \beta'(0) = \beta'(L) = 0, \quad \chi(0) = u_0(X_0), \quad \chi(T) = \beta(X_0). \tag{7.7}$$

The unique solvability, i.e. existence and uniqueness of the solution of the inverse problem (7.1)–(7.6), was established in [47]. With some slight corrections, this theorem reads as follows.

Theorem 7.2.1 *Suppose that* $u_0(x), \beta(x) \in \mathbb{W}_2^4(0, L)$, *and* $\chi(t) \in \mathbb{W}_2^2(0, T)$ *satisfy* (7.7) *and that* $S_0 \neq 0$. *Also, assume that:*

(i) $M := \chi'(0) - u_0''(X_0) \neq 0, \quad m := \dfrac{\chi'(T) - \beta''(X_0)}{M} \neq 0,$

(ii) $u_0'''(0) = u_0'''(L) = \beta'''(0) = \beta'''(L) = 0,$

(iii) $\lambda_1 < 1, 4\lambda_2\lambda_3 - (1 - \lambda_1)^2 \leq 0, \lambda_4 < 1,$

where

$$\lambda_1 := \frac{2}{m^2M^2} \max\left\{M^2 + \frac{4L^2\|\chi''\|^2}{\pi^2}, 4L\|\theta\|^2 + Lm^2\|u_0'''\|^2\right\},$$
$$\lambda_2 := \frac{2}{M^2} \max\left\{\frac{4L^6}{\pi^4m^4}, 1\right\}, \quad \lambda_3 := \frac{2\|\theta'\|^2}{m^2} + \frac{4\|\chi''\|^2}{M^2}\left(\frac{2\|\theta\|^2}{m^2} + \|u_0'''\|^2\right),$$
$$\lambda_4 := \frac{1}{m^2M^2} \max\{M^2 + 2L^3z + 4L^2\|\chi''\|^2, 4L^3z + 4L^3\|\theta'\|^2 + 2Lm^2\|u_0'''\|^2\},$$
$$\theta(x) = \beta'''(x) - mu_0'''(x), \quad z = \frac{1 - \lambda_1}{2\lambda_2}.$$

Then the inverse problem given by equations (7.1)–(7.6) *has a unique solution* $r(t) \in \mathbb{W}_2^1(0, T)$, $s(x) \in \mathbb{W}_2^2(0, L)$ *and*
$u(x, t) \in \mathbb{W}_2^{4,2}(D_T) \cap C(0, T; \mathbb{W}_2^4(0, L)) \cap C(0, L; \mathbb{W}_2^2(0, T))$.

Note that in the above theorem, $\mathbb{W}_2^k(\Omega)$, with $k \in \{1, 2, 4\}$ and $\Omega = (0, L)$ or $(0, T)$, denotes the Sobolev space of functions consisting of all elements of $L^2(\Omega)$ having generalised derivatives up to order k inclusively in $L^2(\Omega)$. Also, we denote

$$\mathbb{W}_2^{4,2}(D_T) := \{u \in L^2(D_T) | \partial_x^j u \in L^2(0, L), j = \overline{1, 4}, \text{ and } \partial_t^i u \in L^2(0, T), i = 1, 2\}.$$

Finally, $C(0, T; \mathbb{W}_2^4(0, L))$ denotes the space of continuous mappings from $(0, T)$ to $\mathbb{W}_2^4(0, L)$ and $C(0, L; \mathbb{W}_2^2(0, T))$ denotes the space of continuous mappings from $(0, L)$ to $\mathbb{W}_2^2(0, T)$. The norms $\|\chi''\|$ and $\|u_0'''\|$ are understood in $L^2(0, T)$ and $L^2(0, L)$, respectively. Also, the norms of θ and θ' are in $L^2(0, L)$.

Although the inverse problem (7.1)–(7.6) has a unique solution it is still ill-posed because it violates the continuous dependence upon the input data (7.4) and (7.5). In the next section we will demonstrate how the BEM discretising numerically the heat equation (7.1) can be used together with the regularisation in order to obtain a stable solution.

7.3 The boundary element method (BEM)

In this section, we use the numerical procedure for discretising the inverse problem (7.1)–(7.6) by using the BEM which results in the following boundary integral equation:

$$\begin{aligned}\eta(x)u(x,t) = &\int_0^t \left[G(x,t,\xi,\tau)\frac{\partial u}{\partial n(\xi)}(\xi,\tau) - u(\xi,\tau)\frac{\partial G}{\partial n(\xi)}(x,t,\xi,\tau)\right]_{\xi\in\{0,L\}} d\tau \\ &+ \int_0^L G(x,t,y,0)u(y,0)\,dy + \int_0^L \int_0^T G(x,t,y,\tau)r(\tau)s(y)\,d\tau dy, \\ &(x,t) \in [0,L] \times (0,T]. \end{aligned} \tag{7.8}$$

Using the same discretisation as described in Section 2.3 which has been used so far as in previous chapters, we obtain

$$\eta(x)u(x,t) = \sum_{j=1}^{N} \left[A_{0j}(x,t)q_{0j} + A_{Lj}(x,t)q_{Lj} - B_{0j}(x,t)h_{0j} - B_{Lj}(x,t)h_{Lj}\right] + \sum_{k=1}^{N_0} \left[C_k(x,t)u_{0,k} + D_k^r(x,t)s_k\right], \tag{7.9}$$

where

$$D_k^r(x,t) = \int_{x_{k-1}}^{x_k} \int_0^t G(x,t,y,\tau)r(\tau)\, d\tau\, dy = \sum_{j=1}^{N} d_{j,k}(x,t)r_j, \tag{7.10}$$

where $d_{j,k}(x,t) = \int_{x_{k-1}}^{x_k} \int_{t_{j-1}}^{t_j} G(x,t,y,\tau)\, d\tau\, dy$ for $j = \overline{1,N}$, $k = \overline{1,N_0}$. The double integral source term $d_{j,k}(x,t)$ can be evaluated analytically to be given by

$$d_{j,k}(x,t) = \begin{cases} 0 & ;\ t \le t_{j-1}, \\ J(x,t,x_{k-1},t_{j-1}) - J(x,t,x_k,t_{j-1}) & \\ +\dfrac{(x-x_{k-1})^2}{4} - \dfrac{(x-x_k)^2}{4} & ;\ t_{j-1} < t \le t_j,\ x \le x_{k-1}, \\ J(x,t,x_{k-1},t_{j-1}) - J(x,t,x_k,t_{j-1}) & \\ -\dfrac{(x-x_{k-1})^2}{4} - \dfrac{(x-x_k)^2}{4} & ;\ t_{j-1} < t \le t_j,\ x_{k-1} < x \le x_k, \\ J(x,t,x_{k-1},t_{j-1}) - J(x,t,x_k,t_{j-1}) & \\ -\dfrac{(x-x_{k-1})^2}{4} + \dfrac{(x-x_k)^2}{4} & ;\ t_{j-1} < t \le t_j,\ x > x_k, \\ J(x,t,x_{k-1},t_{j-1}) - J(x,t,x_k,t_{j-1}) & \\ -J(x,t,x_{k-1},t_j) + J(x,t,x_k,t_j) & ;\ t > t_j, \end{cases}$$

where

$$J(x,t,x_k,t_j)=\left(\frac{(x-x_k)^2}{4}+\frac{t-t_j}{2}\right)\operatorname{erf}\left(\frac{x-x_k}{2\sqrt{t-t_j}}\right)+\frac{\sqrt{t-t_j}}{2\sqrt{\pi}}(x-x_k)\exp\left(-\frac{(x-x_k)^2}{4(t-t_j)}\right).$$

By applying (7.9) at the boundary element nodes $(0,\tilde{t}_i)$ and $(L,\tilde{t}_i)$ for $i=\overline{1,N}$ and the homogeneous Neumann boundary condition (7.3), i.e. $q_{0j}=q_{Lj}=0$, we obtain the system of $2N$ equations

$$-B\mathtt{h}+C\mathtt{u}_0+D^r\mathtt{s}=\underline{0}, \tag{7.11}$$

where $D^r=\begin{bmatrix}\sum_{j=1}^N d_{j,k}(0,\tilde{t}_i)r_j\\ \sum_{j=1}^N d_{j,k}(L,\tilde{t}_i)r_j\end{bmatrix}_{2N\times N_0}$.

For the direct problem, we can find now the boundary temperatures $u(0,\tilde{t}_i)$ and $u(L,\tilde{t}_i)$ from (7.11) as

$$\mathtt{h}=B^{-1}(C\mathtt{u}_0+D^r\mathtt{s}). \tag{7.12}$$

Furthermore, the interior temperatures $u(X_0,\tilde{t}_i)$ for $i=\overline{1,N}$ from the additional condition condition (7.4) can be approximated similarly as in (6.16), i.e. $[u(X_0,\tilde{t}_i)]_N=\left[\chi(\tilde{t}_i)\right]_N$. Applying this in (7.9) it gives

$$-B^I\mathtt{h}+C^I\mathtt{u}_0+D^{rI}\mathtt{s}=\underline{\chi}, \tag{7.13}$$

where $D^{rI}=\left[\sum_{j=1}^N d_{j,k}(X_0,\tilde{t}_i)r_j\right]_{N\times N_0}$. Whereas the final temperature $u(\tilde{x}_k,T)$ for $k=\overline{1,N_0}$ from the overdetermination (7.5) can be approximated as $[u(\tilde{x}_k,T)]_{N_0}=\left[\beta(\tilde{x}_k)\right]_{N_0}$. Applying this in (7.9) it gives

$$-B^{III}\mathtt{h}+C^{III}\mathtt{u}_0+D^{rIII}\mathtt{s}=\underline{\beta}, \tag{7.14}$$

where

$$B^{III} = \Big[B_{0j}(\tilde{x}_k, T) \quad B_{Lj}(\tilde{x}_k, T)\Big]_{N_0 \times 2N}, \qquad C^{III} = \Big[C_k(\tilde{x}_k, T)\Big]_{N_0 \times N_0},$$
$$D^{rIII} = \Big[\textstyle\sum_{j=1}^{N} d_{j,k}(\tilde{x}_k, T) r_j\Big]_{N_0 \times N_0}.$$

7.4 Solution of inverse problem

In this section, we wish to obtain simultaneously the unknown components $r(t)$ and $s(x)$ of the multiplicative source term in the inverse problem (7.1)–(7.6) by using the BEM together with a classical minimisation process. The conditions (7.4)–(7.6) are imposed by minimising the nonlinear least-squares function

$$\mathbb{F}_0(r, s) := \sum_{i=1}^{N} \left(u(X_0, \tilde{t}_i) - \chi(\tilde{t}_i)\right)^2 + \sum_{k=1}^{N_0} \left(u(\tilde{x}_k, T) - \beta(\tilde{x}_k)\right)^2 + (s(X_0) - S_0)^2. \tag{7.15}$$

Here, the approximated temperatures $u(X_0, \tilde{t}_i)$ and $u(\tilde{x}_k, T)$, as introduced earlier in (7.13) and (7.14), respectively, are now employed into the above objective function with the initial guesses $\underline{\mathrm{r}}_0$ and $\underline{\mathrm{s}}_0$ for functions r and s, respectively. Whereas $s(X_0)$ is approximated the same as in (6.20). Then, applying the approximations (7.12)–(7.14) we obtain

$$\begin{aligned}\mathbb{F}_0(\underline{\mathrm{r}}, \underline{\mathrm{s}}) =& \| - B^I B^{-1}(C\mathrm{u}_0 + D^r \underline{\mathrm{s}}) + C^I \mathrm{u}_0 + D^{rI} \underline{\mathrm{s}} - \underline{\chi}\|^2 \\ &+ \| - B^{III} B^{-1}(C\mathrm{u}_0 + D^r \underline{\mathrm{s}}) + C^{III} \mathrm{u}_0 + D^{rIII} \underline{\mathrm{s}} - \underline{\beta}\|^2 \\ &+ (s(X_0) - S_0)^2, \end{aligned} \tag{7.16}$$

where $\underline{\mathrm{r}} = (r_j)_N$ and $\underline{\mathrm{s}} = (s_k)_{N_0}$. The minimisation of (7.16) is performed using the *lsqnonlin* routine from the MATLAB Optimisation Toolbox. This routine attempts to find the minimum of a sum of squares by starting from some arbitrary initial guesses $\underline{\mathrm{r}}_0$ and $\underline{\mathrm{s}}_0$. Note that we have compiled this routine with the following default parameters:

- Algorithm = Trust-Region-Reflective.
- Maximum number of objective function evaluations, 'MaxFunEvals' = $100 \times (N + N_0 + 1)$.
- Maximum number of iterations, 'MaxIter' = 400.
- Termination tolerance on the function value, 'TolFun' = 10^{-10} to 10^{-6}.
- Termination tolerance, 'TolX' = 10^{-10} to 10^{-6}.

Of course, finding a global minimiser to a nonlinear optimisation problem is not an easy task since the functional (7.15), which is in general not convex, i.e. the Hessian of $\mathbb{F}$ is not positive definite. As a consequence it may have local minima in which a descent method tends to get stuck, if the underlying inverse problem is ill-posed, [14, p.17]. In the next section we shall elaborate more on the choice of the initial guess for the iterative routine, as well as on incorporating regularisation in the functional (7.15) in order to ensure convergence to the desired stable solution.

7.5 Numerical examples and discussion

This section presents three benchmark test examples in order to test the accuracy and stability of the numerical methods introduced in Sections 7.3 and 7.4. The RMSEs for $r(t)$ and $s(x)$, defined in (2.49) and (6.28), respectively, are used to evaluate the accuracy of the numerical results.

7.5.1 Example 1

We consider a benchmark test example with $T = 1$, $L = 1/10$, $X_0 = 1/20$, and the initial data (7.2) given by

$$u_0(x) = u(x, 0) = 0, \quad x \in [0, L]. \tag{7.17}$$

For the direct problem (7.1)–(7.3) we also need the input source data

$$r(t) = -\frac{e^t}{40}\left(400\pi^2 t^2 - 400\pi^2 t + t^2 + t - 1\right), \quad s(x) = 40\cos(20\pi x). \tag{7.18}$$

In order to test the BEM accuracy for the direct problem given by equation (7.1) with the source given by the product of the functions in (7.18), subject to the homogenous Neumann boundary condition (7.3) and the initial condition (7.17), the numerical results are compared with the analytical solution given by

$$u(x,t) = e^t(t - t^2)\cos(20\pi x). \tag{7.19}$$

The exact expressions for the inputs (7.4)–(7.6) are given by

$$\begin{cases} \chi(t) = u(1/20, t) = -(t - t^2)e^t, \quad \beta(x) = u(x, 1) = 0, \\ S_0 = s(1/20) = -40. \end{cases} \tag{7.20}$$

As defined in Theorem 7.2.1, we then have $S_0 = -40 \neq 0$, $M = -1 \neq 0$, $m = -e \neq 0$, $\theta(x) = \beta(x) = u_0(x) \equiv 0$, $\lambda_1 = 0.2962 < 1$, $\lambda_2 = 2$, $\lambda_3 = 0$, $4\lambda_2\lambda_3 - (1 - \lambda_1)^2 = -0.4953 \leq 0$, $z = 0.1759$, and $\lambda_4 = 0.2613 < 1$ which satisfy all the conditions (i)–(iii) for existence and uniqueness of the solution.

As the specified boundary conditions (7.3) are of Neumann type, the boundary unknowns in the BEM are represented by the Dirichlet data $u(0,t)$ and $u(L,t)$, as given by (7.12). Once all the boundary data has been obtained accurately, equations (7.13) and (7.14) can be employed explicitly and with no need of interpolations to obtain the temperatures $u(\frac{1}{20}, \tilde{t}_i)$ and $u(\tilde{x}_k, 1)$ for $i = \overline{1, N}$ and $k = \overline{1, N_0}$, respectively. The RMSE of the direct problem results are shown in Table 7.1 and it can be concluded that the BEM numerical solutions are convergent to their corresponding exact values, as the number of boundary elements increases. Whereas Figure 7.1 displays the analytical and numerical results of $\chi(t)$ and $\beta(x)$ and very good agreement can be observed.

Next we consider the inverse problem given by equations (7.1), (7.3), (7.17) and

Table 7.1: The RMSE for $u(0,t)$, $u(0.1,t)$, $\chi(t)$ and $\beta(x)$, obtained using the BEM for the direct problem with $N = N_0 \in \{10, 20, 40\}$, for Example 1.

$N = N_0$	RMSE			
	$u(0,t)$	$u(0.1,t)$	$\chi(t)$	$\beta(x)$
10	5.01E-3	5.01E-3	5.64E-3	8.51E-2
20	1.03E-3	1.03E-3	1.75E-3	4.51E-2
40	8.17E-4	8.17E-4	9.69E-4	2.30E-2

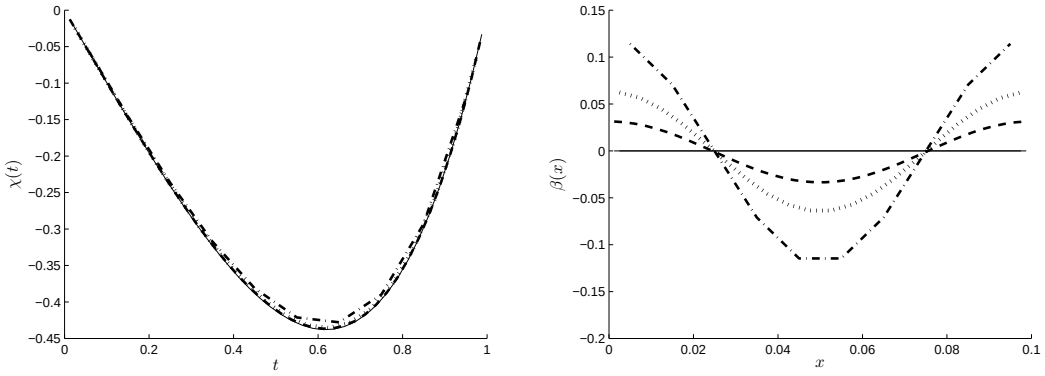

(a) (b)

Figure 7.1: The analytical (——) and numerical results for (a) $\chi(t)$ and (b) $\beta(x)$ obtained using the BEM for the direct problem with $N = N_0 \in \{10\ (- \cdot -), 20\ (\cdots), 40\ (- - -)\}$, for Example 1.

(7.20). The numerical solution can be obtained, as described in Section 7.4, by minimising the objective function (7.15). Preliminary numerical investigations showed that the initial guesses r_0 and s_0 cannot be so arbitrary in order for the minimisation process to converge globally. After many trials, we decided to illustrate the numerical results obtained by considering the initial guess as

$$\begin{cases} \mathrm{r}_0 = \mathrm{r} + random('\text{Normal}', 0, \sigma_r, N, 1), \\ \mathrm{s}_0 = \mathrm{s} + random('\text{Normal}', 0, \sigma_s, N_0, 1), \end{cases} \tag{7.21}$$

with the standard deviations σ_r and σ_s, respectively, given by

$$\sigma_r = p_0 \times \max_{t\in[0,T]} |r(t)|, \quad \sigma_s = p_0 \times \max_{x\in[0,L]} |s(x)|, \tag{7.22}$$

where p_0 is a percentage of perturbation. Hereafter, unless otherwise specified, we present results obtained with $p_0 = 100\%$ perturbed initial guess (which is quite far from the exact solution (7.18)) and $N = N_0 = 20$, we also have set parameters TolFun = TolX = 10^{-6} for the MATLAB optimisation toolbox *lsqnonlin* to solve the inverse problem.

Figure 7.2(a) shows the unregularised objective function $\mathbb{F}_0$ which converges in 39 iterations and the numerical results for $r(t)$, $s(x)$, $u(0,t)$, $u(0.1,t)$ are displayed in Figures 7.2(b)–7.2(e), respectively. As we can see in these figures, the numerical results are inaccurate and partially unstable in Figure 7.2(c).

In order to improve the accuracy and stability, we apply a Tikhonov regularisation process based on minimising the penalised objective function

$$\mathbb{F}_\lambda(\underline{\mathrm{r}},\underline{\mathrm{s}}) := \mathbb{F}_0(\underline{\mathrm{r}},\underline{\mathrm{s}}) + \lambda\left(\|R\underline{\mathrm{r}}\|^2 + \|R\underline{\mathrm{s}}\|^2\right), \tag{7.23}$$

where $\lambda > 0$ is a regularisation parameter to be prescribed, and R is a (differential) regularising matrix as introduced in Section 1.6. Initially, we have applied the first- and second-order regularisations based on minimising the objective function (7.23) as

$$\mathbb{F}_\lambda(\underline{\mathrm{r}},\underline{\mathrm{s}}) = \mathbb{F}_0(\underline{\mathrm{r}},\underline{\mathrm{s}}) + \lambda\left(\sum_{i=1}^{N-1}(r_{i+1}-r_i)^2 + \sum_{k=1}^{N_0-1}(s_{k+1}-s_k)^2\right), \tag{7.24}$$

$$\mathbb{F}_\lambda(\underline{\mathrm{r}},\underline{\mathrm{s}}) = \mathbb{F}_0(\underline{\mathrm{r}},\underline{\mathrm{s}}) + \lambda\left(\sum_{i=2}^{N-1}(-r_{i+1}+2r_i-r_{i-1})^2 + \sum_{k=2}^{N_0-1}(-s_{k+1}+2s_k-s_{k-1})^2\right), \tag{7.25}$$

respectively.

By trial and error, among various regularisation parameters $\lambda \in \{10^{-9},\ldots,10^2\}$, we have found, as illustrative stable results, those obtained with $\lambda_{opt} = 10^{-5}$ which are shown in Figure 7.3. As we can see in this figure, applying orders one or two regularisations (7.24) or (7.25) yield stable, but rather inaccurate results, especially near the endpoints of the intervals of definition of the functions involved, see Figure

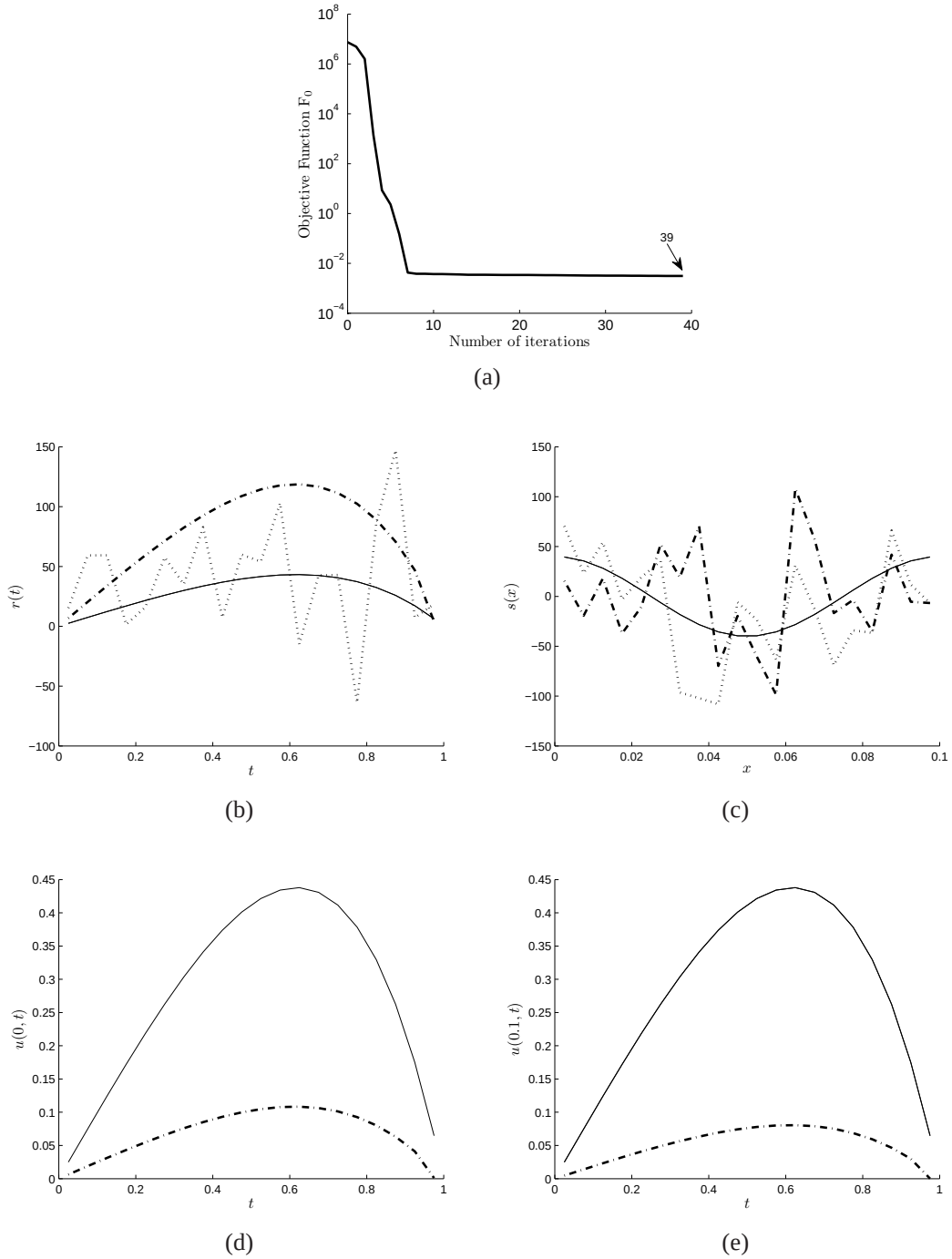

Figure 7.2: (a) The objective function $\mathbb{F}_0$ and the numerical results for (b) $r(t)$, (c) $s(x)$, (d) $u(0,t)$, (e) $u(0.1,t)$ obtained with no regularisation $(- \cdot -)$, for exact data for Example 1. The corresponding analytical solutions are shown by continuous line (——) in (b)–(e) and the $p_0 = 100\%$ perturbed initial guesses are shown by dotted line $(\cdots)$ in (b) and (c).

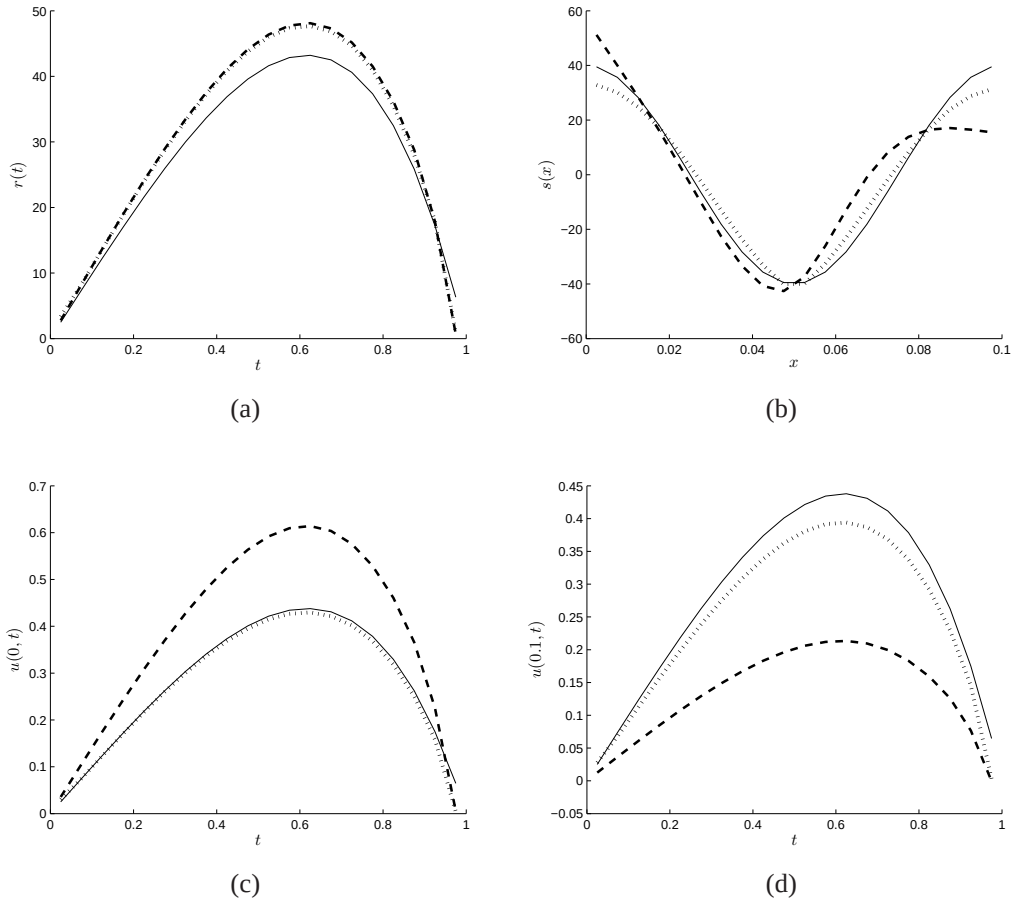

Figure 7.3: The numerical results for (a) $r(t)$, (b) $s(x)$, (c) $u(0,t)$, (d) $u(0.1,t)$ obtained with the first-order regularisation $(\cdots)$ and the second-order regularisation $(---)$ with regularisation parameter $\lambda_{opt} = 10^{-5}$, for exact data for Example 1. The corresponding analytical solutions are shown by continuous line (——).

7.3(b). In order to improve on these inaccuracies we have then investigated a hybrid combination of first- and second- order regularisations given by

$$\mathbb{F}_\lambda(\mathbf{r},\mathbf{s}) = \mathbb{F}_0(\mathbf{r},\mathbf{s}) + \lambda\Bigg((r_1 - r_2)^2 + (-r_{N-1} + r_N)^2 + \sum_{i=2}^{N-1}(-r_{i+1} + 2r_i - r_{i-1})^2 + (s_1 - s_2)^2 + (-s_{N_0-1} + s_{N_0})^2 + \sum_{k=2}^{N_0-1}(-s_{k+1} + 2s_k - s_{k-1})^2\Bigg). \quad (7.26)$$

According to (7.23) and (7.26), the differential regularisation matrix R is given by

$$R = \begin{bmatrix} 1 & -1 & 0 & 0 & . \\ -1 & 2 & -1 & 0 & . \\ 0 & -1 & 2 & -1 & . \\ . & . & . & . & . \end{bmatrix}. \tag{7.27}$$

In the regularisation process, we need to choose an appropriate regularisation parameter λ which balances accuracy and stability. Here, we use the L-curve method to find the regularisation parameter λ. Figure 7.4(a) shows the L-curve obtained by plotting the solution norm $\sqrt{\|R\mathrm{r}\|^2 + \|R\mathrm{s}\|^2}$ versus the residual norm $\sqrt{\mathbb{F}_0(\mathrm{r}, \mathrm{s})}$ for various values of λ when R is given by (7.27). From this figure it can be seen that the corner of the L-curve occurs nearby $\lambda_L = 10^{-5}$, with other appropriate values between the wide range 10^{-6} to 10^{-4}. With this value of the regularisation parameter, the regularised objective function $\mathbb{F}_\lambda$ and the numerical results are shown in Figures 7.4(b)–7.4(f). From Figure 7.4(b) it can be seen that convergence for the regularised objective function $\mathbb{F}_\lambda$ is achieved within 15 iterations. Also, in comparison with the previous Figures 7.3(a)–7.3(d), very good agreement between the exact and the regularised numerical solutions is now obtained, as illustrated in Figures 7.4(c)–7.4(f), respectively. All results are summarised in terms of the RMSE in Table 7.2. Various initial guesses (7.21) with $p_0 \in \{40, 60, 80, 100\}\%$ in (7.22) have been investigated in order to test the robustness of the minimisation procedure with respect to the independence on the initial guess. From Table 7.2 it can be seen that whilst the choice of the initial guess seems to matter for the accuracy of the unregularised solution; i.e. $\lambda = 0$, this restriction disappears when regularisation with $\lambda_L = 10^{-5}$ is imposed. This shows that the numerical regularisation method employed is robust with respect to the independence on the initial guess.

To test the stability of the BEM combined with the nonlinear regularisation, we solve the inverse problem when random noises are added to the input functions $\chi(t)$

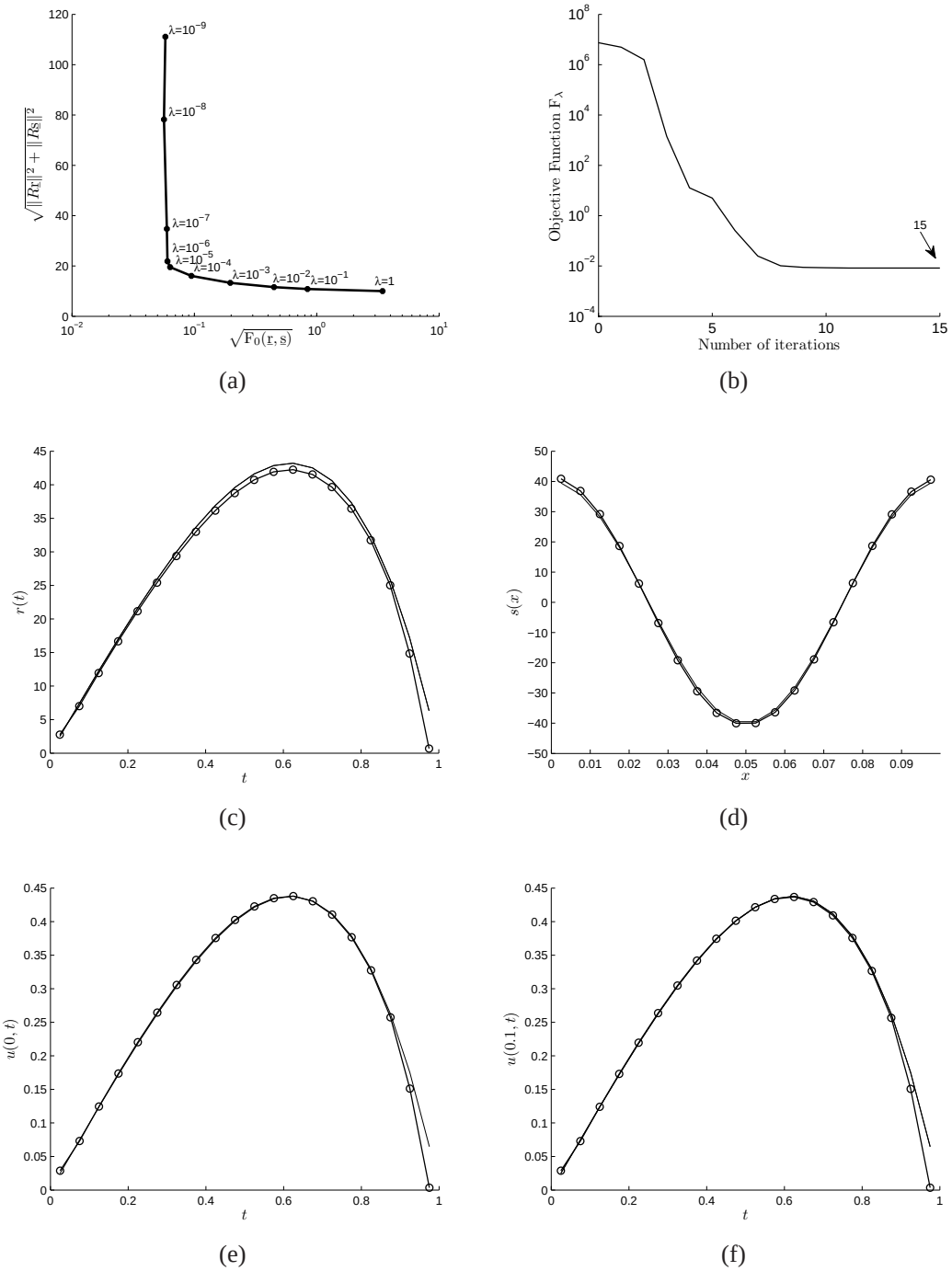

(a) (b)

(c) (d)

(e) (f)

Figure 7.4: (a) The L-curve criterion, (b) the objective function $\mathbb{F}_\lambda$, and the numerical results $(-\circ-)$ for (c) $r(t)$, (d) $s(x)$, (e) $u(0,t)$, (f) $u(0.1,t)$ obtained with the hybrid-order regularisation (7.26) with regularisation parameter $\lambda_L = 10^{-5}$ suggested by L-curve, for exact data Example 1. The corresponding analytical solutions are shown by continuous line (——) in (c)–(f).

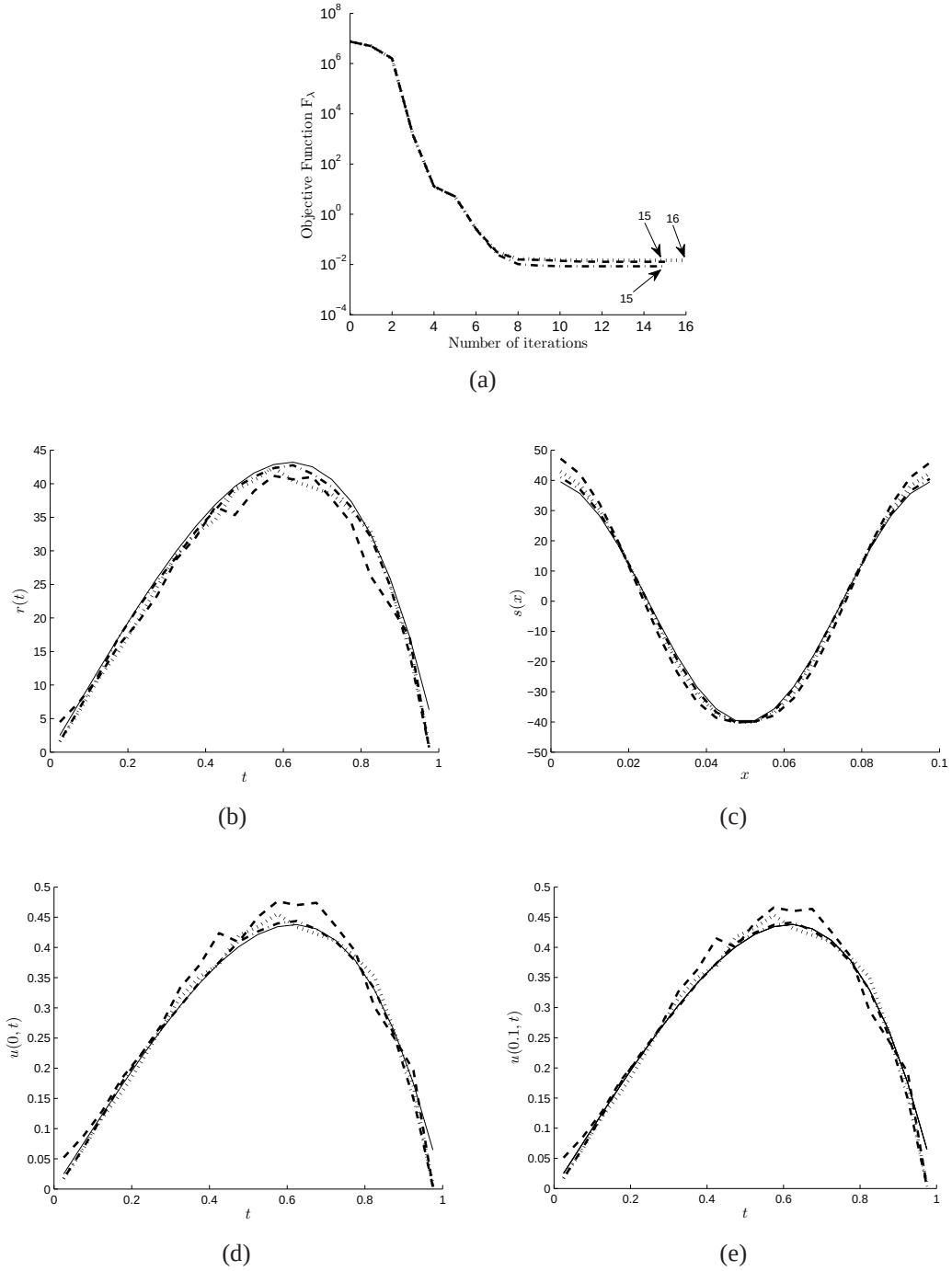

Figure 7.5: (a) The objective function $\mathbb{F}_\lambda$ and the numerical results for (b) $r(t)$, (c) $s(x)$, (d) $u(0,t)$, (e) $u(0.1,t)$ obtained with the hybrid-order regularisation (7.26) with regularisation parameter $\lambda_L = 10^{-5}$ suggested by L-curve for $p \in \{1(-\cdot-), 3(\cdots), 5(--)\}\%$ noisy data, for Example 1. The corresponding analytical solutions are shown by continuous line (——) in (b)–(e).

Table 7.2: The RMSE for $r(t)$, $s(x)$, $u(0,t)$, $u(0.1,t)$ for exact data, Example 1.

$p_0(\%)$	parameter λ	RMSE			
		$r(t)$	$s(x)$	$u(0,t)$	$u(0.1,t)$
40%	0	6.349	18.47	4.72E-2	3.27E-2
	λ_L=1E-5	1.528	0.819	1.49E-2	1.53E-2
60%	0	9.752	26.70	1.14E-1	8.12E-2
	λ_L=1E-5	1.513	0.767	1.48E-2	1.50E-2
80%	0	25.83	44.93	1.99E-1	2.74E-1
	λ_L=1E-5	1.526	0.812	1.48E-2	1.47E-2
100%	0	53.70	54.24	2.34E-1	2.54E-1
	λ_L=1E-5	1.529	0.819	1.47E-2	1.48E-2

and $\beta(x)$ as

$$\begin{cases} \underline{\chi}^{\epsilon} = \underline{\chi} + random('\text{Normal}', 0, \sigma_{\chi}, N, 1), \\ \underline{\beta}^{\epsilon} = \underline{\beta} + random('\text{Normal}', 0, \sigma_{\beta}, N_0, 1), \end{cases} \tag{7.28}$$

with the standard deviations σ_χ and σ_β given by

$$\sigma_{\chi} = p \times \max_{t\in[0,T]} |\chi(t)|, \quad \sigma_{\beta} = p \times \max_{x\in[0,L]} |\beta(x)|, \tag{7.29}$$

respectively. The numerical results obtained with $\lambda_L = 10^{-5}$, are illustrated in Figure 7.5. From Figure 7.5(a) it can be seen that convergence of the hybrid-order regularised objective functional (7.26) is rapidly achieved within 15-16 iterations for $p \in \{1,3,5\}\%$. Furthermore, Figures 7.5(b)–7.5(e) show that stable and accurate numerical results are obtained for all amounts of noise p. Also, as expected, the numerical solutions become more accurate as the amount of noise p decreases.

7.5.2 Example 2

In Example 1, all conditions for the existence and uniqueness of Theorem 7.2.1 were satisfied. We now consider an example which has the analytical solution, [48],

$$u(x,t) = (e^{3t} - e^{-t})\cos(x), \quad r(t) = e^{3t}, \quad s(x) = 4\cos(x), \tag{7.30}$$

where $T = 0.3$, $L = \pi$. One can easily check that the homogeneous Neumann conditions (7.3) are satisfied and that the initial condition (7.2) is also homogeneous, as given in (7.17). Taking $X_0 = 0.75$ we obtain that the input data (7.4)–(7.6) are given by

$$\begin{cases} \chi(t) = u(0.75, t) = (e^{3t} - e^{-t})\cos(0.75), \\ \beta(x) = u(x, 0.3) = (e^{0.9} - e^{-0.3})\cos(x), \\ S_0 = s(0.75) = 4\cos(0.75). \end{cases} \tag{7.31}$$

From this we have $S_0 = M = 4\cos(0.75) \neq 0$, $u_0(x) \equiv 0$, $m = e^{0.9} \neq 0$, $\theta(x) = (e^{0.9} - e^{-0.3})\sin(x)$, $\lambda_1 = 5.3719$, $\lambda_2 = 0.2518$, $\lambda_3 = 24.928$, $z = -8.6813$, $\lambda_4 = 14.654$. One can then observe that the conditions (i) and (ii) of Theorem 7.2.1 are satisfied, but the condition (iii) has been violated. Whilst a solution obviously exists, as given by equations (7.30), one cannot guarantee yet that this solution is unique.

We have solved first the direct problem given by equations (7.1) (with r and s given by (7.30)), (7.3) and (7.17) using the BEM with various numbers of boundary elements $N = N_0 \in \{5, 10, 20\}$ and the numerical results for $\chi(t)$ and $\beta(x)$ presented in Figure 7.6 show rapid convergence and excellent agreement with the analytical solution (7.31). Afterwards, we have solved the inverse problem given by equations (7.1), (7.3), (7.17) and (7.31) in order to retrieve the temperature $u(x, t)$ and the heat source components $r(t)$ and $s(x)$ given analytically by (7.30). We have taken boundary elements $N = N_0 = 20$ and the arbitrary initial guesses $\mathrm{r}_0 = 0$ and $\mathrm{s}_0 = 0$.

We first consider the case of exact data. The convergence of the unregularised objective function $\mathbb{F}_0$ achieved within 56 iterations using the *lsqnonlin* routine with TolFun = TolX = 10^{-10} is illustrated in Figure 7.7(a). Also, the RMSEs of solutions r and s are shown in Figure 7.7(b) by dash line $(\cdots)$ and dot line $(---)$, respectively. The numerical solutions for r and s obtained after 56 iterations are shown by dash-dot line $(-\cdot-)$ in Figures 7.7(c) and 7.7(d), respectively. Very good agreement between the numerical and analytical solutions for s can be observed, whilst the numerical solution for r is stable but slightly away from the analytical solution. We then look

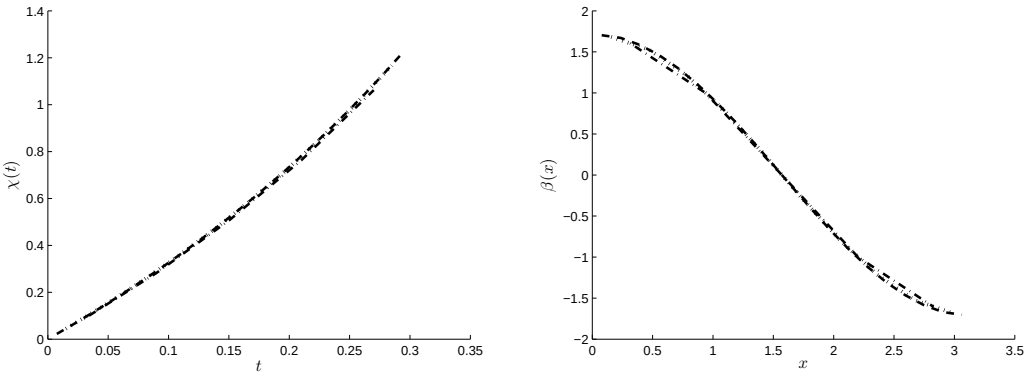

(a) (b)

Figure 7.6: The analytical (——) and numerical results for (a) $\chi(t)$ and (b) $\beta(x)$ obtained using the BEM for the direct problem with $N = N_0 \in \{5(- \cdot -),\ 10(\cdots),\ 20(- - -)\}$, for Example 2.

more closely at Figure 7.7(b) and observe that the minimum of RMSEs is at iteration 31 instead of 56. Therefore, we have tried solving the inverse problem with the fixed iteration at 31, and the numerical results become more accurate, as illustrated by the circle markers $(\circ\circ\circ)$ in Figures 7.7(c) and 7.7(d). Further, we have applied the hybrid-order regularisation procedure (7.26) with the regularisation parameter $\lambda_{opt} = 2 \times 10^{-4}$ (chosen by the trial and error) and the results are shown in Figure 7.8. Figure 7.8(a) displays the convergence of the regularised functional (7.26) achieved within 28 iterations. Also, results for RMSEs and the solutions for r and s are shown in

Table 7.3: The RMSE for $r(t)$ and $s(x)$, for the noise levels $\epsilon_0 \in \{0, 0.01, 0.1\}$, for Example 2.

Noise level	No. of iterations	parameter λ	RMSE	
			$r(t)$	$s(x)$
No noise	56	0	6.3068E-2	1.5492E-1
	31 (fixed)	0	2.6668E-2	1.4751E-1
	28	λ_{opt}=2E-4	5.6471E-2	1.1003E-1
	23 (fixed)	λ_{opt}=2E-4	1.9713E-2	6.4412E-2
$\epsilon_0 = 0.01$	27	λ_{opt}=4E-4	6.3004E-2	1.0886E-1
	21 (fixed)	λ_{opt}=4E-4	2.8829E-2	6.5281E-2
$\epsilon_0 = 0.1$	17	λ_{opt}=2	5.2212E-2	3.0714E-2

Figures 7.8(b)–7.8(d). From Figure 7.8(b) one can see that the minimum of the RMSEs occurs after 23 iterations. By comparing Figures 7.7 and 7.8 one can conclude that the inclusion of some small regularisation yields slightly more accurate and stable results.

Next, we consider the stability of the numerical solution when the noise is present

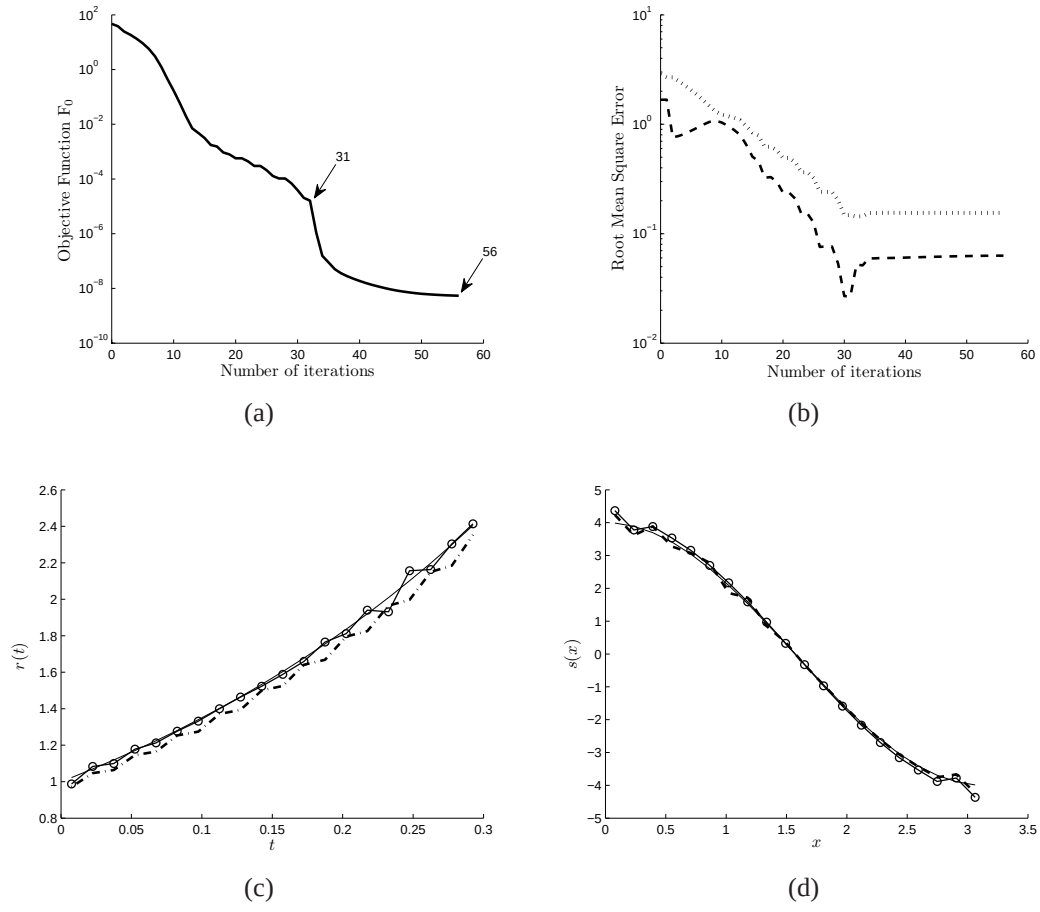

Figure 7.7: (a) The objective function $\mathbb{F}_0$, (b) the RMSEs for $r(t)$ $(- - -)$ and $s(x)$ $(\cdots)$ obtained with no regularisation for exact data, and the numerical results for (c) $r(t)$ and (d) $s(x)$ obtained using the minimisation process after 56 unfixed iterations $(- \cdot -)$, and 31 fixed iterations $(\circ \circ \circ)$, for Example 2. The corresponding analytical solutions (7.30) are shown by continuous line (——) in (c) and (d).

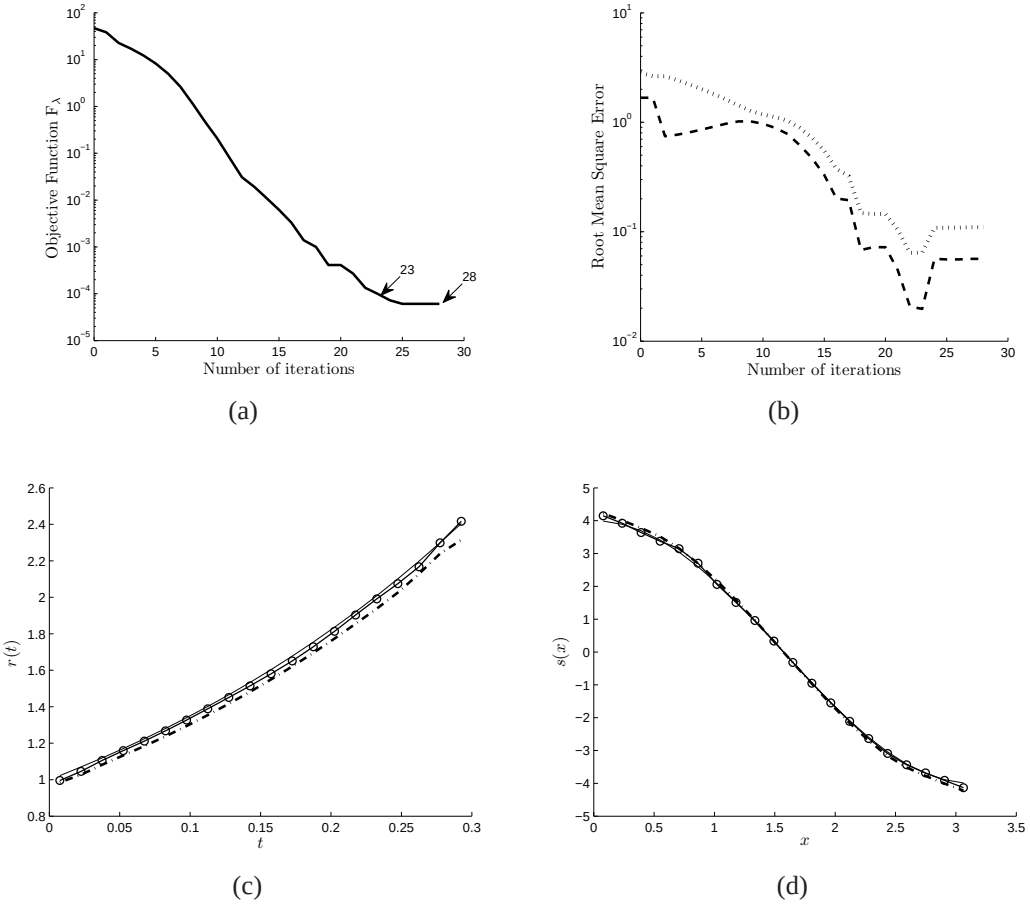

Figure 7.8: (a) The objective function $\mathbb{F}_\lambda$, (b) the RMSEs for $r(t)$ $(- - -)$ and $s(x)$ $(\cdots)$ obtained using the hybrid-order regularisation (7.26) with regularisation parameter $\lambda_{opt} = 2 \times 10^{-4}$ for exact data, and the numerical results for (c) $r(t)$ and (d) $s(x)$ obtained using minimisation process after 28 unfixed iterations $(- \cdot -)$, and 23 fixed iterations $(\circ \circ \circ)$, for Example 2. The corresponding analytical solutions (7.30) are shown by continuous line (——) in (c) and (d).

in the input data (7.4) and (7.5). As in [48], the noise was defined by

$$\begin{cases} \chi^\epsilon(\tilde{t}_i) = \chi(\tilde{t}_i)\left(1 + \dfrac{\epsilon_0}{\sqrt{\sum_{i=1}^N \chi^2(\tilde{t}_i)}} rand(i)\right), \quad i = \overline{1, N}, \\ \beta^\epsilon(\tilde{x}_k) = \beta(\tilde{x}_k)\left(1 + \dfrac{\epsilon_0}{\sqrt{\sum_{k=1}^N \beta^2(\tilde{x}_k)}} rand(k)\right), \quad k = \overline{1, N_0}, \end{cases} \tag{7.32}$$

where $rand(\cdot)$ is a random variable generated by the MATLAB command from a nor-

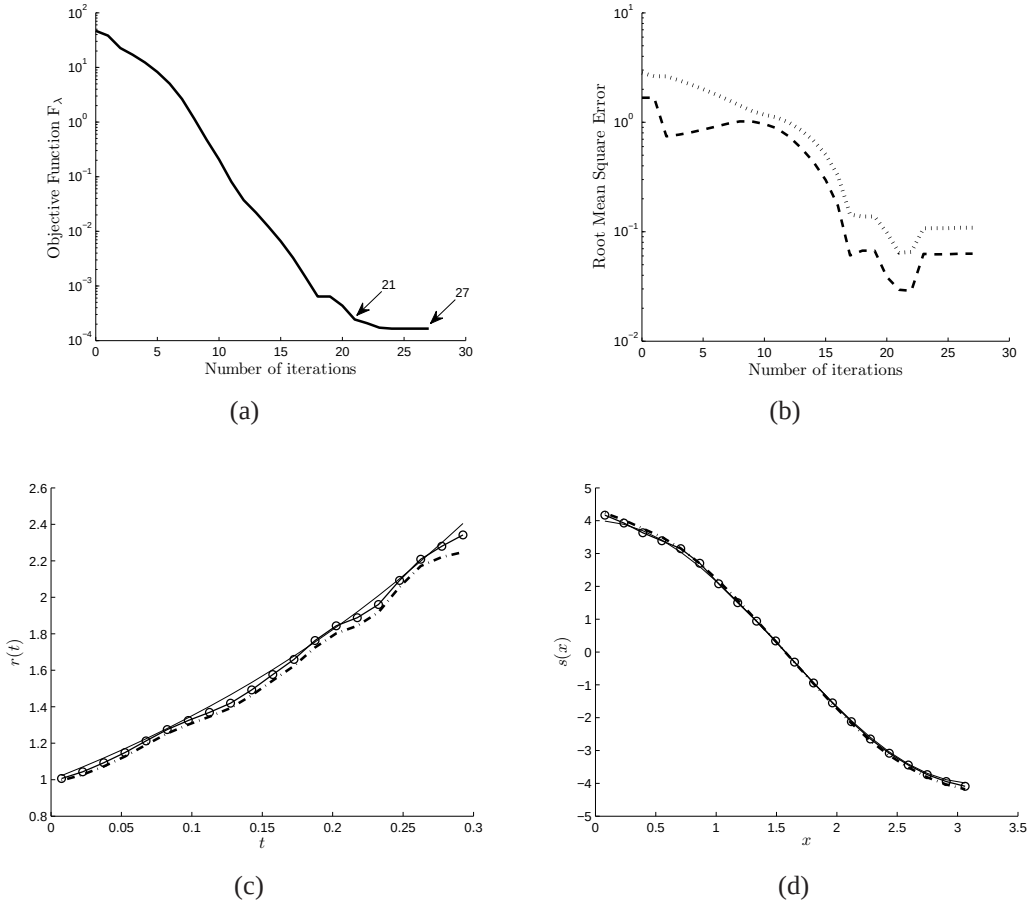

Figure 7.9: (a) The objective function $\mathbb{F}_\lambda$, (b) the RMSEs for $r(t)$ $(- - -)$ and $s(x)$ $(\cdots)$ obtained using the hybrid-order regularisation (7.26) with regularisation parameter $\lambda_{opt} = 4 \times 10^{-4}$ for noise level $\epsilon_0 = 0.01$, and the numerical results for (c) $r(t)$ and (d) $s(x)$ obtained using the minimisation process after 27 unfixed iterations $(- \cdot -)$, and 21 fixed iterations $(\circ\, \circ\, \circ)$, for Example 2. The corresponding analytical solutions (7.30) are shown by continuous line (——) in (c) and (d).

mal distribution with mean zero and unit standard deviation, and ϵ_0 represents the noise level. Remark that the noise (7.32) is multiplicative, whilst the noise in (7.28), Example 1, is additive. For $\epsilon_0 = 0.01$, Figure 7.9 illustrates the results obtained using the hybrid-order regularisation (7.26) with regularisation parameter $\lambda_{opt} = 4 \times 10^{-4}$. The convergence of the regularised objective function achieved within 27 iterations is shown in Figure 7.9(a), whilst the minimum RMSEs of r and s occur after 21 iterations, as can be seen in Figure 7.9(b). Numerical solutions for r and s obtained after

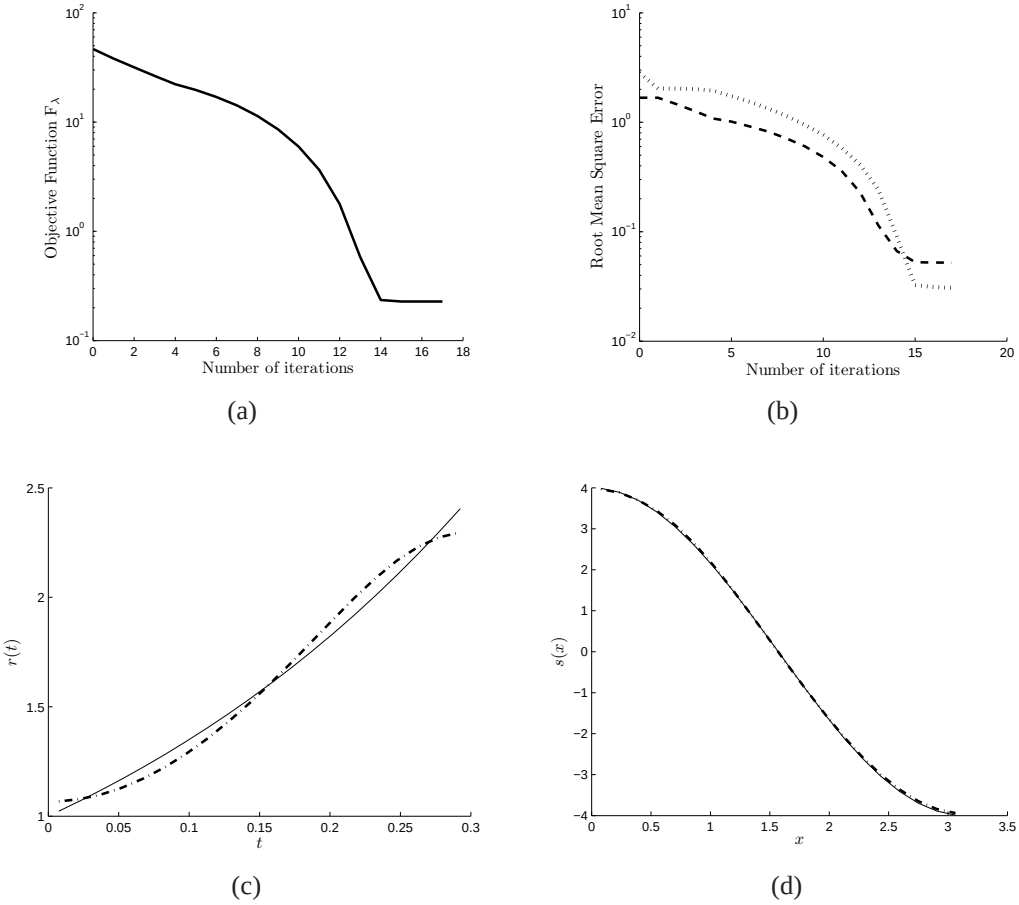

Figure 7.10: (a) The objective function $\mathbb{F}_\lambda$, (b) the RMSEs for $r(t)$ $(- - -)$ and $s(x)$ $(\cdots)$ obtained using the hybrid-order regularisation (7.26) with regularisation parameter $\lambda_{opt} = 2$ for noise level $\epsilon_0 = 0.1$, and the numerical results $(- \cdot -)$ for (c) $r(t)$ and (d) $s(x)$ obtained using the minimisation process after 17 (unfixed) iterations, for Example 2. The corresponding analytical solutions (7.30) are shown by continuous line (——) in (c) and (d).

27 (unfixed) and 21 (fixed) iterations are displayed in Figures 7.9(c) and 7.9(d), respectively. As expected, the conclusions from Figure 7.9 obtained for a low level of noise $\epsilon_0 = 0.01$ are very much the same as the those from Figure 7.8 obtained for no noise $\epsilon_0 = 0$. From both Figures 7.8(c), 7.8(d) and 7.9(c), 7.9(d) one can observe that the numerical results are accurate and stable. Furthermore, there is little difference in the results obtained whether we stop (fix) the iteration process at the minimum of the RMSEs shown in Figures 7.8(b) and 7.9(b) or, if we let the iteration process running

(unfix) until converge of the regularised objective function is achieved.

Next, we consider a large amount of noise, such as $\epsilon_0 = 0.1$, included in (7.32) and the numerical results are shown in Figure 7.10. First, one can observe from Figure 7.10(a) that the convergence of the objective function (7.26) is rapidly achieved within 17 iterations and the monotonic decreasing curve has a somewhat different shape than that recorded in Figure 7.8(a) for no noise $\epsilon_0 = 0$ or in Figure 7.9(a) for a low amount noise $\epsilon_0 = 0.01$. Also, interestingly, unlike in Figures 7.8(b) and 7.9(b) where the RMSEs show a minimum before the iteration process has finished, in Figure 7.10(b) no such minimum occurs. Therefore, in Figures 7.10(c) and 7.10(d) we present only numerical results for r and s, respectively, obtained after 17 (unfixed) iterations with $\lambda_{opt} = 2$. From these figures it can be seen that the numerical solutions are stable, with an unexpected very high accuracy in predicting the s component in Figure 7.10(d). For completeness and clarity the RMSEs of Figures 7.7(b)–7.10(b) are given in numbers in Table 7.3. From this table, and also from Figure 7.10(b), it can be seen that for $\epsilon_0 = 0.1$ the component $s(x)$ is predicted more accurately than the $r(t)$ component, whilst the prediction for $\epsilon_0 \in \{0, 0.01\}$ is reversed.

Finally, we report that the numerical results presented in this example are comparable in terms of accuracy and stability with the numerical results obtained recently in [48] using a different method of successive approximants previously developed in [47].

7.5.3 Example 3

The previous examples possessed an analytical (smooth) solution available explicitly and they were tested in order to verify the accuracy and stability of the numerical method employed. In this subsection, we consider a severe test example represented

by the non-smooth source components

$$r(t) = \begin{cases} t, & 0 \leq t \leq 1/2, \\ 1-t, & 1/2 < t \leq 1 = T, \end{cases} \tag{7.33}$$

$$s(x) = \begin{cases} x, & 0 \leq x \leq 1/20, \\ 0.1-x, & 1/20 < x \leq 1/10 = L, \end{cases} \tag{7.34}$$

where $L = 1/10$, $T = 1$, $X_0 = 1/20$. We also take the homogeneous initial temperature (7.17). This example does not have an analytical solution for the temperature $u(x,t)$ readily available. Therefore, in such a situation the data (7.4) and (7.5) is simulated numerically by solving the direct problem (7.1) with the multiplicative source given by the product of the functions in (7.33) and (7.34), subject to the homogeneous boundary and initial conditions (7.3) and (7.17). The BEM numerical solutions for the data $\chi(t) = u(0.2,t)$ and $\beta(x) = u(x,1)$ are shown in Figure 7.11 for various numbers of boundary elements $N = N_0 \in \{10, 20, 40\}$. From this figure the convergence of the numerical solution, as the number of boundary elements increases, can be observed.

Next we consider the inverse problem given by equations (7.1), (7.3), (7.6) with

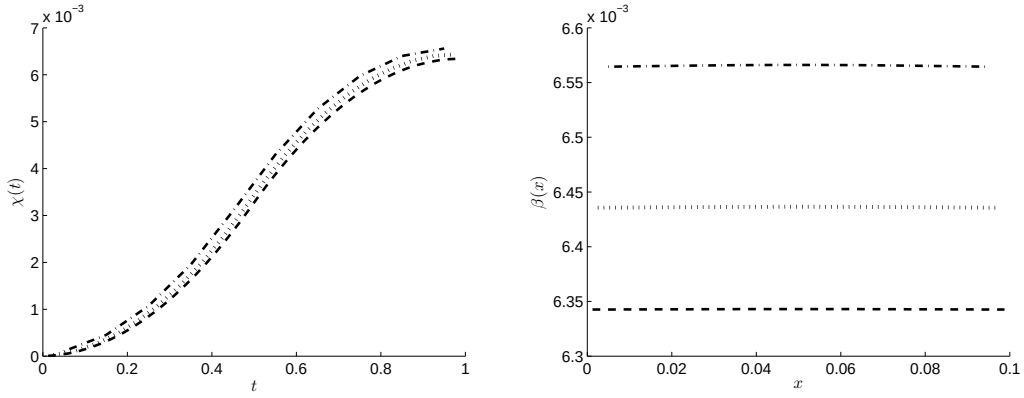

(a) (b)

Figure 7.11: The numerical results for (a) $\chi(t)$ and (b) $\beta(x)$ obtained using the BEM for the direct problem with $N = N_0 \in \{10(-\cdot-),\ 20(\cdots),\ 40(---)\}$, for Example 3.

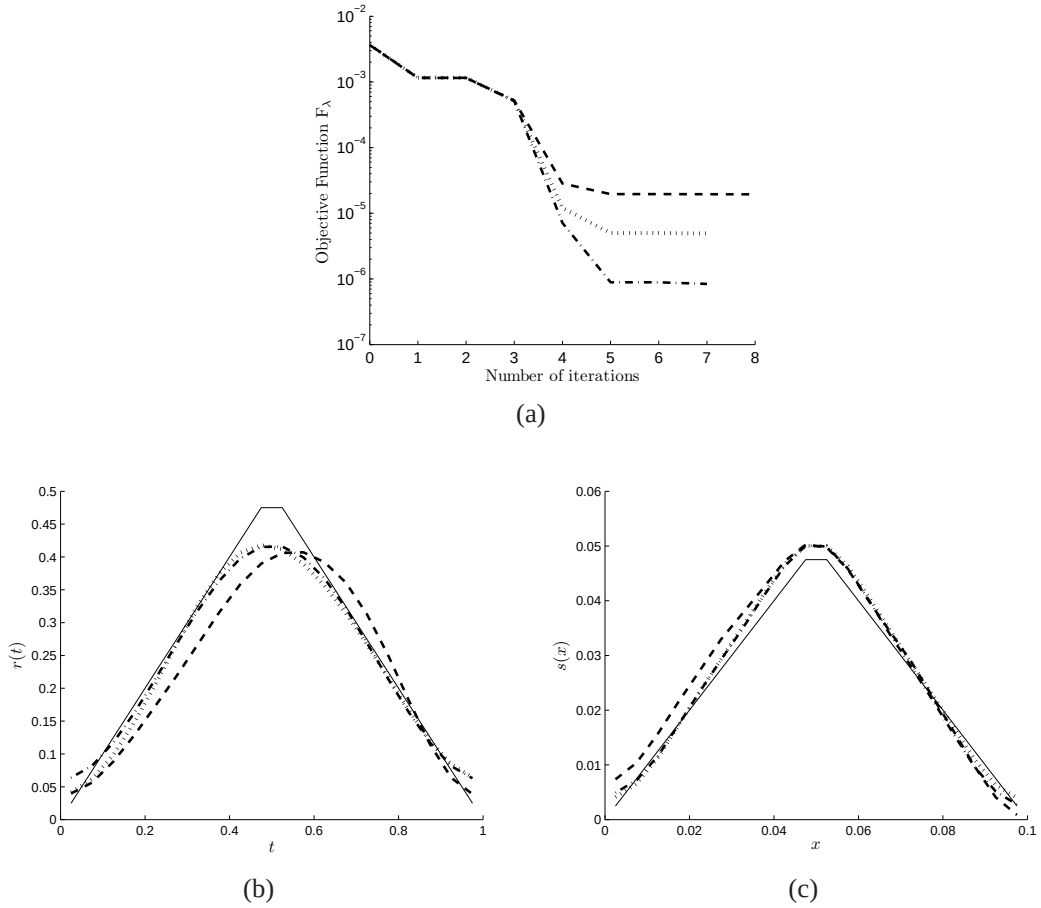

(a)

(b) (c)

Figure 7.12: (a) The objective function $\mathbb{F}_\lambda$ and the numerical results for (b) $r(t)$ and (c) $s(x)$ obtained with the hybrid-order regularisation (7.26) with regularisation parameter $\lambda = 2 \times 10^{-4}$ for $p \in \{1(- \cdot -),\ 5(\cdots),\ 10(- - -)\}\%$ noisy data for Example 3. The corresponding analytical solutions (7.33) and (7.34) are shown by continuous line (——) in (b) and (c).

$S_0 = s(1/20) = 1/20$ specified, (7.17), and the additional measured data (7.4) and (7.5) which has been simulated numerically in Figure 7.11. We pick from Figure 7.11 the numerical BEM solutions obtained with $N = N_0 = 20$ and we further perturb this data with noise, as in (7.28). We took as initial guesses $\mathrm{r}_0 = \mathrm{s}_0 = 0$, and we initiated the iterative minimisation process of the hybrid-order regularisation functional (7.26), as described in Example 1. The numerical results obtained with $\lambda_{opt} = 2 \times 10^{-4}$ (found by trial and error) are shown in Figure 7.12 for $p \in \{1, 5, 10\}\%$ noise generated as in (7.28). From Figure 7.12(a) it can be seen that the convergence of the functional (7.26)

is rapidly achieved within 7-8 iterations using the *lsqnonlin* routine with TolFun = TolX = 10^{-6}. Also, Figures 7.12(b) and 7.12(c) show that stable and accurate numerical solutions for both $r(t)$ and $s(x)$ are obtained for all the amounts of noise p.

In closure, although not illustrated, we report that the same good performance has been recorded when attempting to reconstruct even discontinuous source components.

7.6 Conclusions

In this chapter, inverse source problems with homogeneous Neumann boundary conditions together with specified interior and final time temperature measurements have been considered to find the space- and the time-dependent components of a multiplicative source function. The numerical discretisation was based on the BEM combined with a nonlinear Tikhonov regularisation procedure via the *lsqnonlin* routine from the MATLAB. For a wide range of test examples, the obtained results indicate that stable and accurate numerical solutions have been achieved. The identification of both multiplicative $r(t)s(x)$ and additive $r_1(t)+s_1(x)$ components of space- and time-dependent sources of the form $r(t)s(x) + r_1(t) + s_1(x)$ can also be considered, [47], but its numerical implementation is deferred to a future work.

Chapter 8

General Conclusions and Future Work

8.1 Conclusions

The aim of this thesis was to solve various inverse source problems for the (one-dimensional) heat equation by using the BEM to find the time-dependent heat source function, presented in Chapters 2–5, and space- and time-dependent heat source functions for additive and multiplicative cases, presented in Chapters 6 and 7, respectively. Several types of conditions such as non-local, non-classical, periodic, fixed point, time-average and integral have been considered as boundary or overdetermination conditions.

The BEM has been used as the main numerical approach for discretising the linear heat equation with a heat source present. In Chapter 1 we have described the BEM for discretising the heat equation. With this method, the heat equation is first multiplied by the fundamental solution and then integrated with the assistance of Green's identity. This leads to a boundary integral equation which can be discretised with resulting integral coefficients that can be evaluated analytically. The initial and boundary conditions are also imposed.

In an inverse problem, additional conditions are required to determine uniquely the unknown functions. However, this information has to come from measurements which are contaminated with noise unavoidably. If the problem is ill-posed then small errors

in the measurement data result in highly and unbounded output solutions. Therefore, regularisation methods need to be employed to deal with this instability.

In this thesis, many regularisation methods have been utilised together with the BEM. A popular regularisation method, the Tikhonov regularisation, has been used with orders zero, one and two. Additionally, for comparison, the TSVD method has also been considered in Chapters 3 and 6. Moreover, in Chapter 4, the smoothing spline technique has been considered as a regularisation method for seeking a regularised first-order derivative of a noisy function.

Regularisation methods require a proper choice of the regularisation parameter. There are many methods such as the L-curve method, the GCV criterion, and the discrepancy principle which are all popular and successful methods for choosing the regularisation parameter. The L-curve method is the simplest method for choosing the regularisation parameter. This method suggests choosing the parameter at the corner of the L-curve which is a plot of the solution norm versus the corresponding residual for many positive regularisation parameters. Alternatively, we have also used the GCV criterion in order to indicate a regularisation parameter, this method is based on the minimising the GCV function of various positive regularisation parameters. When the amount of noise is known, the discrepancy principle was proposed to be another method for choosing the regularisation parameter. This method is more rigorous since it requires the knowledge of the noise level with which the input data is contaminated. Furthermore, in Chapter 6, the selection of two regularisation parameters has been based on the L-surface method, this method is a natural extension of the L-curve method used for the selection of a single regularisation parameter. For comparison, the simple trial and error technique has also been employed, i.e. various regularisation parameters were tested with gradually increasing value until oscillations in the numerical solutions have been stabilised.

To test the accuracy and stability of the BEM combined with regularisation methods, numerical examples consisting of various cases of unknown functions, such as smooth continuous, non-smooth continuous and discontinuous functions, have been

illustrated and compared with their analytical solutions, where available. Otherwise, in the cases where the analytical solution for the temperature is not available, we have used the numerical solution of the corresponding direct problem and set the mesh size to be different in the corresponding inverse problem presented in Chapters 3 and 5. This is in order to avoid committing an inverse crime, see [32].

In summary, all numerical results with/without noise contamination have been found to be accurate and stable. In Chapter 2, the determination of the time-dependent heat source function and the temperature subjected to three general boundary conditions has been considered. These three conditions have been distinguished to be six separate cases of boundary and overdetermination conditions and generating six inverse problems. Some cases were found to be ill-conditioned; then the Tikhonov regularisation with orders zero, one and two have been used on both exact and noisy data. Whereas other cases were found to be well-conditioned and the use of BEM has processed well for the inverse problem with no use of regularisation for the exact data, but the regularisation was still needed when noise was present.

In Chapter 3, the identification of the time-dependent heat source and the temperature subjected to a periodic boundary condition, a Robin boundary condition and an integral overdetermination condition has been considered. The BEM has been developed and combined with two regularisation methods; the Tikhonov regularisation and the TSVD method. A couple of benchmark test examples have been presented in order to illustrate the accuracy of the numerical results. No regularisation was required in the case of exact data and we found that the least-squares procedure and the SVD method produced the same accurate numerical results. When noise was added, the L-curve method and the discrepancy principle were selected for the appropriate choice of the regularisation parameter, when using the Tikhonov regularisation of orders zero, one and two, and the truncation level, when using the TSVD. Numerical results obtained by using the BEM combined with either the TSVD or the zeroth-order Tikhonov regularisation have been formed similar. The higher-order regularisation for smooth source recovery gave more accurate results than the lower-order ones, while for non-smooth

sources the conclusion was reversed.

In Chapter 4, we have investigated the reconstruction of the time-dependent blood perfusion coefficient and the temperature in the bioheat equation subjected to the same boundary and overdetermination conditions as in Chapter 3. A simple transformation reduced the bioheat equation to be the classical heat equation, but now the overdetermination condition contained the unknown source function. Two numerical examples have been solved using the BEM. One example has been considered together with the Tikhonov regularisation combined with the higher-order (of accuracy) finite difference and use the GCV method as the choice of regularisation parameter. The second example has used the BEM together with a smoothing spline technique for differentiating a noisy function with a *priori* and a *posteriori* choices of the regularisation parameters.

Chapter 5 presented an identification of the time-dependent heat source and the temperature for the heat equation subjected to the non-classical boundary and integral overdetermination conditions. We have utilised the same technique as before based on the BEM together with the Tikhonov regularisation method. Three benchmark test examples have been considered with smooth and non-smooth continuous source functions to illustrate the accuracy and stability of the numerical results. Utilising the GCV method as choice of regularisation parameter has performed well to obtain stable and accurate solution in all the investigated examples. We have also found that there was not much significant difference value of the regularisation parameter given by the discrepancy principle or the trial and error technique.

In Chapter 6, we have investigated the more challenging identification of two unknown source functions; the time- and space-dependent components of an additive heat source and the temperature in the one-dimensional heat equation subjected to interior point and time integral overdetermination conditions. The BEM was combined with either the Tikhonov regularisation or the TSVD to solve the inverse problem with various selections of the regularisation parameter and the truncation level based on the L-curve method, the discrepancy principle and the GCV criterion when a single regularisation parameter was considered. We have also extended the analysis to the case

when two regularisation parameters were present and chose these parameters by using the L-surface method.

The final case of inverse heat source problem presented in Chapter 7 was a nonlinear case study. This consisted of the simultaneous determination of multiplicative space- and time-dependent source components and the temperature for the heat equation subject to homogeneous Neumann boundary condition, specified interior, and final time temperature measurements. The numerical discretisation was based on the BEM combined with a Tikhonov regularisation procedure. The resulting nonlinear optimisation problem was solved using the MATLAB routine $lsqnonlin$. The hybrid-order combination of the first- and second-order Tikhonov regularisation has achieved a stable and accurate numerical solution.

Throughout the thesis, the retrieved numerical results were found to be accurate and stable concluding the reliability of the BEM combined with the various regularisation techniques for solving a wide range of inverse source problems for the heat equation.

8.2 Future work

As we have studied so far, the use of the BEM combined with regularisation methods can be developed for solving inverse source problems for the heat equation under various types of boundary and overdetermination conditions. This supports the idea that the BEM combined with regularisation methods can also perform well in other related possible future work, as follows.

(i) An inverse source problem related to that of Chapter 5 and given by the follow-

ing system of equations:

$$\begin{cases} u_t = u_{xx} + r(t)f(x,t), \quad (x,t) \in \overline{D}_T, \\ u(x,0) = u_0(x), \quad x \in [0,1], \\ u(0,t) = 0, \quad t \in (0,T], \\ u_t(1,t) + u_x(1,t) + \varphi(u(1,t)) = 0, \quad t \in (0,T], \\ \int_0^1 u(x,t)\,dx = E(t), \quad t \in [0,T], \end{cases} \tag{8.1}$$

where φ is a given nonlinear function, has recently been investigated in [50] but with no numerical study. It would be interesting to study the numerical reconstruction of the time-depending heat source $r(t)$ and the temperature $u(x,t)$ satisfying this inverse problem by using the BEM together with the regularisation methods presented in this thesis.

(ii) Another possible future work for the one-dimensional study is the combination of the identifications in Chapters 6 and 7 for a more general heat source containing both additive and multiplicative components, see [47]. This work is an identification of finding the time-dependent source functions $r(t), r_1(t)$, the space-dependent source functions $s(x), s_1(x)$ and the temperature $u(x,t)$ which satisfy the heat equation

$$u_t(x,t) = u_{xx}(x,t) + r(t)s(x) + r_1(t) + s_1(x), \quad (x,t) \in D_T, \tag{8.2}$$

subject to the initial condition (1.7), the homogeneous Neumann boundary condition (7.3), and the additive measurements

$$u(X_0,t) = \chi(t), \quad u(X_1,t) = \chi_1(t), \quad t \in [0,T], \tag{8.3}$$

$$u(x,T_1) = \beta_1(x), \quad u(x,T_2) = \beta_2(x), \quad x \in [0,L], \tag{8.4}$$

at the fixed sensor locations $0 \leq X_0 < X_1 \leq L$ and the fixed times $0 < T_1 < T_2 \leq T$.

Fixing conditions are also required as

$$r(T_1) = \gamma_1, \quad r(T_2) = \gamma_2, \quad s(X_0) = S_0, \quad s_1(X_0) = \check{S}_0, \tag{8.5}$$

where the functions χ, χ_1, μ_1, μ_2 and the constants γ_1, γ_2, S_0, $\check{S}_0$ are given. This inverse problem is very challenging because it is nonlinear study and the Matlab routine $lsqnonlin$ will be required.

(iii) The multi-dimensional inverse source problem for the heat equation is also very interesting to study further with the BEM. The following inverse source problem can be further studied, see Cannon [8] and Yamamoto [62]. Let Ω be a bounded domain in $\mathbb{R}^n$, $n = 1, 2, 3$. Then, one can consider the inverse problem of finding the temperature $u(\mathbf{x}, t)$ for $(\mathbf{x}, t) \in \Omega \times (0, T)$ and the space-dependent heat source $f(\mathbf{x})$ for $\mathbf{x} \in \Omega$, satisfying the transient heat conduction equation

$$\frac{\partial u}{\partial t}(\mathbf{x}, t) = \nabla^2 u(\mathbf{x}, t) + r(t) f(\mathbf{x}), \quad (\mathbf{x}, t) \in \Omega \times (0, T), \tag{8.6}$$

subject to the initial condition

$$u(\mathbf{x}, 0) = u_0(\mathbf{x}), \quad \mathbf{x} \in \overline{\Omega}, \tag{8.7}$$

and the overspecified Cauchy boundary data

$$u(\mathbf{x}, t) = \beta(\mathbf{x}, t), \quad (\mathbf{x}, t) \in \partial\Omega \times (0, T), \tag{8.8a}$$

$$\frac{\partial u}{\partial n}(\mathbf{x}, t) = \vartheta(\mathbf{x}, t), \quad (\mathbf{x}, t) \in \Gamma \times (0, T), \tag{8.8b}$$

or

$$\frac{\partial u}{\partial n}(\mathbf{x}, t) = \vartheta(\mathbf{x}, t), \quad (\mathbf{x}, t) \in \partial\Omega \times (0, T), \tag{8.9a}$$

$$u(\mathbf{x}, t) = \beta(\mathbf{x}, t), \quad (\mathbf{x}, t) \in \Gamma \times (0, T), \tag{8.9b}$$

where $\Gamma \subset \partial\Omega$ is a non-empty open subset of the boundary $\partial\Omega$, and r, u_0, β and ϑ are known functions.

Bibliography

[1] Ahmadabadi, M. N., Arab, M., and Maalek-Ghaini, F. (2009). The method of fundamental solutions for the inverse space-dependent heat source problem. *Engineering Analysis with Boundary Elements*, **33**, 1231–1235.

[2] Beilina, L., Thanh, N. T., Klibanov, M. V., and Fiddy, M. A. (2014). Reconstruction from blind experimental data for an inverse problem for a hyperbolic equation. *Inverse Problems*, **30**, 025002 (24 pages).

[3] Belge, M., Kilmer, M., and Miller, E. L. (2002). Efficient determination of multiple regularization parameters in a generalized L-curve framework. *Inverse Problems*, **18**, 1161–1183.

[4] Bourgeois, L., Chaulet, N., and Haddar, H. (2011). Stable reconstruction of generalized impedance boundary conditions. *Inverse Problems*, **27**, 095002 (26 pages).

[5] Bourgeois, L., Chaulet, N., and Haddar, H. (2012). On simultaneous identification of a scatterer and its generalized impedance boundary conditions. *SIAM Journal on Scientific Computing*, **34**, 1824–1848.

[6] Bourgeois, L. and Haddar, H. (2010). Identification of generalized impedance boundary conditions in inverse scattering problems. *Inverse Problems and Imaging*, **4**, 19–38.

[7] Cakoni, F. and Kress, R. (2013). Integral equation method for the inverse obstacle

problem with generalized impedance boundary condition. *Inverse Problems*, **29**, 015005 (19 pages).

[8] Cannon, J. R. (1968). Determination of an unknown heat source from overspecified boundary data. *SIAM Journal on Numerical Analysis*, **5**, 275–286.

[9] Cannon, J. R. (1984). *The One-dimensional Heat Equation*. Addison-Wesley Publishing Company, Menlo Park, California.

[10] Cannon, J. R. and Hoek, J. (1986). Diffusion subject to the specification of mass. *Journal of Mathematical Analysis and Applications*, **115**, 517–529.

[11] Cannon, J. R., Lin, Y., and Wang, S. (1991). Determination of a control parameter in a parabolic partial differential equation. *Journal of the Australian Mathematical Society, Series B*, **33**, 149–163.

[12] Chen, Z., Lu, Y., Xu, Y., and Yang, H. (2008). Multi-parameter Tikhonov regularization for linear ill-posed operator equations. *Journal of Computational Mathematics*, **26**, 37–55.

[13] Elden, L., Berntsson, F., and Reginska, T. (2000). Wavelet and Fourier methods for solving the sideways heat equation. *SIAM Journal on Scientific Computing*, **21**, 2187–2205.

[14] Engl, H. W. and Kügler, P. (2005). Nonlinear inverse problem: Theoretical aspects and some industrial applications. In Capasso, V. and Périaux, J., editors, *Multidisciplinary Methods for Analysis Optimization and Control of Complex Systems*, volume 6 of *the series Mathematics in Industry*, pages 3–47. Springer, Berlin.

[15] Farcas, A. and Lesnic, D. (2006). The boundary element method for the determination of a heat source dependent on one variable. *Journal of Engineering Mathematics*, **54**, 375–388.

[16] Hansen, P. C. (2001). The L-curve and its use in the numerical treatment of inverse problems. In Johnston, P., editor, *Computational Inverse Problems in Electrocardiology*, pages 119–142. WIT Press, Southampton.

[17] Hasanov, A. (2007). Simultaneous determination of source terms in a linear parabolic problem from the final overdetermination: Weak solution approach. *Journal of Mathermatical Analysis with Applications*, **330**, 766–779.

[18] Hazanee, A., Ismailov, M. I., Lesnic, D., and Kerimov, N. B. (2013). An inverse time-dependent source problem for the heat equation. *Applied Numerical Mathematics*, **69**, 13–33.

[19] Hazanee, A., Ismailov, M. I., Lesnic, D., and Kerimov, N. B. (2015). An inverse time-dependent source problem for the heat equation with a non-classical boundary condition. *Applied Mathematical Modelling*, in press (available online).

[20] Hazanee, A. and Lesnic, D. (2013). Reconstruction of an additive space- and time-dependent heat source. *European Journal of Computational Mechanics*, **22**, 304–329.

[21] Hazanee, A. and Lesnic, D. (2014). A time-dependent coefficient identification problem for the bioheat equation. In Szczygiel, I., Nowak, A., and Rojczyk, M., editors, *ICIPE2014 8th International Conference on Inverse Problems in Engineering*, pages 127–136. Silesian University of Technology, May 12-15, 2014, Poland.

[22] Ionkin, N. I. (1977). Solution of a boundary-value problem in heat conduction with a non-classical boundary condition. *Differential Equations*, **13**, 294–304.

[23] Ismailov, M. I. and Kanca, F. (2011). An inverse coefficient problem for a parabolic equation in the case of nonlocal boundary and overdetermination conditions. *Mathematical Methods in the Applied Sciences*, **34**, 692–702.

[24] Ismailov, M. I., Kanca, F., and Lesnic, D. (2011). Determination of a time-dependent heat source under nonlocal boundary and integral overdetermination conditions. *Applied Mathematics and Computation*, **218**, 4138–4146.

[25] Ivanchov, M. (2003). *Inverse Problems for Equations of Parabolic Type*. VNTL Publishers, Lviv.

[26] Ivanchov, M. I. (2001). Inverse problem for a multidimensional heat equation with an unknown source function. *Matematychni Studii*, **16**, 93–98.

[27] Ivanchov, N. I. (1993). Inverse problems for the heat-conduction equation with nonlocal boundary conditions. *Ukrainian Mathematical Journal*, **45**, 1186–1192.

[28] Ivanchov, N. I. (1995). On the determination of unknown source in the heat equation with nonlocal boundary conditions. *Ukrainian Mathematics Journal*, **47**, 1647–1652.

[29] Johansson, B. T. and Lesnic, D. (2007). A variational method for identifying a spacewise dependent heat source. *IMA Journal of Applied Mathematics*, **72**, 748–760.

[30] Johansson, B. T. and Lesnic, D. (2008). A procedure for determining a spacewise dependent heat source and the initial temperature. *Applicable Analysis*, **87**, 265–276.

[31] Kabanikhin, S. I. (2008). Definitions and examples of inverse and ill-posed problems. *Journal of Inverse and Ill-posed Problems*, **16**, 317–357.

[32] Kaipio, J. and Somersalo, E. (2007). Statistical inverse problems: Discretization, model reduction and inverse crimes. *Journal of Computational and Applied Mathematics*, **198**, 493–504.

[33] Kerimov, N. B. and Ismailov, M. I. (2012). An inverse coefficient problem for the heat equation in the case of nonlocal boundary conditions. *Journal of Mathematical Analysis and Applications*, **396**, 546–554.

[34] Kerimov, N. B. and Ismailov, M. I. (2015). Direct and inverse problems for the heat equation with a dynamic type boundary condition. *IMA Journal of Applied Mathematics*, accepted.

[35] Kuzhuget, A. V., Beilina, L., Klibanov, M., Sullivan, A., Nguyen, L., and Fiddy, M. A. (2000). Blind experimental data collected in the field and an approximately globally convergent inverse algorithm. *Inverse Problems*, **28**, 095007 (33 pages).

[36] Langer, R. E. (1932). A problem in diffusion or in the flow of heat for a solid in contact with a fluid. *Tohoku Mathematical Journal*, **35**, 360–375.

[37] Lesnic, D. (2009). Identification of the time-dependent perfusion coefficient in the bio-heat conduction equation. *Journal of Inverse and Ill-posed Problems*, **17**, 753–764.

[38] Lesnic, D., Elliott, L., and Ingham, D. B. (1998). The boundary element solution of the Laplace and biharmonic equations subjected to noisy boundary data. *International Journal for Numerical Methods in Engineering*, **43**, 479–492.

[39] Lesnic, D., Elliott, L., Ingham, D. B., Knipe, R. J., and Clennell, B. (1996). The identification of hydraulic conductivities of composite rocks. In Jones, G., Fisher, Q., and Knipe, R. J., editors, *Faulting, Fault Sealing and Fluid Flow in Hydrocarbon Reservoirs: Abstracts*, pages 113–114.

[40] Morozov, A. (1966). On the solution of functional equations by the method of regularization. *Soviet Mathematics Doklady*, **7**, 414–417.

[41] Nakhushev, A. M. (1995). *Equations of Mathematical Biology*. Vysshaya Shkola, Moscow, (in Russian).

[42] Petrov, Y. P. and Sizikov, V. S. (2005). *Well-posed, Ill-posed and Intermediate Problems*. VSP, The Netherlands.

[43] Prilepko, A. I., Orlovsky, D. G., and Vasin, I. A. (2000). *Methods for Solving Inverse Problems in Mathematical Physics*. M. Dekker, New York.

[44] Prilepko, A. I. and Solov'ev, V. V. (1988). Solvability theorems and Rothe's method for inverse problems for a parabolic equation. I. *Differential Equations*, **23**, 1230–1237.

[45] Prilepko, A. I. and Tkachenko, D. S. (2003). Inverse problem for a parabolic equation with integral overdetermination. *Journal of Inverse and Ill-Posed Problems*, **11**, 191–218.

[46] Samarskii, A. A. (1980). Some problems in differential equations theory. *Differential Equations*, **16**, 1221–1228.

[47] Savateev, E. G. (1995). On problems of determining the source function in a parabolic equation. *Journal of Inverse and Ill-Posed Problems*, **3**, 83-102.

[48] Shi, C., Wang, C., and Wei, T. (2014). Numerical solution for an inverse heat source problem by an iterative method. *Applied Mathematics and Computation*, **244**, 577–597.

[49] Skerget, P. and Brebbia, C. A. (1985). Time dependent non-linear potential problems. In Brebbia, C. A., editor, *Boundary Element Research*, pages 63–86. Springer-Verlag, Berlin.

[50] Slodicka, M. (2015). A parabolic inverse source problem with a dynamic boundary condition. *Applied Mathematics and Computation*, **256**, 529–539.

[51] Slodicka, M., Lesnic, D., and Onyango, T. T. M. (2010). Determination of a time-dependent heat transfer coefficient in a nonlinear inverse heat conduction problem. *Inverse Problems in Science and Engineering*, **18**, 65–81.

[52] Thanh, N. T., Beilina, L., Klibanov, M., and Fiddy, M. A. (2014). Reconstruction of the refractive index from experimental backscattering data using a globally convergent inverse method. *SIAM Journal on Scientific Computing*, **36**, B273–B293.

[53] Trucu, D. (2009). *Inverse Problems for Blood Perfusion Identification*. PhD Thesis, University of Leeds.

[54] Trucu, D., Ingham, D. B., and Lesnic, D. (2008). Inverse time-dependent perfusion coefficient identification. *Journal of Physics: Conference Series*, **124**, 012050 (28 pages).

[55] Trucu, D., Ingham, D. B., and Lesnic, D. (2010). Inverse temperature-dependent perfusion coefficient reconstruction. *International Journal of Non-Linear Mechanics*, **45**, 542–549.

[56] Trucu, D., Ingham, D. B., and Lesnic, D. (2011). Reconstruction of the space- and time-dependent blood perfusion coefficient in bio-heat transfer. *Heat Transfer Engineering*, **32**, 800–810.

[57] Twomey, S. (1963). On the numerical solution of Fredholm integral equations of the first kind by the inversion of the linear system produced by quadrature. *Journal of the Association for Computing Machinery*, **10**, 97–101.

[58] Vogel, C. R. (1996). Non-convergence of the L-curve regularization parameter selection method. *Inverse Problems*, **12**, 535–547.

[59] Wei, T. and Li, M. (2006). High order numerical derivatives for one-dimensional scattered noisy data. *Applied Mathematics and Computation*, **175**, 1744–1759.

[60] Wrobel, L. C. (2002). *The Boundary Element Method: Applications in Thermo-Fluids and Acoustics*, Vol.1. John Wiley & Sons, New York.

[61] Xiong, X., Yan, Y., and Wang, J. (2011). A direct numerical method for solving inverse heat source problems. *Journal of Physics: Conference Series*, **290**, 012017 (10 pages).

[62] Yamamoto, M. (1993). Conditional stability in determination of force terms of heat equations in a rectangle. *Mathematical and Computer Modelling*, **18**, 79–88.

[63] Yan, L., Fu, C. L., and Yang, F. L. (2008). The method of fundamental solutions for the inverse heat source problem. *Engineering Analysis with Boundary Elements*, **32**, 216–222.

[64] Yan, L., Yang, F. L., and Fu, C. L. (2009). A meshless method for solving an inverse spacewise-dependent heat source problem. *Journal of Computational Physics*, **228**, 123–136.

[65] Yan, L., Yang, F. L., and Fu, C. L. (2010). A new numerical method for the inverse source problem from a Bayesian perspective. *International Journal for Numerical Methods in Engineering*, **85**, 1460–1474.

[66] Yang, F. and Fu, C. L. (2010). A simplified Tikhonov regularization method for determining the heat source. *Applied Mathematical Modelling*, **34**, 3286–3299.

[67] Yang, L., Dehghan, M., Yu, J. N., and Luo, G. W. (2011). Inverse problem of time-dependent heat sources numerical reconstruction. *Mathematics and Computers in Simulation*, **81**, 1656–1672.

[68] Yi, Z. and Murio, D. A. (2004a). Source term identification in 1-D IHCP. *Computers and Mathematics with Applications*, **47**, 1921–1933.

[69] Yi, Z. and Murio, D. A. (2004b). Source term identification in 2-D IHCP. *Computers and Mathematics with Applications*, **47**, 1517–1533.